Novel Probabilistic-based Framework for Improved History Matching of Shale Gas Reservoirs

by

Francis Nzubechukwu Nwabia

A thesis submitted in partial fulfillment of the requirements for the degree of

Doctor of Philosophy

in

Petroleum Engineering

Department of Civil and Environmental Engineering
University of Alberta

Abstract

Hydraulically fractured horizontal wells are widely adopted for the development of tight or shale gas reservoirs. The presence of highly heterogeneous, multi-scale, fracture systems often renders any detailed characterization of the fracture properties challenging. The discrete fracture network (DFN) model offers a viable alternative for explicit representation of multiple fractures in the domain, where the comprising fracture properties are defined in accordance with specific probability distributions. However, even with the successful modelling of a DFN, the relationship between a set of fracture parameters and the corresponding production performance is highly nonlinear, implying that a robust history-matching workflow capable of updating the pertinent DFN model parameters is required for calibrating stochastic reservoir models to both geologic and dynamic production data.

This thesis will develop an integrated approach for the history matching of hydraulically fractured reservoirs. First, multiple realizations of the DFN model are constructed with conditioning data based on available geological information such as seismic data, well logs, and rate transient analysis (RTA) interpretations, which are useful for inferring the prior probability distributions of relevant fracture parameters. A pilot point scheme and sequential indicator simulation are employed to update the distributions of fracture intensities which represent the abundance of secondary fractures (NFs) in the entire reservoir volume. Next, the model realizations are upscaled into an equivalent continuum dual-porosity dual-permeability model and subjected to numerical multiphase flow simulation. The predicted production performance is compared with the actual recorded responses. Finally, the DFN-model parameters are adjusted following an indicator-based probability perturbation method. Although the probability perturbation technique has been applied to update facies distributions in the past, its application in modeling DFN distributions is limited.

An indicator formulation is proposed to account for the non-Gaussian nature of the DFN parameters. The algorithm aims at minimizing the objective function while reducing the uncertainties in the unknown fracture parameters.

The novel probabilistic-based framework is applied to estimate the posterior probability distributions of transmissivity of the primary fracture (T_{pf}), transmissivity of the secondary induced fracture (T_{sf}) and secondary fracture intensity (P^{sf}_{32L}), secondary fracture aperture (r_e), length and height (L and H), in a multifractured shale gas well in the Horn River Basin. An initial realization of the DFN model is sampled from the prior probability distributions using the Monte Carlo simulation. These probability distributions are updated to match the production history, and multiple realizations of the DFN models are sampled from the updated (posterior) distributions accordingly. The key novelty in the developed probabilistic approach is that it accounts for the highly nonlinear relationships between fracture model parameters and the corresponding flow responses, and it yields an ensemble of DFN realizations calibrated to both static and dynamic data, as well as the related upscaled flow-simulation models. The results demonstrate the utility of the developed approach for estimating secondary fracture parameters, which are not inferable from other static information alone.

Preface

Chapter 3 of this thesis has been published as Nwabia, F. N., & Leung, J. Y. (2020). Inference of Hydraulically Fractured Reservoir Properties from Production Data Using the Indicator-Based Probability Perturbation Assisted History-Matching Method. *Journal of Petroleum Science and Engineering*, 198, 108240. I was responsible for the conceptualization, model construction, formal analysis, and writing the original draft. Leung, J. Y was the supervisory author and was involved in concept formation, project administration, data curation and reviewing and editing the manuscript.

Chapter 4 of this thesis has been published as Nwabia, F. N., & Leung, J. Y. (2021). Probabilistic history matching of multi-scale fractured reservoirs: Integration of a novel localization scheme based on rate transient analysis. *Journal of Natural Gas Science and Engineering*, 94, 104067. I was responsible for the conceptualization, model construction, formal analysis, and writing the original draft. Leung, J. Y was the supervisory author and was involved in concept formation, project administration, data curation and reviewing and editing the manuscript.

A version of chapter 5 has been published as Nwabia, F. N., & Leung, J. Y. (2021). Incorporating the Variability of Uncertain DFN Model Parameters of a Hydraulically Fractured Reservoir during Probability-Based Assisted History Matching: Findings and Deductions. *In 3rd International Discrete Fracture Network Engineering Conference.* I was responsible for the conceptualization, model construction, formal analysis, and writing the original draft. Leung, J. Y was the supervisory author and was involved in concept formation, project administration, data curation and reviewing and editing the manuscript.

A version of Chapter 6 will be submitted for publication as Nwabia, F.N., & Leung, J.Y. A Robust Probabilistic History Matching Framework for the Characterization of Fracture Network Parameters of Shale Gas Reservoirs. I was responsible for the conceptualization, model construction, formal analysis, and writing the original draft. Leung, J. Y was the supervisory author and was involved in concept formation, project administration, funding acquisition, data curation and reviewing and editing the manuscript.

Chapters 1, 2 and 7 are originally written by Francis Nwabia and have never been published before.

Dedicated to my family

for their love, perpetual support, discipline, and inspiration.

Acknowledgements

First, I owe a profound gratitude and praises to Almighty God for His blessings, directions, and inspiration to conclude this chapter of my life.

I would like to express my sincere gratitude to my supervisor, Dr. Juliana Leung for her guidance, encouragement, mentorship, consistent engagements, and the opportunity to learn and work under her honored tutelage. I am most grateful for her care and stellar supervision throughout my research. I also want to thank my supervising committee members, Dr. Hassan Dehghanpour and Dr. Jeff Boisvert for their insights and invaluable contributions. I would also acknowledge the immense support from my mentor, Dr. James Arukhe.

To the team at Dr. Leung's research group of the University of Alberta, I say a very big thank you for the interesting times, stimulating technical conversations and your friendships.

I acknowledge the financial support of PTDF & TETFund Nigeria, University of Alberta and NSERC for this research through grants and scholarship. Sincere thanks to Schlumberger, MathWorks®, ©KAPPA and Golder Associates for providing the academic licenses for the Petrel & Eclipse simulation tools, MATLAB, Topaze NL Module, and FracMan, respectively.

Finally, I want to specially acknowledge the endless support of my wife Sandra Francis-Nwabia, daughter Chizaram Nwabia and son Jachike Nwabia, my parents Hyginus (late) and Lucy Nwabia, and my siblings – Chukwuma, Chinyere, Nonso, Onyinye, Oluchukwu, Ndidiamaka (late), Chukwudi and John. Your love and support brought me this far.

Table of Contents

List of Tables

List of Figures

List of Symbols

A_{cm}	Total matrix surface area draining into fracture system, ft^2
A_{cw}	Wellface cross-sectional area, ft^2
A_m	Area of a surface area open to flow in a given flow direction
A_r	Area of fracture *r*
b	Nearest neighbor fracture intensity constant parameter
B	Formation volume factor
b_s or P_{wfs}	Simulated bottom hole pressure
b_h or P_{wfh}	Historical bottom hole pressure
c	Nearest neighbor fracture intensity model empirical constant
C	Production information influencing the simulation event
c_{frac}	Fracture compressibility (p_{frac} and s_{frac} for primary and secondary fracture)
c_{fluid}	Fluid compressibility
c_t	Total compressibility
$d_{x,f}$	Distance between a location x and the nearest major feature
d	Production data
d_m	Distance from the open surface to the center of the matrix block
e_{eq}	Equivalent radius
F_{ij}, F_{kk}	Element of fracture tensor in the 3 × 3 matrix
f_{target}	Historical data
f^i	Simulated data
g	Gravitational constant
G	Forward model
G_p	Cumulative gas production
h	Reservoir or formation thickness
h_f	Fracture height
I^l	Indicator variable of step *l*
I^{l+1}	Indicator variable of step *l+1*
k_f	Fracture permeability
k_m	Matrix permeability

k_z, k_y	Vertical and horizontal permeability
k, k'	Category indicators variable for steps l and l+1 respectively
k_{ij} or $\overline{\overline{k}}$	Permeability tensor
K, K'	Category for indicator variable I
L_i, L_j, L_k or L_f	Fracture spacings in x, y, and z directions
L_w	Producing well interval length
m	Model parameters
m	Slope
N	Total number of fractures in a grid cell
n_{ir}, n_{jr}	i^{th} and j^{th} components of the unit normal vector **n** corresponding to the fracture plane r
n	Normal unit vector
Obj_{opt}	Optimal objective function
Obj_{tol}	Predefined tolerance for objective function
ΔO	Objective function
$\mathrm{Obj}_{\mathrm{optimal}}$	Optimal objective function
$\mathrm{Obj}_{\mathrm{tolerance}}$	Predefined tolerance for objective function
ΔO	Objective function
p	Predicted
P_f	Fracture pressure
P_D	Dimensionless pressure
P_i	Initial reservoir pressure
P_m	Matrix pressure
P_{ref}	Reference pressure
P_{wf}	Bottom Hole Pressure
$m(P)$	Pseudo pressure
$\overline{P}$	Average pressure
$P^{sf}{}_{32G}$	Global fracture intensity of the secondary induced fracture
$P\{I(u)\}$	Probability of the indicator at location u
P_{32L}	Local fracture intensity
P_{32G}	Global fracture intensity

$m(P)$	Pseudo pressures
Qg_s	Simulated gas production rate
Qg_h	Historical gas production rate
Qw_s	Simulated water production rate
Qw_h	Historical water production rate
q_D	Dimensionless flow rate
Q_{DA}	Dimensionless cumulative
q_{ref}	Reference rate (gas)
q_τ	Production rate (gas) with time
$Q_{(t)}$	Cumulative production as a function of time
r_{Dn}	Deformation or perturbation parameter for n number of distinct type of model parameters (r_{Dnopt} - optimal perturbation parameter)
r_e	Fracture aperture
r_w	Wellbore radius
S_{frac}	Fracture storativity
t	Time
T	Reservoir temperature
t_{ca}	Pseudo material balance time
t_{dxf}	Dimensionless time
t_e	Equivalent time or material balance time
T_r	Transmissivity of fracture plane r
T_{pf}	Transmissivity of the primary fracture
T_{sf}	Transmissivity of the secondary fracture
u	Location vector
$\mathbf{u}$	Vector of state variables
V	Grid cell volume
V_m	Volume of the matrix block or matrix control volume
V_t	Total volume of bounding matrix
x_1, x_2	Fracture spacing (also d_1, d_2)
X_f	Effective fracture half-length
$x^{(1)}$, $x^{(2)}$	Points on a function

x^{low}, x^{high}	Lower and upper bounds for search interval corresponding to a unimodal function
z_i	Real gas deviation factor at initial reservoir pressure
Zw	Well distance from the lower reservoir boundary
δ_{ij}	Kroenecker's delta
ρ	Fluid density
μ, μ_g	Fluid viscosity, Gas viscosity
ω	Storativity ratio
λ	Interporosity coefficient
σ	Shape factor
φ	Ratio of equal distances to overall interval distance
ϕ_f	Fracture porosity
ϕ_m	Matrix porosity

Acronyms

CCFV	Cell centered finite volume
CFD	Conditional finite domain
CVFE	Control volume finite element
DFN	Discrete fracture network
DPDK	Dual porosity dual permeability
EDFM	Embedded discrete fracture model
EnKF	Ensemble Kalman Filter
GSLIB	Geostatistical software library
HRB	Horn River Basin
MBAL	Material balance
MBT	Material balance time
MCMC	Markov Chain Monte Carlo
MFE	Mixed finite element
MPFA	Multi-point flux approximation
NFs	Natural fractures
PPM	Probability perturbation method
PV	Pore volume
PSS	Pseudo steady state
RFT	Repeat formation tester
RHS	Right hand side
RNP	Rate normalized pressure
RTA	Rate transient analysis
SBS	Spatial bootstrap
SISIM	Sequential indicator simulation
SRV	Stimulated reservoir volume
STGIIP or G_i	Gas initially in place
WBHP	Well bottom hole pressure
WGPR	Well gas production rate
WWPR	Well water production rate

Chapter 1: Introduction

1.1 BACKGROUND

The basin-centered continuous accumulations, otherwise known as the unconventional reservoirs, cannot produce economic volumes of hydrocarbon without stimulation treatments such as fracturing and steam injection. These types of reservoirs (shale gas and shale oil, coalbed methane, gas hydrates, deep gas, heavy oil and (or) natural bitumen and shallow biogenic gas) are often characterized by low recovery factor, low matrix permeability, uncertain hydrocarbon-water contact, large in-place volumes, lack of traditional traps or seal, and abnormal pressures. Shale, in particular, the most abundant source rock for conventional reservoirs and self-sourcing cap rock for unconventional oil and gas fields is a fine-grained fissile or laminated sedimentary rock formed from the compaction of silt and clay-size mineral particles (clay size < silt size < sand size); less than $\frac{1}{256th}$ mm in diameter particles.

The combination of horizontal drilling and hydraulic fracturing, also called hydraulically fractured horizontal wells, as shown in Fig. 1-1, has contributed to the improved production of unconventional (tight and shale) reservoirs in recent years. This technique involves horizontal directional drilling of well into the tight formation and the use of water, sand, and chemicals at high pressures to create fissures in the shale rock, which increases permeability and allows hydrocarbon to escape. The commercial application of this method was successful in the nineties and as of 2012, about 2.5 million fracturing jobs had been performed worldwide on both oil and gas wells with an adequate flow from the reservoirs (shale gas, tight gas, and tight oil).

Although the use of hydraulically fractured horizontal wells has some recorded successes, the presence of highly heterogeneous, multi-scale fracture systems often renders any detailed characterization of the fracture properties, a necessity for future prediction of the reservoir, challenging. The complex geometries of the secondary fractures and the significant disparity in permeability between the matrix and fracture systems pose particular challenges to the flow simulation and intensify the nonlinearity between the fracture model parameters and flow responses. There is, therefore, a need for a robust and efficient process to update both hydraulic and secondary fracture parameters integrating both static (e.g., logs) and dynamic data (e.g., rate and pressure measurements) for reliable production forecast and to facilitate reservoir management or optimize development strategies.

1.2 SIMULATION APPROACHES FOR PROPER REPRESENTATION OF COMPLEX FRACTURE SYSTEMS

Many different strategies are available for the numerical multiphase simulation of fractured reservoir systems. They primarily differ on how the geometries of the fracture systems are described and how the fracture-matrix fluid flow is presented. The choice of simulation approach reflects the complexity of the fracture characteristics (e.g., geometry, intensity, and scales) in capturing the matrix and fracture flow interactions. The dual porosity formulation considers fracture systems as the flow path directly connected with the wellbore and inter-porosity flow from matrix system to fracture system while ignoring the flow from the matrix to the wellbore (Barenblatt et al., 1960; Warren and Root, 1963; Al-Ghamdi and Ershaghi, 1996). The consideration of both the fracture system and the matrix block as fluid flow pathways into the wellbore with additional inter-porosity flow between matrix and fracture systems, otherwise called dual permeability model (or DPDK – dual-porosity dual-permeability) was proposed as improvements to the DP model (Hu and Huang, 2002; Degraff et al., 2005; Uba et al., 2007). It widely depends on the assumption that the fractures should be densely populated and well connected (Sun and Schechter, 2015; Kumar et al., 2019) to prevent the overestimation of fracture connectivity. Due to these limitations, DFN modeling, which explicitly specifies the actual geometries and locations of individual fractures using local refinement to discretize the volume near fractures in the computational domain, serves as a substitute. In situations where the detailed description of the actual geometries and locations of individual fractures are necessary, local grid refinement (LGR) can be applied in the fracture regions to represent these fracture elements in the computational domain explicitly. Despite that the DFN model approach can offer a more accurate representation of the complex fracture system than the DP or DPDK models, it suffers computational constraints, thus demanding the need to upscale the DFN models into equivalent dual permeability models as often adopted in most commercial simulation tools (Sarda et al., 2001; Nejadi et al., 2017; Nwabia and Leung, 2020).

The advanced higher-order discretization schemes such as control-volume finite-element (CVFE), cell-centered finite-volume (CCFV or multi-point flux approximation MPFA) and mixed finite-element methods (MFE), have been developed (Monteagudo & Firoozabadi, 2004; Sandve et al., 2012; Zidane & Firoozabadi, 2014; Liu et al., 2020) to simulate fluid flow in fracture systems using unstructured grids accurately. Each of these techniques has its own merits and limitations; for example, the CVFE design is computationally efficient, but it does not maintain flux continuity for a heterogeneous porous medium; the MFE method, which is locally flux-continuous and conservative, can be computationally expensive, as both the velocity and pressure fields are evaluated concurrently. While the use of unstructured grids suffers from high cost of computation as a result of too many gridblocks required to conform to hydraulic fractures, the local grid refinement suffers the same constraint due to the difficulty in representing fracture orientation (Cipolla et al., 2010). The recent and widely adopted embedded discrete fracture model (EDFM) discretizes fractures into structured cubical matrix cells (Li and Lee 2008; Shakiba et al., 2018). The EDFM is computationally efficient in calculating fluid transport within SRV since fractures are modeled explicitly within the matrix grid without refinement. These simulation tools used for the representation of complex fracture systems have peculiar limitations associated with adaptability for the scope of a study, computational efficiency, and the assumptions used for the formulation.

1.3 PROBLEMS WITH THE METHODS FOR CHARACTERIZING FRACTURED RESERVOIR SYSTEMS

In reservoir systems where both hydraulic and secondary fractures are present, secondary data such as seismic can improve predictions of fracture intensity in between the wells. In this thesis, fracture intensity at pilot (e.g., well) locations are used as conditioning data in a sequential indicator simulation to populate secondary fractures to the rest of the domain. Reservoir model parameters are adjusted during history matching such that the model predictions can closely reproduce the historical data (e.g., flow rates and pressures). History matching is inherently an ill-posed inverse problem with non-unique solutions. For fractured reservoir systems, a set of initial models (or realizations) are constructed by incorporating various static or geological data, and the models are subjected to flow simulation and an optimization scheme to adjust the fracture parameters until the mismatch between the predicted response and the actual historical data is minimized.

The goals of most probabilistic history-matching schemes are: (a) to estimate the posterior distributions corresponding to the unknown model parameters; and (b) to sample a set of updated models (or realizations) from those distributions; the variability exhibited by those realizations facilitates the uncertainty quantification and assessment. A particularly important aspect of fractured reservoir history matching is the capability to handle the probability distributions of any forms, without assuming that it follows a Gaussian distribution. Stochastics search algorithms (e.g., genetic algorithm, simulated annealing), optimization-based methods (e.g., maximum a-posterior), and sampling-based (e.g., gradual deformation), have been used to either update equivalent model parameters or update parameters of the discrete fractures. A combined gradient simulator and the adjoint method was formulated by Cui and Kellar (2005) to update the flow properties of a reservoir based on the correlation between fracture intensity and fracture permeability, matrix permeability, and a coupling factor. Gradient-based optimization techniques require several gradient calculations and are thus not computationally efficient. De Lima et al. (2012) implemented the gradual deformation approach to estimate realizations of fault distribution (i.e., spatial locations, intensity, and length). However, despite the ease of the implementation of the gradual deformation method, it only works for modeling properties that follow a Gaussian distribution, and this is an invalid assumption for most fracture properties. The MCMC has been applied to calibrate subsurface models and quantify its uncertainties in a Bayesian probabilistic framework (Maucec et al., 2007). The gap with MCMC is that it tends to require a large number of forward simulations, especially when dealing with a large number of unknown model parameters. The implementation of stochastic search algorithms to estimate fracture distribution have also proven useful in reservoir studies. Ensemble-based techniques such as Ensemble Kalman Filter or EnKF (Aanonsen et al., 2009; Emerick and Reynolds, 2011) and ensemble smoother or EnS (Chai et al., 2018; Chang and Zhang, 2018), which utilize the covariance matrix to update an ensemble of parameters, have also gained wide attention for their advantages in data assimilation and uncertainty quantification. Its major limitation is that it assumes multi-Gaussian distribution on model and data variables and a linear relationship between all variables, and these assumptions do not hold for fractured reservoirs, rendering the convergence behavior of other ensemble-based methods, including EnKF, to be compromised. Emerick and Reynolds (2012) assessed the results of a very long MCMC as a reference solution to scrutinize the sampling performance of the ensemble-based methods by combining MCMC with EnKF. Despite acknowledging a high data mismatch, the outcome identified improvements when compared to EnKF alone. Although these extensions/hybrid formulations may retain the idea of utilizing an ensemble, they do not rely on linear update and are not appropriate for highly non-Gaussian variables; therefore, it is argued that they could offer only partial approximation of the true distribution.

1.4 PROBLEM STATEMENT

Hydraulically fractured reservoirs are characterized by very complex fracture systems and heterogeneities. The significant challenges usually encountered in characterizing these types of reservoirs include: the inadequate constraining information for the proper description of the fracture networks, inability of optimization algorithms to handle fracture parameters whose distributions are non-Gaussian, the uncertainties posed in the nonlinear relationship between the fracture parameters and updated upscaled reservoir model properties, and the rationale for formulating localization schemes for reliable history matching process.

These limitations can be resolved by developing a novel technique poised with the ability to properly characterize the complexities inherent in such reservoirs while being within appropriate computational efficiency and cost. Consequently, integrating the description of fracture network systems using information from microseismic data and RTA estimates into the formulation of an efficient probabilistic history matching workflow provides a means for improving the characterization of multi-scale fractured reservoirs.

Therefore, the problem statement of this thesis is *"development of a robust probabilistic history matching framework aimed at improving existing history matching routines for the characterization of multi-scaled hydraulically fractured reservoirs"*.

1.5 RESEARCH OBJECTIVES

The main objective of this research is to develop a practical probabilistic-based assisted history matching workflow for characterizing and updating fracture network parameters of multi-scale hydraulically fractured reservoirs while honoring both static geological data and dynamic information. The developed history matching workflow integrated both dynamic production data and static information into the probability perturbation method to specifically address the following objectives.

1. Describe fracture network systems using conditioning data from microseismic information and RTA estimates.

2. Handle the spatial variability of the secondary fractures in the reservoir, including those in the vicinity of the hydraulic fractures and those disconnected from the hydraulic fractures, by incorporating a pilot-point parameterization scheme and sequential simulation in an indicator-based PPM workflow.

3. Formulate a localization scheme based on RTA-derived flow regimes for reliable history matching.

4. Handle the uncertainties associated with the non-linear relationship between fracture network parameters and reservoir flow response for both Gaussian and non-Gaussian uncertain fracture network parameters.

5. Update the posterior probability distributions of the hydraulic and secondary fractures of a shale gas reservoir – Horn River Basin.

1.6 LIMITATIONS OF RESEARCH

(i) The forward model does not couple the flow computations with geomechanics calculations, thus, the impact of stress changes in the reservoir on production is not explicitly captured.

(ii) The research workflow is implemented for a (water-wet) dry gas reservoir where the gas remains in the gas phase during pressure depletion in the reservoir.

(iii) The hydraulic fractures are modeled as elongated penny-shaped fissures.

(iv) The DPDK model is used to represent the matrix – fracture fluid flow in the fractured reservoir system comprising of both hydraulic and secondary fractures.

1.7 DISSERTATION STRUCTURE

This is a paper-based thesis with a total of 7 chapters. Chapters 3, 4, 5 are already published articles, and chapter 6 has been submitted for publication. Each of these articles comprises a specific introduction, literature review, methodology, conclusion, and references. The bibliography at the end of the thesis is the combination of the references from individual chapters of the reports.

Chapter 1 presents a general background in terms of the motivation, the problem statement and research objectives. Chapter 2 reviews the relevant literature associated with the characterization of fractured reservoirs and production history matching approaches.

Chapter 3 discusses the probabilistic-based history matching workflow formulation and the practical applications for updating Gaussian and non-Gaussian fracture parameters in case studies.

Chapter 4 explores the integration of an RTA-constrained localization scheme for the formulated history matching workflow in Chapter 3 for a reliable history matching of hydraulically fractured reservoirs. In this chapter, the result derived from RTA was used to constrain the initial probability distribution of uncertain fracture parameters. The flow regimes were used to formulate a localization scheme for history matching. Chapter 5 employs the developed workflow to assess the impact of the variability of fracture parameters across hydraulic fracture stages during history matching and update of fracture parameters. Chapter 6 describes a robust assisted history matching workflow for updating fracture network parameters for hydraulic and secondary fractures (NFs). In this chapter, the pilot-point parameterization scheme and sequential simulation are integrated into the indicator-based PPM workflow to handle the spatially varying secondary fracture distribution, and the parameters of both hydraulic and secondary fractures of a reservoir in the Horn River Basin were characterized and updated.

The conclusions of the thesis, the relevant contributions, and applications are presented in Chapter 7, along with recommendations for future work.

1.8 REFERENCES

Aanonsen, S. I., Oliver, D. S., Reynolds, A. C., Vallès, B. 2009. The Ensemble Kalman Filter in Reservoir Engineering – A Review. SPE-117274-PA. SPE J. 14(03): 393–412. SPEJ Sept. 2009. https://doi.org/10.2118/117274-PA

Al-Ghamdi, A., Ershaghi, I. 1996. Pressure transient analysis of dually fractured reservoirs. SPE 26959-PA. SPE J. 1(1): 93–100. doi:10.2118/26959-PA

Barenblatt, G. I., Zheltov, Y. P., Kochina, I. N. 1960. Basic concepts in the theory of seepage of homogeneous liquids in fissured rocks, J. Appl. Math. Mech., Engl. Transl. 24(5): 1286-1303. https://doi.org/10.1016/0021-8928(60)90107-6

Chai, Z., Tang, H., He, Y., Killough, J., Wang, Y. 2018. Uncertainty Quantification of the Fracture Network with a Novel Fracture Reservoir Forward Model. SPE-191395-MS. SPE Annual Technical Conference and Exhibition, Dallas, Texas. https://doi.org/10.2118/191395-MS

Chang, H., and D. Zhang. 2018. History Matching of Stimulated Reservoir Volume of Shale-Gas Reservoirs Using an Iterative Ensemble Smoother. SPE-189436-PA. SPE Journal 23 (2): 346-366. https://doi.org/10.2118/189436-PA

Cipolla, C., L., Lolon, E. P., Erdle, J. C., Rubin, B. 2010. Reservoir Modeling in Shale-Gas Reservoirs. SPE Res Eval & Eng, 13 (2010): 638–653. doi:https://doi.org/10.2118/125530-PA

Cui, H., Kelkar, M. 2005. Automatic History Matching of Naturally Fractured Reservoirs and a Case Study. SPE-94037-MS. Western Regional Meeting, Irvine, California, 30 March-1 April. https://doi.org/10.2118/94037-MS

Degraff, J.M., Meurer, M.E., Landis, L.H., Lyons, S. 2005. Fracture network modeling and dual-permeability simulation of carbonate reservoirs. SPE 10954-MS. international petroleum technology conference, Doha, Qatar. doi:10.2118/10954-MS

De Lima, A., Lange, A., Schiozer, D.J., 2012. Assisted History-Matching for the Characterization and Recovery Optimization of Fractured Reservoirs using Connectivity Analysis. SPE 154392. SPE Europec/EAGE Annual Conference. https://doi.org/10.2118/154392-MS

Emerick, A. A., Reynolds, A. C. 2011. History Matching a Field Case Using the Ensemble Kalman Filter With Covariance Localization. SPE -141216-PA. SPE Res Eval & Eng 14 (04): 443-452. https://doi.org/10.2118/141216-PA

Emerick, A. A., Reynolds, A. C. 2012. Combining the ensemble Kalman Filter with Markov-chain Monte Carlo for Improved History Matching and Uncertainty Characterization. SPE-141336-PA. SPE J. 17(2): 418–440. https://doi.org/10.2118/ 141336-PA

Hu, B.X., Huang, H. 2002. Stochastic analysis of reactive solute transport in heterogeneous, fractured porous media: a dual-permeability approach. Trans. Porous Med. 48(1): 1–39. doi:10.1023/A:1015671227317

Kumar, S., Rey, A., Dufour, G., Ogunyomi, B. 2019. Understanding Fluid Flow Behavior in Fractured Reservoir using Dual Porosity Dual Permeability and Discretized Fracture Model. SPE-196038-MS. SPE Annual Technical Conference and Exhibition, Calgary, Alberta, Canada. doi:https://doi.org/10.2118/196038-MS.

Li, L., Lee, S.H. 2008. Efficient field-scale simulation of black oil in a naturally fractured reservoir through discrete fracture networks and homogenized media. SPE-103901-PA. SPE Res. Eval. & Eng. 11(4): 750-758. https://doi-org /10.2118/103901-PA

Liu, Y., Liu, L., Leung, J. Y., Moridis, G. J. 2020. Sequentially Coupled Flow and Geomechanical Simulation with a Discrete Fracture Model for Analyzing Fracturing Fluid Recovery and Distribution in Fractured Ultra-Low Permeability Gas Reservoirs. Journal of Petroleum Science and Engineering, 189, 107042. https://doi.org/10.1016/j.petrol.2020.107042

Maucec, M., Douma, S. G., Hohl, D., Leguijt, J., Jimenez, E., Datta-Gupta, A. 2007. Streamline-Based History Matching and Uncertainty--Markov-Chain Monte Carlo Study of an Offshore Turbidite Oil Field. SPE-109943-MS. SPE Annual Technical Conference and Exhibition, California, USA. https://doi.org/10.2118/109943-MS

Monteagudo, J.E.P., and Firoozabadi, A. 2004. Control-Volume Method for Numerical Simulation of Two-Phase Immiscible Flow in Two-and Three-Dimensional discrete-Fractured Media, Water Resour. Res., 40, W07405, http://dx.doi.org/10.1029/2003WR002996

Nejadi, S., Trivedi, J.J., Leung, J. 2017. History Matching and Uncertainty Quantification of Discrete Fracture Network Models in Fractured Reservoirs. Journal of Petroleum Science and Engineering 152(2017) 21–32. http://dx.doi.org/10.1016/j.petrol.2017.01.048

Nwabia, F.N., and J.Y. Leung. 2020. Probabilistic History Matching of Multi-Scale Fractured Reservoirs: Integration of a Novel Localization Scheme Based on Rate Transient Analysis. SPE-199988-MS. SPE Canada Unconventional Resources Conference, Calgary, Canada. https://doi.org/10.2118/199988-MS

Sandve, T.H., Berre, I., Nordbotten, J.M. 2012. An Efficient Multi-Point Flux Approximation Method for discrete Fracture–Matrix Simulations. Journal of Computational Physics. 231(09), 3784–3800. https://doi.org/10.1016/j.jcp.2012.01.023

Sarda, S., Jeannin, L., Bourbiaux, B. 2001. Hydraulic Characterization of Fractured Reservoirs: Simulation on Discrete Fracture Models. SPE Reservoir Simulation Symposium, Houston, Texas, USA. SPE-66398-MS. https://doi-org/10.2118/66398-MS.

Shakiba, M., de Araujo Cavalcante Filho J., Sepehrnoori, K. 2018. Using Embedded Discrete Fracture Model (EDFM) in Numerical Simulation of Complex Hydraulic Fracture Networks Calibrated by Microseismic Monitoring Data. Journal of Natural Gas Science and Engineering, 55(2018), 495-507. ISSN 1875-5100. https://doi.org/10.1016/j.jngse.2018.04.019

Sun, J., Schechter, D. S. 2015. Optimization-Based Unstructured Meshing Algorithms for Simulation of Hydraulically and Naturally Fractured Reservoirs with Variable Distribution of Fracture Aperture, Spacing, Length and Strike. SPE-170703-PA. SPE Res. Eval & Eng 18(04): 463 – 480. https://doi-org /10.2118/170703-PA

Uba, H.M., Chiffoleau, Y., Pham, T., Divry, V., Kaabi, A., Thuwaini, J. 2007. Application of a hybrid dual-porosity/ dual-permeability representation of large-scale fractures to the simulation of a giant carbonate reservoir. SPE 105560-MS. SPE middle east oil and gas show and conference, Bahrain. doi:10.2118/105560-MS

Warren, J.E., Root, P.J. 1963. The Behavior of naturally Fractured Reservoirs. SPE 426-PA. SPE J. 3(3), 245–255 (1963). http://doi:10.2118/426-PA

Zidane, A., Firoozabadi, A. 2014. An Efficient Numerical Model for Multicomponent Compressible Flow in Fractured Porous Media, Advances in Water Resources 74 (2014) 127–147. https://doi.org/10.1016/j.advwatres.2014.08.010

APPENDIX – *Figures*

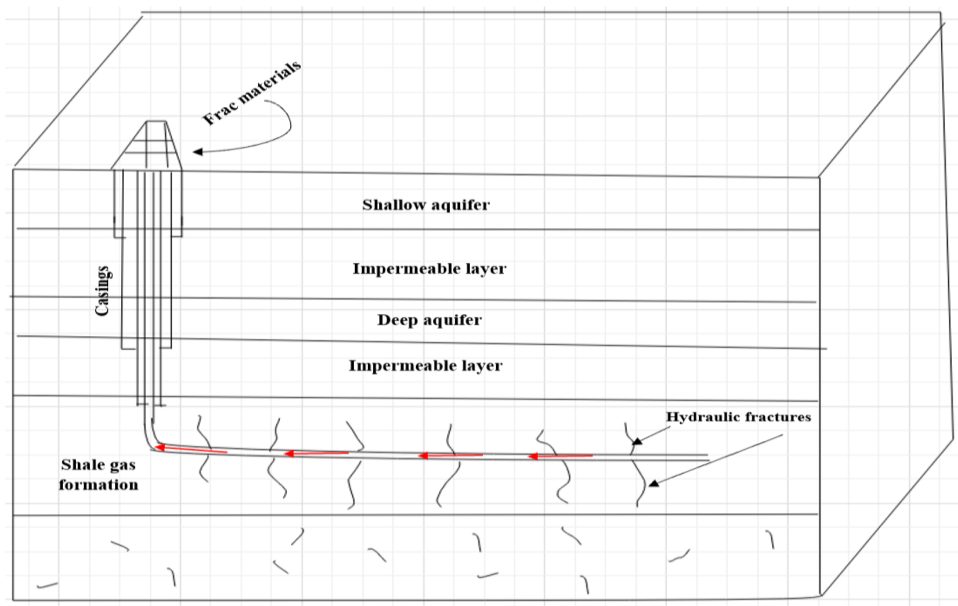

Fig. 1-1: Schematic depiction of hydraulic fracturing for shale gas.

Chapter 2: Literature Review

2.1 OVERVIEW

This chapter gives an insight into different approaches of quantifying, representing, and managing uncertainties in subsurface systems. Detailed discussions and limitations of different probability-based sampling techniques used in history matching are also presented. It should be noted that this thesis is written in a paper-based structure and therefore contains specific literature reviews peculiar to each of the publications presented in different chapters.

2.2 QUANTIFICATION OF UNCERTAINTIES IN SUBSURFACE SYSTEMS

Subsurface systems with a large pool of natural resources are abound with several complexities and require proper characterization. These systems are usually studied and measured at the surface based on collated data to improve knowledge and volume calculations. Despite studies and modeling performed on these systems on different scales (including local, regional, or global scales), it is plagued with several uncertainties, mostly due to lack of data, measurement errors and lack of understanding of the elemental phenomena and processes taking place. Generally, there is no unique representation or interpretation of the subsurface model for decision-making purposes. A reasonable numerical model comprising of geostatistical inputs is usually needed to relate available data and improve the understanding of the subsurface. Therefore, the quantification of uncertainty in subsurface systems is a crucial part of the decision-making process in the characterization of a reservoir and is discussed in this thesis in the context of uncertainties in input parameters and uncertainty management (uncertainty presentation, multiple realizations and decision making under uncertainty).

2.2.1 Uncertainties in Input Parameters

Input parameters in the form of histogram means, standard deviation and sample range are mostly assumed to be fixed whereas they have some inherent uncertainty which requires assessment. Reduction of these associated uncertainty in input parameters improves accuracy of results from modeling. Methods such as the conventional Bootstrap (BS), spatial Bootstrap (SBS) and Conditional Finite Domain (CFD) has been developed for the purpose of quantifying uncertainties in such statistical parameters.

The BS method is based on random sampling with replacement notwithstanding the form of data probability density function. It is a form of statistical resampling technique that can quantify uncertainty by simply resampling from the original data. It assumes that the data are independent and is representative of the entire population, and, therefore, may not be adaptable for reservoir data which usually have some level of correlations. Neufeld and Deutsch (2007) developed *boot-avg* code based on the resampling technique. The SBS method is applied to spatial data with correlated structure and quantifies uncertainty only of order one in histogram. The limitation with this approach is that for spatially dependent data, the application of conventional bootstrap will amount to the loss of the correlation. Solow (1985) created spatial dependency for SBS by describing covariance matrix to the bootstrap. Deutsch (2004) created the GSLIB-like code premised on efficient matrix simulation procedure by relaxing the independence assumptions of bootstrap through resampling with correlation.

For SBS, the following steps are used.

- Gather the representative data.
- Compute the 3-D variogram of the data set.
- Lower and upper triangular matrices (LU) simulation.

- Calculate the necessary statistical parameters.
- Redo step 3 severally and
- Assemble the distribution of uncertainty in the statistic.

Despite that the SBS has the ability to handle the problem of data independency, there is an increase in uncertainty as the spatial correlation increases since it does not account for all possible data in the area of interest.

The CFD technique assesses the uncertainty in the histogram mean by accounting for the size of the domain and the local conditioning data. It is a stochastic approach based on a multivariate Gaussian distribution. Compared to SBS, CFD quantifies the uncertainty of any order in the histogram and has a decreasing uncertainty in sample mean as the range of correlation increases (Babak and Deutsch; 2008).

2.2.2 Uncertainty Management

Decision analysis on subsurface systems involves; consideration of all possible inherent uncertainties, the complexity of the system, multiple objectives and time factor involved in quantifying the uncertainties. The decisions made in the study of these subsurface systems usually depend on how best the uncertainties inherent in these systems are understood, presented, and managed.

2.2.2.1 Uncertainty Presentation

It is certain that due to lack of complete knowledge of relevant geophysical, geological and reservoir engineering parameters of subsurface systems, it is impossible to reduce the limiting uncertainties to zero. This necessitates the need to carefully investigate, capture and present the important parameters affecting the system in a good manner to avoid underestimation and overestimation in decisions which can mostly lead to bad outcomes. The use of probability distributions, quantiles, sensitivity analysis, spider diagrams and tornado chats are some of the popular methods of representing and understanding uncertainty. Probability distributions will be discussed in this section.

2.2.2.1.1 Probability Distributions

Since uncertainties in model parameters are majorly due to lack of knowledge, the uncertainties are usually incorporated in the input data (individual parameters) in the form of histogram (or maybe variogram) forming different realizations. Probability distributions (probability density function PDF) is constructed by drawing smooth curve fit through a vertically normalized histogram. It is differentiated from a histogram due to its involvement with continuous data rather discrete data. In the context of subsurface systems studies, the minimum, P90 (actual recovery ≥ estimate with probability of at least 90%), mode, median or P50 (actual recovery ≥ estimate with probability of at least 50%), mean, P10 (actual recovery ≥ estimate with probability of at least 10%), and maximum, are the common terms used in quantifying reserve uncertainty according to the *Guidelines for Application of the Petroleum Resources Management System* (2011), Fig. 2-1.

2.2.2.1.2 Screening Techniques

Simplified approaches are useful in identifying the non-influential inputs of a computer model before using the more advanced sensitivity analysis methods for systems with many input parameters. This simplified screening methods keep the number of model evaluations small (Scheidt et al., 2018). The use of a screening technique is computationally economical making sensitivity evaluation subjective to parameter ranking based on their importance. The one-at-a-time and the Morris methods are the popular screening techniques in subsurface systems modeling.

The one-at-a-time method proposed by Daniel, 1973 involves varying the input parameters one after another while keeping other input parameters fixed at a nominal value or a baseline. This simple process enables visualization of the effects of changing one parameter at a time and this is best expressed using Tornado charts. The Morris, 1991 method is best adapted for models with large number of input parameters and is based on repeated sampling of randomized one-at-a-time designs. It measures the global sensitivity using a set of local derivatives (elementary effects) taken at points sampled throughout the parameter space.

2.3 UNCERTAINTY ASSESSMENT WITH MULTIPLE MODELS AND REALIZATIONS

The understanding that uncertainty is not an inherent characteristic of reservoirs but rather due to lack of knowledge about the reservoir implies that it can be modeled while bearing in mind that it has no objective measure.

Generally, to appropriately manage uncertainty associated with different aspects of reservoir management, there is need for a method or tool capable of evaluating a complete range of uncertainties by identifying the relevant elements of uncertainty and filtering out the irrelevant ones, and implement the processes that can reduce the uncertainties to an acceptable level by refining both the interpretation and model, and gathering more data when the existing information cannot be refined further.

Construction of multiple 3D models (either by changing a parameter or performing stochastic simulation, etc.) serves as a way to assess the cumulative impact of data, interpretation, and modeling uncertainties on reservoir management decisions. For a 3D model, the uncertainty analysis follows the workflow proposed by Gringarten (2009):

- Evaluation and quantification of the uncertainties of all parameters involved in the model construction.
- Integration of the evaluated and quantified uncertainties – through the construction of a complete reservoir model.
- Analysis of the impact of constructing multiple models based on the criteria used to make a decision and
- Perform iterations targeted at reducing the uncertainties until risks are sufficiently minimized to allow decision making.

A way of looking at model uncertainty is seeing it as multiple realizations of a geostatistical-based process where stochastic simulations reproduce input parameters due to ergodicity (fluctuations around the input parameters), with a resultant variability in responses. It is believed that the only way to assess the cumulative impact of all uncertainties is to construct multiple realizations through a combination of scenario-based and stochastic simulations i.e., by repeating stochastic simulation process (e.g., Monte Carlo method, Gaussian simulation etc.) using different random paths or seeds (Amarante et al., 2019).

2.4 PROBABILITY APPROACHES FOR PRODUCTION HISTORY MATCHING

The major goal of history matching is to improve how reservoirs are represented so as to make reliable predictions of production rate and consequently optimize future field developments. The conventional "manual" trial and error approach or standard history matching techniques which uses limited number of models for prediction can only make global modifications and local adjustments which are not always geologically realistic and does not handle static uncertainties. The probabilistic approaches for production history matching incorporate uncertainty quantification as an ensemble to improve forecasting or prediction.

The assessment of uncertainty in estimated reservoir parameters requires sampling from the posterior distribution of the parameters, and this is implemented efficiently using the Bayesian methods (Lee, 1997).

2.4.1 Bayesian Approach

In simple terms, the Bayesian approach aims to determine the probability distribution of model parameters based on Bayes' theorem (Bayes et al., 1763) which describes the probability of an event based on prior knowledge of conditions that might be related to the event. This probabilistic approach is useful in calibrating model parameters considered as random variables characterized by a probability density function, whilst having 'subjective beliefs' during calibration defined by a joint posterior distribution of parameters.

Mathematically, the probability function of a particular parameter defined according to Bayes theorem is given as,

$$P(\alpha \mid \beta) = \frac{P(\beta \mid \alpha).P(\alpha)}{P(\beta)} \qquad (2\text{-}1)$$

Where;

α represents the model parameter; β is the observations or experimental data; $P(\alpha \mid \beta)$ is the posterior probability function (posterior beliefs having accounted for β) or the conditional probability of event α occurring given that β is true; $P(\alpha)$ is the prior probability distribution (modeler prior beliefs); $P(B \mid \alpha)$ is the likelihood function of the observations; and $P(\beta)$ is the probability of observations.

Important advantages of the Bayesian approach noted to be adaptable for production history matching include; (1) treating inverse problems as a well-posed problem (i.e. has a uniquely determined solution that depends continuously on its data) in an expanded stochastic space, (2) providing point estimates (maximum and medians) and posterior probability distribution function, and (3) providing more flexibility in the regularization or while adding information (stochastic regularization is the minimum mean square estimation of a random parameter that is normally distributed when the data are also normally distributed) (Emery, 2016).

Some probabilistic approaches referenced on Bayesian concept and some other useful probabilistic methods for production history matching are discussed in the following sections.

2.4.1.1 Markov Chain Monte Carlo

Markov Chain Monte Carlo (MCMC) method derives its meaning from the individual terms "Markov" which assume that predictions for the future state of a system (or model parameters) depend entirely on the current state of the system and "Chain" implying that there are many iterations of Monte Carlo random sampling. This therefore means that in MCMC, the distributions from which sampling is done depends on the current state of the system (related to bayesianism). During the process, each iterative step consists of a proposal and an acceptance step and as the iterative steps continue, the Markov chain converges to a desired fixed distribution. The basic method of the MCMC is simple and is derived from Metropolis algorithm.

1. Start with a guess of the parameters, θ_1. Calculate the probability for this guess, P_1.
2. Guess a second set of parameters, randomly drawn from a Normal multivariate solution centered on θ_1. The Normal distribution is known as the proposal density, or jumping distribution. The normal sampling distributions for each of the parameters are assumed to

be independent, with Gibbs sampling. Call the new set of sampled parameters θ_1 and calculate its probability as P_2.

3. Calculate the acceptance ratio $R = \frac{P_2}{P_1}$.
4. Pick a random number r between 0 and 1. If R>r, then new best guess is $\theta_1 = \theta_2$, go to step 3. If $R \leq r$, go to step 2. The idea of using the current guess to change the sampling region defines the MCMC.
5. The algorithm terminates after some fixed (large) number of iterations that attains the desired distribution. The posterior probability distributions of the parameters is the distributions of the accepted values of the parameters at the various iterations.

Note that the parameters of the normal sampling distribution in step 2 depend only on the current best guess, thus MCMC.

The described technique can generate realizations conditioned to hard data as well as honor the reference statistics. The major challenge in using MCMC is its requirement of large number of iterations to converge to a stationary distribution mainly due to low acceptance ratios for transitions to a new state when the number of parameters in a model is large.

2.4.1.2 Kalman Filtering and EnKF

The Kalman Filtering developed by Rudolf Kalman (1960) is essentially a set of mathematical equations that minimizes the estimated error covariance by applying a predictor – corrector type estimator when some presumed conditions are satisfied. It provides a recursive computational procedure for minimizing quadratic function of estimation error for a linear dynamic system with statistical noise and inaccuracies. There is a basic assumption in Kalman filtering that the system dynamics are linear and that measurements and errors follow a Gaussian distribution.

The following stochastic differential equation describes the Kalman filter as a method of estimating the current state of a process.

$$x_k = A_k x_{k-1} + B_k u_k + w_{k-1} \tag{2-2}$$

Where A_k represents the state transition model, B_k the control input model applied to the control vector u_k. w_{k-1} is the process noise with mean zero and covariance Q:

$$P(w) \sim N(0, Q) \tag{2-3}$$

Let z be the measurement defined as:

$$z_k = H_k x_k + v_k \tag{2-4}$$

Where H_k represents the observation model, and the v_k represent the measurement noise with mean zero and covariance of R:

$$P(v) \sim N(0, R) \tag{2-5}$$

The priori state estimate based on the knowledge of the system at step k is defined as $\overset{*}{x}_k$, and the posterior state estimate at step k, based on the measurement z_k , is defined as $\hat{x}_k$.

Let the prior estimate error be $e_k^* = x_k - \overset{\wedge *}{x}_k$ and the posterior error $e_k = x_k - \hat{x}_k$.

Error covariance matrices measure the correctness of the state estimates.

The priori estimate error covariance is defined as:

$$P_k^* = E[e_k^* e_k^{*T}] \tag{2-6}$$

The posteriori estimate error covariance is defined as:

$$P_k = E[e_k e_k^T] \tag{2-7}$$

Now, the posteriori state estimation $\hat{x}_k$ is defined as a linear combination of the priori estimate $\hat{x}_k^*$ and the weighted difference between an actual measurement and the predicted measurement:

$$\hat{x}_k = \hat{x}_k^* + K(z_k - H\hat{x}_k^*) \tag{2-8}$$

Where K represents the Kalman gain and it also minimizes the posteriori noise covariance:

$$K = \left(P_k^* H^T\right) / (HP_k^* H^T + R)^{-1} \tag{2-9}$$

The Kalman filter can operate in two different stages; prediction and updating. While the prediction phase utilizes the current state to estimate the state of the next step, the updating phase uses the priori estimates and the current observations to improve the state estimate.

The Kalman filter as is most history matching algorithms minimizes the mean square error. The expected value (or rather the mean) of the squared error in the posteriori estimate error is:

$$E\left[(x_k - \hat{x}_k)^2\right] \tag{2-10}$$

Note that to minimize the expected value of the squared error is the same as minimizing the trace of the posteriori estimate error covariance matrix P_k. It can be said that this trace is minimized when its derivative with respect to the gain is set to zero, thus leading to Kalman gain which minimizes the mean square error.

There has also been some useful extensions and generalizations to the Kalman filters method including extended Kalman filter (known to be the nonlinear version of the Kalman filter, which linearizes about an estimate of the current mean and covariance), the unscented Kalman filter (particularly useful when the predict and update functions are highly nonlinear, thus poor performance with the use of extended Kalman filters. This deterministic sampling is used to pick minimal set of sample points or sigma points around the mean to propagate through the nonlinear functions and the ensemble Kalman filter (a Monte Carlo based technique in which an ensemble of model states are used to approximate the covariance matrices used in the updating process).

The ensemble Kalman filter (EnKF) is a Monte Carlo implementation of the Bayesian update problem. EnKF represent the distribution of the system state using a collection of state vectors, called an ensemble, and replace the covariance matrix by the sample covariance computed from the ensemble. The ensemble is assumed a random sample, but the ensemble members are really not independent – the EnKF ties them together. An advantage of EnKF is that advancing the PDF in time is achieved by simply advancing each member of the ensemble.

The Kalman filters and its extensions are very useful algorithms for history matching but not without some challenges. The main challenge of the EnKF is the Gaussian assumption of the prior joint probability distribution and thus difficulty in convergence to the correct distribution if the prior joint probability distribution has non-Gaussian contribution. The non-linearity in the dynamic model, the non-Gaussianity of state variables distribution and the limitations of the ensemble size (highly dependent on the size and characteristic of the initial ensemble) result in non-physical updates during the analysis.

2.4.1.3 Gradual Deformation Method

This is a stochastic method introduced in Hu (2000) to constrain history matches to simple statistics and was further remodified to handle dependent realizations in Hu (2002). The method utilizes the fact that certain linear combinations of independent Gaussian fields maintain second order statistics. It is the continuous perturbation of an initial realization of a prior model in a way that the perturbed realization matches better the data **d** and the same time honors a prior model. While the perturbations in this method are gradual or continuous (as the name implies), the variable being perturbed can be discrete or categorical (Caers, 2007).

The implementation of this method requires that a standard Gaussian random variable V or standard Gaussian vector $\boldsymbol{V}$ can be represented as a linear combination of two independent standard Gaussian variables V_1 and V_2 or standard Gaussian vectors $\boldsymbol{V_1}$ and $\boldsymbol{V_2}$ sharing the same covariance matrix; equations below.

$$V = V_1 \cos r + V_2 \sin r$$

$$\boldsymbol{V} = \boldsymbol{V_1} \cos r + \boldsymbol{V_2} \sin r \qquad \text{(true for any value of } r\text{)} \tag{2-11}$$

Some important points to note;

- Components of $\boldsymbol{V_1}$ and $\boldsymbol{V_2}$ of vector $\boldsymbol{V}$ can be correlated or uncorrelated.
- When correlation of the components of $\boldsymbol{V_1}$ is expressed in a variance-covariance matrix C, and the components of $\boldsymbol{V_2}$ share the same covariance, then the components of $\boldsymbol{V}$ also have the same variance-covariance matrix C.
- r is the perturbation parameter of variable $\boldsymbol{V_1}$.
- If r=0, $\boldsymbol{V} = \boldsymbol{V_1}$.
- If r increases, any outcome of $\boldsymbol{V}$ becomes "gradually" different from the corresponding outcomes of $\boldsymbol{V_1}$ in the limit case.
- If $r = \pi/2$, $\boldsymbol{V} = \boldsymbol{V_2}$
- $\boldsymbol{V_1}$ and $\boldsymbol{V_2}$ must be independent random vectors.

Generally, the gradual deformation method is relatively a straightforward process with an easy implementation for an existing history matching framework. However, its application to only systems that can be represented by a Gaussian distribution makes it unsuitable for complex geologies or systems which cannot be derived from a Gaussian distribution.

2.4.1.4 *Probability Perturbation Method*

The probability perturbation method (PPM) introduced by Caers (2003) is a flexible data integration method applicable to solve non-linear inverse problems where there is complex geology. The process follows a different course from the normal Bayesian inverse models which usually rely on prior and likelihood distribution and sampling from posterior distribution. Rather, sampling in this method consists of perturbing the probability models used to generate the model realization, creating a chain of realizations which converge to match any type of data.

The concept of PPM is to incorporate production data mismatch as a piece of secondary information during history matching to generate new realizations. It uses the following parameterization to translate production data mismatch into a piece of secondary information:

$$P(A \mid C) = (1 - r_c)i + r_c P(A) \tag{2-12}$$

where $P(A)$ is the marginal distribution of the event A (the unconditional probability of A or the prior probability distribution or the modelers prior belief) representing the global proportion of A over the entire domain. C represents the production data. r_c is the perturbation parameter and i is the realization of binary indicator variables for any physical property or parameter at the grid blocks.

Referencing on the equation above, if $r_c = 0$, $P(A|C) = i$, resulting in a realization similar to i. However, when $r_c = 1$, $P(A|C) = P(A)$, resulting in a different binary indicator variable or realization equiprobable to i. A blend of i and another equiprobable realization will be obtained if r_c is between 0 and 1. Thus, by adjusting r_c, the indicator variable is perturbed.

$P(A|C)$ does not depend on the production data mismatch, C, rather it is considered to be dependent on the resulting realization of the binary indicator which simply implies that the production data depends on the choice of r_c.

A good history match using PPM is achieved when the mismatch between the forward model and actual data d_2 (otherwise called objective function) is optimal or minimal. This is possible with an optimal value of the perturbation parameter r_c.

$$O(r_c) = \| g(i^{(1)}(u_j, r_c)) - d_2 \| \tag{2-13}$$

where $O(r_c)$ is the objective function as a function of r_c; g is the forward model and $\{i^{(1)}(u_j,r_c), j=1,...,N\}$ is a generated perturbation.

Using the method to perturb the initial realization can only reduce the objective function but not achieve a global minimum. The probability perturbation algorithm below is employed in an iterative way to further reduce the objective function and achieve a global optimal match.

- choose random seed
- generate an initial realization
- Until an optimal value of r_c is found

  (i) Minimize to get $r^{opt}{}_c$

  $$O(r_c) = \| g(i^{(1)}(u_j, r_c)) - d_2 \|$$

  (ii) Change random seed

  (iii) Assign

  $$i^{(0)}(u_j) \leftarrow i^{(1)}(u_j, r_c^{opt}), \forall j$$

In the use of PPM algorithm for production history matching, the production data can be integrated through an optimization process (such as Dekker Brent 1-D derivative-free optimization method) while the PPM serve as the main engine for the production data integration (Johansen, 2008). The entire process consists of an inner loop where the optimization scheme such as Brent's algorithm (Brent, 1973) can be used to obtain a local optimal value or r_D for a given initial realization, and an outer loop where a different initial realization of model parameters is explored. The method does not require a particular type of distribution to represent the perturbed parameter, thus it is able to represent reservoir fracture parameters which is usually not smooth (non-Gaussian); a very flexible advantage it has over other methods such as gradual deformation and Kalman filtering whose parameters are represented by Gaussian distributions.

APPENDIX - *Figures*

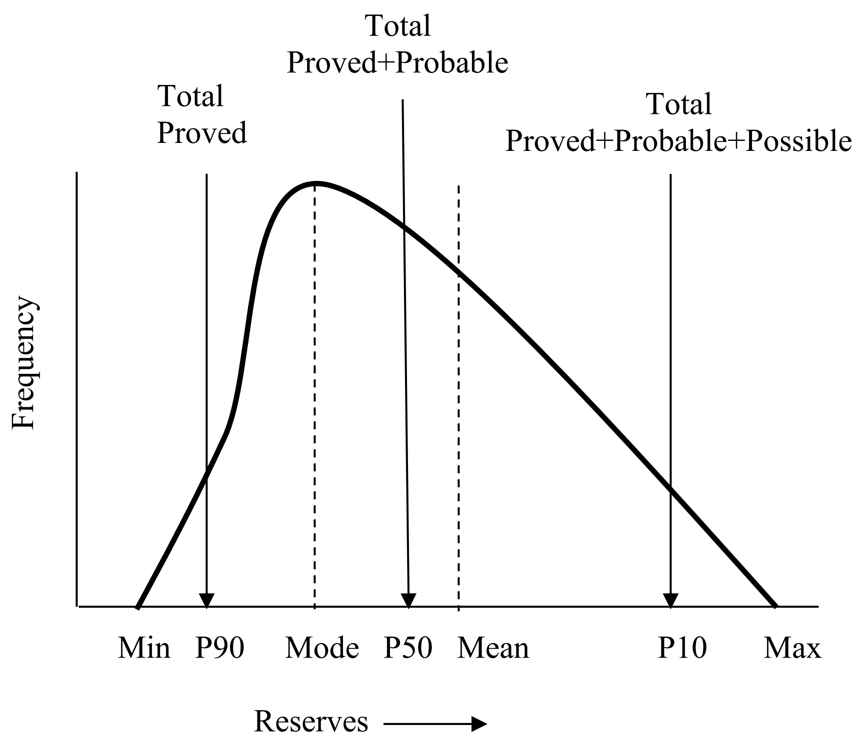

Fig. 2-1: Showing reserve distributions with some common terms relating to reserve uncertainty

Chapter 3: Inference of Hydraulically Fractured Reservoir Properties from Production Data Using the Indicator-Based Probability Perturbation Assisted History-Matching Method

3.1 OVERVIEW

Hydraulically fractured horizontal wells are widely adopted for the development of tight or shale gas reservoirs. The presence of highly heterogeneous, multi-scale, fracture systems often render any detailed characterization of the fracture properties challenging. Discrete fracture network (DFN) model offers a viable alternative for explicit representation of multiple fractures in the domain, where the comprising fracture properties are defined in accordance with specific probability distributions. However, even with the successful modelling of a DFN, the relationship between a set of fracture parameters and the corresponding production performance is highly nonlinear, implying that a robust history-matching workflow capable of updating the pertinent DFN model parameters is required for calibrating stochastic reservoir models to both geologic and dynamic production data.

This thesis proposes an integrated approach for the history matching of hydraulically fractured reservoirs. First, multiple realizations of the DFN model are constructed conditioning to available geological information such as seismic data and well logs, which are useful for inferring the prior probability distributions of relevant fracture parameters. Next, the models are upscaled into equivalent continuum dual-permeability model and subjected to numerical multiphase flow simulation. The predicted production performance is compared with the actual recorded responses. Finally, the DFN-model parameters are adjusted following an indicator-based probability perturbation method. Although the probability perturbation technique has been applied to update facies distributions in the past, its application in modeling DFN distributions is limited. To account for the non-Gaussian nature of the DFN parameters, an indicator formulation is proposed. The algorithm aims at minimizing the objective function, while reducing the uncertainties in the unknown fracture parameters.

The method is applied to estimate the posterior probability distributions of the transmissivity of the primary fracture (T_{pf}), transmissivity of the secondary induced fracture (T_{sf}) and global fracture intensity (P^{sf}_{32G}) in a multifractured shale gas well in the Horn River Basin. An initial realization of the DFN model are sampled from the prior probability distributions using the Monte Carlo simulation. These probability distributions are updated to match the production history, and multiple equi-probable realizations of the DFN models are sampled from the updated (posterior) distributions accordingly. The final sampled realizations of the DFN model are consistent with both static geological information and dynamic production history.

3.2 INTRODUCTION

The combination of horizontal drilling and hydraulic fracturing, or otherwise known as hydraulically fractured horizontal wells, has contributed the improved production from unconventional (tight and shale) reservoirs in recent years. The presence of highly heterogeneous, multi-scale fracture systems often renders any detailed characterization of the fracture properties challenging. Complexities such as the secondary fracture geometries and the striking difference between permeabilities of the matrix and fracture systems constitute distinct challenges to the flow simulation and intensify the nonlinearity between the fracture model parameters and flow responses (Wang and Leung, 2015). Thus, formulating an efficient workflow that integrates both static (e.g., logs) and dynamic data (e.g., rate and pressure measurements) to update hydraulic and secondary fracture parameters in a discrete fracture network model remains challenging.

First, numerical simulation of multiphase flow in fractured porous media is challenging. The choice of simulation approach should reflect the complexity of the fracture characteristics (e.g., geometry, intensity, and scales), while capturing the matrix and fracture flow interactions. The dual-porosity (DP) model considers the fracture system as the only flow path that is directly connected to the wellbore; although inter-porosity flow between the matrix and fracture systems is accounted for, inter-porosity flows within the matrix system and to the wellbore are ignored (Warren and Root, 1963; De Swaan, 1976; Bui et al., 2000). An improved form of the DP model is termed the dual-porosity dual-permeability (DPDK) model, as it considers all inter-porosity flows between the matrix system, fracture network, and the wellbore (Hu and Huang, 2002; Al-Shaalan et al., 2003; Van Heel et al., 2008). In the DPDK framework, the flow transfer terms are formulated as functions of the shape factor, pressure gradients, and several other physical parameters. A major pitfall is its difficulty in fully capturing the effects of capillarity and gravity into the formulation of shape factor. Equivalent models consisting of matrix and fracture domains have also been used to represent the fractured medium in the DP or DPDK modeling frameworks. Other more sophisticated techniques are available to incorporate features of a discrete fracture model, where the actual geometries and locations of individual fractures are explicitly specified in the computational domain. This generally requires discretizing the domain with unstructured meshes. Several finite element and finite volume methods, such as control-volume finite-element (CVFE), cell-centered finite-volume (CCFV or multi-point flux approximation MPFA) and mixed finite-element methods (MFE), have been developed (Monteagudo & Firoozabadi, 2004; Sandve et al., 2012; Zidane & Firoozabadi, 2014; Liu et al., 2020). Each of these techniques has its own merits and limitations; for example, the CVFE design is computationally efficient, but it does not maintain flux continuity for a heterogeneous porous medium; the MFE method, which is locally flux-continuous and conservative, can be computationally expensive, as both the velocity and pressure fields are evaluated concurrently. More recently, the Embedded Discrete Fracture Models (EDFM) has been widely adopted. Each matrix cell is divided into a set of sub-segments divided by various discrete fractures located within the cell. An updated connectivity/transmissibility list is used for computing the flow between matrix and fracture segments (Shakiba et al., 2018). The transmissibility calculations take into account the orientation and size of individual fractures. Given that pressure distribution along each fracture is not explicitly calculated, the overall computational cost is reduced.

The DP model is used in this work because of its ease of implementation. The presented workflow is not specific to a particular flow simulation strategy, so other aforementioned simulation techniques can also be adopted readily. The specification of a dual continuum reservoir simulation model requires assigning equivalent porous medium properties to each reservoir cell consisting of both matrix and fracture continua (Nejadi et al., 2017). These equivalent properties refer to the permeability tensor and shape parameters obtained by appropriate upscaling techniques (Bourbiaux et al., 1998, Bogdanov et al., 2007). The Oda upscaling technique is a commonly adopted analytical approach developed by Oda (1985). Other flow-based upscaling techniques (including both local and other advanced local-global schemes) have also been developed (Chen et al., 2003).

A second challenge is associated with the inference of distributions of fracture properties from dynamic (flow and pressure) data. History matching is in itself an inverse problem with non-unique solutions. This is a process by which all data (various sources and scales) are integrated. Typically, a set of initial models (or realizations) are constructed by incorporating various static or geological data. The models are then subjected to flow simulation and an optimization scheme to adjust the model parameters until the mismatch between the predicted response and the actual historical data is minimized. In the case of fractured reservoirs, the uncertain model parameters may include different fracture parameters (e.g., size, location, intensity, orientation). The goals of most probabilistic history-matching schemes are to (a) estimate the posterior distributions corresponding to the unknown model parameters and (b) to sample a set of updated models (or realizations) from those distributions; the variability exhibited by those realizations facilitates the uncertainty quantification and assessment. A particularly important aspect of fractured reservoir history matching is the capability to probability distributions of any forms without the assumption of Gaussianity.

Different approaches, such as stochastics search (e.g., genetic algorithm, simulated annealing), sampling-based (e.g., gradual deformation), and optimization-based methods (e.g., maximum a-posterior), are available to characterize fracture network models. While the equivalent model parameters are updated in some cases, the discrete fracture properties are updated in others. Cui and Kellar (2005) adopted a gradient-based technique, where the sensitivity coefficients of production data with respect to the fracture intensity were computed using a gradient simulator and the adjoint method; correlations between fracture intensity and fracture permeability, matrix permeability, and a certain coupling factor were used to update these pertinent flow parameters. Others have applied alternative global search techniques. Hu and Jenni (2005) designed a gradual deformation routine to tune an object-based Boolean model for predicting the location, shape, and size of various heterogeneous features from production data. An approach called the probability perturbation method (PPM), which is adopted in this work, was previously used by Hoffman

(2004) and Suzuki et al. (2007) for production history matching. Hoffman (2004) formulated a PPM workflow to estimate the uncertain locations and proportions of calcite bodies in a North Sea reservoir integrating both water rates and repeat formation tester (RFT) data. Suzuki et al. (2007) applied the PPM workflow for history matching of a synthetic naturally fractured reservoir. In their study, fracture density (e.g., fracture count per volume) was the unknown parameter; a multi-scale approach was adopted where both large-scale distribution and local-scale variations were estimated; however, hydraulically fractured tight/shale wells were not analyzed in that work; in particular, additional relevant fracture parameters (e.g., aperture, permeability) and their distributions were not considered. It has been widely established that PPM can handle non-Gaussian probability distributions, as no particular assumptions of the model parameter distributions are necessary; these previous works did not explicitly present examples where the model parameters are highly non-Gaussian.

De Lima et al. (2012) subsequently employed the gradual deformation technique to estimate realizations of fault distribution (i.e., intensity, length, and spatial locations). Chai et al. (2016) proposed a two-stage Markov Chain Monte Carlo method with embedded discrete fracture modeling for characterizing different porosity distributions corresponding to the organic matrix, inorganic matrix, secondary fractures, and hydraulic fractures of shale reservoirs. Other researchers have applied various stochastic search algorithms to estimate fracture distribution. Chen et al. (2019) designed a multi-scale (two-way) strategy for the history-matching of dual-porosity models: an evolutionary algorithm was used to calibrate coarse-scale static and dynamic parameters from average field pressure, well bottom-hole pressures, and repeat formation tester (RFT) data, while the streamline simulation was performed to fine-tune local fracture permeability to match the specific well bottom-hole pressures. Many ensemble-based techniques (e.g., Ensemble Kalman filter, or EnKF, and ensemble smoother) have also gained wide attention due to its merits in data assimilation and uncertainty quantification. The basic form of EnKF assumes multi-Gaussian distribution for all model and data variables and a linear relationship between them; unfortunately, none of these assumptions would hold for fractured reservoirs. A Bayesian updating scheme is involved to minimize the mismatch function. Modifications were proposed to partially address these limitations: iterative updating to alleviate issues related to nonlinearity and alternative parameterization schemes to transform the non-Gaussian distributions into Gaussian ones. Nejadi et al. (2015) employed EnKF to characterize hydraulic fracture parameters (e.g., half-length and transmissivity) and induced fracture parameters (e.g., length, transmissivity, intensity) using a DPDK simulation model. This approach was also employed in Nejadi et al. (2017) for inferring fracture orientation, conductivity, permeability tensors, and intensity for a naturally fractured reservoir. Although these extensions/hybrid formulations may retain the idea of utilizing an ensemble, they do not rely on linear update and are not appropriate for highly non-Gaussian variables; therefore, it is argued that they could offer only partial approximation of the true distribution.

The literature review highlights a number of unresolved issues pertinent to production history-matching of multi-scale fractured reservoirs. The gradient-based optimization techniques are robust, but the computation of gradients (sensitivity coefficients) can be computationally expensive. Stochastic search algorithms, such as simulated annealing and the genetic algorithm may also require many iterations to converge. A sampling-based technique, namely the probability perturbation method, is preferred, as it does not require gradient calculations and exhibits good convergence property; it facilitates the estimation of the posterior probability distribution, from which multiple realizations can be sampled. This approach has been used to calibrate permeability distribution in conventional reservoirs (Kashib et al. 2006) and naturally fractured reservoir permeability distribution, which was conditioned to a prescribed fracture density model (Suzuki et al. 2007). However, there was no previous application for unconventional reservoirs where both hydraulic and secondary fractures are present.

The objective of this research is, therefore, to formulate an indicator-based probability perturbation method for history-matching production data in a reservoir system consisting of both hydraulic and secondary (natural) fractures: the discrete fracture network (DFN) model parameters are updated, and the DFN model will be upscaled into a DPDK model for flow simulation. This framework is used to characterize both local and global fracture parameters. A significant advantage is that the uncertainties in fracture parameters are represented by multiple equi-probable DFN realizations and their corresponding upscaled flow-simulation models. Many previous studies focus on updating the upscaled models, without offering a direct means of transferring that upscaled model parameters back to a set of DFN model parameters. In addition, the proposed indicator-based formulation of the probability perturbation method is flexible in the handling of non-Gaussian fracture model parameters. The developed workflow is applied in a synthetic case study of a hydraulically fractured shale reservoir in the Horn River basin.

3.3 METHODOLOGY

3.3.1 Generation of an Initial Realization of the Discrete Fracture Network Model

The Fisher et al. (2005) conceptualization of a complex hydraulic fracture system was adopted to construct the DFN model using FRACMAN® (Golder Associates, 2018). Each hydraulic fracture stage is modeled using a primary fracture (an elongated penny-shaped crack) intersected by many randomly-distributed secondary fractures. These secondary fractures may represent any complex induced (or natural) fractures connected to the primary fracture – Fig. 3-1. Fracture properties, such as the location, size, orientation, intensity, aperture, and transmissivity, are defined for both the primary and secondary fractures. The Fisher distribution (Fisher, 1953) is used to define the orientation parameters of the induced fractures. In principle, different orientation parameters should be defined for each hydraulic fracturing stage, and these parameters can be inferred from geomechanical and microseismic data, if available.

The transmissibilities of the primary (T_{pf}) and induced fractures (T_{sf}), as well as the global induced fracture intensity ($P^{sf}{}_{32G}$), are the uncertain history-matching parameters. Updating of the uncertain parameters based on production histories is achieved during history matching. For a certain value of $P^{sf}{}_{32G}$, individual secondary fractures are populated following a prescribed nearest neighbor model, where the local fracture intensity ($P^{sf}{}_{32L}$) decreases exponentially with distance to the primary fracture:

$$\mathrm{P}_{32L}(x) = \mathrm{c}\mathrm{e}^{-b\partial_{x,f}}, \tag{3-1}$$

where c is an empirical constant; ∂ is the distance between location x and the primary fracture plane (according to Dershowitz, 1993). c can be estimated using image log data, possibly gathered from nearby fields, and b controls how quickly the secondary fracture intensity would decrease with distance away from the primary fracture; its value is calculated from the mean distance between the location x and the primary fracture and is defined as

$$\overline{\partial}_{x,f} = b^{-1}. \tag{3-2}$$

Static data such as cores, well logs, and microseismic interpretations can be used to infer prior distributions of various fracture parameters; for example, aperture, height in relation to the bed thickness, density or spacing, orientation, and dip are fracture parameters derivable from cores, while the approximate trend and plunge of both primary and secondary fractures can be inferred from microseismic responses. It should be emphasized that although static data is useful for interfering the prior distributions and offering an approximation of SRV, static data alone is typically insufficient to resolve all relevant parameters of a hydraulic fracture system, such as secondary fracture parameters (P^{sf}_{32G}, T_{sf}); hence, dynamic data is needed to reduce the uncertainty.

3.3.2 Discrete-Fracture-Network Model Upscaling

The DFN model is transformed into an equivalent DPDK simulation model (Fig. 3-2) based on a static upscaling scheme (Oda 1985). Given that the induced fractures are well connected and densely populated, the Oda upscaling scheme is assumed applicable (Dershowitz et al., 2000).

The upscaled DPDK model parameters include fracture porosity, Oda permeability tensor, and matrix-fracture coupling in the form of shape factor. In particular, the fracture porosity is defined as the total fracture volume (average cross-sectional area× aperture) divided by the cell volume. The Oda permeability tensor is computed by projecting the fracture isotropic permeability onto the fracture plane and then scaling it according to the fracture porosity. The orientation of a fracture inside a grid cell is described by a unit normal vector **n**. The mass moment of inertia of all fracture normals distributed over a unit sphere is obtained as:

$$N = \int_{\Omega} n_i n_j E(\boldsymbol{n}) d\Omega \tag{3-3}$$

where $\boldsymbol{\Omega}$ is the integration domain corresponding to the surface of a unit sphere, N is the number of fractures in $\boldsymbol{\Omega}$, n_i and n_j are the components of **n**, and $E(n)$ represents the probability density function describing the number of fractures whose unit normals are oriented within $d\boldsymbol{\Omega}$.

The resultant 3 × 3 fracture permeability tensor describing the directional permeability for the upscaled grid cell is given by the following matrix:

$$K_{ij} = \frac{1}{12}(F_{kk}\delta_{ij} - F_{ij}) \tag{3-4}$$

where K_{ij} is an element in the permeability tensor, F_{ij} is the corresponding element of the fracture tensor: it projects the permeability to the direction of **n** and expresses the flux along **n**, assuming the fractures are impermeable in a direction parallel to their unit normals. It is calculated by summing the contributions from N individual fractures within the upscaled grid block, weighted by their area and transmissivity as in Eq. (3-5); δ_{ij} is the Kroenecker's delta.

$$F_{ij} = \frac{1}{V}\sum_{r=1}^{N} A_r T_r n_{ir} n_{jr} \quad , \tag{3-5}$$

where V is the grid cell volume, N is the total number of fractures in the grid cell, n_{ir} and n_{jr} denote the i^{th} and j^{th} components of the unit normal vector corresponding to the fracture plane r, A_r is the area of fracture plane r and T_r is the transmissivity of fracture plane r.

Finally, the shape factor, or sigma factor (with a dimension of 1/length^2), provides a measure of the fracture-matrix interaction or interporosity flow between the matrix and fracture domains. It is represented mathematically according to Kazemi et al. (1976) as:

$$Sigma = 4\left(\frac{1}{L_i^{\,2}} + \frac{1}{L_j^{\,2}} + \frac{1}{L_k^{\,2}}\right) \quad , \tag{3-6}$$

where L_i, L_j, and L_k refer to the fracture spacing in the x, y and z directions.

In most practical applications, fractures could be non-orthogonal and irregularly oriented within a grid block). For such complex scenarios where multiple disconnected matrix blocks separated by thin fracture planes are present in a grid block, the regional dimensions (perpendicular to the fracture surface areas) become the fracture spacings. In most of these applications, the shape factor is used directly in the simulators in such a way that the contact area open to flow direction is preserved. Kazemi et al. (1992) introduced a formulation for the generalized shape factor as:

$$Sigma = \frac{1}{V_m} \sum_s \frac{A_m}{d_m} . \tag{3-7}$$

V_m represents the matrix volume within the grid block, A_m is the area open to flow between a segment of the fracture plane and its neighboring matrix block, d_m is the distance from that open flow surface to the center of the corresponding neighboring matrix block, and sigma is computed by summing over all such open surfaces within that particular grid block. This formulation was further generalized by Heinemann et al. (2011) for two specific scenarios. For matrix with isotropic permeability, the distance should be calculated by selecting a point j on the fracture plane segment, such that a line connecting i to the center of the neighboring matrix block is orthogonal to the surface A_j:

$$Sigma = \frac{1}{V_m} \sum_{j=1}^{N} \frac{A_j}{d_j} . \tag{3-8}$$

N refers to the total number fracture plane segments. For an anisotropic matrix, the distance must be k-orthogonal to the surface:

$$Sigma = \frac{1}{V_m} \sum_{j=1}^{N} A_j \frac{\left| \overline{\overline{k}} \,.\, \mathbf{n}_j \right|}{\left| d_j \right|} . \tag{3-9}$$

$\overline{\overline{k}}$ is the permeability tensor.

3.3.3 *Numerical Flow Simulation*

Material balance, momentum balance, phase behavior descriptions, and numerous auxiliary equations are implemented in numerical simulation to model multiphase fluid flow. A commercial black-oil simulator (Schlumberger, 2017) is employed. This system of nonlinear differential equations for the DP formulation is solved numerically based on finite-difference and finite-volume methods:

$$d = G(\mathbf{m}, \mathbf{u}) . \tag{3-10}$$

u and **m** represent the estimated state variables (pressure and saturation) and the model parameters, respectively; d is simulated data after model simulation G, which depends on the principles of material balance, momentum balance, phase behavior descriptions, and numerous auxiliary equations.

3.3.4 Probability Perturbation Method

The probability perturbation method (PPM) can be used to effectively integrate production dynamics during the history-matching process (Caers, 2003; Kashib and Srinivasan, 2006). In PPM, instead of tuning the specific unknown model parameters, such as a particular geostatistical realization of fracture intensity, the probability distributions corresponding to these model parameters are perturbed; in other words, instead of attempting to construct one history-matched realization of the DFN model, the goal is to infer the posterior probability distributions of numerous DFN parameters such that multiple realizations of the DFN model can be sampled. The variability exhibited by these realizations is expected to capture the uncertainty in the model parameters and reflect the non-unique nature of an inverse problem.

The technique does not depend on the conventional Bayesian decomposition of posterior into the likelihood of observing the data and a prior belief, but rather utilizes pre-posterior distributions (probability of the model parameters given some subset of the data). It enables a fast non-iterative updating scheme to generate new realizations of the uncertain model parameters, and this aspect differs from other methods, such as MCMC, which requires a large number of iterations to converge to a stationary distribution due to low acceptance ratios for transitions to a new state, especially when the number of unknown model parameters is large. The convergence behavior of other ensemble-based methods, such as EnKF, may also be compromised if the prior and posterior are non-Gaussian. In Emerick and Reynolds (2012), a hybrid method where MCMC is combined with EnKF to improve sampling efficiency, a very long chain was used as the reference solution to scrutinize the sampling performance of several ensemble-based methods with 100 realizations; the comparison showed that either MCMC or EnKF alone may not be efficient.

Another drawback with EnKF is that, in its simplest form, EnKF assumes multi-Gaussian distribution on model and data variables and a linear relationship between all variables (Aanonsen et al. 2009; Emerick and Reynolds, 2012). Both these assumptions do not hold for fractured reservoirs. Modifications were proposed to address these limitations partially: iterative updating to alleviate issues related to nonlinearity (Li and Reynolds 2009; Chen and Oliver, 2012) and alternative parameterization schemes to transform the non-Gaussian distributions into Gaussian ones (Linde et al., 2015). One of our previous works also employed a re-sampling scheme and a parameterization formulation to account for non-Gaussian model parameters and nonlinear multi-phase flow processes in an EnkF framework (Nejadi et al., 2015). However, the choice of an appropriate parameterization scheme for 3D fracture parameters is not established. In the end, there is still debate that though these extensions/hybrid formulations may retain the idea of utilizing an ensemble, they do not rely on linear update or transformation of space; they could offer only partial approximation of the true distribution.

Similar to previous PPM implementations, as cited previously, an indicator formulation is adopted here to account for the non-Gaussian nature of DFN parameters. The probability distributions of the uncertain parameters (i.e., P^{sf}_{32G}, T_{pf} and T_{sf}) are perturbed according to the indicator-based formulation proposed in Kashib and Srinivasan (2006):

$$P\{I^{l+1}(u)=k \mid I^{l}(u)=k,\ C\}=r_D.P\{I(u)=k^{'}\}\forall k^{'}\neq k$$
$$P\{I^{l+1}(u)=k \mid I^{l}(u)=k,\ C\}=1-\sum_{k^{i}\neq k} r_D\ .P\{I(u)=k^{'}\}. \tag{3-11}$$

The formulation describes the probability of transitioning from the indicator category k at step l to the category k' at step l+1 using the deformation factor $r_D \in [0,1]$. The probability $P\{I(u) = k'\}$ is the prior probability (inferred from static/geologic data) while $P\{I^{l+1}(u) = k|I^{l}(u) = k, C\}$ is the posterior probability. As r_D tends towards 1, more perturbation of the probabilities is resulted. If $r_D = 0$, there is no perturbation, and the probability of staying at category k at step l+1 is 1.0; if $r_D = 1$, the probability of staying at category k at step l+1 is 0. Thus, the indicator-based formulation, together with the r_D adjustment facilitates the perturbation of both Gaussian and non-Gaussian distributions. u represents the unknown T_{sf}, T_{pf} and P_{32G} as points in the domain.

At the end of each perturbation step, a set of updated DFN parameters are sampled and used to generate a new DFN model. The model is subsequently upscaled into a DPDK model for flow simulation. The advantage of this approach, instead of perturbing the DPDK model parameters directly, is that it facilitates the sampling of DFN realizations and the corresponding upscaled DPDK models to be conducted in a consistent fashion. Suppose one were to perturb the DPDK mode parameters directly. In that case, there is no unique way to reconstruct the posterior probability distributions or even to sample realizations, of the corresponding DFN parameters based on those updated DPDK parameters alone. This parameterization scheme helps to preserve the non-linear relationship between a given set of DFN parameters and the associated reservoir flow response. As the perturbation is performed in the DFN space, no down-scaling is actually required; after each perturbation step, there is a DFN model associated with the upscaled DPDK model.

The PPM workflow is described in Fig. 3-3. To attain the global optimal, the workflow is divided into an inner loop, where the Brent 1D optimization scheme (Brent, 1973) is used to obtain a local optimal value of r_D for a given initial realization, and an outer loop, where a different initial realization of the model parameters is explored. Denotations are marked in the figure to describe the sections of the workflow indicating the two loops.

$$\Delta O = \int \left(\frac{Q_{g_s}(t) - Q_{g_h}(r_D^*, t)}{Q_{g_{h\max}}(r_D^*, t)} \right)^2 dt + \int \left(\frac{Q_{w_s}(t) - Q_{w_h}(r_D^*, t)}{Q_{w_{h\max}}(r_D^*, t)} \right)^2 dt + \int \left(\frac{b_s(t) - b_h(r_D^*, t)}{b_{\max}(r_D^*, t)} \right)^2 dt. \tag{3-12}$$

Eq. (3-12) is the normalized objective function, where Q_g, Q_w and b representing the gas production, water production and Bottom-hole pressure, respectively; the subscripts s, h and max

denote the simulation prediction, historical data, and the upper limit (maximum value) for that particular variable, respectively.

During the probability perturbation, Brent's algorithm is applied to search for the optimal r_D corresponding to the local minima of the objective function based on a certain initial realization of the model parameters. This algorithm is effective in locating the minimum of a single-variable function by utilizing the concepts of golden section search and parabolic interpolation, which are summarized in Eq. (3-13).

$$\frac{x^{(2)} - x^{low}}{x^{high} - x^{low}} = \frac{x^{high} - x^{(1)}}{x^{high} - x^{low}} = \varphi = 0.618. \tag{3-13}$$

where x^{low} and x^{high} are the lower and upper bounds for the search interval corresponding to an unimodal function; $x^{(1)}$ and $x^{(2)}$ are points on the function such that the distances from x^{low} to $x^{(2)}$ and $x^{(1)}$ to x^{high} are exactly the same. Either $x^{(1)}$ and $x^{(2)}$ is selected as the minima for the next search interval. The process is repeated until the minimum is below a certain predefined tolerance. φ is the ratio of equal distances to the overall interval distance ($x^{high} - x^{low}$), which is a factor akin to what is applied in the golden section search algorithm. The algorithm is computationally efficient as objective function evaluation is only required at the equal-distance points (i.e., $x^{(1)}$, $x^{(2)}$ etc.) and the convergence speed is fast. The method is used to estimate the optimal value of r_D corresponding to a given initial realization of the unknown parameters. The inner loop is then repeated using a different initial realization, as denoted by the outer loop. With the implementation of the entire workflow for the PPM, the following uncertain parameters are updated:

- Global fracture intensity of the secondary (induced) fractures (P^{sf}_{32G}).
- Transmissivity of the secondary fracture (T_{sf}).
- Transmissivity of the primary fracture (T_{pf})

New model realizations are generated for each update of these parameters until an optimal objective function is achieved based on a predefined tolerance.

Following the approach described by Caers (2007) and Kashib and Srinivasan (2006), the PPM algorithm, as implemented in this work, is summarized below;

- Generate an initial realization $I^l(u)$ with seed s
- Until a history match of data is achieved
    - Change the random seed
    - Until the search for r_D yields r_D^{opt}
        - (i) Guess a value for r_D
        - (ii) Calculate $P\{I^{l+1}(u) = k|I^l(u) = k, C\}$
        - (iii) Generate a new realization $I^{l+1}(u, r_D)$
        - (iv) Evaluate objective function as a function of $I^{l+1}(u, r_D)$
    - Set $I^{l+1}(u,r_D^{opt}) \rightarrow I^l(u)$

Although the PPM formulation has been applied in other studies in the literature, this thesis is the first to illustrate how this method can be formulated to infer/characterize parameters associated with hydraulic and secondary fractures from dynamic data. In particular, previous studies, those that are cited in the introduction and earlier in this section, focused on characterizing the distribution of a single unknown parameter (e.g., absolute permeability, facie, or fracture intensity). This thesis, however, attempts to history match multiple unknown parameters simultaneously, corresponding to different scales and prior distributions. Another contribution is that, despite it having been widely established that PPM can handle non-Gaussian probability distributions, previous works did not often explicitly present examples where the model parameters are highly non-Gaussian. Two different case studies are presented to show how the results would differ if the "true" distributions of the unknown model parameters are indeed non-Gaussian.

3.4 REFERENCE CASE STUDY

To demonstrate the functionality of the proposed PPM implementation, an example corresponding to a horizontal shale gas well consisting of four stages of hydraulic fracturing is presented.

3.4.1 Model Description

The model dimension is 800 ft. × 800 ft. × 250 ft. (with 50 × 50 × 10 grid cells along the x-, y-, and z- directions, respectively). The reference model representing a multifractured shale gas well in the Horn River Basin is created. Each hydraulic fracturing stage is modeled as a primary (main) fracture plane intersected by a set of secondary (smaller) fractures. The trend and plunge of each primary fracture were inferred from interpreted microseismic events (Nejadi et al., 2015). The trend is defined as the horizontal angle in the x-y plane measured away from the north (i.e., positive y-axis), while the plunge is defined as the vertical angle between the fracture plane and the horizontal (x-y) plane. The microseismic observations show that the orientation of fracture growth (as defined by Fisher (1953) distribution) is along the NE direction (i.e., with an average pole trend of 140˚). These values are used to populate the primary and secondary fracture planes in the reference model.

The properties of the fracture and matrix systems in the DPDK model are determined via analytical upscaling of the DFN model (Oda, 1985). It is then subjected to numerical flow simulation to compute the production profiles for a period of 12 months. The 12-month production profiles of water production rate, gas production rate, and bottom-hole pressure (P_{wf}) are considered as the *historical* data in this case study. The uncertain DFN model parameters to be history-matched are P^{sf}_{32G}, T_{sf}, and T_{pf}. It should be emphasized that in the reference case, these three parameters are constants for the entire domain. Given that the history-matching problem is ill-posed with non-unique solutions, the objective for applying the PPM workflow is to infer the univariate distributions of P^{sf}_{32G}, T_{sf}, and T_{pf}, from which multiple sets of solutions, while honoring the production histories, can be sampled. It should also be noted that in this case study, the forward model incorporates only the flow simulation, and geomechanics calculations are not coupled. In addition, history matching of other reservoir parameters such as relative permeability or compaction tables has not been considered. These additional aspects can be integrated into future work. However, it should be mentioned that the proposed workflow is very flexible and can be readily extended to incorporate additional uncertain model parameters.

A preliminary history-match is conducted to determine, approximately, the potential mismatch in the objective function (although it could be quite high) and assess the upper and lower bounds of individual model parameters. This step is essential to examining the sensitivity of the production responses with respect to variations in the uncertain parameters. Table 3-1 summarizes the other (i.e., known) DFN model and the corresponding upscaled dual-permeability model parameters. The orientation parameters for the secondary fractures are assumed similar to those of the primary fractures. As explained previously in the methodology, the nearest-neighbor model and Fisher distribution (Fisher, 1953) are used to populate the secondary fractures in accordance to the location of the primary fractures. Values of storativity for the primary and secondary fractures are similar to those reported in Cinco-ley (1996).

Table 3-1: Data for the discrete fracture network model and the dynamic dual permeability (DPDK) simulation model.

Discrete Fracture Network Parameters:	
Primary Fractures	
Aperture	1.0×10^{-3} feet
Storativity	1.0×10^{-2}
Trend (Stage 1)	247˚
Trend (Stage 2)	244˚
Trend (Stage 3)	177˚
Trend (Stage 4)	226˚
Plunge (Stage 1)	55˚
Plunge (Stage 2)	29˚
Plunge (Stage 3)	69˚
Plunge (Stage 4)	19˚
Compressibility	0.231 $psia^{-1}$
Secondary Fractures	
Storativity	1.83×10^{-2}
Aperture	1.97 10^{-5} feet
Trend	Similar to primary fractures
Plunge	
Compressibility	
Dual Permeability Model Parameters:	
Number of grids	50 × 50 × 10
Model dimensions	800 × 800 × 250 $feet^3$
Matrix Permeability	0.0005 to 0.0007 mD
Matrix Porosity	6%
Reservoir depth	6400 feet
Initial reservoir pressure	5000 psi

3.4.2 Workflow Validation

In this section, the workflow described in Fig. 3-3 is applied to history match the historical production data corresponding to the reference case. An initial realization of the DFN model is constructed and upscaled; it is carried out within the FracMan® software facilitated by the use of macros. The macro is an editable script consisting of a set of function calls for creating and upscaling the DFN models. The macro can be executed repeatedly within a loop, enabling the generation of multiple DFN realizations at each iteration or updating step. The rest of the PPM workflow is implemented in Matlab™ R2018a (MathWorks, 2018).

3.4.2.1 Case #1 – Gaussian Fracture Parameters

It is assumed that the three unknown parameters (P^{sf}_{32G}, T_{pf}, and T_{sf}) would follow the Gaussian distribution. Thirty indicator levels are used to parameterize each of the three unknown model variables. The midpoint corresponding to each level is used during the back-transform. Fig. 3-4(a) shows the initial distributions of the three uncertain model parameters.

3.4.2.2 Case #2 – Non-Gaussian Fracture Parameters

This case illustrates the application of the probabilistic history-matching framework, if the distributions of the various uncertain fracture parameters are non-Gaussian. It is assumed that the distributions for three unknown parameters (P^{sf}_{32G}, T_{pf} and T_{sf}) are unknown and could possibly be non-Gaussian. Once again, thirty indicator levels are used to parameterize each of the three unknown model variables. However, in this case, the initial distributions for some of three unknown parameters are assumed non-Gaussian: P^{sf}_{32G} is log-normally distributed, while T_{sf} and T_{pf} are bi-modally and normally distributed, respectively. Fig. 3-4(b) shows the initial distributions of the uncertain model parameters.

3.4.2.3 *Case #3 – Gaussian and Non-Gaussian Fracture Parameters for a Complex DFN*

A more complex DFN case, as shown in Fig. 3-1(b), is analyzed next. This example consists of the same multi-stage hydraulic fracture system, where a more complex set of secondary fractures are present in each stage of the primary fracture. This, the global fracture intensity of the secondary fracture (P^{sf}_{32G}) is higher compared to that in *Case #1* and *Case #2*. The same three unknown parameters (P^{sf}_{32G}, T_{pf} and T_{sf}) are considered. Thirty indicator levels are used to parameterize each of the unknown variables; two particular sub-cases are examined: **(a)** Gaussian distributions are assumed for all three parameters; **(b)** non-Gaussian distributions are assumed for some variables, where P^{sf}_{32G} is log-normally distributed, while T_{sf} and T_{pf} are bi-modally and normally distributed, respectively. Figs. 3-5(a) & 3-5(b) shows the initial distributions of the uncertain model parameters.

3.5 RESULTS AND DISCUSSION

The quality of the history match of the reference models' historical data is measured based on the mismatch in the objective function; the iterations are terminated if the objective function in Eq. (3-7) is less than 5 %. It is observed that the mismatch would be around or reduced below this tolerance after approximately 39 iterations, which is equivalent to roughly three outer loops, with each comprising 13 inner loop iterations.

Selected successive changes in the prior and posterior distributions from iteration l to iteration $l+i$ are shown in Figs. 3-6(a), 3-6(b) and 3-7(a) & 3-7(b) for cases #1, #2 and #3; this figure depicts the probabilities for either staying at the current category k at step l+1 or transitioning to category k' at step $l+1$. In the figure, each row represents a particular outer loop (1, 2, and 3), while individual figures along the row depict selected inner loop iterations from counter $i = l$ to i = l+1.

The profiles of gas production rate, water production rate, and P_{wf} corresponding to the posterior distributions are compared with the historical data, and three additional realizations are subsequently sampled; the corresponding profiles of the gas production rate, water production rate, and P_{wf} of all three history-matched realizations are shown in Figs. 3-8(a), 3-8(b) and 3-9(a) & 3-9(b).

Tables (3-2, 3-3, 3-4 and 3-5) summarize the mean of the distributions of the model parameters for the initial and updated realizations. Notwithstanding the different set-up between Case #1 and Case #2 (i.e., Gaussian vs. non-Gaussian distributions of unknown model parameters), a reduction in the model parameter uncertainty is observed after the history matching process, reflecting the conditioning effect in the model uncertainty due to the integration of additional dynamic data. The history-matched results obtained in both demonstrations of Case #3, as shown in Tables 3-4 and 3-5, reflect an increase in $P^{sf}{}_{32G}$, resembling that of the reference model. The results presented in Figs. 3-6 – 3-7 further suggest the final updated distributions for $P^{sf}{}_{32G}$ *and* T_{sf} remain non-Gaussian.

A single deterministic "true" (reference) reservoir is used, and a certain set of prior distributions are assumed for all unknown variables. In all practical applications, some additional static (geological studies or microseismic data) must be used to infer these prior distributions (as mentioned in section 3.4.1). This particular aspect (inference of a prior) is universal to all history-matching and dynamic data integration methods. However, as shown in the case studies, despite the initial models being quite different from the reference model (Tables 3-2 – 3-5), the final updated models are remarkably close to the reference model. This behavior implies that despite a set of incorrect initial models being used, the history matching workflow is capable of progressively perturbing the posteriors to match the actual production data.

Table 3-2: Summary of the uncertain DFN model parameter distribution for the reference, initial and updated realizations (Case #1).

Uncertain Parameter	Reference Model	Initial Model (Mean values)	Updated Model (Mean values)
Global Fracture Intensity (P^{sf}_{32G}), /ft.	0.092	0.152	0.059
Transmissivity T_{sf}, ft^2/sec	31.160	84.970	28.875
Transmissivity T_{pf}, ft^2/sec	449.56	680.100	571.450

Table 3-3: Summary of the uncertain DFN model parameter distribution for the reference, initial and updated realizations (Case #2).

Uncertain Parameter	Reference Model	Initial Model (Mean values)	Updated Model (Mean values)
Global Fracture Intensity (P^{sf}_{32G}), /ft.	0.092	0.120	0.079
Transmissivity T_{sf}, ft^2/sec	31.160	112.625	32.110
Transmissivity T_{pf}, ft^2/sec	449.56	888.900	412.500

Table 3-4: Summary of the uncertain DFN model parameter distribution for the reference, initial and updated realizations (Case #3a).

Uncertain Parameter	Reference Model	Initial Model (Mean values)	Updated Model (Mean values)
Global Fracture Intensity (P^{sf}_{32G}), /ft.	0.092	0.104	0.2418
Transmissivity T_{sf}, ft^2/sec	31.160	103.670	99.910
Transmissivity T_{pf}, ft^2/sec	449.560	848.300	524.250

Table 3-5: Summary of the uncertain DFN model parameter distribution for the reference, initial and updated realizations (Case #3b).

Uncertain Parameter	Reference Model	Initial Model (Mean values)	Updated Model (Mean values)
Global Fracture Intensity (P^{sf}_{32G}), /ft.	0.092	0.050	0.1713
Transmissivity T_{sf}, ft^2/sec	31.160	80.125	55.845
Transmissivity T_{pf}, ft^2/sec	449.560	571.450	441.500

The procedure adopted in this work demonstrates the possibility of estimating DFN model parameters using dynamic flow data by incorporating complex fluid flow physics and direct perturbation of the probabilities of DFN model parameters, from which DFN models can be sampled and upscaled into the equivalent DPDK models. Thus, this approach is more suitable for handling the non-linear relationship between the DFN parameters and flow response. It offers a means of estimating parameters related to secondary (e.g., induced) fractures (P^{sf}_{32G} and T_{sf}) based on production data, which may not be readily inferred from well logs and microseismic interpretations.

3.6 CONCLUSION

- A probabilistic workflow for perturbing the probability distributions of uncertain fracture parameters has been developed to characterize hydraulically fractured reservoirs from static and dynamic (production) observations.
- An indicator formulation is adopted to facilitate the modeling of uncertain distributions of three particular global fracture parameters (primary fracture conductivity, secondary fracture conductivity, and global fracture intensity).
- The method is flexible in handling both Gaussian and non-Gaussian uncertain fracture parameters and can be implemented to characterize other uncertain fracture parameters, such as fracture aperture, length, and height.
- The method is more suitable for handling the non-linear relationship between discrete fracture network parameters and reservoir flow response. This was achieved by the perturbation of

DFN parameters in the DFN space instead of the upscaled reservoir parameters, thus reducing possible errors associated with upscaled reservoir parameters.

- An important benefit of this method is that the uncertainties in fracture parameters are quantified using multiple equi-probable DFN models and their corresponding upscaled flow-simulation models.
- It is recommended that this technique be applied to analyzing other complex field cases involving multiple well pads (with more than one well) and extended to characterize naturally fractured reservoirs.

3.7 REFERENCES

Aanonsen, S. I., Oliver, D. S., Reynolds, A. C., Vallès, B. 2009. The Ensemble Kalman Filter in Reservoir Engineering – A Review. SPE-117274-PA. SPE J. 14(03): 393–412. SPEJ Sept. 2009. https://doi.org/10.2118/117274-PA

Ahmed, R., Edwards, M.G., Lamine, S., Huisman, B.A.H., Pal, M. 2015. Three-Dimensional Control-Volume Distributed Multi-Point Flux Approximation coupled with a Lower-Dimensional Surface Fracture Model. Journal of Computational Physics, 303 (2015), 470 – 497. https://doi.org/10.1016/j.jcp.2015.10.001

Al-Shaalan, T.M., Fung, L.S.K., Dogru, A.H. 2003. A Scalable Massively Parallel Dual-Porosity Dual-Permeability Simulator for Fractured Reservoirs with Super-k Permeability. SPE 84371-MS, SPE Annual Technical Conference and Exhibition, 5–8 Oct 2003, Denver, Colorado. https://doi:10.2118/84371-MS

Bogdanov, I.I., Mourzenko, V.V., Thovert, J.F., Adler, P.M. 2007. Effective Permeability of Fractured Porous Media with Power-Law Distribution of Fracture Sizes. Phys. Rev. E, 76 (036309), 1–15.

Bourbiaux, B., Cacas, M.C., Sarda, S., Sabathier, J.C. 1998. A Rapid and Efficient Methodology to Convert Fractured Reservoir Images into a Dual-Porosity Model. Oil & Gas Science and Technology. 53 (6), 785–799. https://doi.org/10.2516/ogst:1998069

Brent, R.P. 1973. Algorithms for Minimization without Derivatives. Prentice- Hall, Englewood Cliffs, New Jersey. ISBN: 0-13-022335-2.

Bui, T.D., Mamora, D.D., Lee, W.J. 2000. Transient Pressure Analysis for Partially Penetrating Wells in Naturally Fractured Reservoirs. SPE 60289-MS, SPE Rocky Mountain Regional/Low Permeability Reservoirs Symposium and Exhibition, Denver, Colorado, 12–15 Mar 2000. https://doi:10.2118/60289-MS

Caers, J. 2003. History Matching Under Training-Image-Based Geological Model Constraints. SPE-74716-PA. SPE Journal 8(03). https://doi.org/10.2118/74716-PA

Caers, J. 2007. Comparing the Gradual Deformation with the Probability Perturbation Method for Solving Inverse Problems. Mathematical Geology 39(1), 27-52. https://doi.org/10.1007/s11004-006-9064-6

Chai, Z., Yan, B., Killough, J.E., Wang, Y. 2016. An Efficient Method for Fractured Shale Reservoir History Matching: The Embedded Discrete Fracture Multi-Continuum Approach. SPE-181765-MS. SPE Annual Technical Conference and Exhibition, 26 -28 September, Dubai, UAE. https://doi.org/10.2118/181765-MS

Chen, H., Yang, C., Datta-Gupta, A., Zhang, J., Chen, L., Liu, L., Chen, B., Cui, X., Shi, F., Bahar, A. 2019. A Hierarchical Multiscale Framework for History Matching and Optimal Well Placement for a HPHT Fractured Gas Reservoir, Tarim Basin, China. IPTC-19314-MS. International Petroleum Technology Conference, 26 – 28 March, Beijing China. https://doi.org/10.2523/IPTC-19314-MS

Chen, Y., Durlofsky, L.J., Gerristen, M., Wen, X.H. 2003. A Coupled Local-Global Upscaling Approach for Simulating Flow in Highly Heterogeneous Formations. Advances in Water Resources 26 (10), 1041–1060. https://doi.org/10.1016/S0309-1708(03)00101-5

Chen, Y and Oliver, D.S. 2012. Ensemble Randomized Maximum Likelihood Method as an Iterative Ensemble Smoother, Math. Geosci., 44(1), 1–26. https://doi-org/10.1007/s11004-011-9376-z

Chow, C.C. 2015. Sampling from a Probability Distribution. Scientific Clearing House.https://sciencehouse.wordpress.com/2015/06/20/sampling-from-a-probability-distribution/

Cinco-ley, H. 1996. Well-Test Analysis for Naturally Fractured Reservoirs. SPE-31162-JPT. Journal of Petroleum Technology 48(01), 51 – 54. https://doi.org/10.2118/31162-JPT

Cui, H., Kelkar, M. 2005. Automatic History Matching of Naturally Fractured Reservoirs and a Case Study. SPE-94037-MS. Western Regional Meeting, Irvine, California, 30 March-1 April. https://doi.org/10.2118/94037-MS

De Lima, A., Lange, A., Schiozer, D.J., 2012. Assisted History-Matching for the Characterization and Recovery Optimization of Fractured Reservoirs using Connectivity Analysis. SPE 154392. SPE Europec/EAGE Annual Conference. https://doi.org/10.2118/154392-MS

Dershowitz, W.S. 1993. Geometric Conceptual Models for Fractured Rock Masses: Implications for Groundwater Flow and Rock Deformation. ISRM-EUROCK-1993-010, Second European Conference of the International Society for Rock Mechanics, Lisbon, Portugal, 21–24 June. https://www.onepetro.org/conference-paper/ISRM-EUROCK-1993-010

Dershowitz, B., LaPointe, P., Eiben, T., Wei, L. 2000. Integration of Discrete Feature Network Methods with Conventional Simulator Approaches. SPE Res Eval & Eng 3 (2): 165-170. SPE-62498-PA. http://dx.doi.org/10.21186/62498-PA

De Swaan, O.A. 1976. Analytical solutions for determining naturally fractured reservoir properties by well testing. SPE 5346-PA. SPE J. 16(3), 117–122. https://doi:10.2118/5346-PA

Emerick, A.A., Reynolds, A.C. 2012. Combining the Ensemble Kalman Filter with Markov-Chain Monte Carlo for Improved History Matching and Uncertainty Characterization. SPE-141336-PA. SPE Journal 17 (2): 418–440. https://doi-org/10.2118/141336-PA

Endo, H. K., and Long, J. S. 1984. A Model for Investigating Mechanical Transport in Fracture Networks. Water Resources Research, 20(10), 1390-1400. https://doi:10.1029/WR020i010p01390

Fisher, R.A. 1953. Dispersion on a Sphere. The Royal Society of London. Series A, Mathematical and Physical Sciences. Volume A217 (1130), 295-305. https://doi.org/10.1098/rspa.1953.0064

Fisher, M.K., Wright, C.A., Davidson, B.M., Goodwin, A.K., Fielder, E.O., Buckler, W.S., Steinsberger, N.P. 2003. Integrating Fracture Mapping Technologies to Optimize Stimulations in the Barnett Shale. SPE-77441-PA. SPE Production & Facilities 20 (02), 85-93. https://doi.org/10.2118/77441-PA

Golder Associates. 2018. FRACMAN 7.70 User Documentation. Copyright 1999 – 2018.

Heinemann, Z. E., Mittermeir, G. M. 2011. Derivation of the Kazemi–Gilman–Elsharkawy Generalized Dual Porosity Shape Factor. Transp Porous Med 91, 123–132. https://doi-org./10.1007/s11242-011-9836-4

Hoffman, T.B., Caers, J. 2004. History Matching with the Probability Perturbation Method – Application to a North Sea Reservoir. Paper A009 presented at European Conference on the Mathematics of Oil Recovery, 30 August – 2 September 2004, Cannes, France.

Hu, B.X., Huang, H. 2002. Stochastic analysis of reactive solute transport in heterogeneous, fractured porous media: a dual-permeability approach. Trans. Porous Med. 48(1), 1–39 (2002). https://doi:10.1023/A:1015671227317

Hu, L.Y., Jenni, S., 2005. History Matching of Object-Based Stochastic Reservoir Models. SPE Journal 10 (3), 312–323. https://doi.org/10.2118/81503-PA

Jo, H. 2013. Optimal Fracture Spacing of a Hydraulically Fractured Horizontal Wellbore to Induce Complex Fractures in a Reservoir Under High In-Situ Stress Anisotropy. IPTC-16717-MS. International Petroleum Technology Conference, 26-28 March, Beijing, China. https://doi-org/10.2523/IPTC-16717-MS

Johansen, K., Caers, J., Suzuki, S. 2007. Hybridization of the Probability Perturbation Method with Gradient Information. Comput Geos 11, 319 – 331 (2007). https://doi.org/10.1007/s10596-007-9055-9

Kashib, T., Srinivasan, S. 2006. A Probabilistic Approach to Integrating Dynamic Data in Reservoir Models. Journal of Petroleum Science and Engineering 50(3–4), 241 – 257. https://doi.org/10.1016/j.petrol.2005.11.002

Kazemi, H., Merrill, L.S., Porterfield, K.L., Zeman, P.R. 1976. Numerical Simulation of Water-Oil Flow in Naturally Fractured Reservoirs. SPE-5719-PA. SPE Journal 16(6), 317-326. https://doi.org/10.2118/5719-PA

Kazemi, H., Gilman, J.R., Elsharkawy, A.M. 1992. Analytical and Numerical Solution of Oil Recovery from Fractured Reservoirs Using Empirical Transfer Functions. SPE-19849-PA. SPE Reserv. Eng. 7(2), 219–227. https://doi-org/10.2118/19849-PA

Khani, H., Hamdi, H., Nghiem L., Chen, Z., Sousa, C.S. 2018. Geologically Consistent History Matching of SAGD Process Using Probability Perturbation Method. SPE-189770-MS. SPE Canada Heavy Oil Technical Conference, Calgary, 13-14 March. https://doi.org/10.2118/189770-MS

Li, G and Reynolds, A.C. 2009. Iterative Ensemble Kalman Filters for Data Assimilation. SPE-109808-PA. SPE Journal 14(3), 496–505. https://doi-org/10.2118/109808-PA

Linde, N., Renard, P., Mukerji, T, and Caers, J. 2015. Geological Realism in Hydrogeological and Geophysical Inverse Modeling: A Review. Advances in Water Resources, 86 (Part A), 86-101. https://doi.org/10.1016/j.advwatres.2015.09.019

Liu, Y., Liu, L., Leung, J. Y., and Moridis, G. J. 2020. Sequentially coupled flow and geomechanical simulation with a discrete fracture model for analyzing fracturing fluid recovery and distribution in fractured ultra-low permeability gas reservoirs. Journal of Petroleum Science and Engineering, 189, 107042.

Long, J. S., Remer, J. S., Wilson, C. R., & Witherspoon, P. A. 1982. Porous Media Equivalents for Networks of Discontinuous Fractures. Water Resources Research, 18(3), 645-658. https://doi:10.1029/WR018i003p00645

MathWorks. 2018. MATLAB Documentation. Retrieved August 14, 2018. https://www.mathworks.com/help/matlab/index.html

Monteagudo, J.E.P., and Firoozabadi, A. 2004. Control-Volume Method for Numerical Simulation of Two-Phase Immiscible Flow in Two-and Three-Dimensional discrete-Fractured Media, Water Resour. Res., 40, W07405, http://dx.doi.org/10.1029/2003WR002996

Nejadi, S., Leung, J.Y., Trivedi, J.J., Virues, C. 2015. Integrated Characterization of Hydraulically Fractured Shale-Gas Reservoirs - Production History Matching. SPE-171664-PA. SPE Res Eval & Eng, 18 (04), 481–494. https://doi.org/10.2118/171664-PA

Nejadi, S., Trivedi, J.J., Leung, J. 2017. History Matching and Uncertainty Quantification of Discrete Fracture Network Models in Fractured Reservoirs. Journal of Petroleum Science and Engineering 152(2017), 21–32. http://dx.doi.org/10.1016/j.petrol.2017.01.048

Oda, M. 1985. Permeability Tensor for Discontinuous Rock Masses. Geotéchnique 35 (4), 483 – 495. https://doi.org/10.1680/geot.1985.35.4.483

Oliver, D., Chen, Y., 2011. Recent Progress on Reservoir History Matching: A Review. Computational Geosciences. 15(1), 185–221. https://doi.org/10.1007/s10596-010-9194-2

Pyrcz, M.J., Deutsch, C.V. 2014. Geostatistical Reservoir Modeling. Oxford University Press. ISBN: 978-0-19-973144-2.

Rwechungura, R.W., Dadashpour, M., Kleppe, J. 2011. Advanced History Matching Techniques Reviewed. SPE -142497-MS. SPE Middle East Oil and Gas Show and Conference, 25 – 28 September, Manama, Bahrain. https://doi.org/10.2118/142497-MS

Sahimi, M. 2011. Flow and Transport in Porous Media and Fractured Rock (2nd ed.). Weinheim: Wiley-VCH.

Sandve, T.H., Berre, I., Nordbotten, J.M. 2012. An Efficient Multi-Point Flux Approximation Method for discrete Fracture–Matrix Simulations. Journal of Computational Physics. 231(09), 3784–3800. https://doi.org/10.1016/j.jcp.2012.01.023

Schlumberger, 2017. ECLIPSE Reference Manual Version 2017.2.

Schlumberger, 2017. ECLIPSE Technical Description Version 2017.2.

Shakiba, M., de Araujo Cavalcante Filho J., Sepehrnoori, K. 2018. Using Embedded Discrete Fracture Model (EDFM) in Numerical Simulation of Complex Hydraulic Fracture Networks

Calibrated by Microseismic Monitoring Data. Journal of Natural Gas Science and Engineering, 55(2018), 495-507. ISSN 1875-5100. https://doi.org/10.1016/j.jngse.2018.04.019

Suzuki, S., Daly, C., Caers, J.K., Mueller, D., 2007. History Matching of Naturally Fractured Reservoirs using Elastic Stress Simulation and Probability Perturbation Method. SPE-95498-PA. SPE J. 12 (1), 118–129. https://doi.org/10.2118/95498-PA

Van Heel, A.P.G., Boerrigter, P.M., Van Dorp, J.J. 2008. Thermal and Hydraulic Matrix-Fracture Interaction in Dual Permeability Simulation. SPE 102471-PA. SPE Reservoir Evaluation Eng. 11(4), 735–749 (2008). http://doi:10.2118/102471-PA

Wang, M. and Leung, J.Y. 2015. Numerical Investigation of Fluid-Loss Mechanisms during Hydraulic Fracturing Flow-Back Operations in Tight Reservoirs. Journal of Petroleum Science and Engineering 133: 85-102

Warren, J.E., Root, P.J. 1963. The Behavior of naturally Fractured Reservoirs. SPE 426-PA. SPE J. 3(3), 245–255. http://doi:10.2118/426-PA

Zidane, A., Firoozabadi, A. 2014. An Efficient Numerical Model for Multicomponent Compressible Flow in Fractured Porous Media, Advances in Water Resources 74 (2014) 127–147. https://doi.org/10.1016/j.advwatres.2014.08.010

APPENDIX – *Figures*

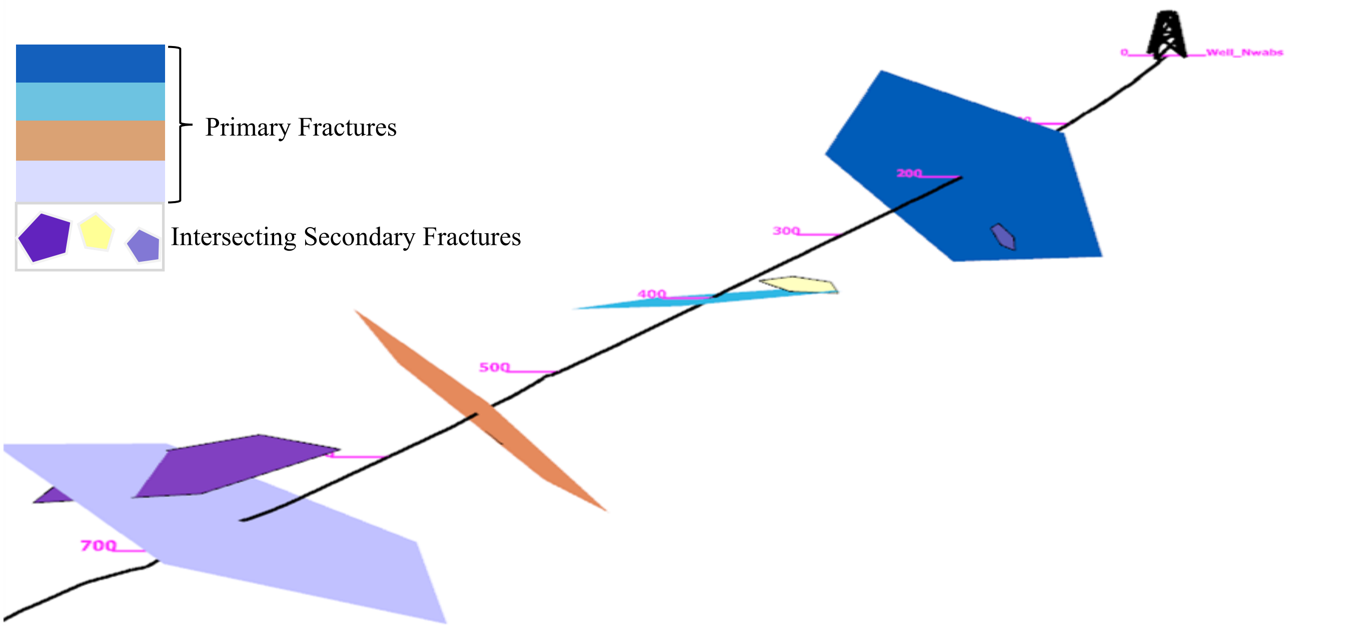

(a)

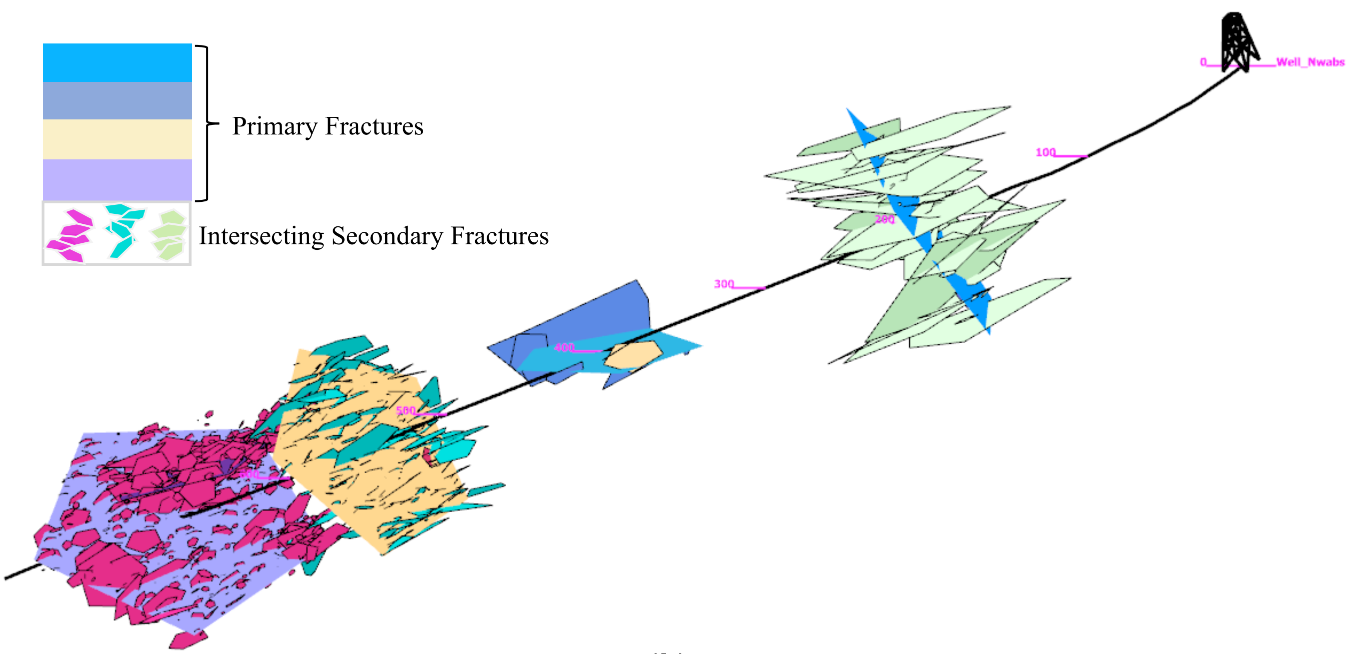

(b)

Fig. 3-1: Diagram showing the well, the primary fractures and secondary induced fractures intersecting the primary fractures for (a) Cases #1-2, and (b) Case #3.

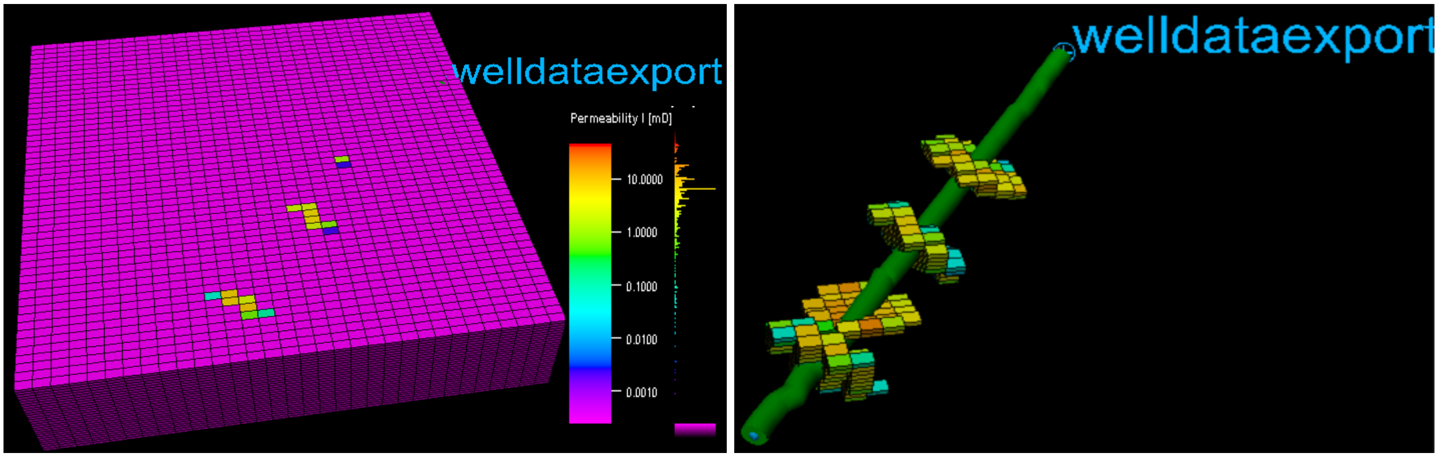

(a) **(b)**

Fig. 3-2: (a) Nested model grid – with the variable of fracture PERMX is shown; (b) 1D filter of the variable of fracture PERMX.

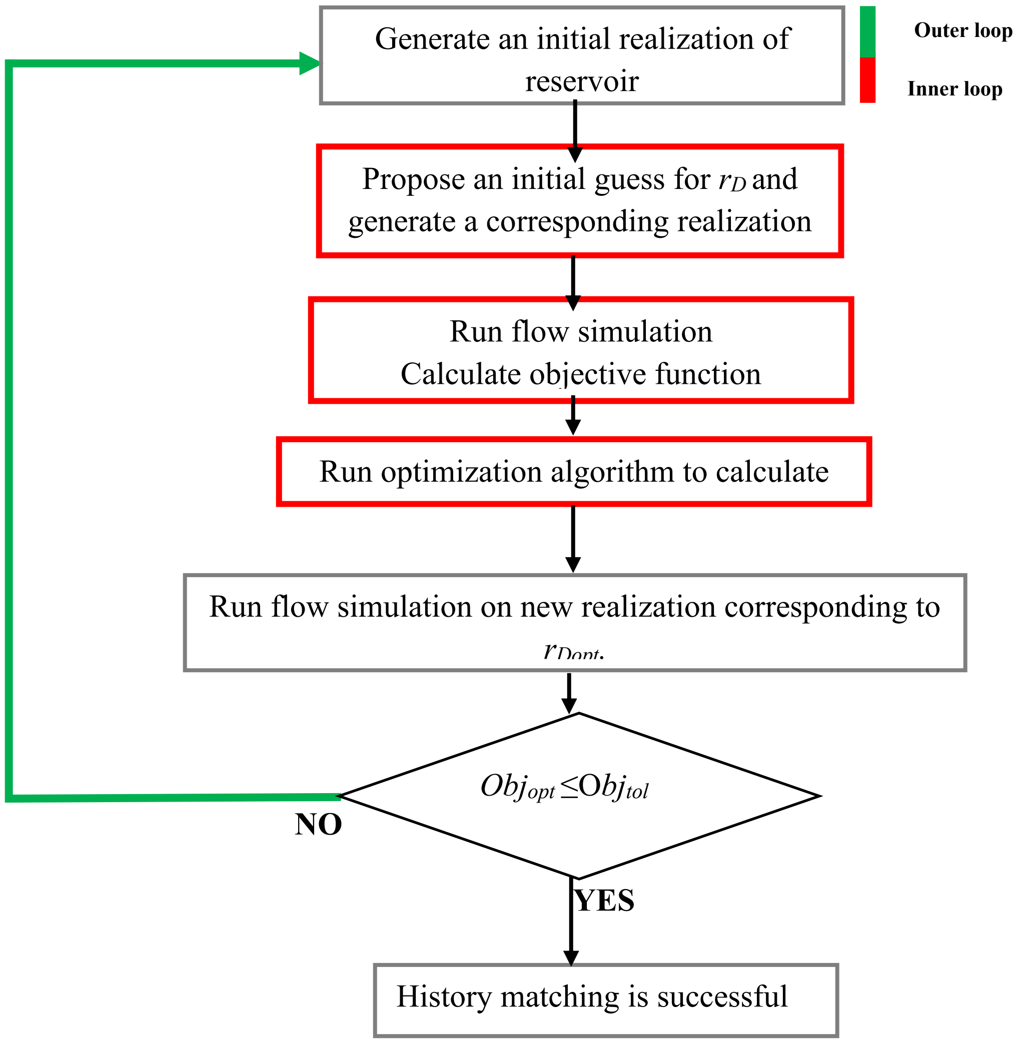

Fig. 3-3: Flowchart describing the probability perturbation method and objective function minimization workflow.

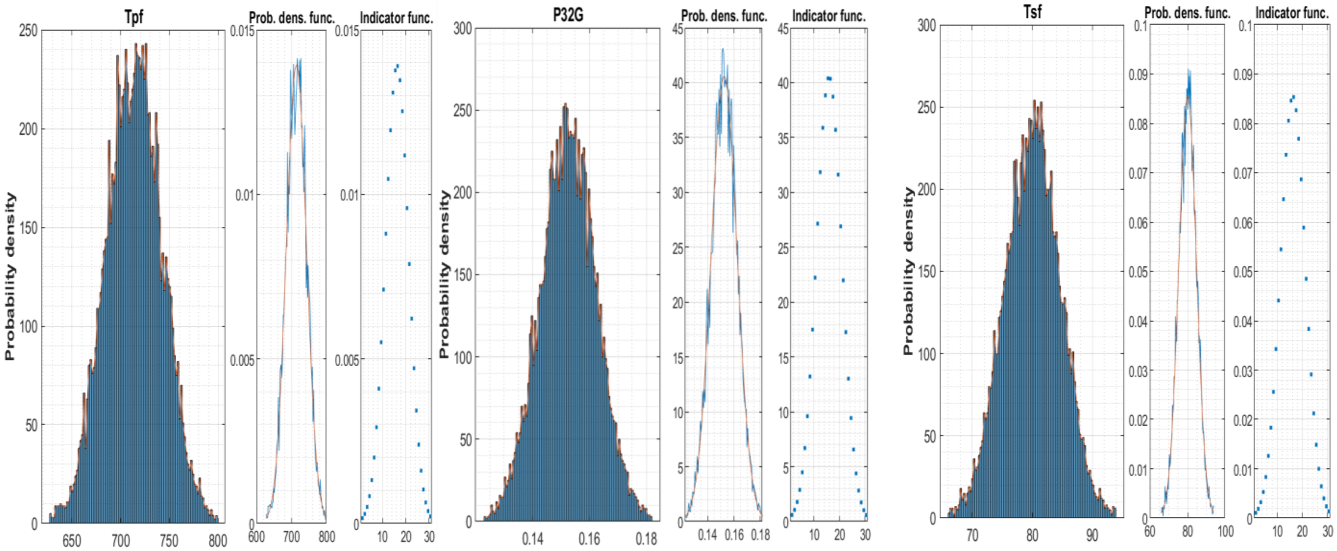

(a)

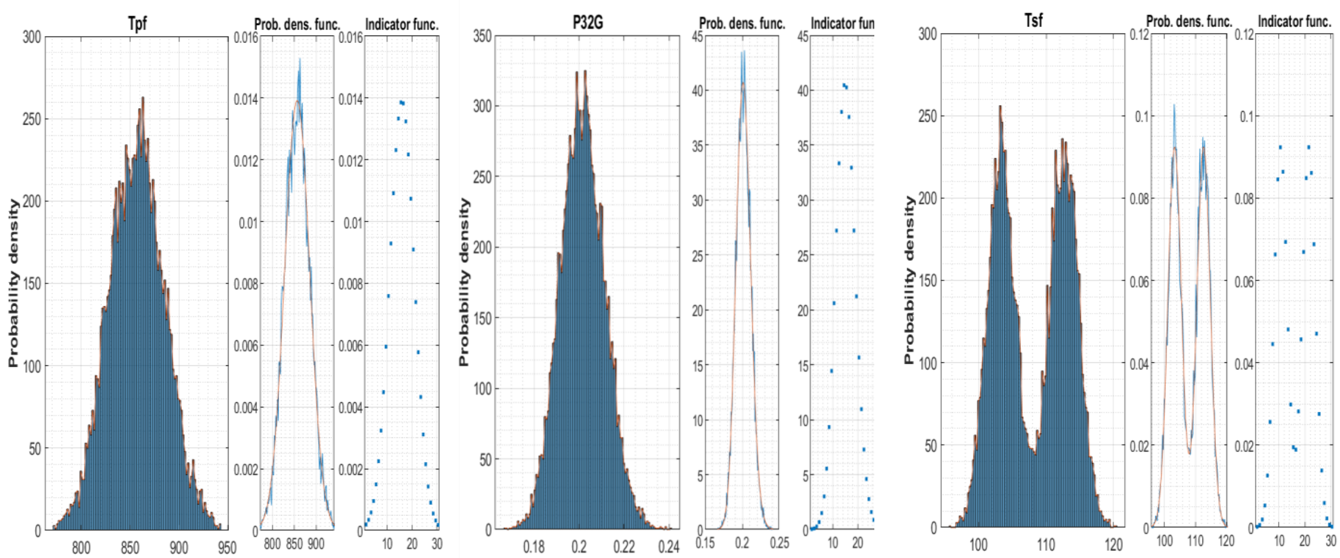

(b)

Fig. 3-4: Initial probability density functions of T_{pf}, P^{sf}_{32G} and T_{sf} for

(a) *Case #1* and (b) *Case #2*.

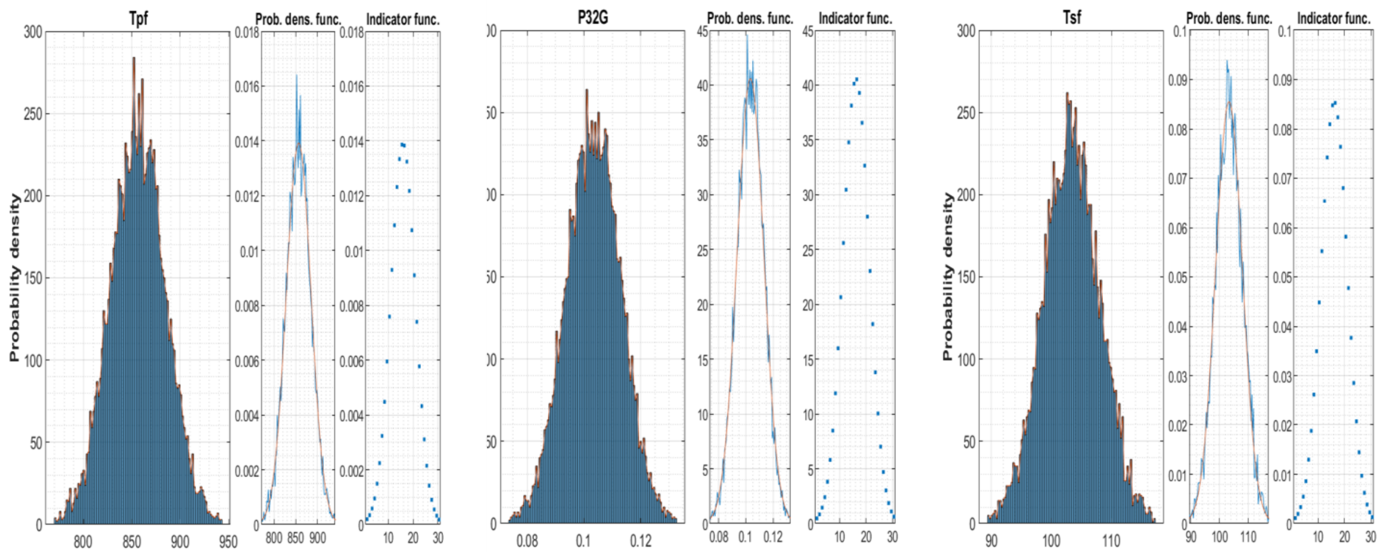

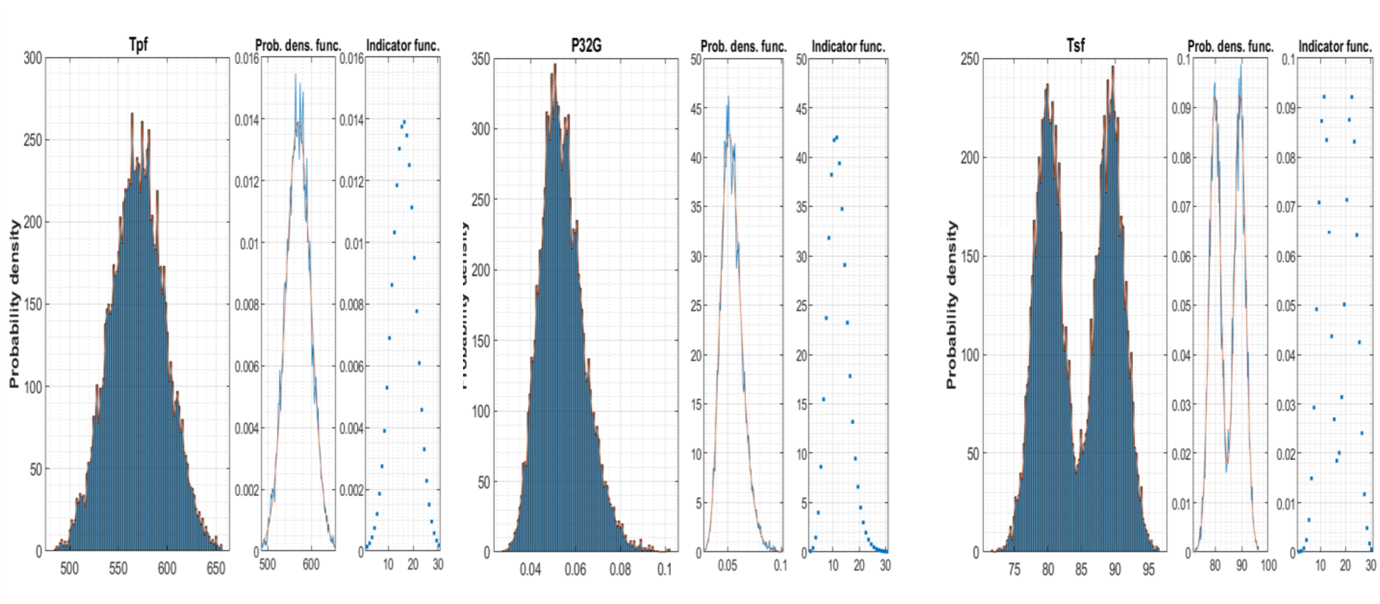

(b)

Fig. 3-5: Initial probability density functions of T_{pf}, P^{sf}_{32G} and T_{sf} for *Case #3* – (a) Gaussian and (b) non-Gaussian.

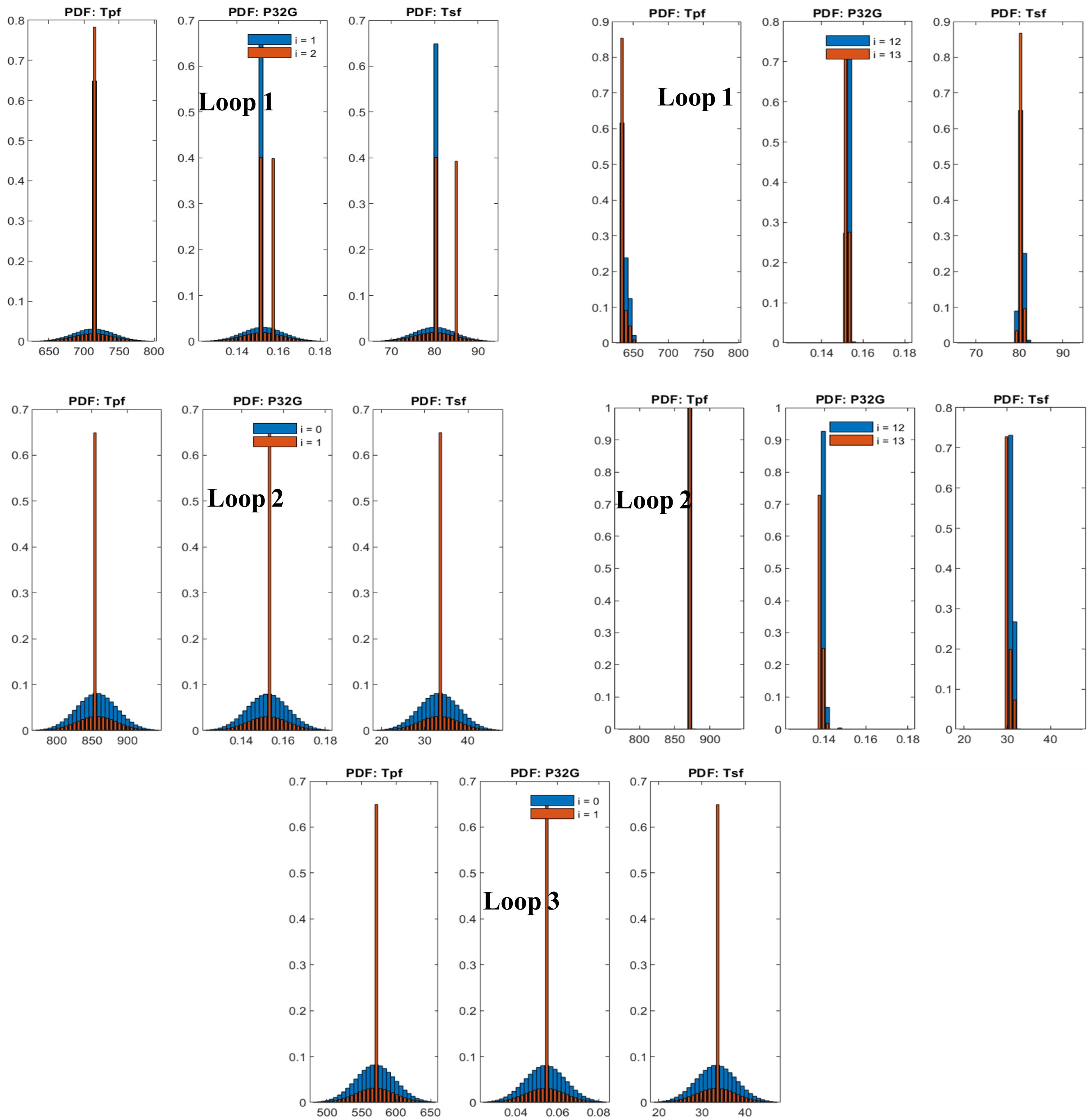

PDF: Tpf
PDF: P32G
PDF: Tsf
i = 1
i = 2
Loop 1
PDF: Tpf
PDF: P32G
PDF: Tsf
i = 12
i = 13
Loop 1
PDF: Tpf
PDF: P32G
PDF: Tsf
i = 0
i = 1
Loop 2
PDF: Tpf
PDF: P32G
PDF: Tsf
i = 12
i = 13
Loop 2
PDF: Tpf
PDF: P32G
PDF: Tsf
i = 0
i = 1
Loop 3

(a)

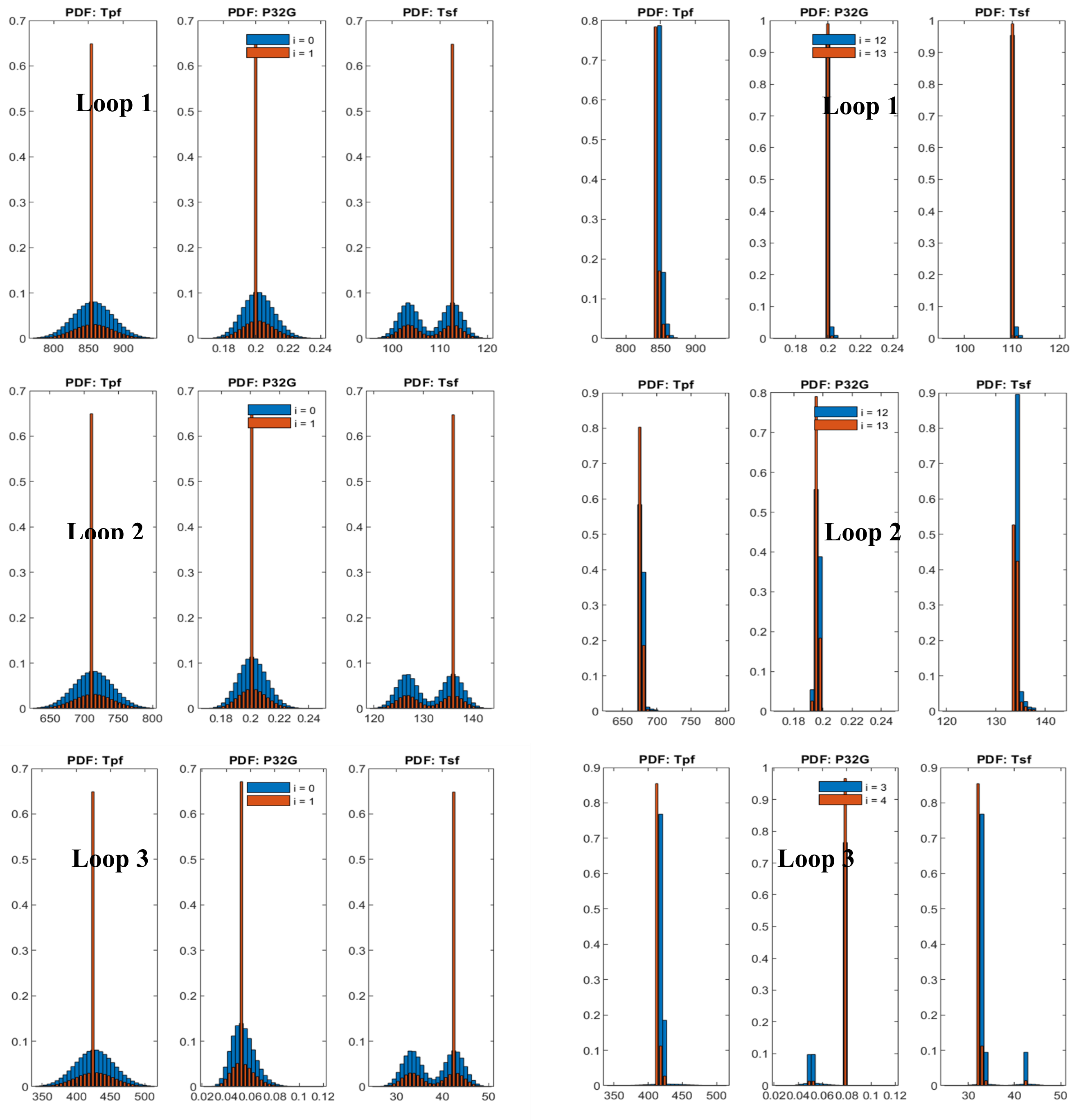

Fig. 3-6: Comparison between (selected) prior and posterior distributions for the iterations steps *i* to *i*+1 for different loops corresponding to (a) *Case #1* and (b) *Case #2*.

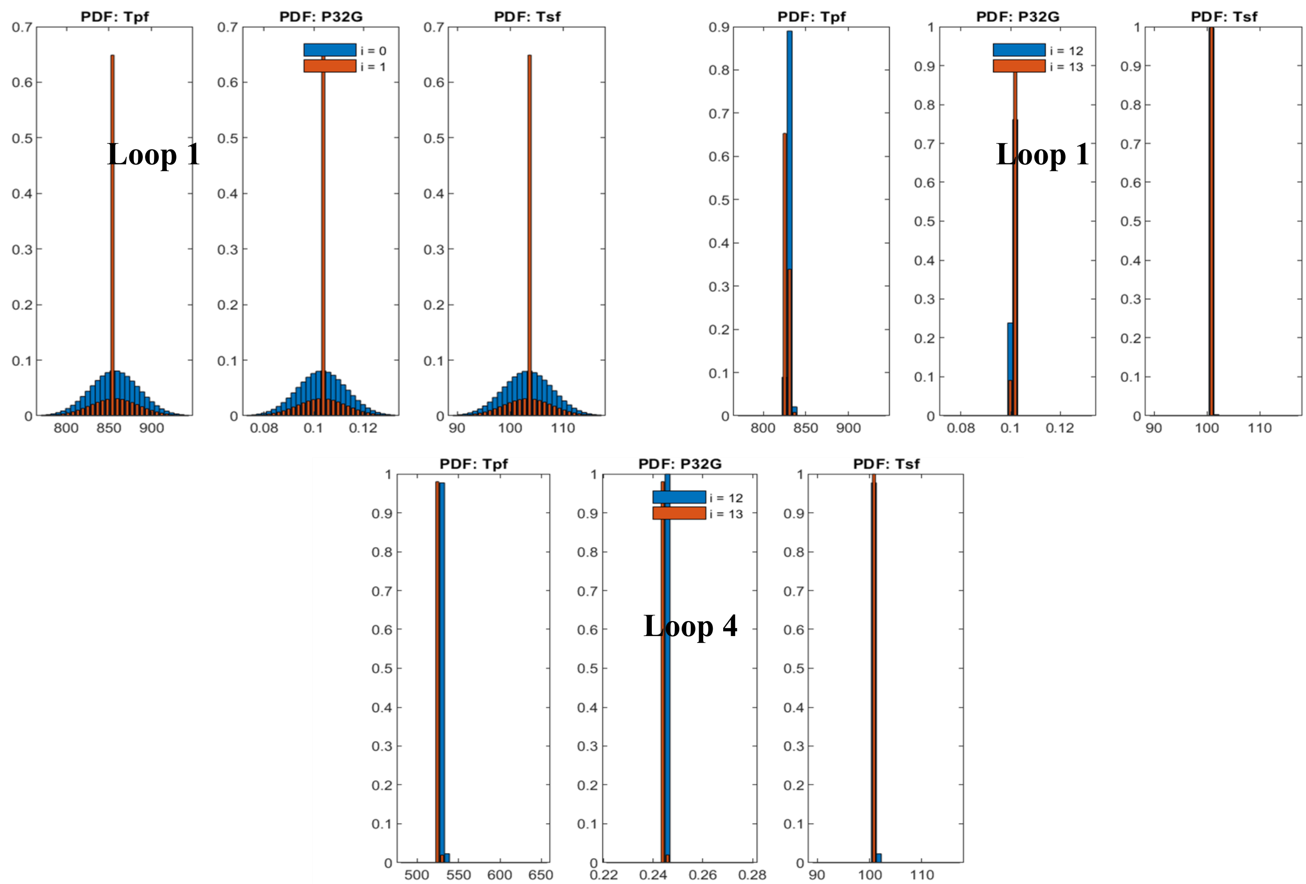

PDF: Tpf
PDF: P32G
PDF: Tsf
i = 0
i = 1
Loop 1
PDF: Tpf
PDF: P32G
PDF: Tsf
i = 12
i = 13
Loop 1
PDF: Tpf
PDF: P32G
PDF: Tsf
i = 12
i = 13
Loop 4

(a)

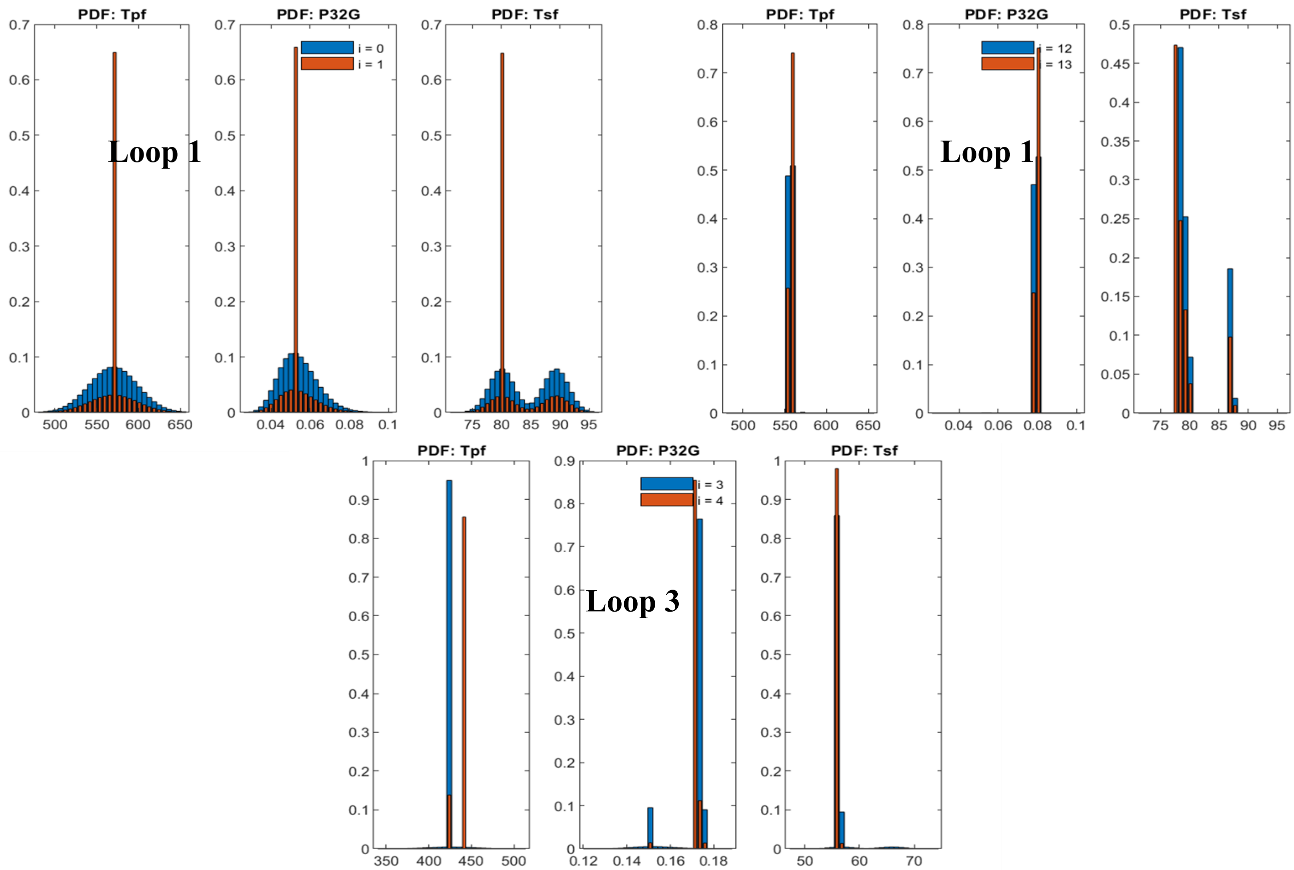

(b)

Fig. 3-7: Comparison between (selected) prior and posterior distributions for the iterations steps *i* to *i*+1 for different loops corresponding to

Case #3 – (a) Gaussian and (b) non-Gaussian

Note: *i* refer to *l* (iterative index).

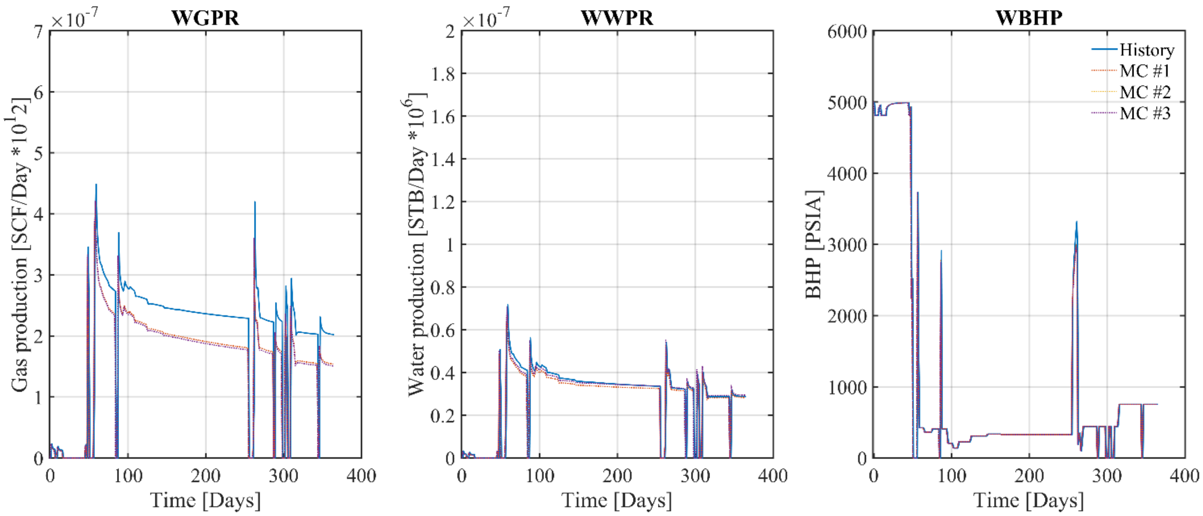

(a)

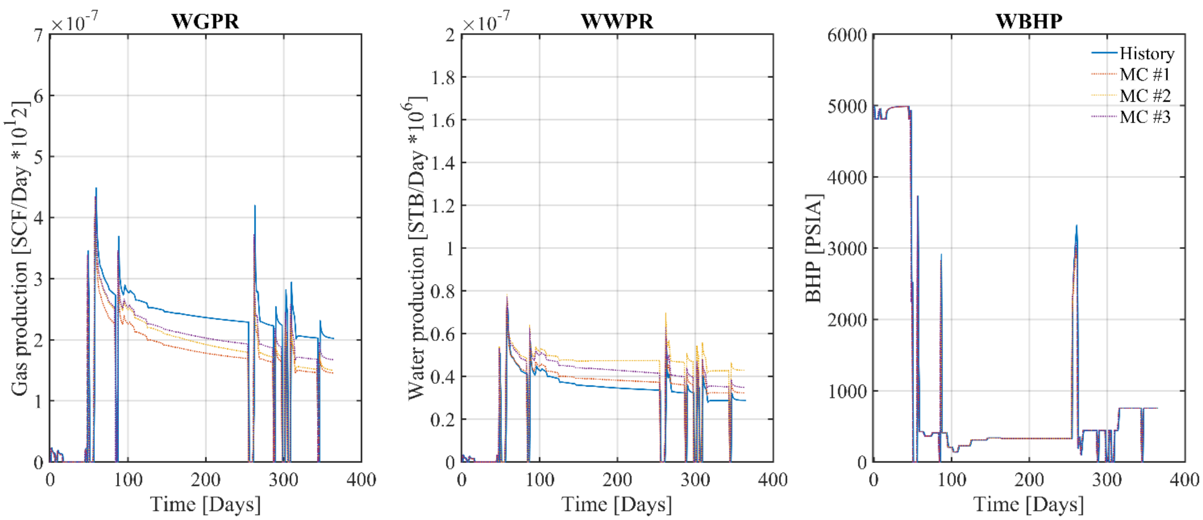

(b)

Fig. 3-8: Gas production, water production and BHP profiles corresponding to equi-probable history matched realizations sampled from the final posterior probability distributions for (a) *Case #1* and (b) *Case #2*.

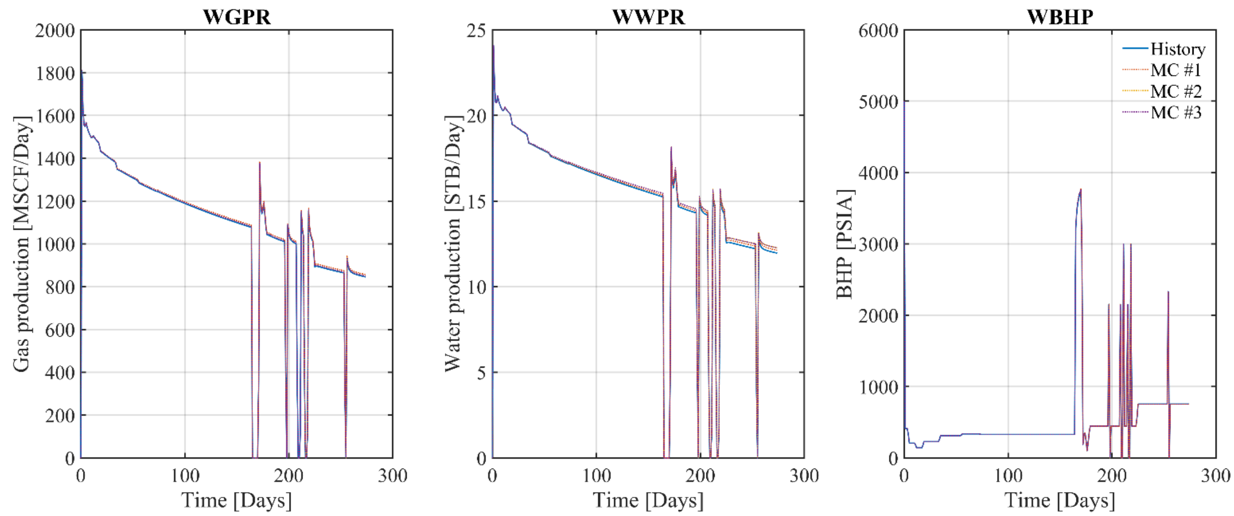

(a)

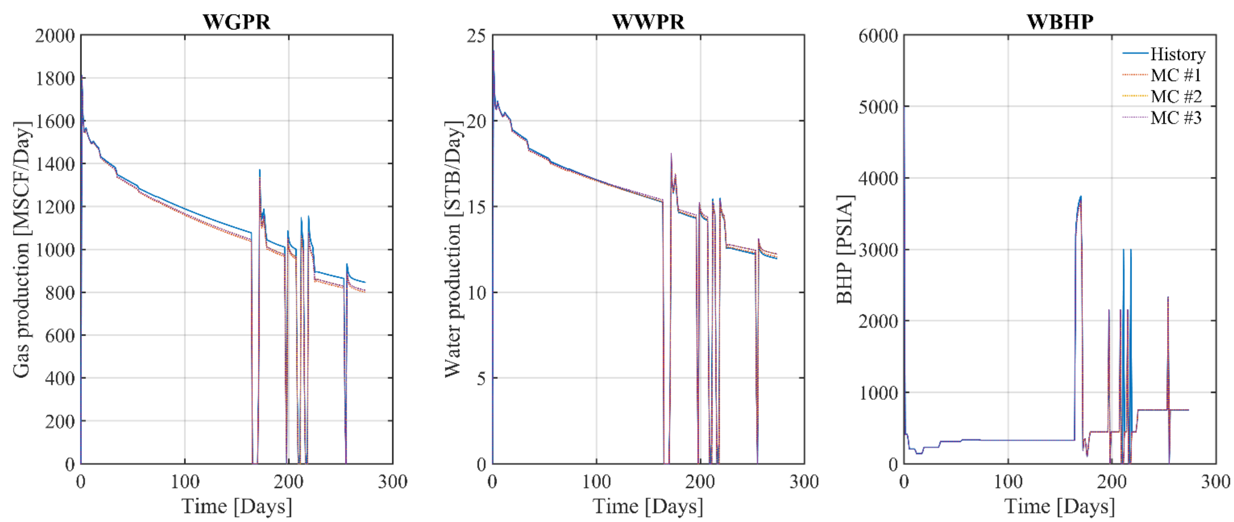

(b)

Fig. 3-9: Gas production, water production and BHP profiles corresponding to equi-probable history matched realizations sampled from the final posterior probability distributions for *Case #3* – (a) Gaussian and (b) non-Gaussian.

Chapter 4: Probabilistic History Matching of Multi-Scale Fractured Reservoirs: Integration of a Novel Localization Scheme Based on Rate Transient Analysis

4.1 OVERVIEW

A new assisted history-matching workflow is presented, where rate transient analysis (RTA) results are used to constrain not only the initial discrete fracture network (DFN) models, the interpreted flow regimes are also used to formulate a localization scheme for more efficient updating of the pertinent DFN model parameters. The outcome is an ensemble of DFN realizations that are calibrated to both geologic and dynamic production data.

RTA interpretations and other pertinent geological data are used to infer the prior probability distributions of the unknown fracture parameters, from which an ensemble of initial DFN models is sampled. The DFN models are subjected to numerical multiphase flow simulation. The fracture parameters are adjusted following an indicator-based probability perturbation method, which is capable of minimizing the objective function and reducing the uncertainties in the unknown fracture parameters simultaneously. A key feature is that the flow regimes identified from RTA are used to formulate a localization strategy, where individual segments of the production data are used to tune only a specified subset of the unknown model parameters.

In a case study, the method is applied to characterize the probability distributions of four parameters in a multifractured shale gas well: primary fracture transmissivity, aperture of the secondary fracture, transmissivity of the secondary induced fracture, and global fracture intensity. Their probability distributions are updated following the proposed approach to match the production history. Multiple realizations of the DFN model are sampled.

A key novelty is that the proposed probabilistic approach facilitates the representation of uncertainties in fracture parameters via multiple DFN models and their corresponding upscaled flow-simulation models. A more comprehensive and robust approach is presented for integrating specific RTA interpretations and estimations into various steps of the history-matching process.

4.2 INTRODUCTION

Detailed characterization of highly heterogeneous, multi-scale, fracture systems, which are commonly observed in hydraulically fractured unconventional reservoirs, is often challenging. Complex fracture geometries compounded with the significant disparity in permeability between the matrix and fracture systems can pose particular challenges. Flow simulation of a discrete fracture network (DFN) model can be computationally demanding considering the highly nonlinear relationships between various fracture model parameters and the corresponding flow responses (Wang and Leung, 2015; Liu et al., 2019). It remains challenging to construct a set of DFN models and update both the hydraulic and secondary fracture parameters by integrating both static (e.g., logs) and dynamic data (e.g., rate and pressure measurements).

The first issue is the integration of data and measurements from diverse sources and scales. Fracture properties, such as size, aperture, compressibility, orientation, storativity, transmissivity, intensity, half-length, permeability, are generally not known a priori. Certain image logs may be used to infer the statistics of these parameters. Data acquired from recorded microseismic activities has been useful in determining the direction of fractures regarding their trend (the angle measured from the North in the $x-y$ plane) and plunge (the vertical angle measured from the horizontal $x-y$ plane). Rate transient analysis (RTA) can be used to assess flow regimes and certain fracture parameters from production data. There are many existing RTA models in the literature corresponding to different flow regimes and boundary conditions. Some of the early works is that of Bello et al. (2010), which developed an analytical model for a dual-porosity medium entailing five identifiable flow regimes. Ezulike et al. (2015) identified three flow regimes similar to those in Bello's model and further extended the analysis to late-time pseudo-steady state flow due to inter-fracture interference. Ali et al. (2013) also performed an analysis on the triple-porosity model, which assumes sequential flows from matrix to micro-fractures, macro-fractures, and finally to the horizontal well while identifying six different flow regimes. Recently, Wang (2018) incorporated many additional mechanisms in their analytical models, including secondary fracture networks, non-Darcy flow, non-uniform stimulated reservoir volume, gas desorption in nanopores, and heterogeneous completion across multiple stages, for analyzing various flow regimes in fractured shale gas well production. Despite the development of many new models over the years, the main limitation, however, is that the analytical models used in RTA often invoke many assumptions, such as constant parameter values and specific boundary conditions. Nevertheless, interpretations derived from RTA can be used as initial guesses for more rigorous (detailed) history matching analysis (Yue et al., 2016).

The second concern is connected to the numerical simulation of multiphase flow in fractured porous media. Fractured reservoir simulation approaches can be categorized depending on how the fracture geometry is represented and how the matrix and fracture flow interactions are captured. The dual-porosity (DP) model considers the fracture system as the only flow path directly connected to the wellbore; although inter-porosity flow between the matrix and fracture systems is accounted for, inter-porosity flows within the matrix system and to the wellbore are ignored (De Swaan, 1976; Warren and Root, 1963; Bui et al., 2000). An improvement to the DP model, which is the dual-porosity dual-permeability (DPDK) model, was proposed, and it considers all inter-porosity flows between the fracture network, matrix system, and the wellbore (Hu and Huang, 2002; Al-Shaalan et al., 2003; Van Heel et al., 2008). In the DPDK model, the flow transfer terms are formulated as functions of the shape factor, pressure gradients, and several other physical parameters. A major drawback is that it is difficult to fully capture the information pertinent to multiphase flow, in terms of capillarity and gravity, into the formulation of the shape factor. In the DP or DPDK modeling framework, the fractured medium is represented with an equivalent model consisting of matrix and fracture domains. There is also an assumption that the fractures should be densely populated for this model to work efficiently (Ahmed et al., 2015). Alternative approaches have been developed to alleviate these limitations by incorporating the discrete fracture model, where the actual geometries and locations of individual fractures are prescribed in the computational domain explicitly. An unstructured mesh is used to discretize a domain with randomly-distributed fractures. Various finite element and finite volume methods, such as control-volume finite-element (CVFE), cell-centered finite-volume (CCFV or multi-point flux approximation MPFA), and mixed finite-element methods (MFE), have been developed (Monteagudo and Firoozabadi, 2004; Sandve et al., 2012; Zidane and Firoozabadi, 2014; Liu et al., 2020). There are some limitations with these techniques; for example, the CVFE scheme does not preserve flux continuity for heterogeneous porous medium, while the MFE method, which is locally flux-continuous and conservative, can be computationally expensive, as both the velocity and pressure fields are estimated simultaneously. In recent years, the use of Embedded Discrete Fracture Models (EDFM) is becoming more popular. The discrete fractures are integrated within the conventional matrix cells (Shakiba et al., 2018). In this work, the DPDK model is used to capture the interporosity flows between the fracture network, matrix system, and wellbore. To construct a dual continuum reservoir simulation model, equivalent porous medium properties such as permeability tensor and shape parameters are assigned to each reservoir cell consisting of both matrix and fracture continua via upscaling techniques (Nejadi et al., 2017). A commonly-adopted analytical approach was developed by Oda (1985). More advanced flow-based upscaling techniques and local-global upscaling schemes have also been developed (Chen et al., 2003).

The third concern is the inference of distributions of fracture properties from dynamic (flow and pressure) data. History matching is a process by which dynamic data is integrated to infer the uncertain model parameters: fracture parameters (e.g., intensity, location, orientation, size) are perturbed until the simulation prediction is consistent with the actual dynamic data. This is an inverse problem, and its solutions are non-unique. Several techniques, including stochastics search (e.g., simulated annealing, genetic algorithm), optimization-based methods (e.g., maximum a-posterior), and sampling-based (e.g., gradual deformation), have been utilized to characterize fracture network models. In some cases, the equivalent model parameters are updated, while discrete fracture properties are updated in others. Cui and Kellar (2005) calculated the sensitivity coefficients of production data with respect to the fracture intensity using a gradient simulator and the adjoint method; correlations between fracture intensity and fracture permeability, matrix permeability, and a certain coupling factor were used to update these pertinent flow parameters. Yet, the gradient-based optimization techniques can be computationally expensive due to the gradient calculations. Hu and Jenni (2005) formulated a gradual deformation method to calibrate an object-based Boolean model for estimating the shape, location, and size of various heterogeneous features from production data. De Lima et al. (2012) applied gradual deformation to estimate realizations of fault distribution (i.e., intensity, length, and spatial locations). However, despite the ease of the implementation of the gradual deformation method, it is only applicable for modeling properties that follow a Gaussian distribution, and this is generally not a valid assumption for fracture properties. Suzuki et al. (2007) applied the probability perturbation method

(PPM) to estimate large-scale fracture distribution and local-scale variations in fracture densities for a naturally fractured reservoir without considering hydraulic fracture stages. Chai et al. (2016) proposed a two-stage Markov Chain Monte Carlo (MCMC) method with embedded discrete fracture modeling for characterizing different porosity distributions corresponding to the organic matrix, inorganic matrix, secondary fractures, and hydraulic fractures of shale reservoirs. The problem with MCMC is that it requires numerous iterations to converge to a stationary distribution due to low acceptance ratios for transitions to a new state, particularly when the number of unknown model parameters is large. Other researchers have applied various stochastic search algorithms to estimate fracture distribution. Chen et al. (2019) developed a multi-scale approach for history-matching of dual-porosity models: an evolutionary algorithm was used to calibrate coarse-scale static and dynamic parameters from average field pressure, well bottom-hole pressures, and repeat formation tester (RFT) data, while the streamline simulation was performed to fine-tune local fracture permeability to match the specific well bottom-hole pressures. Ensemble-based techniques (e.g., Ensemble Kalman filter, or EnKF, and ensemble smoother) have also gained wide attention for their advantages in data assimilation and uncertainty quantification. The convergence of EnKF is guaranteed if multi-Gaussian distributions can be assumed for the model and data variables, as well as if a linear relationship between all variables exists. These assumptions are generally not applicable for fractured reservoirs, rendering the convergence behavior of other ensemble-based methods, including EnKF, to be compromised. Improvements on the EnKF formulation, such as iterative updating to mitigate concerns associated with nonlinearity (Chen and Oliver, 2012) and alternative parameterization schemes to transform the non-Gaussian distributions into Gaussian ones (Linde et al., 2015), were proposed. Nejadi et al. (2015) employed EnKF to characterize hydraulic fracture parameters (e.g., half-length and transmissivity) and induced fracture parameters (e.g., length, transmissivity, intensity) using a DPDK simulation model. A similar technique was used in Nejadi et al. (2017) to infer fracture orientation, conductivity, permeability tensors, and intensity for a naturally fractured reservoir. Emerick and Reynolds (2012) combined MCMC with EnKF, and the results showed some improvement compared to EnKF alone; however, the data mismatch was still quite high. They assessed the results of a very long MCMC as a reference solution to scrutinize the sampling performance of the ensemble-based methods. In the end, there is still debate that though these extensions/ hybrid formulations may retain the concept of utilizing an ensemble, they no longer depend on a linear update or transformation of space and are not appropriate for highly non-Gaussian variables, implying that they could offer only a partial approximation of the true distribution.

The literature review has revealed several arguable issues relevant to production history-matching of multi-scale fractured reservoirs. The description of DFN models with little or no data counters the idea of proper representation of fractured reservoirs. Values obtained from thorough RTA study and microseismic data serve as an ideal substitute to constrain the description of DFN and further localization of dynamic history matching. The gradient-based optimization techniques are robust, but the computation of gradients (or the sensitivity coefficients) can be computationally expensive. Stochastic search algorithms, such as simulated annealing and the genetic algorithm, may also require many iterations to converge. A sampling-based technique, namely the probability perturbation method, is used for this research, as it does not require gradient calculations and can easily handle non-Gaussian fracture parameters; it facilitates the estimation of the posterior probability distribution, from which multiple realizations can be sampled. The PPM approach has been implemented to calibrate permeability distribution in conventional reservoirs (Kashib et al.,

2006) and naturally fractured reservoir permeability distribution, conditioned to a prescribed fracture density model (Suzuki et al., 2007).

The objective of this thesis is to propose a new workflow for incorporating RTA-derived information into an indicator-based probability perturbation method for history-matching production data in a system consisting of both hydraulic and secondary (induced) fractures: in addition to utilizing the RTA results to constrain the initial distributions of various fracture properties (e.g., transmissivity, aperture, or intensity), information related to the flow regimes is used to formulate a localization scheme, where individual segments of the production data are used to tune only a specified subset of the unknown model parameters. Therefore, the RTA results are used in two different ways to constrain the overall history-matching workflow. The adoption of localization strategies in other settings has improved the convergence behavior of many history-matching problems that are generally ill-posed. In the proposed method, the global and local discrete fracture network (DFN) model parameters are updated, and the DFN model is subsequently upscaled into a DPDK model for multiphase flow simulation. A significant advantage of the technique is that the uncertainties in fracture parameters are represented by multiple DFN realizations and their corresponding upscaled flow-simulation models. Many previous studies focus on updating the upscaled models, without offering a direct means of transferring that upscaled model parameters back to a set of DFN model parameters. The outcome is an ensemble of DFN realizations that are calibrated to both geologic and dynamic production data. The developed workflow is applied in a synthetic case study of a hydraulically fractured shale reservoir in the Horn River basin.

4.3 METHODOLOGY

4.3.1 Rate Transient Analysis of Production Data

In the RTA study, a dual-porosity reservoir model is employed to represent the hydraulic fracture and background matrix; it is assumed that a hydraulically-fractured horizontal well is located in the center of the rectangular domain with no-flow outer boundaries (Blasingame et al., 1990; Bourdet, 2002). The fractured horizontal well model commonly used for unconventional gas analysis and production forecasting is adapted here, as represented in Fig. 4-1.

The analysis is performed on the plot of rate normalized pressure versus square root of time and the log-log plot of rate normalized pressure (*RNP*) integral, as well as its derivative, versus equivalent time (t_e) (as shown in Fig. 4-2 and Fig. 4-3, respectively). The equations for the identified flow regimes are presented in Appendix A.1. The *RNP* integral and its derivative are defined according to Eq. (4-1) and Eq. (4-2), respectively. Relevant model parameters, including fracture half-length (X_f), total matrix surface area draining into fracture system (A_{cm}), matrix permeability (k_m) and stimulated reservoir volume (*SRV*) can be obtained from different identifiable flow regimes.

$$\frac{1}{t_e}\int_0^{t_e}\frac{q_{ref}}{q(\tau)}(m(P_i)-m(P(\tau)))d\tau \text{ versus } t_e \tag{4-1}$$

$$\frac{\partial}{\partial lnt_e}\left(\frac{1}{t_e}\int_0^{t_e}\frac{q_{ref}}{q(\tau)}(m(P_i)-m(P(\tau)))d\tau\right)\text{versus } t_e \tag{4-2}$$

where $t_e=\dfrac{Q(t)}{q(t)}$ is the equivalent time, otherwise called material balance time and it is a time function that transforms the variable-rate solution into an equivalent constant-rate solution. The integral of *RNP* and its derivative are often preferred, instead of its direct form, as they help to preserve the signatures corresponding to the flow regimes and suppress the noise or fluctuations commonly observed in the derivative of *RNP* versus t_e plot.

The dashed blue lines represent the boundary model where the distance from the well to the North and South boundaries are the same, and the distance to the East and West boundaries are also the same. The two nodes can be adjusted to control the distances to the boundaries. These flow regimes can be identified:

1. Transient linear flow: half-slope representing flow from the matrix into the primary fractures with infinite conductivity: A_{cm} can be obtained from this segment after determining k_m from the psedo state-state flow regime.
2. Pseudo steady-state or SRV flow: unit slope representing pressure interference between consecutive hydraulic fractures. $k_m$and X_f can be determined from the intercept and slope, respectively. Since X_f is determined, SRV (= 2 × L_w × X_f × h) can be obtained from this segment.

The normalized rate cumulative plot (Fig. 4-4) is also employed to estimate the initial in-place gas volume. A straight line with a negative slope can be identified during the boundary-dominated flow regime. Thus, this is transformed into a simple relationship between the dimensionless rate and cumulative as defined below:

$$q_D = \frac{1422Tq}{kh(m(P_i) - m(P_{wf}))} \tag{4-3}$$

$$Q_{DA} = \frac{4.5Tz_i\mathrm{STGIIP}(m(P_i) - m(\overline{P})}{\phi hAP_i(m(P_i) - m(P_{wf}))} \tag{4-4}$$

$$\frac{q}{(m(P_i) - m(p_{wf})} \text{ versus } \frac{\mathrm{STGIIP}(m(Pi) - m(\overline{P}))}{(m(P_i) - m(p_{wf})} \tag{4-5}$$

The plot of Eq. (4-5) with an assumed value of STGIIP iteratively converges to a value of STGIIP (compared with the assumed value) identified as an intercept on the x-axis.

From the RTA results, the following parameters are estimated, and they are used subsequently in the numerical simulation model: X_f, k_m and A_{cm}. For the remaining four fracture parameters (transmissivities of the primary (T_{pf}) and induced fractures (T_{sf}), global induced fracture intensity (P^{sf}_{32G}), the secondary fracture aperture r_e), the RTA estimates will be used to infer the initial distributions, while the posterior distributions will be updated in the probabilistic history-matching framework in the next step. First, the Latin hypercube sampling technique is applied with the RTA procedure to generate random samples of these four parameters – considering that model parameter estimation is an inverse problem, multiple sets of values could match the data. This sampling approach helps to determine a reliable range for each parameter, which is subsequently used to define the initial distributions of the DFN model parameters. This approach ensures that the initial DFN models used in the next step are constrained to the RTA estimates. Details are discussed later in section 4.4.1.

4.3.2 Generation of Initial Realization of Discrete Fracture Network Models

The Fisher et al. (2005) formulation for a complex hydraulic fracture system was adopted to construct the DFN model using FRACMAN® (Golder Associates, 2018): each hydraulic fracture stage is modeled using a primary fracture (an elongated penny-shaped fissure) that is intersected by randomly-distributed secondary (induced) fractures connected to the primary fracture – Fig. 4-5. The secondary fractures are the induced fractures initiated as cracks on the hydraulic fracture surfaces. Since natural fractures are not considered here, their impacts on the hydraulic fracture geometry, as well as reactivation of natural fractures, are not modeled. In this work, it is assumed that the primary and induced secondary fractures are the most dominant features. Fracture properties, such as orientation, intensity, aperture, location, size, and transmissivity, are defined for both primary and secondary fractures. The Fisher distribution (Fisher, 1953) is used to define the orientation parameters of the induced fractures. Parameters of the Fisher distribution should be defined separately for individual hydraulic fracturing stages and can be estimated from geomechanical and microseismic data.

Transmissivities of the primary (T_{pf}) and induced fractures (T_{sf}), global induced fracture intensity (P^{sf}_{32G}), as well as the secondary fracture aperture r_e, are the uncertain history-matching parameters considered in this research. Updating of the uncertain parameters based on production histories will be achieved during history matching. Individual secondary fractures are assigned following a prescribed nearest neighbor model, where the local fracture intensity (P_{32L}) decreases exponentially with distance to the primary fracture:

$$\mathrm{P}_{32L}(x) = \mathrm{c}e^{-bd_{x,f}} \tag{4-6}$$

Where c and b are empirical constants; d is the distance between location x and the primary fracture plane (Dershowitz, 1993).

4.3.3 Discrete-Fracture-Network Model Upscaling

The DFN model is transformed into an equivalent DPDK simulation model (Fig. 4-6) based on a static upscaling scheme (Oda, 1985). The Oda upscaling scheme is assumed to be suitable and applicable for this thesis; it is computationally faster than the flow-based upscaling schemes (it can be calculated without running any flow simulations). In addition, it is assumed that the induced fractures are well connected to the primary fracture (Dershowitz et al., 2000).

The upscaled DPDK model parameters include fracture porosity, Oda permeability tensor, and matrix-fracture coupling in the form of shape factor. In particular, the fracture porosity is defined as the total fracture volume (average cross-sectional area × aperture) divided by the cell volume. The Oda permeability tensor is computed by first projecting the isotropic fracture permeability onto the fracture plane and then scaling it according to the fracture porosity. The resultant 3 × 3 permeability tensor is given by the following matrix:

$$K_{ij} = \frac{1}{12}(F_{kk}\delta_{ij} - F_{ij}) \tag{4-7}$$

Where K_{ij} is an element in the permeability tensor, F_{ij} is the element of fracture tensor (facilitates fracture flow as a vector along the unit normal from the fracture plane and is calculated by adding the individual fractures within the upscaled grid block, weighted by their area and transmissivity as in Eq. (4-8); δ_{ij} is the Kroenecker's delta.

$$F_{ij} = \frac{1}{V}\sum_{r=1}^{N} A_r T_r n_{ir} n_{jr} \tag{4-8}$$

Where V is the grid cell volume, N is the total number of fractures in a grid cell, n_{ir}, nj_r represents the component of a unit normal to the fracture r, A_r is the area of fracture r and T_r is the transmissivity of fracture r.

Finally, the shape factor, or sigma factor, provides a measure of fracture-matrix interaction, or interporosity flow between the matrix and fracture domains. It is represented mathematically as:

$$Sigma\left(\frac{1}{ft^2}\right) = 4\left(\frac{1}{L_i^{\ 2}} + \frac{1}{L_j^{\ 2}} + \frac{1}{L_k^{\ 2}}\right) \tag{4-9}$$

Where L_i, L_j, and L_k refer to the fracture spacings in the x, y, and z directions.

4.3.4 Probability Perturbation History Matching Using Flow Regime-Localization Scheme

A commercial black-oil simulator (Schlumberger, 2017) is employed to model multiphase fluid flow.

PPM effectively integrates production data dynamically during the history-matching process (Caers 2003; Kashib and Srinivasan, 2006). It substitutes the tuning of specific unknown model parameters, such as a particular geostatistical realization of fracture intensity, with the tuning of the probability distributions corresponding to these model parameters. This is accomplished via a deformation parameter, r_D.

The probability perturbation method (PPM) is a perturbation approach based on the Bayesian updating framework. It perturbs or updates the posterior probability distribution directly based on the mismatch with the production histories. Similar to other ensemble-based techniques, multiple realizations can be sampled from the posterior distributions, facilitating the analysis of many realizations of the uncertain model parameters. Secondly, it is a non-iterative updating scheme and does not assume Gaussian distributions. Therefore, PPM is adopted here due to its flexibility with non-Gaussian distributions and non-linear updating. The main disadvantage of PPM is that the perturbation is based on a perturbation factor, and in some implementations, this can be a limiting step. However, in the formulation shown here, an efficient 1D optimization scheme is adopted, as suggested by others in the literature (Caers 2003; Kashib and Srinivasan, 2006).

An indicator formulation is adopted here to account for the non-Gaussian nature of DFN parameters. In particular, probability distributions of the uncertain parameters (i.e., P^{sf}_{32G}, T_{pf}, r_e, and T_{sf}) are perturbed according to the indicator-based formulation proposed in Kashib and Srinivasan (2006):

$$P\{I^{l+1}(u) = k \mid I^{l}(u) = k,\ C\} = r_D . P\{I(u) = k^{'}\} \forall k^{'} \neq k$$

$$P\{I^{l+1}(u) = k \mid I^{l}(u) = k,\ C\} = 1 - \sum_{k^{i} \neq k} r_D \ . P\{I(u) = k^{'}\} \tag{4-11}$$

The formulation describes the probability of transitioning from the indicator category k at step l to the category k' at step l+1 using the perturbation factor $r_D \in [0,1]$. The probability $P\{I(u) = k'\}$ is the prior probability while $P\{I^{l+1}(u) = k|I^{i}(u) = k, C\}$ is the posterior probability. As r_D tends towards 1, more perturbation of the probabilities results. If $r_D = 0$, there is no perturbation, and the probability of staying at category k at step l+1 is 1.0.; if $r_D = 1$, the probability of staying at category k at step l+1 is 0. u represents the unknown T_{sf}, r_e, T_{pf} and P^{sf}_{32G} as points in the domain.

The PPM framework is described in Fig. 4-7. To arrive at the global optimal, the workflow is divided into an inner loop, where the Brent 1D optimization scheme (Brent, 1973) is used to obtain a local optimal value of r_D for a given initial realization, and an outer loop, where a different initial realization of the model parameters is explored. Denotations are marked in the figure to describe the sections of the workflow indicating the two loops. In Fig. 4-7, the first step is to generate a set of initial realizations based on previously-derived RTA results. It should be emphasized that the RTA step is not repeated at the beginning of every outer loop; it is simply necessary to ensure all initial realizations are constrained by the RTA estimated distributions, as discussed earlier.

$$\Delta O = \int \left(\frac{Q_{g_s}(t) - Q_{g_h}(r_D^*, t)}{Q_{g_{h\max}}(r_D^*, t)} \right)^2 dt + \int \left(\frac{Q_{w_s}(t) - Q_{w_h}(r_D^*, t)}{Q_{w_{h\max}}(r_D^*, t)} \right)^2 dt + \int \left(\frac{b_s(t) - b_h(r_D^*, t)}{b_{\max}(r_D^*, t)} \right)^2 dt \tag{4-12}$$

Eq. (4-12) defines the normalized objective function based on the L2 norm corresponding to the mismatch between historical data and simulation prediction, where Q_g, Q_w, and b represent the gas production, water production, and Bottom-hole pressure, respectively, and the subscripts s, h and max denote the simulation prediction, historical data, and the upper limit (maximum value) for that particular variable, respectively.

In the inner loop, the Brent's algorithm is applied to search for the optimal r_D corresponding to the local minima of the objective function based on a certain initial realization of the model parameters. This algorithm effectively locates the minimum of a single-variable function by utilizing the concepts of golden section search and successive parabolic interpolation, which are summarized in Eq. (4-13).

$$\frac{x^{(2)} - x^{low}}{x^{high} - x^{low}} = \frac{x^{high} - x^{(1)}}{x^{high} - x^{low}} = \varphi = 0.618 \tag{4-13}$$

Where x^{low} and x^{high} are the lower and upper bounds for the search interval corresponding to a unimodal function; $x^{(1)}$ and $x^{(2)}$ are points on the function such that the distances from x^{low} to $x^{(2)}$ and $x^{(1)}$ to x^{high} are exactly the same. Either $x^{(1)}$ and $x^{(2)}$ is selected as the minima for the next search interval. The process is repeated until the minimum is below a certain pre-defined tolerance. φ is the ratio of equal distances to the overall interval distance ($x^{high} - x^{low}$), which is a factor akin to what is applied in the golden section search algorithm. The Brent algorithm in the inner loop is computationally efficient as objective function evaluation is only required at the equal-distance points (i.e., $x^{(1)}$, $x^{(2)}$, etc.), and the convergence speed is fast. The efficiency of the designed workflow is therefore associated with the Brent algorithm. The method is used to estimate the optimal value of r_D corresponding to a given initial realization of the unknown parameters. The inner loop is then repeated using a different initial realization, as denoted by the outer loop.

A novel localization strategy is incorporated based on the flow regimes identifiable from RTA. The RTA-derived flow regimes are used to constrain which model parameters can be perturbed or updated based on different parts of the production data. The early-time data is used to adjust the parameters describing the hydraulic fractures. The late-time data is used to adjust the secondary fracture parameters; this is because secondary fractures generally remain un-propped, and their aperture and hydraulic conductivity strongly depend on the inner-fracture fluid pressure; communication between the secondary and hydraulic fractures is significant during the late time after much of the water in the active secondary fractures has been displaced by gas influx from the matrix (Ezulike and Dehghanpour, 2015). A localization scheme is designed: (1) the early-time data is used to perturb and optimize only T_{pf}; (2) the late-time data is used to perturb and optimize T_{sf}, P^{sf}_{32G}, r_e, while T_{pf} remains fixed at its optimal value from stage (1).

4.4 REFERENCE CASE STUDY

To demonstrate the functionality of the proposed PPM implementation, a model representing a particular horizontal shale gas well comprising of four stages of hydraulic fracturing in the Horn River Basin is presented. The data is extracted from a field example presented in an earlier work by Nejadi et al. (2015) and as adapted from Nwabia and Leung (2021).

4.4.1 Model Description

The model dimension is 244 m × 244 m × 76 m (with 50 × 50 × 10 grid cells along the x-, y-, and z- directions, respectively). Each hydraulic fracturing stage is modeled as a primary (main) fracture plane intersected by a set of secondary (smaller) fractures.

Table 4-1 shows a summary of the DFN model parameters. Fracture orientation, including the trend (horizontal angle in the x-y plane measured away from the north, i.e., positive y-axis) and plunge (vertical angle between the fracture plane and the horizontal x-y plane) of each primary fracture can be inferred from microseismic interpretations. For this particular well, the microseismic observations show that the orientation of fracture growth is along the NE direction (i.e., pole trend of 140˚) (Nejadi et al., 2015).

As discussed in section 4.3.1, values of X_f, A_{cm}, k_m, and SRV are estimated directly from the RTA results and are used for the construction of the reference DFN model. The following equations are used to compute the relevant DFN model parameters, which are used to constrain the initial distribution of the four uncertain fracture properties (P^{sf}_{32G}, T_{pf}, T_{sf}, and r_e) that are updated in the PPM workflow:

$$P_{32G}(/ft) = \frac{A_{cm}\text{(total area of fractures)}}{V_t\ \text{(total volume)}} = \frac{\sum_{1}^{N} 2\frac{L_w}{N}h}{2L_w X_f h} \qquad \text{4-14(a)}$$

$$T_f(ft^2/s) = \frac{k_f \rho g r_e}{\mu} \qquad \text{4-14(b)}$$

$$\lambda = \sigma r_w^2 \frac{k_m}{k_f} \qquad \text{4-14(c)}$$

$$S_{frac} = (c_{fluid} + c_{frac})\rho g r_e \qquad \text{4-14(d)}$$

$$\omega = \frac{(\phi c_t)_f}{(\phi c_t)_f + (\phi c_t)_m} \qquad \text{4-14(e)}$$

P_{32} is a measure of fracture intensity, as defined by Dershowitz (1984); the subscript G denotes a global fracture intensity measure that is constant throughout the entire domain. T_f refers to the transmissivity of either primary, T_{pf}, or secondary, T_{sf}, fracture. In this example, the secondary fractures represent induced/reactivated fractures due to hydraulic fracture; therefore, both T_{pf} and T_{sf} are proportional to the corresponding primary fracture permeability k_f (stages 1 to 4, as shown in Table 4-1). r_e is the secondary fracture aperture. Values of fluid viscosity μ, density ρ, and fluid compressibility c_{fluid} for the gas phase at initial conditions are presented in Table 4-2. g is the gravitational constant. σ is the shape factor defined by the characteristic dimension of the matrix block and the number of normal sets of fracture planes intersecting the matrix block; r_w is the wellbore radius (0.091m). S_{frac} and c_{frac} are the fracture storativity and fracture compressibility, respectively. ω is the storativity ratio describing the fractional contribution of the fractures to the total storativity of the system (i.e., ratio of fracture storativity $(\phi c_t)_f$ to the storativity of the entire matrix-fracture systems $(\phi c_t)_{f+m}$; where ϕ_m and ϕ_f are the matrix porosity (obtained from RTA) and the fracture porosity, respectively; the fracture porosity is defined as the ratio of total fracture volume to the cell volume, and the total fracture volume is computed as $2X_f L_w h$. Primary and secondary fracture compressibility are assigned based on values corresponding to the Muskwa shale, ranging between 0.025 – 0.12 MPa^{-1}, according to Bustin et al. (2008).

Eq. 4-14(a) is used to compute P_{32G}. Eq. 4-14(b) is used to estimate T_{pf}, and T_{sf}; Eq. 4-14(c) is used to estimate k_f. Eq. 4-14(d)-(e) are used to compute r_e, and the values of storativity for both the primary and secondary fractures are similar to those observed by Cinco-ley (1996). As discussed in section 4.3.2, individual secondary fractures are populated according to the nearest neighbor model, where the local fracture intensity (P_{32L}) decreases exponentially with distance to the primary fracture. Analytical upscaling (Oda, 1985) is used to construct the equivalent DPDK model. After the DFN model upscaling, the upscaled model is then subjected to numerical flow simulation (Eclipse-Petrel E&P Software Platform, 2017) to compute the production profiles for a total period of 12 months.

One particular DFN realization is treated as the reference case, from which the *historical* data is extracted for this case study. As discussed in section 4.3.4, the production period is divided into two segments for localization purposes: early time (Day 0 to Day 90) vs. late time (Day 91 to 365).

Therefore, the 12-month production profiles of water production rate, gas production rate, and bottom-hole pressure (P_{wf}) corresponding to the reference case are considered as the historical data.

A preliminary history match is conducted to determine approximately the potential mismatch in the objective function (although it could be quite high) and to assess the level of perturbation (e.g., the bounds corresponding to the model parameters) that may be required during the PPM history-matching step.

Table 4-1: Parameters for the reference discrete fracture network (DFN) model and the corresponding dual permeability (DPDK) simulation model.

Discrete Fracture Network Parameters:	
Primary Fractures	
Storativity, S_{pfrac}	1.0×10^{-6}
Equivalent radius, e_{peq}	(70, 50, 64, 75) ft
Permeability k_f	($k_{f1} = k_{f2}$ 10, k_{f3} 15, k_{f4} 5) mD
Trend (Stage 1)	226˚
Trend (Stage 2)	177˚
Trend (Stage 3)	244˚
Trend (Stage 4)	247˚
Plunge (Stage 1)	19˚
Plunge (Stage 2)	69˚
Plunge (Stage 3)	29˚
Plunge (Stage 4)	55˚
Compressibility, c_{pfrac}	0.000156 psi^{-1}
Secondary Fractures	
Storativity, S_{sfrac}	1.0×10^{-6}
Equivalent radius, e_{seq}	(10, 19, 9, 32) ft

Trend	Assigned based on the nearest neighbor model from the primary fracture
Plunge	
Compressibility, c_{sfrac}	Similar to the primary fracture
Dual Permeability Model Parameters:	
Number of grids	50 × 50 × 10
Model dimensions	800 × 800 × 250 ft^3
Matrix Permeability	0.00004 to 0.00007 mD
Matrix Porosity	6%
Reservoir depth	6425 ft
Initial reservoir pressure	5000 psi

Table 4-2: Reservoir Fluid Properties (Shale Gas).

Gas Density, ρ	0.0507 lb./ft^3
Viscosity, μ	0.015 cp
Compressibility, c_{fluid}	3.99 e-7 psi^{-1}

4.4.2 Workflow Implementation

The designed history matching framework is implemented to perturb the unknown DFN model parameters and to integrate the historical production data for the reference case, as described in section 4.4.1. A FracMan® macro editable script comprising of a set of function calls for creating and upscaling of the DFN models is used to generate a set of initial realizations, as well as the new realizations during each iteration or updating step. The remaining segments of the PPM workflow involving the fluid flow simulation, history matching, and unknown parameter updating are implemented in Matlab® R2020a (MathWorks, 2020) as a central control for the call functions to the other software platforms.

Thirty indicator levels are used to parameterize each of the four unknown (history matching) parameters; P^{sf}_{32G} (lognormal distribution), T_{pf} (Gaussian distribution), r_e (lognormal distribution), and T_{sf} (bimodal distribution). These indicators represent different bins of the categorical parameters, where the midpoints correspond to the levels used during the back-transform. Fig. 4-8 shows the initial distributions of the four uncertain model parameters generated in the outer loop and this will be optimized when the minimum objective function is achieved, calibrated to both geologic and dynamic production data.

4.5 RESULTS AND DISCUSSION

The initial realizations are constructed based on the RTA estimates, with N ranging between 2 and 9 and k_m ranging from 0.0002 to 0.0006 mD. For the reference model, N = 4 and k_m = 0.004 mD. The status of the dynamic history matching is monitored according to the mismatch, and the iterations would terminate if the objective function is lower than a pre-determined tolerance (ΔO_{tol} $\leq$ 10%, according to Eq. 4-12). It is observed that the iterations would stop after approximately 104 to 120 iterations; for example, in this case study, it takes 10 outer loops and 13 inner loops for one particular set of initial realizations.

Selected successive changes in the prior and posterior distributions from iteration l to iteration $l+i$ are shown in Fig. 4-9, representing the probabilities for either staying at the current category k at step $l+1$ or transitioning to category k' at step $l+1$. The rows indicate some selected outer loops, and individual figures along each row represent some selected inner loop iterations corresponding to counter $i = l$ to $i = l+1$. The spikes observed in the figure reveal a reduction in the sampling variance, which indicates a level of convergence to a solution at the particular iteration step. Between loops 1 and 5, only T_{pf} is updated using the early time data. From loop 6 onwards, T_{pf} is not updated, with its value being drawn from the posterior distribution obtained at the end of loop 5, while P^{sf}_{32G}, r_e, and T_{sf} are updated using the late time data. Fig. 4-9 illustrates that the PPM algorithm has satisfactorily retained the non-Gaussian characteristics for different distributions during the parameter updating process, while Gaussian posterior distributions are generally expected with other sampling-based methods, such as EnKF. After obtaining the final posterior probability distributions, two additional realizations are sampled and the profiles of gas production rate, water production rate, and P_{wf} of all three history-matched realizations are shown in Fig. 4-10. A 5% noise is added to the production data. The results confirm that our method is robust and capable of handling noisy data.

Table 4-3 compares the distribution means of the model parameters for the initial and updated realizations. The updated values of the uncertain fracture parameters are different from those of the initial models, indicating that the RTA-derived mean values would only offer possible estimates for the initial models. Table 4-4 shows the comparison between the objective functions of the three history-matched realizations with the set objective function tolerance ($\Delta O_{tol} \leq 10\%$).

For all the uncertain parameters, the updated (history-matched) values are much closer to those in the reference model. In particular, a noticeable variation from the initial model is observed, indicating that the initial model, which is constrained based on RTA estimates alone, could only offer a preliminary estimate. For r_e, although the updated aperture (mean) value of 0.016 ft is not as close to the reference model (mean value of 0.029 ft), it still represents a much better match with the reference model, considering that the initial distribution was much wider and different. The variability exhibited by the final updated models illustrates the non-uniqueness of all history-matching inverse problems.

Table 4-3: Comparison of the uncertain DFN model parameters for the reference case, initial and updated realization.

Uncertain Parameter	Reference Model	Initial Model (Mean Values)	Updated Model (Mean Values)
Global Fracture Intensity (P^{sf}_{32G}), /ft.	0.190	0.250	0.193
Transmissivity T_{sf}, ft^2/sec	32.530	126.340	43.431
Transmissivity T_{pf}, ft^2/sec	357.600	855.100	391.910
Aperture $r_{e,}$ ft.	0.029	0.052	0.016

Table 4-4: Comparison of the objective function of the history matched realizations.

	ΔO_{tol}	Realization #1	Realization #2	Realization #3
0 – 90 days	10%	0.1732%	0.3050%	0.0844%
91 – 365 days	10%	8.7052%	9.5281%	8.5464%

The history matching framework adopted in this thesis demonstrates the possibilities of; handling non-Gaussian fracture parameters, handling the non-linear relationship between the uncertain fracture parameters and upscaled reservoir model properties, and implementing a flow regime-localization scheme for efficient history matching. It further presents a method for evaluating secondary fracture parameters, such as P^{sf}_{32G}, r_e, and T_{sf}; that are not readily inferred from existing well logs and microseismic interpretations.

It is acknowledged that there are limitations associated with the DPDK model for representing fracture geometry and the matrix–fracture flow interactions, as highlighted in the introduction, but considering that the focus of this thesis is to introduce a history-matching workflow for characterizing unknown fracture parameters, the emphasis is on the history matching scheme and less so on the simulation tool. The presented workflow can easily be modified to integrate with more advanced simulation tools (e.g., EDFM). Future studies will incorporate other methods of fluid flow simulation for the multi-stage hydraulically fractured reservoir.

4.6 CONCLUSION AND RECOMMENDATION

a) This research adopted the probability perturbation method for history matching of multi-staged fractured unconventional wells. This method has not been employed for this particular application previously. Most importantly, a new localization scheme based on flow regimes is added.

b) The implementation shows the flexibility of the framework to handle non-Gaussian fracture parameters. The workflow also handles the non-linear relationship between fracture parameters and upscaled reservoir model properties directly by perturbing the probabilities of the uncertain fracture parameters (using a macro file representation of the DFN model).

c) The localization scheme for history matching designed for the method facilitates efficient history matching by perturbation of the impacting parameters of the model according to the specific flow region.

d) A significant advantage of this approach is that the uncertainties in fracture parameters are quantified using multiple DFN models and their corresponding upscaled flow-simulation models.

e) The updated (history-matched) values of the uncertain fracture parameters show a noticeable variation from the initial model; indicating that the initial model, which is constrained based on RTA estimates alone, could only offer a preliminary estimate. A more rigorous history matching procedure, such as that presented in this thesis, is required for properly inferring the inherent uncertainties.

f) Future studies will extend this technique to modeling spatially varying uncertain fracture parameters with a more complex distribution of secondary fractures for several field cases. Effects of natural fractures should also be considered.

4.7 REFERENCES

Ahmed, R., Edwards, M.G., Lamine, S., Huisman, B.A.H., Pal, M. 2015. Three-Dimensional Control-Volume Distributed Multi-Point Flux Approximation coupled with a Lower-Dimensional Surface Fracture Model. Journal of Computational Physics, 303(2015), 470 – 497. https://doi.org/10.1016/j.jcp.2015.10.001

Ali, A.J., Siddiqui, S., Dehghanpour, H. 2013. Analyzing the Production Data of Fractured Horizontal Wells by a Linear Triple Porosity Model: Development of Analysis Equations. Journal of Petroleum Science and Engineering. 112 (2013), 117 – 128. https://doi.org/10.1016/j.petrol.2013.10.016

Al-Shaalan, T.M., Fung, L.S.K., Dogru, A.H. 2003. A Scalable Massively Parallel Dual-Porosity Dual-Permeability Simulator for Fractured Reservoirs with Super-k Permeability. SPE 84371-MS, SPE Annual Technical Conference and Exhibition, Denver, Colorado, 5–8 Oct 2003. https://doi:10.2118/84371-MS

Bello, R.O., Wattenbarger, R.A. 2010. Multi-stage Hydraulically Fractured Shale Gas Rate Transient Analysis. SPE-126754-MS, SPE North Africa Technical Conference and Exhibition, Egypt. https://doi.org/10.2118/126754-MS

Blasingame, T.A., Johnston. J.L., Lee. W.J. 1989. Type-Curves Analysis Using the Pressure Integral Method. SPE-18799-MS. SPE California Regional Meeting, 5 – 7 April, Bakersfield, California. https://doi.org/10.2118/18799-MS

Bourdet, D. 2002. Well Test Analysis: The Use of Advanced Interpretation Models. Handbook of Petroleum Exploration and Production, ISSN 1567-8032; Vol 3. Elsevier Science.

Brent, R.P. 1973. Algorithms for Minimization without Derivatives. Prentice- Hall, Englewood Cliffs, New Jersey. ISBN: 0-13-022335-2.

Bui, T.D., Mamora, D.D., Lee, W.J. 2000. Transient Pressure Analysis for Partially Penetrating Wells in Naturally Fractured Reservoirs. SPE 60289-MS, SPE Rocky Mountain Regional/Low Permeability Reservoirs Symposium and Exhibition, Denver, Colorado, 12–15 Mar 2000. https://doi:10.2118/60289-MS

Bustin, R.M., Bustin, A.M.M., Cui, X., Ross, D.J.K., Pathi, V.S.M., 2008. Impact of Shale Properties on Pore Structure and Storage Characteristics. In: Presented at the SPE Shale Gas Production Conference, Fort Worth, Texas, USA, 16–18 November. SPE 119892. https://doi.org/10.2118/119892-MS

Caers, J. 2003. History Matching Under Training-Image-based Geological Model Constraints. SPE Journal, 8(03), pp.218-226. 10.2118/74716-PA

Caers, J. 2007. Comparing the Gradual Deformation with the Probability Perturbation Method for Solving Inverse Problems. Mathematical Geology 39(1), 27-52. https://doi.org/10.1007/s11004-006-9064-6

Chai, Z., Yan, B., Killough, J.E., Wang, Y. 2016. An Efficient Method for Fractured Shale Reservoir History Matching: The Embedded Discrete Fracture Multi-Continuum Approach. SPE-181765-MS. SPE Annual Technical Conference and Exhibition, Dubai, UAE. https://doi.org/10.2118/181765-MS

Chen, H., Yang, C., Datta-Gupta, A., Zhang, J., Chen, L., Liu, L., Chen, B., Cui, X., Shi, F., Bahar, A. 2019. A Hierarchical Multiscale Framework for History Matching and Optimal Well

Placement for a HPHT Fractured Gas Reservoir, Tarim Basin, China. IPTC-19314-MS. International Petroleum Technology Conference, Beijing China. https://doi.org/10.2523/IPTC-19314-MS

Chen, Y., Oliver, D.S., 2012. Ensemble Randomized Maximum Likelihood Method as an Iterative Ensemble Smoother. Math. Geosci. 44 (1), 1–26. https://doi.org/10.1007/ s11004-011-9376-z

Chen, Y., Durlofsky, L.J., Gerristen, M., Wen, X.H., 2003. A Coupled Local-Global Upscaling Approach for Simulating Flow in Highly Heterogeneous Formations. Advances in Water Resources. 26 (10), 1041–1060. https://doi.org/10.1016/S0309-1708(03)00101-5

Cinco-ley, H. 1996. Well-Test Analysis for Naturally Fractured Reservoirs. SPE-31162-JPT. Journal of Petroleum Technology 48(01). https://doi.org/10.2118/31162-JPT

Cui, H., Kelkar, M. 2005. Automatic History Matching of Naturally Fractured Reservoirs and a Case Study. SPE-94037-MS. Western Regional Meeting, Irvine, California, 30 March-1 April. https://doi.org/10.2118/94037-MS

De Lima, A., Lange, A., Schiozer, D.J., 2012. Assisted History-Matching for the Characterization and Recovery Optimization of Fractured Reservoirs using Connectivity Analysis. SPE 154392. SPE Europec/EAGE Annual Conference. https://doi.org/10.2118/154392-MS

Dershowitz, B., LaPointe, P., Eiben, T. et al. 2000: Integration of Discrete Feature Network Methods with Conventional Simulator Approaches. SPE Res Eval & Eng 3 (2): 165-170. SPE-62498-PA. http://dx.doi.org/10.21186/62498-PA

Dershowitz, W. S. (1984): Rock Joint Systems. Ph.D. Thesis, Massachusetts Institute of Technology, Cambridge, Massachusetts.

Dershowitz, W.S. 1993. Geometric Conceptual Models for Fractured Rock Masses: Implications for Groundwater Flow and Rock Deformation. ISRM-EUROCK-1993-010, Second European Conference of the International Society for Rock Mechanics, Lisbon, Portugal, 21–24 June. https://www.onepetro.org/conference-paper/ISRM-EUROCK-1993-010

De Swaan, O.A. 1976. Analytical Solutions for Determining Naturally Fractured Reservoir Properties by Well Testing. SPE 5346-PA. SPE J. 16(3), 117–122 (1976). https://doi:10.2118/5346-PA

Emerick, A.A., Reynolds, A.C., 2012. Combining the ensemble Kalman Filter with Markov-chain Monte Carlo for Improved History Matching and Uncertainty Characterization. SPE-141336-PA. SPE J. 17 (2), 418–440. https://doi.org/10.2118/ 141336-PA

Ezulike, O.D., Ghanbari, E., Siddiqui, S., Dehghanpour, H. 2015. Pseudo-Steady State Analysis in Fractured Tight Oil Reservoirs. Journal of Petroleum Science and Engineering. 129 (2015), 40 – 47. https://doi.org/10.1016/j.petrol.2015.01.009

Ezulike, O. D., Dehghanpour, H. 2015. A Complementary Approach for Uncertainty Reduction in Post-Flowback Production Data Analysis. Journal of Natural Gas Science and Engineering. 27(2), 1074 – 1091. https://doi.org/10.1016/j.jngse.2015.09.059

Fisher, R.A. 1953. Dispersion on a Sphere. The Royal Society of London. Series A, Mathematical and Physical Sciences. A217 (1130), 295-305. https://doi.org/10.1098/rspa.1953.0064

Fisher, M.K., Wright, C.A., Davidson, B.M., Goodwin, A.K., Fielder, E.O., Buckler, W.S., Steinsberger, N.P. 2003. Integrating Fracture Mapping Technologies to Optimize Stimulations in the Barnett Shale. SPE-77441-PA. SPE Production & Facilities. 20 (02), 85-93. https://doi.org/10.2118/77441-PA

Golder Associates. 2018. FRACMAN 7.70 User Documentation. Copyright 1999 – 2018.

Hu, B.X., Huang, H. 2002. Stochastic Analysis of Reactive Solute Transport in Heterogeneous, Fractured Porous Media: a Dual-Permeability Approach. Trans. Porous Med. 48(1), 1–39. https://doi:10.1023/A:1015671227317

Hu, L.Y., Jenni, S., 2005. History Matching of Object-Based Stochastic Reservoir Models. SPE Journal 10 (3), 312–323. https://doi.org/10.2118/81503-PA

KAPPA Engineering, 2019. Dynamic Data Analysis – v5.20.02 - ©KAPPA 1988 - 2019

Kashib, T., Srinivasan, S. 2006. A Probabilistic Approach to Integrating Dynamic Data in Reservoir Models. Journal of Petroleum Science and Engineering. 50, 241 – 257. https://doi.org/10.1016/j.petrol.2005.11.002

Linde, N., Renard, P., Mukerji, T., Caers, J., 2015. Geological Realism in Hydrogeological and Geophysical Inverse Modeling: A Review. Adv. Water Resour. 86 (Part A), 86–101. https://doi.org/10.1016/j.advwatres.2015.09.019

Liu, Y., Leung, J.Y., Chalaturnyk, R., Virues, C.J.J. 2019. New Insights on Mechanisms Controlling Fracturing Fluid Distribution and its Impacts on Well Performance in Shale Gas

Reservoirs. SPE Production & Operations 34(3): 564-585. https://doi-org/10.2118/185043-PA.

Liu, Y., Liu, L., Leung, J. Y., Moridis, G. J. 2020. Sequentially Coupled Flow and Geomechanical Simulation with a Discrete Fracture Model for Analyzing Fracturing Fluid Recovery and Distribution in Fractured Ultra-Low Permeability Gas Reservoirs. Journal of Petroleum Science and Engineering, 189, 107042. https://doi.org/10.1016/j.petrol.2020.107042

MathWorks, 2020. MATLAB Documentation. https://www.mathworks.com/help/matlab/index.html

Monteagudo, J.E.P., Firoozabadi, A. 2004. Control-Volume Method for Numerical Simulation of Two-Phase Immiscible Flow in Two-and Three-Dimensional discrete-Fractured Media, Water Resources Research. 40(7) (2004) W074051–W0740520, http://dx.doi.org/10.1029/2003WR002996

Nejadi, S., Leung, J.Y., Trivedi, J.J. 2015. Integrated Characterization of Hydraulically Fractured Shale-Gas Reservoirs - Production History Matching. SPE Res Eval & Eng **18** (04): 481–494. SPE-171664-PA. https://doi.org/10.2118/171664-PA.

Nejadi, S., Trivedi, J.J., Leung, J. 2017. History Matching and Uncertainty Quantification of Discrete Fracture Network Models in Fractured Reservoirs. Journal of Petroleum Science and Engineering. 152, 21–32. http://dx.doi.org/10.1016/j.petrol.2017.01.048

Nwabia, F.N., Leung, J.Y. 2021. Inference of Hydraulically Fractured Reservoir Properties from Production Data Using the Indicator-Based Probability Perturbation Assisted History-

Matching Method. Journal of Petroleum Science and Engineering 198, 108240. ISSN 0920-4105. https://doi.org/10.1016/j.petrol.2020.108240

Oda, M. 1985. Permeability Tensor for Discontinuous Rock Masses. Geotéchnique **35** (4): 483 – 495. https://doi.org/10.1680/geot.1985.35.4.483

Sandve, T.H., Berre, I., Nordbotten, J.M. 2012. An Efficient Multi-Point Flux Approximation Method for discrete Fracture–Matrix Simulations. Journal of Computational Physics. 231(09), 3784–3800. https://doi.org/10.1016/j.jcp.2012.01.023

Schlumberger, 2017. ECLIPSE Reference Manual Version 2017.2.

Schlumberger, 2017. ECLIPSE Technical Description Version 2017.2.

Shakiba, M., de Araujo Cavalcante Filho J., Sepehrnoori, K. 2018. Using Embedded Discrete Fracture Model (EDFM) in Numerical Simulation of Complex Hydraulic Fracture Networks Calibrated by Microseismic Monitoring Data. Journal of Natural Gas Science and Engineering, 55(2018), 495-507. ISSN 1875-5100. https://doi.org/10.1016/j.jngse.2018.04.019

Suzuki, S., Daly, C., Caers, J.K., Mueller, D., 2007. History Matching of Naturally Fractured Reservoirs using Elastic Stress Simulation and Probability Perturbation Method. SPE-95498-PA. SPE J. 12 (1), 118–129. https://doi.org/10.2118/95498-PA

Van Heel, A.P.G., Boerrigter, P.M., Van Dorp, J.J. 2008. Thermal and Hydraulic Matrix-Fracture Interaction in Dual Permeability Simulation. SPE 102471-PA. SPE Reservoir Evaluation Eng. 11(4), 735–749. http://doi:10.2118/102471-PA

Wang, H. 2018. Discrete Fracture Networks Modeling of Shale Gas Production and Revisit Rate Transient Analysis in Heterogeneous Fractured Reservoirs. Journal of Petroleum Science and Engineering. 169, 796 – 812. https://doi.org/10.1016/j.petrol.2018.05.029

Wang, M., Leung, J.Y. 2015. Numerical Investigation of Fluid-Loss Mechanisms During Hydraulic Fracturing Flow-Back Operations in Tight Reservoirs. Journal of Petroleum Science and Engineering 133: 85-102. https://doi.org/10.1016/j.petrol.2015.05.013

Warren, J.E., Root, P.J. 1963. The Behavior of naturally Fractured Reservoirs. SPE 426-PA. SPE J. 3(3), 245–255. http://doi:10.2118/426-PA

Yue, M., Leung, J.Y., Dehghanpour, H. 2016. Numerical Investigation of Limitations and Assumptions of Analytical Transient Flow Models in Tight Oil Reservoirs. Journal of Natural Gas Science and Engineering 30: 471-486. https://doi.org/10.1016/j.jngse.2016.01.042

Zidane, A., Firoozabadi, A. 2014. An Efficient Numerical Model for Multicomponent Compressible Flow in Fractured Porous Media, Advances in Water Resources. 74, 127–147. https://doi.org/10.1016/j.advwatres.2014.08.010

APPENDIX – *Figures*

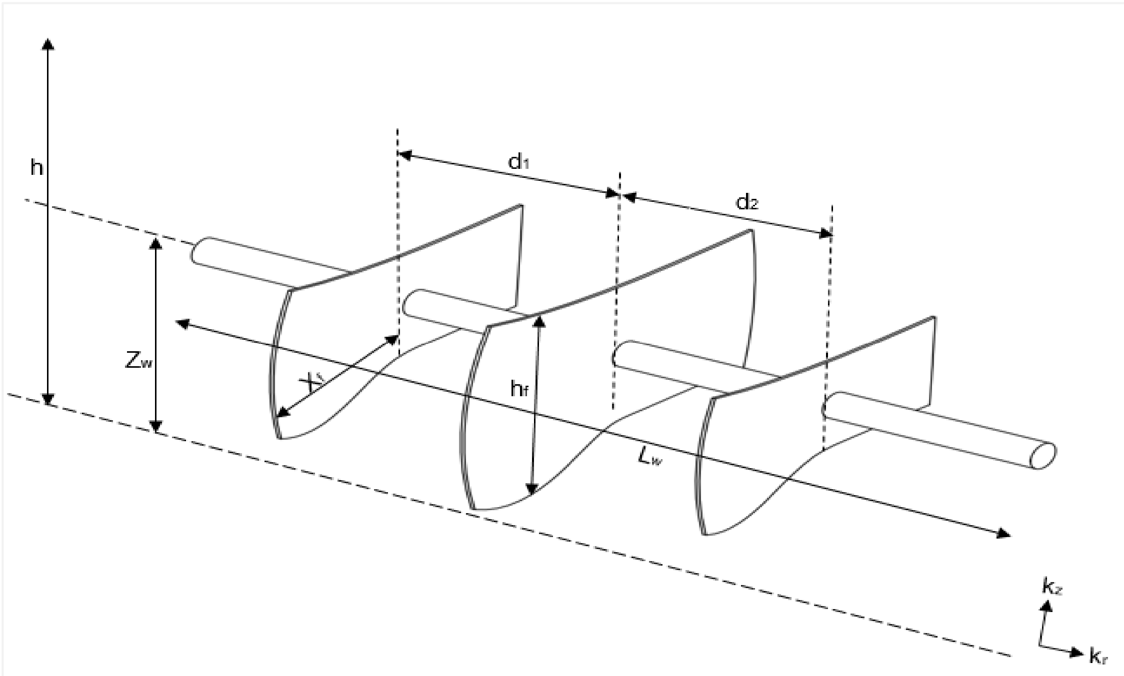

Fig. 4-1: Schematic of a fractured horizontal well and dimensions.

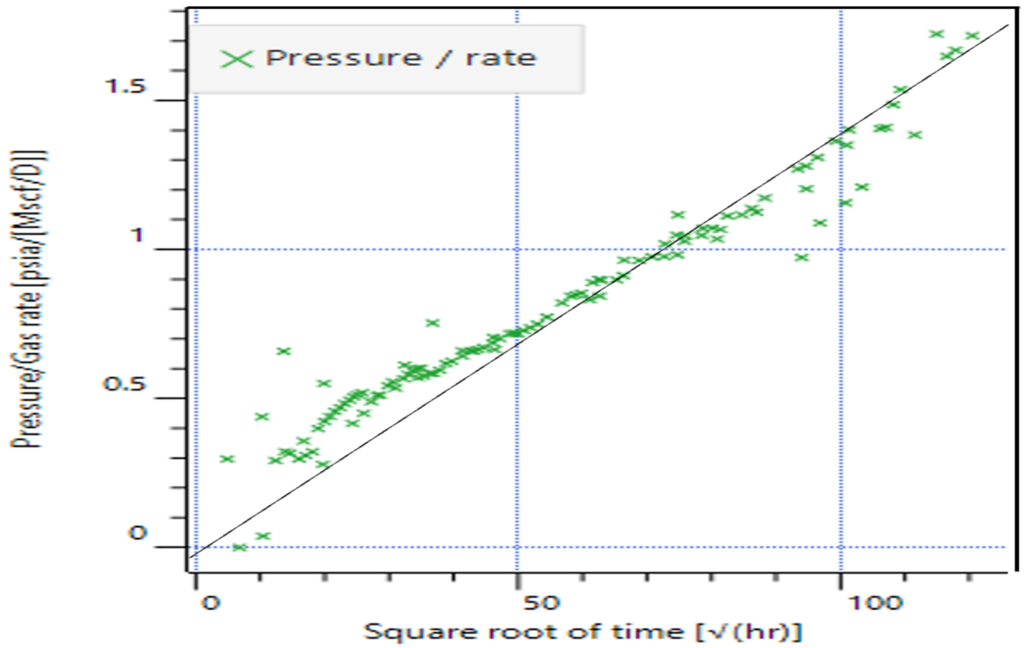

Fig. 4-2: Specialized linear square root plot for gas case

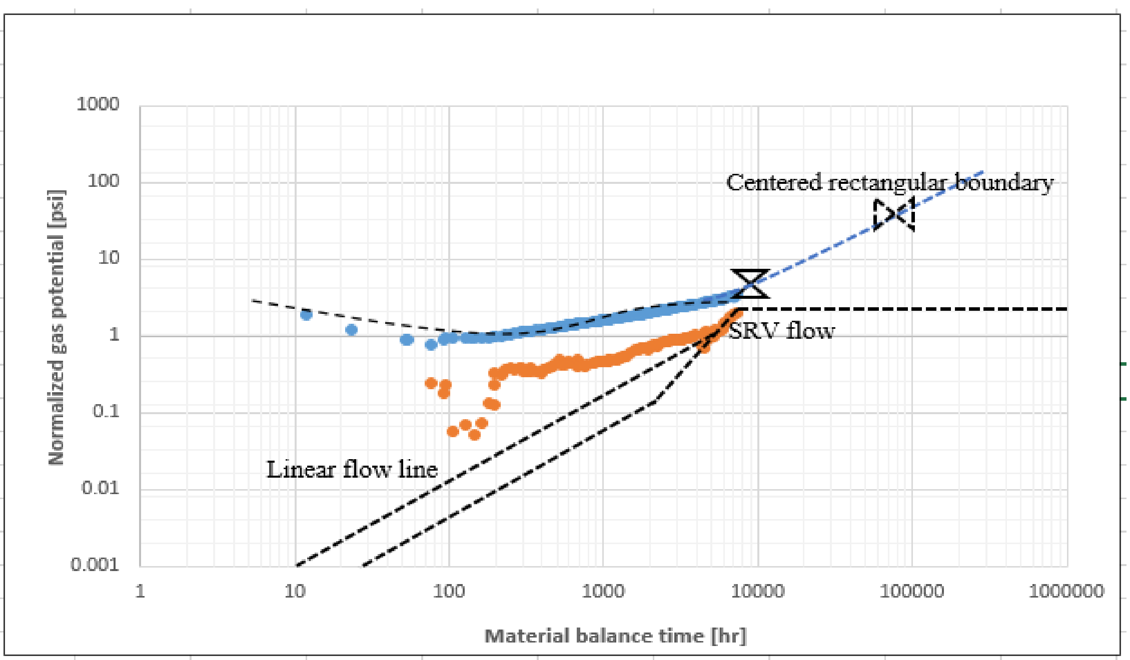

Fig. 4-3: Log-log plot of rate normalized pressure (*RNP*) integral and its derivative versus material balance time (*te*) [blue – integral; brown – derivative].

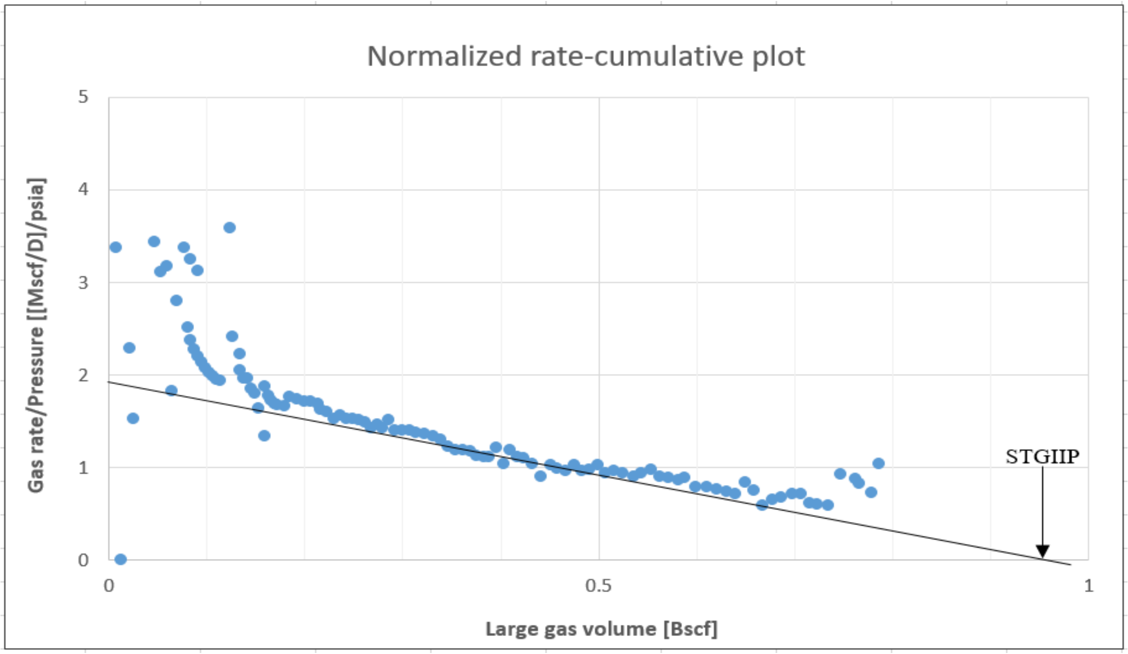

Fig. 4-4: Normalized rate-cumulative plot.

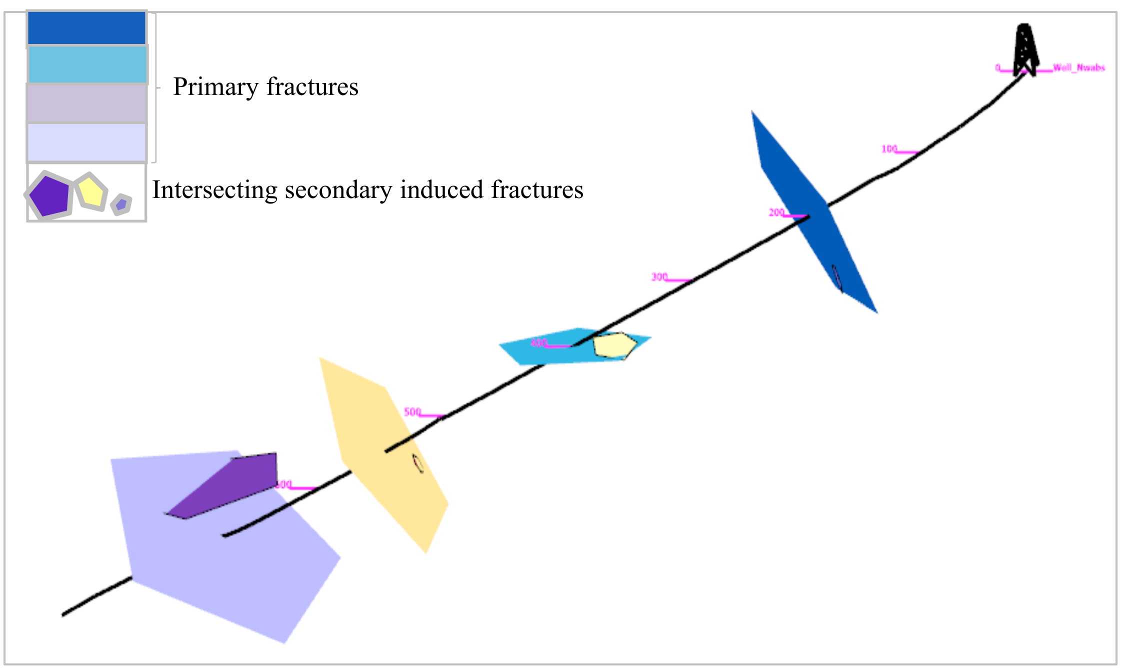

Fig. 4-5: Diagram showing the primary fractures and the intersecting secondary induced fractures.

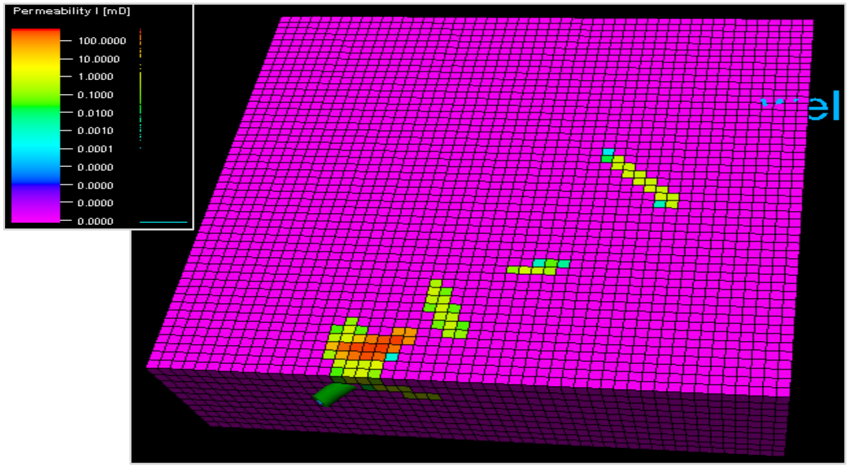

Fig. 4-6: Schematic representation of the upscaled DPDK model with an indication of PERMZ (permeability along the z-direction).

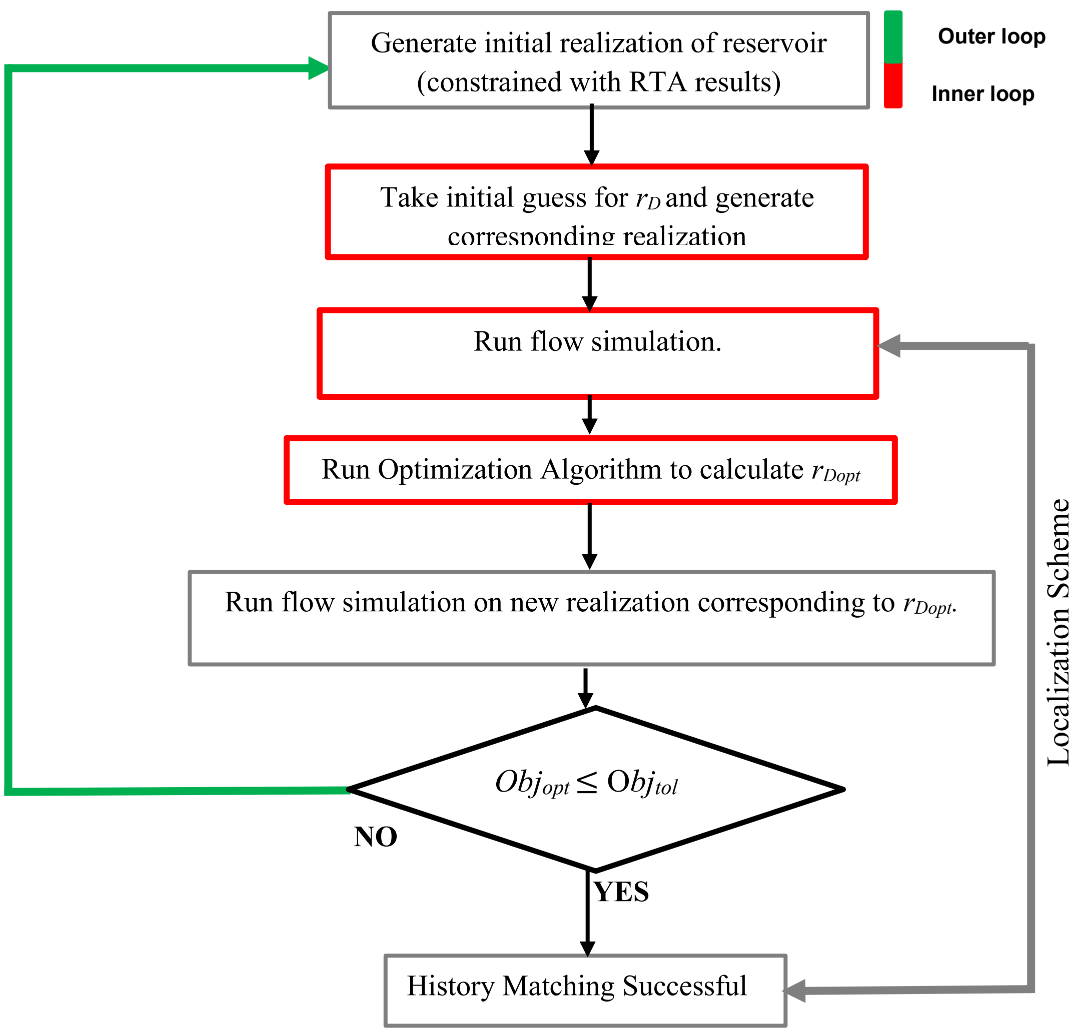

Fig. 4-7: Flowchart describing the procedure for probability perturbation method and objective function optimization.

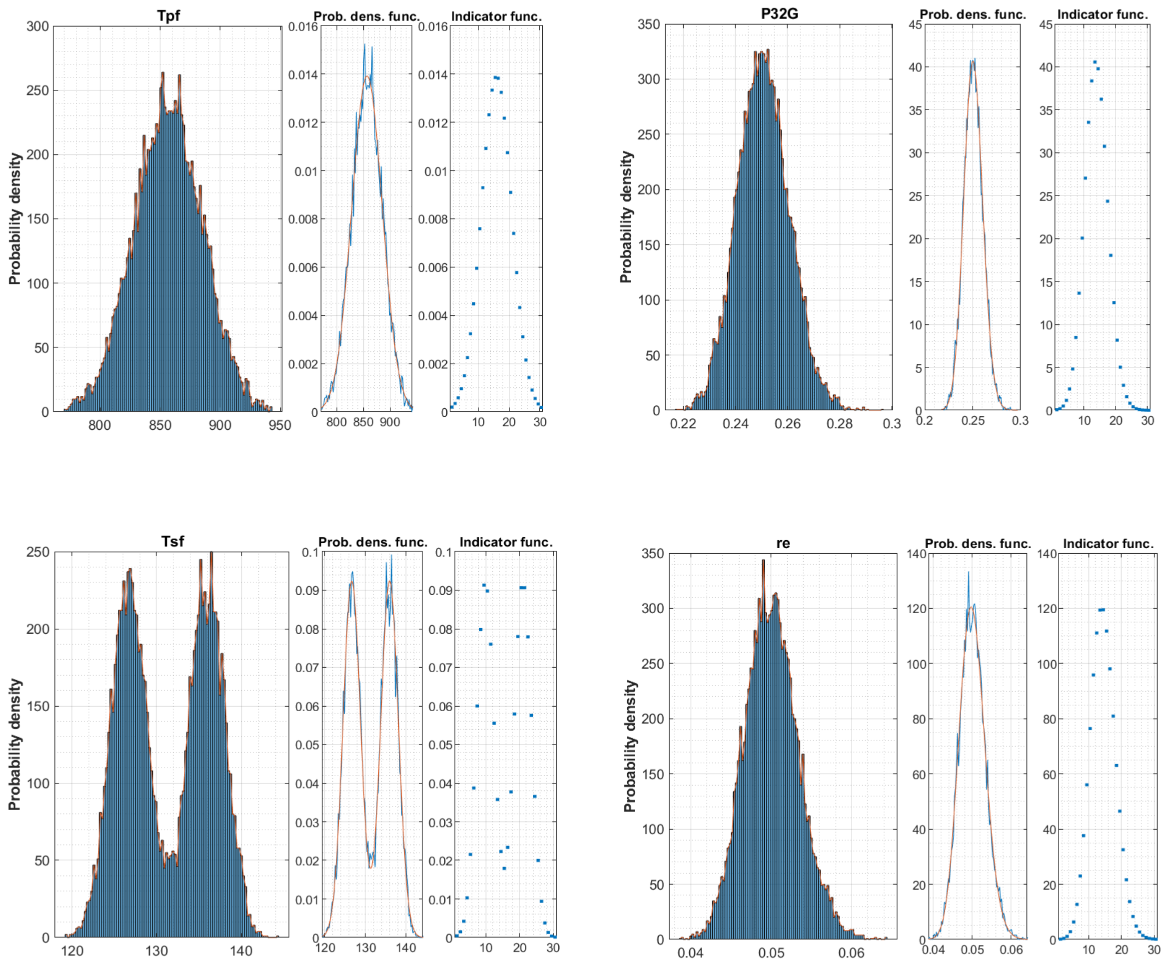

Fig. 4-8: Initial probability density functions of P^{sf}_{32G}, T_{pf}, T_{sf}, and r_e.

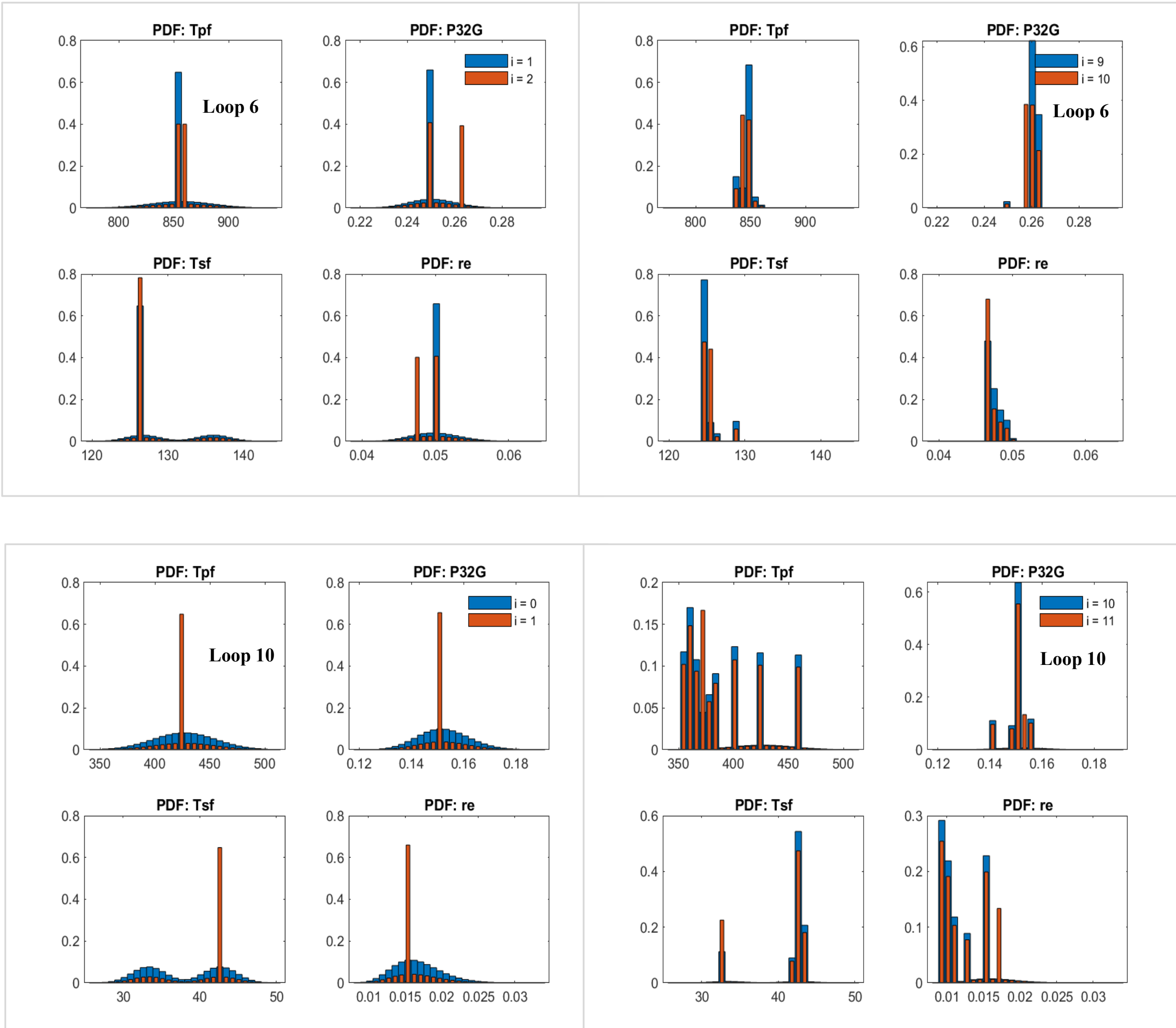

Fig. 4-9: Comparison between (selected) prior and posterior distributions for the iteration step i to i+1, where i = l = iterative index.

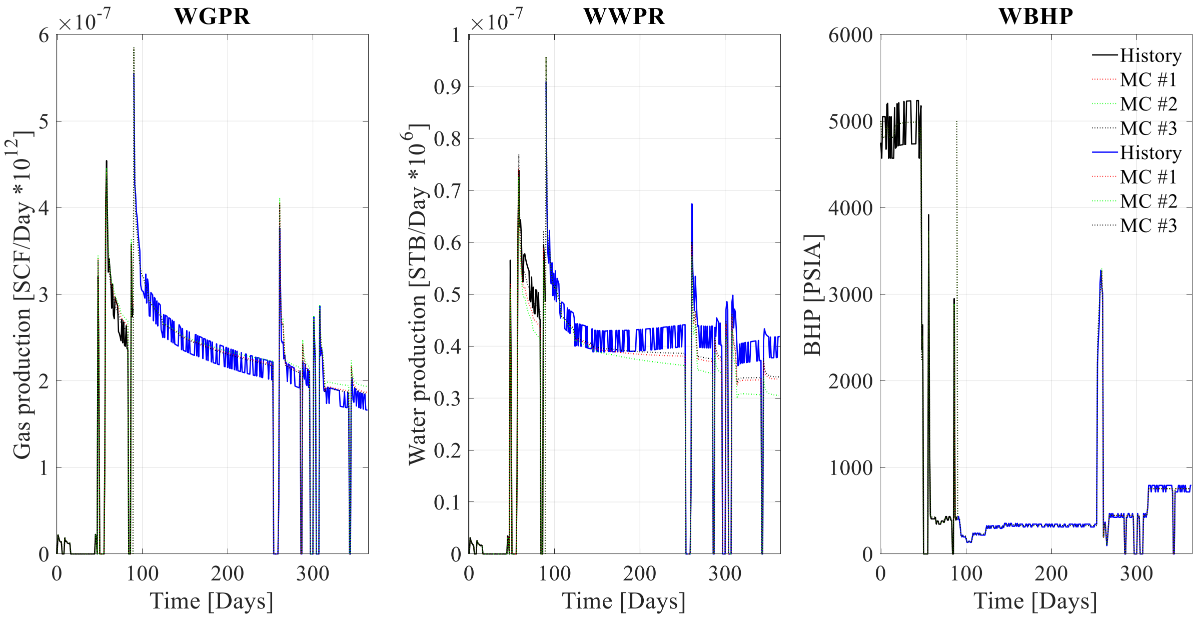

Fig. 4-10: Gas production, water production and BHP profiles of history matched realizations sampled from the final posterior probability distributions

[black – early time; blue – late time).

Chapter 5: Incorporating the Variability of Uncertain DFN Model Parameters of a Hydraulically Fractured Reservoir during Probabilistic-Based Assisted History Matching: Findings and Deductions

5.1 OVERVIEW

Discrete fracture network (DFN) models can explicitly represent the geometrical properties of each individual fracture (e.g., size, orientation, shape, and aperture) and fracture sets, where these comprising fracture properties are sampled from specific probability distributions. Nevertheless, integrating these DFN models during a production history matching remains difficult. A robust model updating technique, with the capabilities of incorporating the variability in the fracture parameters across hydraulic fracture stages and mitigating the uncertainty inherent in the non-linear relationship between a set of fracture parameters and the corresponding upscaled reservoir model properties, is required. It is important to update pertinent DFN model parameters, such that they are calibrated to both stochastic reservoir models and dynamic production data.

Rate transient analysis (RTA) interpretations are used to infer the prior probability distributions of the unknown varying DFN parameters across each stage of the hydraulic fracture and the intersecting secondary fractures associated with each hydraulic fracture stage; an ensemble of the initial DFN models are sampled. This is followed by a numerical multiphase flow simulation of the upscaled model and a comparison between the predicted production responses with the actual historical data. An indicator-based probability perturbation method is then used to minimize the objective function and consequently reduce the uncertainties in the unknown fracture parameters.

An essential detail is those flow regimes identified through RTA study are used to develop a localization scheme, where multiple flow regimes are inferred from the production data, and different portions of the production data are used to perturb specific model parameters corresponding to that particular flow regimes. The adoption of localization schemes is targeted at improving the convergence behavior of such ill-posed inverse problems. The designed probabilistic framework characterizes the posterior probability distributions of twenty-four DFN parameters of a multi-staged (4 stages) hydraulically-fractured horizontal shale gas well in the Horn River Basin: primary fracture transmissivity (T_{pf}), secondary fracture aperture (r_e), secondary fracture transmissivity (T_{sf}), global fracture intensity of the secondary fracture (P^{sf}_{32G}), secondary fracture length (*L)* and height (*H*); The proposed approach does not only sample multiple realizations of the DFN model, but it also updates (through the adopted history matching workflow) the probability distributions of these impacting DFN parameters. The results reveal the flexibility in obtaining unknown secondary fracture parameters that are not easily inferred by other methods such as cores and microseismic interpretations.

5.2 INTRODUCTION

The combination of horizontal drilling and hydraulic fracturing, which is also termed hydraulically fractured horizontal wells, has immensely contributed to the improved production from unconventional (tight and shale) reservoirs in recent years. This practice involves horizontal directional drilling of well into the tight formation along with the injection of water, sand, and chemicals at high pressures to create fissures in the shale rock. Despite the successes with hydraulic fracturing and horizontal drilling, the presence of highly heterogeneous, multi-scale, fracture systems renders any detailed characterization of the fracture properties, a prerequisite for future reservoir forecast, to be difficult. A particular challenge is related to the complex geometries of the secondary fractures (intersected with or reactivated by a hydraulic fracture) – their distribution is generally correlated to the position/orientation of a hydraulic (primary) fracture. Another difficulty stems from the high contrast in permeability between the matrix and fracture systems which amplifies the nonlinearity (uncertainty) between the fracture model parameters and recorded flow responses. Consequently, an efficient procedure, which would mitigate these challenges is essential to update both hydraulic and secondary fracture parameters per stage whilst integrating both static (e.g., core/ logs) and dynamic data (e.g., rate and pressure measurements) for reliable production forecast and to optimize development strategies.

Detailed characterization of fractured reservoirs is firstly challenged by data paucity leading to the combination of information and measurements from different sources. Image logs and results from core data analysis can be used to infer the uncertain statistics of fracture parameters like orientation, half-length, intensity, aperture, height, and permeability. In some cases, acoustic data, such as microseismic events, has been used to infer fracture orientation (e.g., trend and plunge). Analytical models of rate transient analysis (RTA) have been useful for deriving fractured reservoir flow regimes and fracture parameters from production data. One of the early RTA studies was performed by Bello et al., 2010, which presented an analytical model for a dual-porosity medium, and the model was used to analyze production rate data for identifying five flow regimes. Many improved models have since been proposed to capture additional physics in different reservoir settings: shale gas (Agarwal et al., 1999), tight gas (Zuo et al., 2016), and tight oil (Clarkson et al., 2010; Uzun et al., 2016). Although RTA techniques are widely adopted for analyzing production data obtained from hydraulically fractured horizontal wells in tight or shale reservoirs, the major drawback of these analytical models are the many assumptions involved: e.g., homogeneous reservoir properties, rendering it difficult to be integrated for generating stochastic realizations of fracture parameters or DFN models. Yet, there are limited studies that integrate results from these analytical models for constraining DFN models.

The next challenge concerning fractured reservoir characterization is the complexity associated with numerical simulation of multiphase flow in fractured porous media. Detailed representation of discrete fractures (accounting for its geometry and the matrix–fracture flow interaction physics). One common approach is the dual-porosity (DP) model, which is used to represent a fractured medium with an equivalent continuum model. In the DP model, the fracture system is considered as the only flow path directly connected to the wellbore. An alternative, which is the dual-porosity dual-permeability (DPDK) model, considers all inter-porosity flows between the matrix system, fracture network, and the wellbore. With the DPDK models, regularly spaced matrix blocks separated by a fracture network are utilized to replace a domain with randomly-distributed discrete fractures; a set of effective (upscaled) parameters are used to define this equivalent system for fluid flow modeling (Warren and Root, 1963; Kazemi, 1976; Uleberg and Kleppe, 1996; Bui et al., 2000). The method is effective when the fractures are densely populated and well-connected (Vo et al., 2019). In recent years, the Embedded Discrete Fracture Model (EDFM) technique serves as an improvement to the DPDK model and an alternative approach to the more complex DFN flow simulations: complex fracture networks are embedded in a set of structured matrix blocks without utilizing local grid refinement or unstructured gridding (Yu et al., 2018; Torres et al., 2020). Since the main focus of this research is to introduce a history-matching workflow for characterizing unknown fracture parameters, the emphasis is on the history matching scheme and less so on the simulation tool. Thus, the DPDK model is used: equivalent porous medium properties, such as permeability tensor and shape parameters, are assigned to each reservoir cell consisting of both matrix and fracture continua via upscaling techniques (Nwabia and Leung, 2020). The approach developed by Oda, 1985 is used to compute these effective properties

History matching (HM), which is the task of integrating production data to infer the distributions of uncertain model (fracture) properties, is generally an ill-posed inverse problem with non-unique solutions. Optimization-based methods (e.g., maximum a-posterior), ensemble-based methods (Ensemble Kalman Filter - EnKF and Ensemble Smoother - EnS), and sampling-based techniques (e.g., Monte Carlo Markov Chain or MCMC and gradual deformation) are some common HM algorithms, which can be used for characterizing fracture network models, by updating either the equivalent model parameters or specific discrete fracture properties. A number of probabilistic approaches, such as the gradual deformation method first introduced by Hu (2000) and subsequently modified in Hu (2002) can be used for updating probability distributions of uncertain model parameters. However, though the gradual deformation method is easy to implement, it is only applicable for modeling properties that follow a Gaussian distribution, which is generally not a valid assumption for fracture properties. Another technique, the probability perturbation method (PPM) that was developed by Caers, 2003, is more flexible for handling non-Gaussian distributions. In our previous work, Nwabia and Leung (2021), a HM workflow based on the PPM was developed to characterize hydraulic fracture parameters (e.g., primary fracture transmissivity) and induced fracture parameters (e.g., length, aperture, intensity) using a DPDK simulation model); however, variability in fracture parameters across different stages was not considered. Chai et al. (2016) proposed a two-stage MCMC method with EDFM for characterizing different porosity distributions corresponding to the secondary fractures, hydraulic fractures, organic matrix, and inorganic matrix of shale reservoirs. However, the MCMC approach may require several iterations to arrive at a stable converged solution (Tripoppoom, 2019). Ensemble-based methods, such as EnKF (Emerick and Reynolds, 2011) and EnS (Chai et al., 2018; Chang and Zhang, 2018), which utilize the covariance matrix to update an ensemble of parameters, have also gained wide attention for their advantages in data assimilation and uncertainty quantification. Its major limitation is that it assumes multi-Gaussian distribution on model and data variables and a linear relationship between all variables, and these assumptions do not hold for fractured reservoirs.

A PPM workflow that integrates relevant RTA-derived information is applied in this research thesis. It can handle non-Gaussian fracture parameters and facilitate the estimation of the posterior probability distribution, from which multiple realizations can be sampled. Properties derived from RTA are used to constrain the initial distributions of the uncertain fracture parameters (length, height, aperture, intensity, and transmissivity), and the derived flow regimes are used to formulate a localization scheme where individual segments of the production data are used to tune only a specified subset of the unknown model parameters. In contrast to our previous work (Nwabia and Leung, 2021), the unknown hydraulic fracture model parameters can vary among different stages. The proposed PPM framework offers a direct means of updating unknown model parameters in the DFN domain and subsequently upscaling them into a DPDK model for multiphase flow simulation, thus creating the representation of uncertainties in fracture parameters with multiple DFN realizations and their corresponding upscaled flow-simulation models. A case study of a synthetic case of a hydraulically fractured shale reservoir in the Horn River basin is presented.

5.3 STUDY PROCEDURE

5.3.1 Rate Transient Analysis to Constrain DFN Model Parameters

The schematic representation in Fig. 5-1 (*Appendix – B*) shows the fractured horizontal well model commonly used for unconventional gas analysis and production forecasting. It is adapted to represent a four-stage hydraulically fractured horizontal well located in the center of a rectangular domain with no-flow outer boundaries.

The plot of rate normalized pressure and the square root of time and log-log plot of rate normalized pressure (*RNP*) integral and its derivative versus equivalent time (t_e) is analyzed to obtain the dominant flow regimes, where the matrix-fracture area (A_{cm}), matrix permeability (k_m), fracture half-length (X_f) and *SRV* can be derived. Both the *RNP* integral and its derivative are preferred because they are useful for smoothening noisy data. Various flow regimes can be identified from the plot of *RNP* versus t_e. Eq. (5-1) and Eq. (5-2) (in Appendix – A) and equations in Appendix A.1 represent the equations for defining the RNP versus √t, and *RNP* integral and its derivative versus t_e. The equivalent time, otherwise known as the material balance time (*MBT*), is the ratio of the cumulative production as a function of time and fluid (gas) production rate with time, $t_e = \frac{Q(t)}{q(t)}$.

From the RTA, an initial linear flow period corresponding to a half-slope and the pseudo steady-state flow (*PSS*) corresponding to a unit slope are observed. Fracture parameters, such as A_{cm} is estimated from the initial linear flow from the matrix into the hydraulic fracture with infinite conductivity, while properties representing pressure interference between consecutive hydraulic fractures are estimated from the *PSS* flow (k_m, X_f, *SRV*). These estimated fracture properties are used to derive the initial distributions of the hydraulic and induced fracture parameters necessary for the construction of the DFN model (global induced fracture intensity P^{sf}_{32G}, the secondary fracture aperture r_e, transmissivities of the primary T_{pf} and induced fractures T_{sf}).

5.3.2 DFN Modeling Incorporating Unknown Multi-Stage Hydraulic Fracture Properties

In this work, each hydraulic fracturing stage is modeled as an elongated penny-shaped crack (primary fracture) with intersecting randomly distributed secondary or induced fractures connected to the primary fracture, according to Fisher et al., 2005 – Fig. 5-2. The secondary fractures are induced fractures initiated as cracks on the hydraulic fracture surfaces. It is assumed that the hydraulic and induced fractures are the dominant fractures; thus, the impacts of other natural fractures on primary fracture geometry and its reactivation are assumed to be negligible. Each set of induced fractures is specified based on the nearest neighbour model, where the local fracture intensity (P_{32L}) decays exponentially with the distance to the hydraulic fracture – Eq. (5-3) (Appendix – A). The model is based on several empirical parameters: c is typically inferred from image log data; *b* controls how quickly the induced fracture intensity decreases with distance away from the hydraulic fracture; *d* is the distance between location x and the primary fracture plane (Dershowitz, 1993).

The initial distributions of the unknown DFN model parameters (T_{sf}, P^{sf}_{32G}, T_{pf}, r_e, L and H) vary for each individual hydraulic fracture stage, and their updating during history matching will be performed simultaneously for all the fracture stages.

5.3.3 Probability Perturbation and Flow Regime-Based Localized History Matching

The creation of the DFN model with varying unknown fracture parameters across fracture stages is followed by model upscaling and PPM history-matching.

The implications of the DFN model on flow and transport at the regional scale are evaluated by transforming the DFN model into an equivalent DPDK simulation model (in this case matrix-fracture coupling, fracture porosity, and Oda permeability tensor) following Oda, 1985 static upscaling scheme. This scheme is selected since it can be calculated without requiring flow simulations, thus it is more computationally efficient in comparison to other flow-based upscaling schemes. The fracture porosity is calculated as the product of the average cross-sectional area and aperture divided by the cell volume. The 3 × 3 Oda permeability tensor is estimated based on the projection of the fracture isotropic permeability onto the fracture plane and scaling according to the fracture porosity as in Eq. (5-4) – (5-5) (Appendix A). The sigma factor or shape factor creates a means of matrix-fracture interaction and it is represented mathematically in Eq. (5-6) (Appendix – A).

With the DFN upscaling completed, numerical simulation of the DPDK model is performed using ECLIPSE (Schlumberger, 2017) commercial black-oil simulator.

The PPM is an alternative to a traditional Bayesian approach for solving inverse problems which effectively integrates the changes in production data during the history-matching process (Caers, 2003). Through the use of a perturbation parameter r_D, the probability distributions corresponding to model parameters are adjusted instead of directly perturbing the specific unknown model parameters (as implemented in most other HM methods). Thus, it has the flexibility to handle non-Gaussian distributions for model parameters and non-linear relationships between model parameters and the dynamic responses.

Following the proposed indicator-based PPM formulation in Kashib and Srinivasan, 2006 – Eq. (5-7) (Appendix – A), the probabilities of the unknown DFN model parameters (P^{sf}_{32G}, r_e,

T_{pf}, T_{sf}, H, and L) are adjusted and updated. The indicator formulation handles the non-Gaussian nature of the DFN model parameters. Eq. (5-7) describes the probability of transitioning from the indicator category k at step l to the category k' at step $l+1$ using $r_D \in [0,1]$. The probability $P\{I(u) = k'\}$ is the prior probability while $P\{I^{l+1}(u) = k|I^{i}(u) = k, C\}$ is the posterior probability. When r_D approaches 1, the probability of transitioning to another category increases; in other words, if $r_D = 1$, the probability of remaining in category k at step $l+1$ is 0. This is in contrast to $r_D = 0$, when there is no perturbation and the probability of staying in category k at step $l+1$ is 1.0. u represents the unknown parameters: T_{sf}, r_e, T_{pf}, P^{sf}_{32G}, H, and L for each stage.

The PPM framework described in Fig. 5-3 achieves a global minimum through a two-loop process; the inner loop where the 1D optimization scheme is implemented; similar to Kashib and Srinivasan (2006) and Caers (2003), the 1D optimization algorithm by Brent, 1973 is adopted to determine a local optimal value of r_D for a given initial realization, and the outer loop is used for exploring a different initial realization of the model parameters. The normalized objective function corresponding to the mismatch between production history and simulation prediction is presented in Eq. (5-8) (Appendix – A).

The 1D optimization scheme in the inner loop locates the minimum of a single-variable function and uses the concept of golden section search and parabolic interpolations to search for the optimal r_D which corresponds to the local minima of the objective function from any initial realization of the DFN model parameters, as described in Eq. (5-9) (Appendix – A).

x^{high} and x^{low} in Eq. (5-9) are the upper and lower bounds for the search interval corresponding to a unimodal function; $x^{(1)}$ and $x^{(2)}$ are points on the function such that the distances from x^{low} to $x^{(2)}$ and $x^{(1)}$ to x^{high} are exactly the same. Either $x^{(1)}$ and $x^{(2)}$ is selected as the minima for the next search interval. The process is repeated until the minimum is below the pre-defined tolerance. φ is the ratio of equal distances to the overall interval distance ($x^{high} - x^{low}$) and is a factor related to what is applied in the golden section search algorithm. The computational efficiency of the designed workflow is associated with the Brent algorithm as its objective function evaluation is only required at the equal-distance points (i.e., $x^{(1)}$, $x^{(2)}$, etc.). The method is applied and repeated to estimate the optimal value of r_D corresponding to any given initial realization of the unknown parameters.

The flow regimes derived from RTA are incorporated into the workflow as a localization strategy to constrain which of the DFN model parameters is to be updated for different parts of the production data. Since secondary fractures are considered to generally remain un-propped, the communication between the secondary and hydraulic fractures is significant during the late time after much of the water in the active secondary fractures has been displaced by gas influx from the matrix (Ezulike and Dehghanpour, 2015). Thus, hydraulic fracture parameter T_{pf} is perturbed during the early time while the late-time data is used to update the secondary fracture parameters – P^{sf}_{32G}, r_e, T_{sf}, L, and H for all four fracture stages, whereas the already-optimized T_{pf} remain unchanged.

5.4 CASE STUDY

5.4.1 Model Definition

The model represents a four-stage hydraulically fractured reservoir in the Horn River Basin with dimensions of 244 m. × 244 m. × 76 m. (with 50 × 50 × 10 grid cells along the x-, y-, and z-directions, respectively). The primary fractures propagate along a pole trend of 140˚ according to the available microseismic information of the well (Nejadi et al., 2015).

The values of k_m, X_f, A_{cm}, and *SRV* estimated from the RTA results are converted to the relevant DFN parameters (P^{sf}_{32G}, r_e, T_{sf}, L, and H) for the construction of the DFN model. A plot of the *RNP* integral and its derivative versus MBT (t_e) is shown in Fig. 5-4 and the estimated parameters are summarized in Table 5-1 (*Appendix – C*).

The relevant DFN model parameters are useful in constraining the initial distributions of the uncertain fracture parameters according to Eq. (5-10i) – (5-10v) (Appendix – A).

The secondary fractures are the induced fractures, and it is assumed that both T_{pf} and T_{sf} are proportional to the primary fracture permeability k_f for all the four fracture stages according to Eq. (5-10i) (Appendix – A). P^{sf}_{32G} is the fracture intensity defined by Dershowitz, 1984 where *sf* refers to secondary fracture, and the subscript *G* denotes a constant global fracture intensity throughout the entire domain. r_e represents the secondary fracture aperture, while S_{frac} and c_{frac} are the fracture storativity and fracture compressibility, respectively. ω is the storativity ratio described as the fractional contribution of the fractures to the total storativity of the system (i.e., the ratio of fracture storativity $(\phi c_t)_f$ to the storativity of the entire matrix-fracture systems $(\phi c_t)_{f+m}$; where ϕ_m and ϕ_f are the matrix porosity and the fracture porosity, respectively; the fracture porosity is defined as the ratio of total fracture volume to the cell volume, and the total fracture volume is computed as $2X_fL_w h$. Once a DFN model is constructed, it is upscaled as shown in Fig. 5-5 which represents the upscaled DPDK model of permeability along the x-direction.

Summary of the DFN model parameters and the shale gas reservoir fluid properties are presented in Tables 5-2 and 5-3, respectively.

The historical data is a 12 month production history comprising gas and water production rate and flowing bottom-hole pressure (P_{wf}); with a localization scheme designed for early time (0 – 90 days) and late time (91 – 365 days).

5.4.2 Workflow Application

The implementation of the PPM workflow is performed using one DFN realization as a reference case where the historical data is extracted. A first-pass history matching aimed at determining the approximate mismatch in the objective function and evaluating the extent of perturbation that may be required during the PPM history-matching is conducted. An editable macro script in the FracMan® domain containing a set of function calls for constructing and upscaling DFN models is used to create a set of initial realizations during the initialization steps and updated realizations during the updating steps. Other sections of the PPM framework (flow simulation, history matching, and parameter updating) are facilitated from Matlab® 2021a (MathWorks, 2021) central control with call functions to other software platforms.

The twenty-four unknown fracture parameters; T_{pfi} (Gaussian distribution), T_{sfi} (bimodal distribution), P^{sf}_{32Gi} (lognormal distribution), r_{ei} (lognormal distribution), H_i (lognormal distribution), and L_i (lognormal distribution) are parameterized using thirty indicator levels (bins of the unknown parameters) whose midpoints are the levels used for back-transform. i represents fracture stages 1 to 4 implying that the unknown DFN fracture parameters vary across the fracture stages from i = 1 to i = 4. Following the implementation of the PPM workflow, the initial distributions of the uncertain DFN model parameters generated in the outer loop are presented in Fig. 5-6 (Appendix – B).

5.5 RESULTS, FINDINGS, AND DEDUCTIONS

The minimized objective function was achieved with approximately 520 iterations, comprising 10 outer loops where all initial realizations were explored and 52 inner loops. The iterations stop when the mismatch has dropped below a certain tolerance ($\Delta O_{tol} \leq 10\%$).

Fig. 5-7 (Appendix – B) shows the prior and final posterior distributions of the updated mean values of the unknown fracture parameters after history matching using the designed PPM framework. The updated values of T_{pf} (T_{pf1}, T_{pf2}, $T_{pf3,}$ and T_{pf4} for all the four fracture stages) are achieved in the early time based on the novel localization scheme. These values are fixed during the late time to obtain the updated values of T_{sf} (T_{sf1}, T_{sf2}, $T_{sf3,}$ and T_{sf4}) and $P^{sf}{}_{32Gi}$ ($P^{sf}{}_{32G1}$, $P^{sf}{}_{32G2}$, $P^{sf}{}_{32G3}$, $P^{sf}{}_{32G4}$) realized in loop 7, r_e (r_{e1}, r_{e2}, $r_{e3,}$ and r_{e4}) realized in loop 9, and H (H_1, H_2, $H_{3,}$ and H_4) and L (L_1, L_2, $L_{3,}$ and L_4) achieved in Loops 6 and 10 respectively. The figure further shows that the designed workflow preserved the non-Gaussians characteristics of the distributions of the updated parameters.

The gas production rate, water production rate, and bottom-hole pressure profiles for the best three history-matched realizations sampled from the final posterior distributions are presented in Fig. 5-8 (Appendix – B). The comparison between the objective functions of these realizations as presented in Table 5-4 shows that the final model predictions closely match the production histories for all three realizations corresponding to both early and late times. This match can be attributed to the robustness of the designed PPM workflow.

Table 5-5 (Appendix – C) compares the mean values of the updated model parameters with the (true) reference model and mean values of the initial distributions (that are based on the RTA estimates). The twenty-four uncertain model parameters are grouped in the table according to the respective hydraulic fracture stages. The results indicate that the updated model's values closely match the reference model with negligible differences. On the other hand, noticeable discrepancies are observed between the updated and initial models, and this would suggest that the initial models, though constrained with reliable RTA estimates, should be further updated to achieve a better history match.

5.6 CONCLUSION

(i) We have developed and tested a probabilistic-based history matching framework for the updating of the unknown primary and secondary fracture parameters of a hydraulically fractured reservoir in the Horn River Basin.

(ii) A flow regime-based localization scheme incorporated into the workflow enhanced the history matching process by adjusting only specific impacting fracture parameters for specific flow periods.

(iii) The PPM framework is flexible for handling the non-Gaussian fracture parameters, as well as the non-linear relationship between the fracture parameters and the upscaled reservoir model properties, by perturbing the probabilities of the fracture parameters in the DFN domain.

(iv) The noticeable variation between the values of the updated models and the initial models indicates that the initial models constrained by RTA estimates are only possible estimates. The target match between the updated model and the reference model was achieved with negligible differences.

5.7 REFERENCES

Agarwal, R.G, D.C. Gardner, S.W. Kleinsteiber, and D.D. Fussell. 1999. Analyzing Well Production Data Using Combined-Type-Curve and Decline-Curve Analysis Concepts. *SPE Reserv. Eval. Eng.* 2, 478–486.

Bello, R.O., and R.A. Wattenbarger. 2010. Multi-stage Hydraulically Fractured Shale Gas Rate Transient Analysis. SPE-126754-MS. *In Proceedings of the SPE North Africa Technical Conference and Exhibition, Egypt*.

Brent, R.P. 1973. Algorithms for Minimization without Derivatives. Prentice- Hall, Englewood Cliffs, New Jersey. ISBN: 0-13-022335-2.

Bui, T.D., D.D. Mamora, and W.J. Lee. 2000. Transient Pressure Analysis for Partially Penetrating Wells in Naturally Fractured Reservoirs. SPE 60289-MS. *In Proceedings of the SPE Rocky Mountain Regional/Low Permeability Reservoirs Symposium and Exhibition, Denver, Colorado, 12–15 March 2000*.

Caers, J. 2003. History Matching Under Training-Image-based Geological Model Constraints. *SPE Journal*, 8(03), 218-226.

Chai, Z., H. Tang, Y. He, J. Killough, and Y. Wang. 2018. Uncertainty Quantification of the Fracture Network with a Novel Fracture Reservoir Forward Model. SPE-191395-MS. *In Proceedings of the SPE Annual Technical Conference and Exhibition, Dallas, Texas, 24-26 February*.

Chai, Z., B. Yan, J.E. Killough, and Y. Wang. 2016. An Efficient Method for Fractured Shale Reservoir History Matching: The Embedded Discrete Fracture Multi-Continuum Approach. SPE-181765-MS. *In Proceedings of the SPE Annual Technical Conference and Exhibition, Dubai, UAE.*

Chang, H., and D. Zhang. 2018. History Matching of Stimulated Reservoir Volume of Shale-Gas Reservoirs Using an Iterative Ensemble Smoother. SPE-189436-PA. *SPE Journal* 23 (2): 346-366.

Clarkson, C.R, and P.K. Pedersen. 2010. Tight Oil Production Analysis: Adaptation of Existing Rate-Transient Analysis Techniques. SPE-137352-MS. *In Proceedings of the Canadian Unconventional Resources and International Petroleum Conference, Calgary, AB, Canada, 19–21 Oct.*

Dershowitz, W.S. 1993. Geometric Conceptual Models for Fractured Rock Masses: Implications for Groundwater Flow and Rock Deformation. ISRM-EUROCK-1993-010. *In Proceedings of the Second European Conference of the International Society for Rock Mechanics, Lisbon, Portugal, 21–24 June.*

Dershowitz, W. S. 1984. *Rock Joint Systems*. [Doctoral Thesis, Massachusetts Institute of Technology, Cambridge, Massachusetts].

Emerick, A. A., and A.C. Reynolds. 2011. History Matching a Field Case Using the Ensemble Kalman Filter With Covariance Localization. SPE -141216-PA. *SPE Res Eval & Eng* 14 (04): 443-452.

Ezulike, O. D., and H. Dehghanpour. 2015. A Complementary Approach for Uncertainty Reduction in Post-Flowback Production Data Analysis. *Journal of Natural Gas Science and Engineering*. 27(2), 1074 – 1091.

Fisher, M.K., C.A. Wright, B.M. Davidson, A.K. Goodwin, E.O. Fielder, W.S. Buckler, and N.P. Steinsberger. 2003. Integrating Fracture Mapping Technologies to Optimize Stimulations in the Barnett Shale. SPE-77441-PA. *SPE Production & Facilities*. 20 (02), 85-93.

Hu, L. Y. 2000. Gradual Deformation and Iterative Calibration of Gaussian Related Stochastic Models. *Mathematical Geology*. 32(1), 87–108.

Hu, L. Y. 2002. Combination of Dependent Realizations within the Gradual Deformation Method. *Mathematical Geology*. 34(8), 953–963.

Kashib, T., and S. Srinivasan. 2006. A Probabilistic Approach to Integrating Dynamic Data in Reservoir Models. *Journal of Petroleum Science and Engineering*. 50, 241 – 257.

Kazemi, H. 1969. Pressure Transient Analysis of Naturally Fractured Reservoirs with Uniform Fracture Distribution. SPE-2156-A. *SPE J.* 9(04), 451-462.

Liu, S., J. Wei, Y. Ma, X. Liu, and B. Yan. 2021. Numerical simulation on the effect of fractures geometries for shale gas development with discrete fracture network model. *J Petrol Explor Prod Technol*.

MathWorks. 2021. MATLAB Documentation. www.mathworks.com/help/matlab/index.html

Nejadi, S., J.Y. Leung, and J.J. Trivedi. 2015. Integrated Characterization of Hydraulically Fractured Shale-Gas Reservoirs - Production History Matching. SPE-171664-PA. *SPE Res Eval & Eng*. 18 (04): 481–494.

Nwabia, F.N., and J.Y. Leung. 2021. Inference of Hydraulically Fractured Reservoir Properties from Production Data Using the Indicator-Based Probability Perturbation Assisted History-Matching Method. *Journal of Petroleum Science and Engineering* 198, 108240.

Nwabia, F.N., and J.Y. Leung. 2020. Probabilistic History Matching of Multi-Scale Fractured Reservoirs: Integration of a Novel Localization Scheme Based on Rate Transient Analysis. SPE-199988-MS. *In Proceedings of the SPE Canada Unconventional Resources Conference, Calgary, Canada*.

Oda, M. 1985. Permeability Tensor for Discontinuous Rock Masses. *Geotéchnique* 35 (4): 483 – 495.

Schlumberger. 2017. *ECLIPSE Reference Manual Version* 2017.2.

Torres, F., A. Jia, Y. Wei, W. Yunsheng, W. Junlei, X. Hongbing, L. Ning, and M. Jijun. 2020. Comparison of Dual Porosity Dual Permeability with Embedded Discrete Fracture Model for Simulation Fluid Flow in Naturally Fractured Reservoirs. ARMA-2020-1462. *In Proceedings of the 54th US Rock Mechanics/ Geomechanics Symposium, Houston, Texas, USA.*

Tripoppoom, S. 2019. *Assisted History Matching Workflow for Unconventional Reservoirs*. [MSc Thesis, University of Texas at Austin].

Uleberg, K., and J. Kleppe. 1996. Dual Porosity, Dual Permeability Formulation for Fractured Reservoir Simulation. *Paper from the NTNU Trondheim RUTH Seminar*, Stavanger.

Uzun, I., B. Kurtoglu, and H. Kazemi. 2016. Multiphase Rate-Transient Analysis in Unconventional Reservoirs: Theory and Application. *SPE Reserv. Eval. Eng.* 19, 553–566.

Vo, H., J. Kamath, and R. Hui. 2019. High Fidelity Simulation of Recovery Mechanisms in Complex Natural Fracture Systems. SPE-193864-MS. *In Proceedings of the SPE Reservoir Simulation Conference, 10-11 April, Galveston, Texas*.

Warren, J.E., and P.J. Root. 1963. The Behavior of naturally Fractured Reservoirs. SPE 426-PA. *SPE J*. 3(3), 245–255.

Yu, W., K. Wu, M. Liu, K. Sepehrnoori, and J. Miao. 2018. Production Forecasting for Shale Gas Reservoirs with Nanopores and Complex Fracture Geometries Using an Innovative Non-intrusive EDFM Method. SPE 191666. *In Proceedings of the SPE Annual Technical Conference and Exhibition, September 2018, Dallas, Texas.*

Zuo, L, W. Yu, and K. Wu. 2016. A fractional Decline Curve Analysis Model for Shale Gas Reservoirs. *Int. J. Coal Geol.* 163, 140–148.

APPENDIX – A (*Equations)*

$$\frac{1}{t_e}\int_0^{t_e}\frac{q_{ref}}{q(\tau)}(m(P_i)-m(P(\tau)))d\tau \text{ versus } t_e \tag{5-1}$$

$$\frac{\partial}{\partial lnt_e}\left(\frac{1}{t_e}\int_0^{t_e}\frac{q_{ref}}{q(\tau)}(m(P_i)-m(P(\tau)))d\tau\right)\text{versus } t_e \tag{5-2}$$

$$\mathrm{P}_{32L}(x)=\mathrm{ce}^{-bd_{x,f}} \tag{5-3}$$

$$K_{ij}=\frac{1}{12}(F_{kk}\delta_{ij}-F_{ij}) \tag{5-4}$$

F_{ij} is the element of fracture tensor which facilitates fracture flow as a vector along the unit normal from the fracture plane and is calculated by adding the individual fractures within the upscaled grid block, weighted by their area and transmissivity as in Eq. 5-5; δ_{ij} is the Kroenecker's delta and K_{ij} is an element in the permeability tensor.

$$F_{ij}=\frac{1}{V}\sum_{r=1}^{N}A_rT_rn_{ir}n_{jr} \tag{5-5}$$

N is the total number of fractures in a grid cell, n_{ir} and nj_r represents the component of a unit normal to the fracture r, A_r is the area of fracture r, T_r is the transmissivity of fracture r and V is the grid cell volume.

$$Sigma\left(\frac{1}{ft^2}\right)=4\left(\frac{1}{L_i^{\,2}}+\frac{1}{L_j^{\,2}}+\frac{1}{L_k^{\,2}}\right) \tag{5-6}$$

L_i, L_j, and L_k is the fracture spacings in the x, y, and z directions.

$$P\{I^{l+1}(u)=k \mid I^{l}(u)=k,\ C\}=r_D.P\{I(u)=k^{'}\}\forall k^{'}\neq k$$

$$P\{I^{l+1}(u)=k \mid I^{l}(u)=k,\ C\}=1-\sum_{k^{1}\neq k} r_D\ .P\{I(u)=k^{'}\} \tag{5-7}$$

$$\Delta O=\int\left(\frac{Q_{g_s}(t)-Q_{g_h}(r_D^{\ *},t)}{Q_{g_{h\max}}(r_D^{\ *},t)}\right)^2 dt+\int\left(\frac{Q_{w_s}(t)-Q_{w_h}(r_D^{\ *},t)}{Q_{w_{h\max}}(r_D^{\ *},t)}\right)^2 dt+\int\left(\frac{b_s(t)-b_h(r_D^{\ *},t)}{b_{\max}(r_D^{\ *},t)}\right)^2 dt \tag{5-8}$$

$$\frac{x^{(2)}-x^{low}}{x^{high}-x^{low}}=\frac{x^{high}-x^{(1)}}{x^{high}-x^{low}}=\varphi=0.618 \tag{5-9}$$

$$T_f\,(ft^2/s)=\frac{k_f\rho g r_e}{\mu} \tag{5-10i}$$

$$P_{32G}(/ft)=\frac{A_{cm}(\text{total area of fractures})}{V_t\ (\text{total volume})}=\frac{\sum_{1}^{N}2\frac{L_w}{N}h}{2L_w X_f h} \tag{5-10ii}$$

$$S_{frac}=(c_{fluid}+c_{frac})\rho g r_e \tag{5-10iii}$$

$$\omega=\frac{(\phi c_t)_f}{(\phi c_t)_f+(\phi c_t)_m} \tag{5-10iv}$$

$$\lambda=\sigma r_w^2\frac{k_m}{k_f} \tag{5-10v}$$

APPENDIX – B (*Figures)*

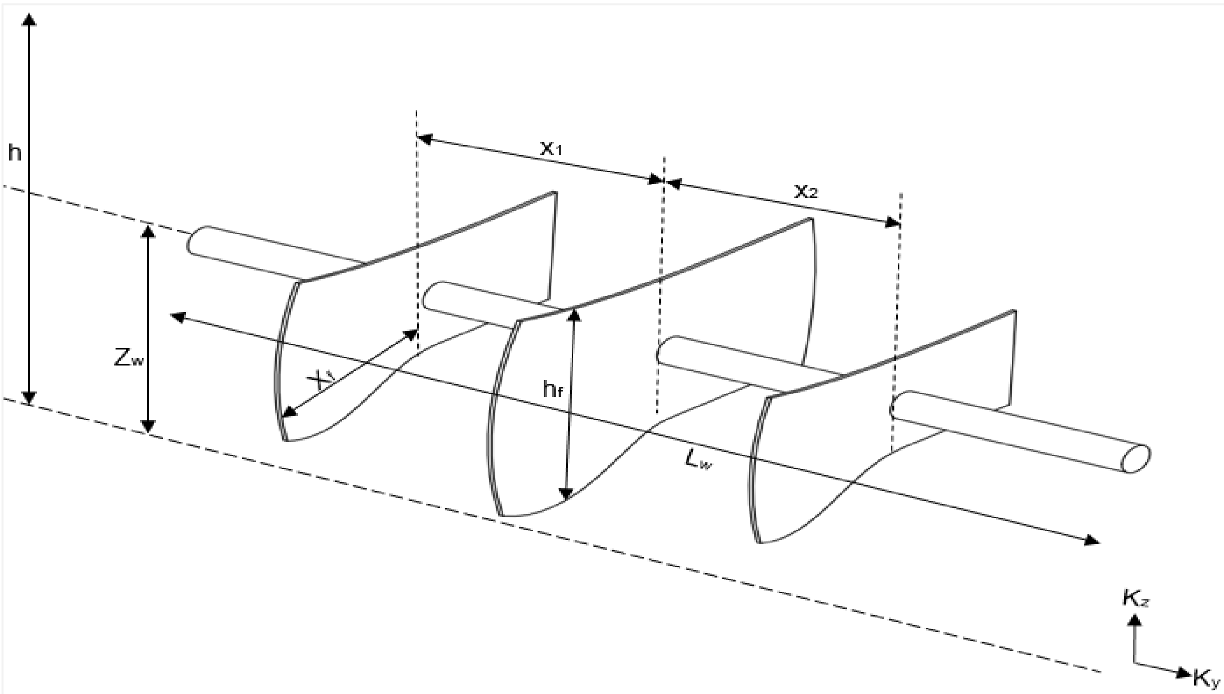

Fig. 5-1: A representation of a fractured horizontal well and dimensions.

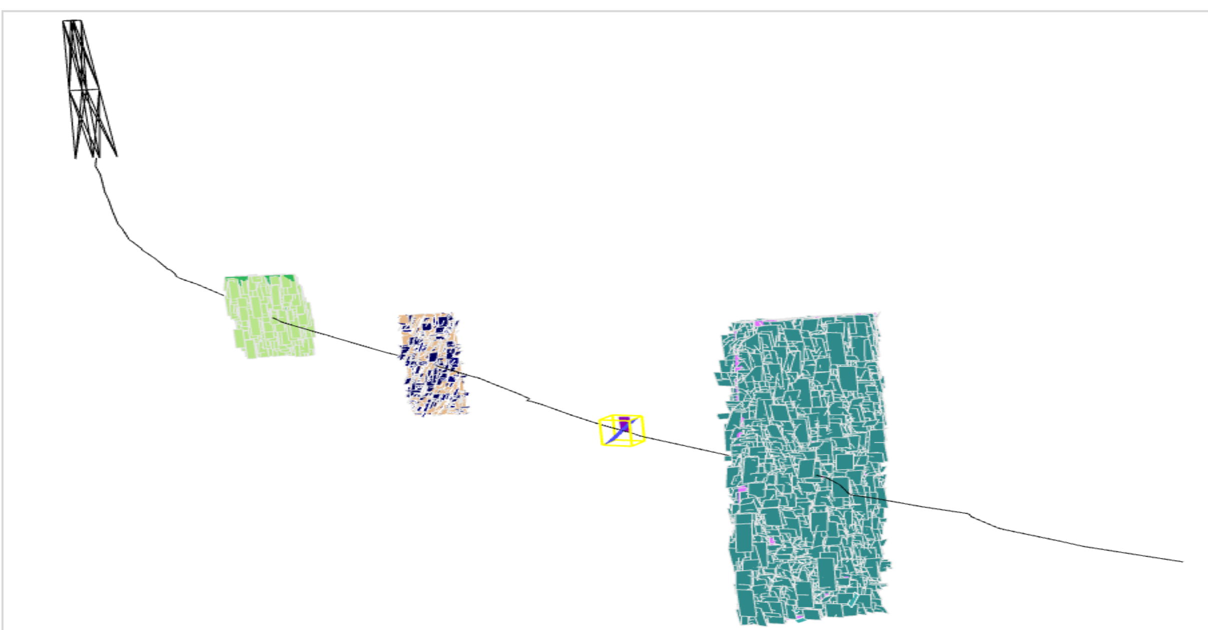

Fig. 5-2: The hydraulic fractures and intersecting secondary induced fractures.

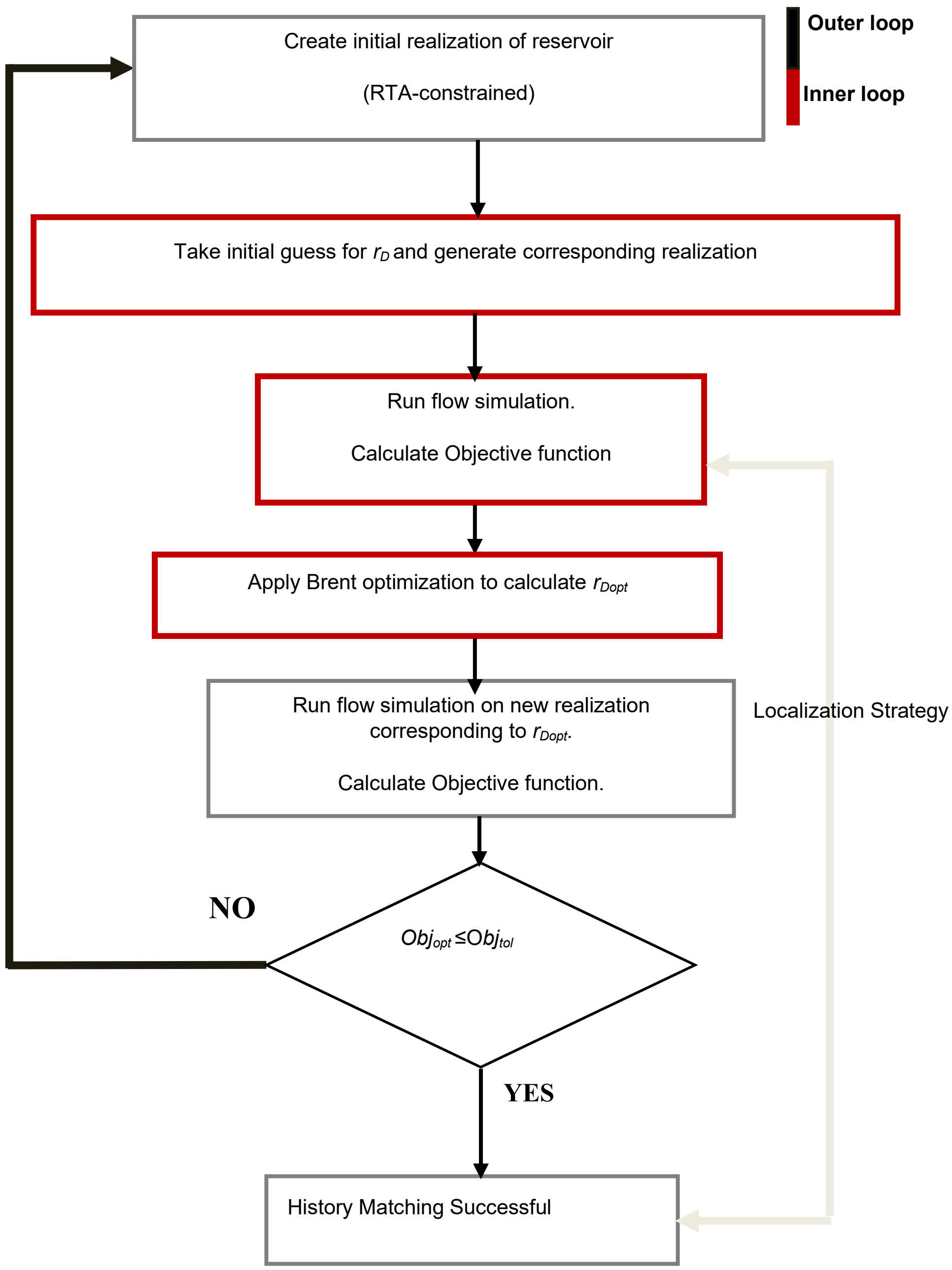

Fig. 5-3: PPM framework and objective function optimization.

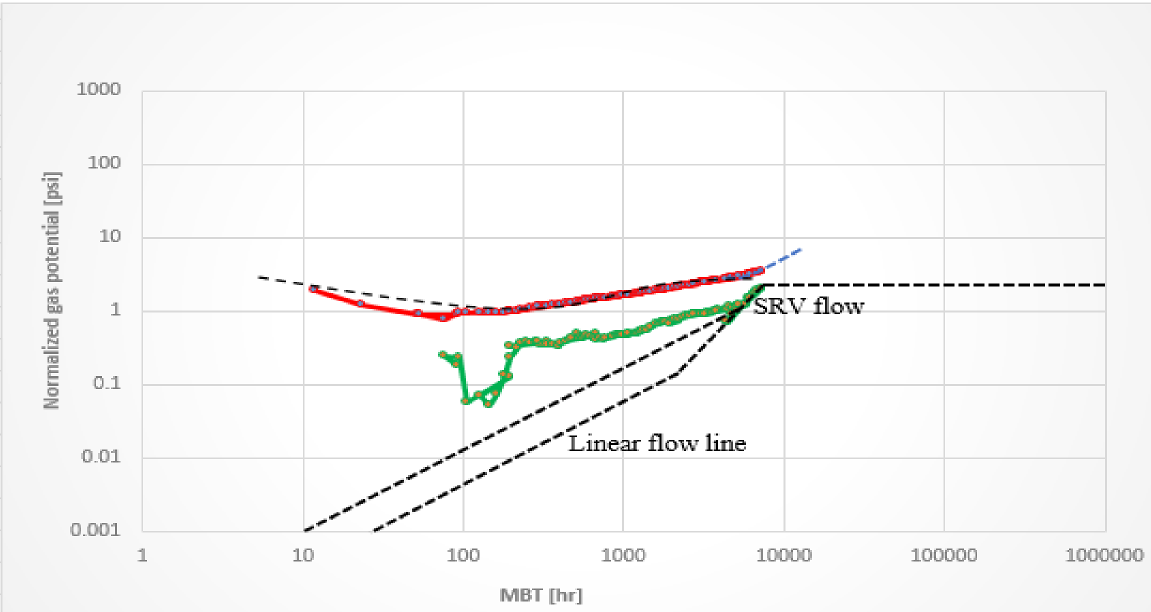

Fig. 5-4: A plot of the *RNP* integral and its derivative versus *MBT* (*te*)

[red – integral; green – derivative].

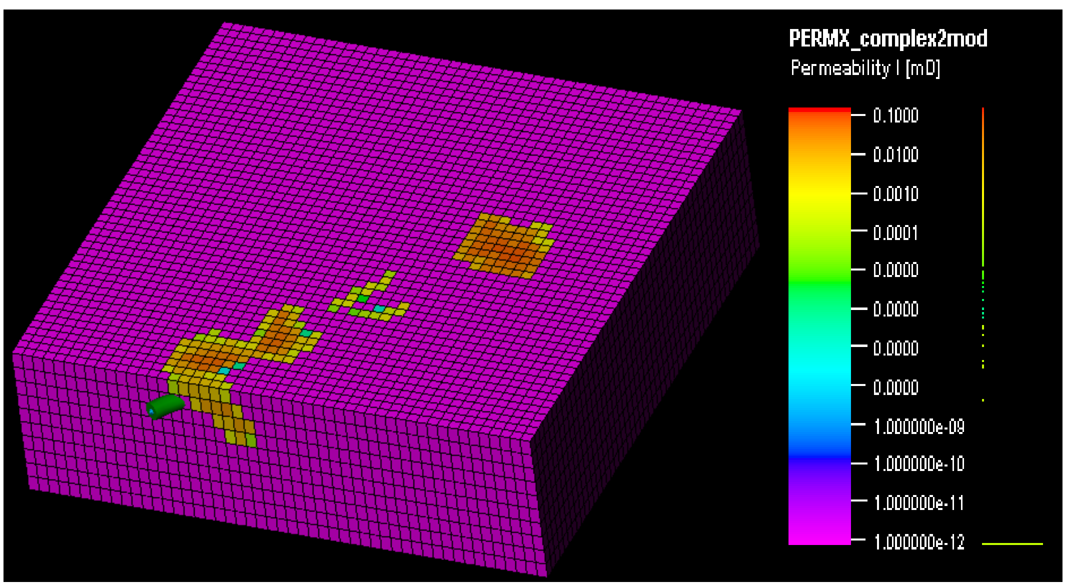

Fig. 5-5: The upscaled DPDK model indicating permeability along the x-direction.

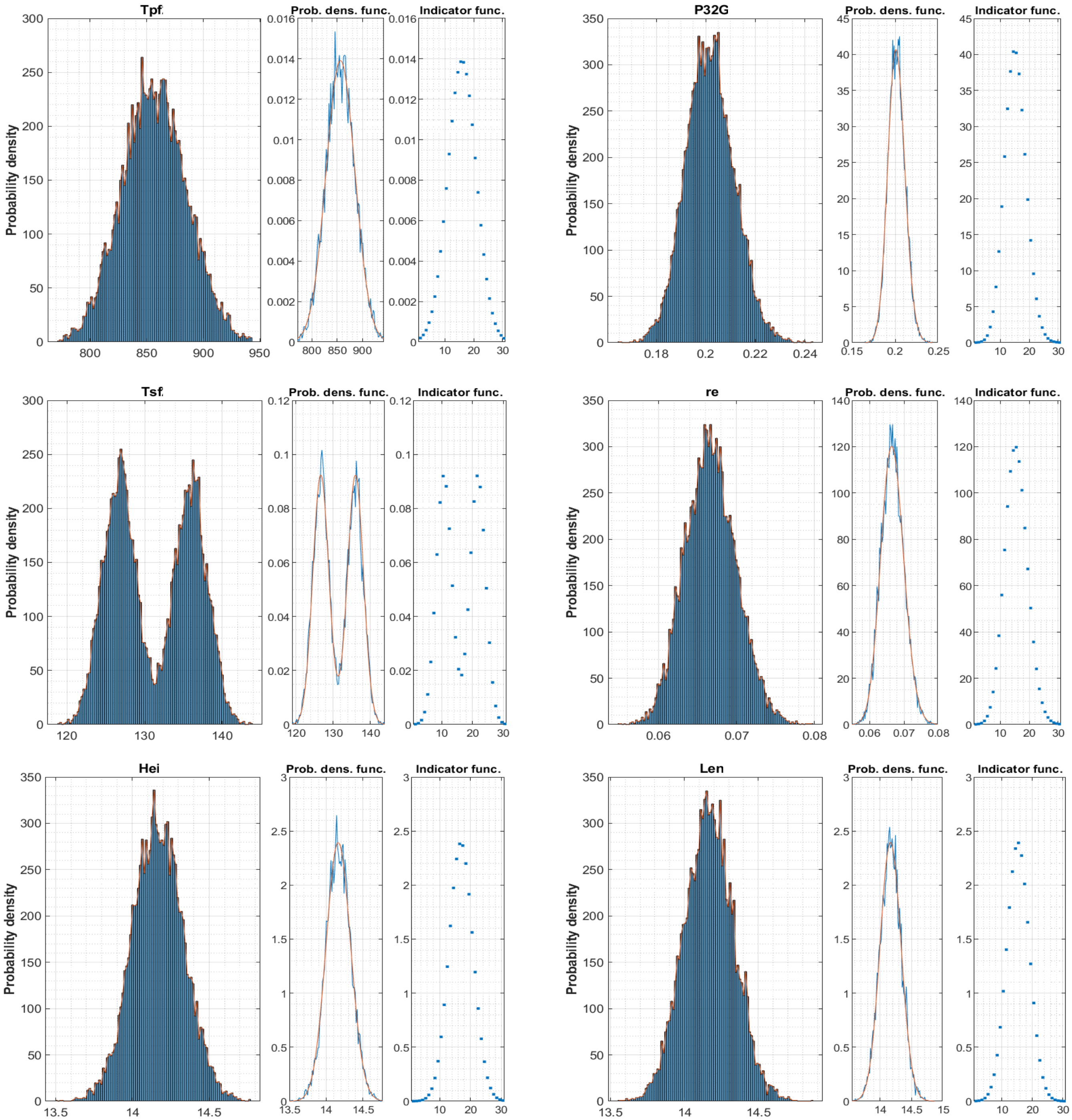

Fig. 5-6: Initial probability density functions of T_{pf}, P^{sf}_{32G}, T_{sf}, r_e, L, and H for all four fracture stages.

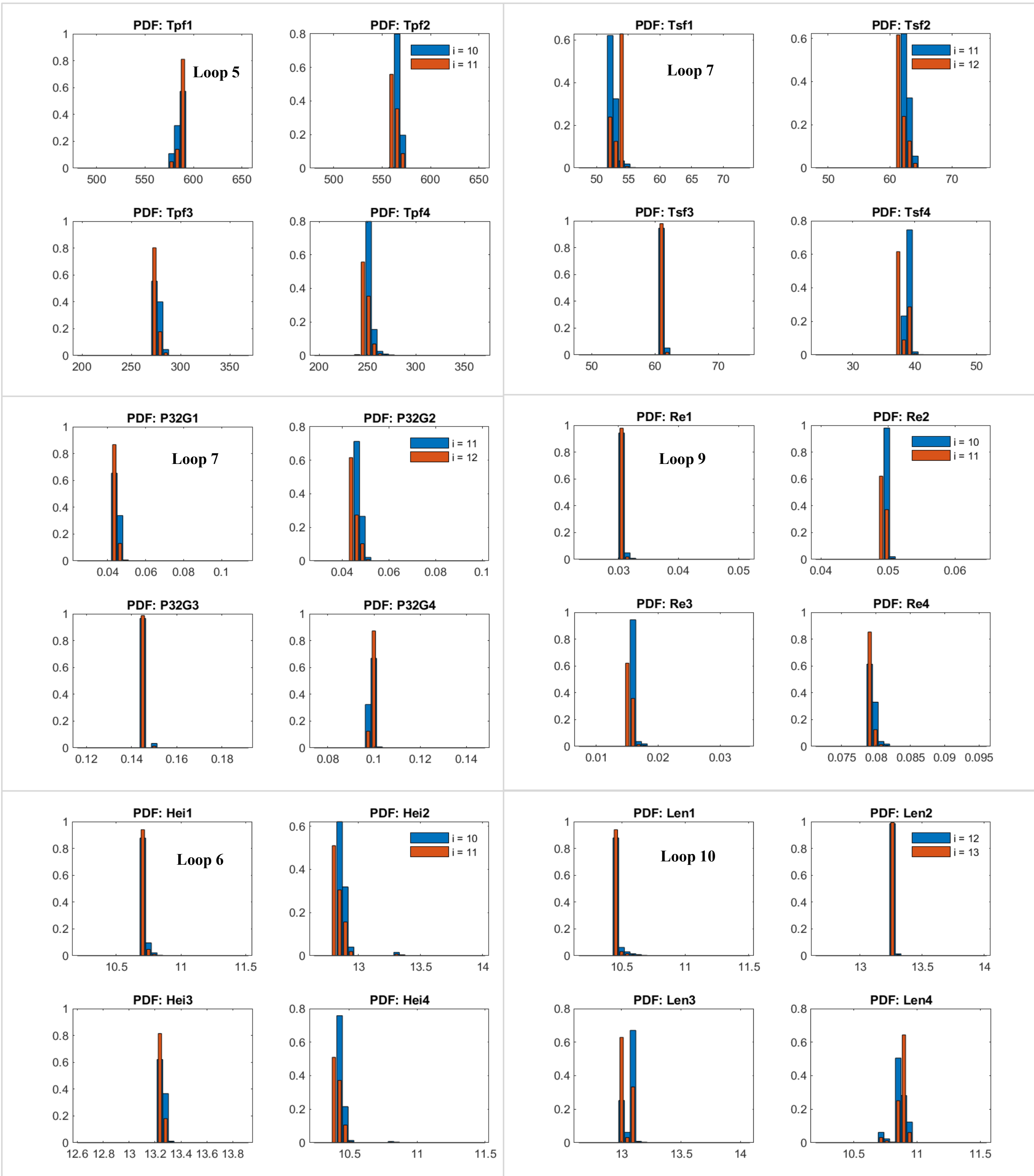

Fig. 5-7: The prior and posterior distributions for the iteration step *i* to *i*+1 of the updated parameters. *i* = *l* = iterative index.

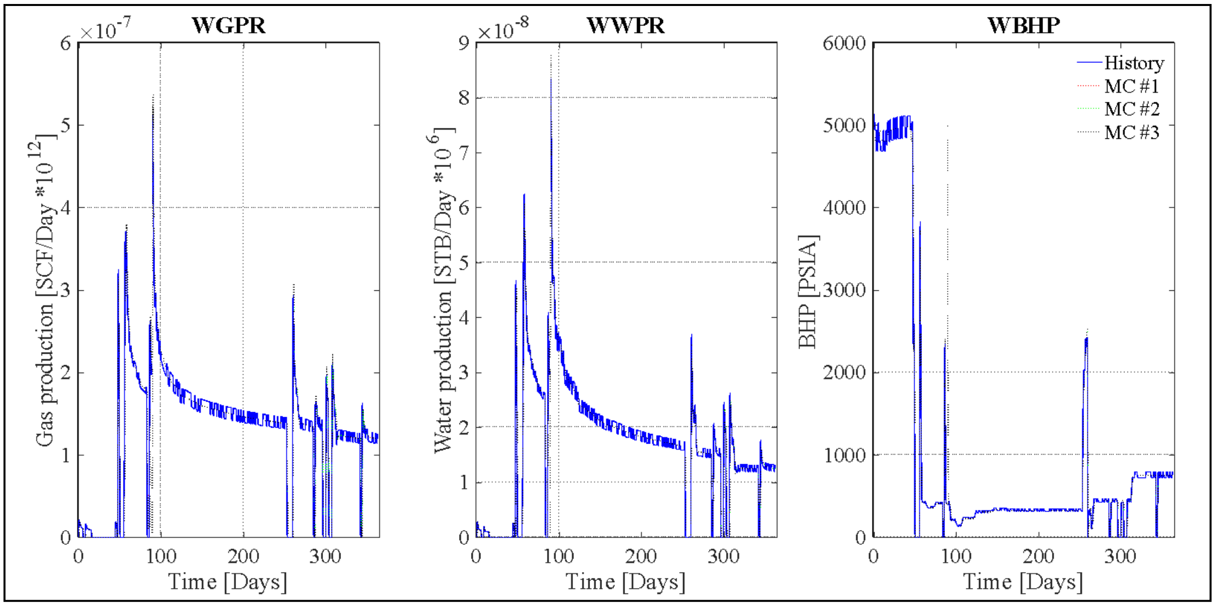

Fig. 5-8: History matched realizations of gas production rate, water production rate, and P_{wf} profiles sampled from the final posterior probability distributions.

APPENDIX – C (*Tables)*

Table 5-1: Preliminary results obtained from the RTA analysis.

Fracture half length, X_f	156 m (512 ft)
Number of traverse fractures, N	4
Producing well interval, L_w	218 m (717 ft)
Porosity, ϕ	0.060
Interporosity coefficient, λ	1.03E-08
Storativity, ω	0.538

Table 5-2: Summary of the reference DFN model parameters and the corresponding DPDK simulation model.

DFN Parameters:	
Primary Fractures	
Storativity, S_{pfrac}	1.0×10^{-6}
Equivalent radius, e_{peq}	(70.3, 50.9, 62.8, 72.7) ft
Permeability k_f	(k_{f1} = k_{f2} 12, k_{f3} 17, k_{f4} 3) mD
Trend (Stage 1)	226˚
Trend (Stage 2)	177˚
Trend (Stage 3)	244˚
Trend (Stage 4)	247˚
Plunge (Stage 1)	19˚
Plunge (Stage 2)	69˚
Plunge (Stage 3)	29˚
Plunge (Stage 4)	55˚
Compressibility, c_{pfrac}	0.000156 psi^{-1}
Secondary Fractures	
Storativity, S_{sfrac}	1.0×10^{-6}
Equivalent radius, e_{seq}	(10, 19, 9, 32) ft
Trend	
Plunge	
Compressibility, c_{sfrac}	Similar to the primary fracture
DPDK Parameters:	
Number of grids	50 × 50 × 10
Model dimensions	244 × 244 × 76 m^3
Matrix Permeability	0.000045 to 0.000075 mD
Matrix Porosity	4 – 6 %
Reservoir depth	1959 m
Initial reservoir pressure	5000 psi

Table 5-3: Shale Gas Reservoir Fluid Properties.

Compressibility, c_{fluid}	3.99 e-7 psi^{-1}
Gas Density, ρ	0.0507 lb./ft^3
Viscosity, μ	0.0155 cp

Table 5-4: Objective function values of the history matched realizations.

Days	ΔO_{tol} **%**	**Realization** #1 %	**Realization** #2 %	**Realization** #3 %
0 - 90	10	0.01590	0.01582	0.01580
91 - 365	10	0.1035	0.0134	0.1031

Table 5-5: Comparison of the uncertain DFN model parameters for the reference case, initial and updated realization for the four stages of the fractures.

Uncertain Parameter	Reference Model	Initial Model	Updated Model
Transmissivity T_{pf}, ft^2/sec	575.650	850.000	585.000
	550.650		563.500
	270.500		273.510
	240.600		250.050
Global Fracture Intensity (P^{sf}_{32G}), /ft.	0.090	0.210	0.041
	0.093		0.042
	0.190		0.142
	0.130		0.105
Transmissivity T_{sf}, ft^2/sec	45.050	135.000	53.420
	52.500		62.180
	50.000		62.050
	32.530		38.700
Aperture r_e, ft.	0.022	0.670	0.030
	0.029		0.048
	0.020		0.015
	0.050		0.078
Height H, ft.	9.010	14.300	10.730
	10.950		12.714
	12.001		13.201
	8.450		10.450
Length L, ft.	8.450	14.250	10.495
	12.000		13.320
	11.005		12.901
	9.000		10.861

Chapter 6: A robust probabilistic history matching framework for the characterization of fracture network parameters of shale gas reservoirs

6.1 OVERVIEW

A novel workflow is presented for characterizing discrete fracture network parameters in tight or shale reservoirs using an indicator-based probability perturbation method. The conditional probability distributions of primary (hydraulic) and secondary fractures are perturbed until a reasonable match with the production history is attained.

A case study for the characterization of the DFN model parameters in a reservoir in the Horn River Basin (HRB) is illustrated, where the posterior probability distributions of primary fracture transmissivity (T_{pf}) at each stage of the hydraulic fracture and secondary fracture aperture (r_e), secondary fracture transmissivity (T_{sf}), global fracture intensity of the secondary fracture (P^{sf}_{32L}), secondary fracture length (L) and height (H) are updated. A pilot point scheme and sequential indicator simulation are employed to update the distributions of P^{sf}_{32L}.

Each realization of the DFN model is upscaled to an equivalent dual-porosity dual-permeability model and subjected to numerical multiphase flow simulation. The predicted production performance is then compared with the historical data. The DFN model parameters are adjusted following an indicator-based probability perturbation method during the history matching process. This workflow accounts for the highly nonlinear relationships between fracture model parameters and the corresponding flow responses, and it yields an ensemble of DFN realizations calibrated to both static and dynamic data, as well as the related upscaled flow-simulation models. The results demonstrate the utility of the developed approach for estimating secondary fracture parameters, which are not inferable from other static information alone.

6.2 INTRODUCTION/ LITERATURE REVIEW

Detailed characterization of primary (hydraulic) fracture (HF) and secondary (i.e., induced or naturally occurring) fractures (SF) in unconventional tight/shale gas reservoirs remains challenging due to the complex heterogeneity in fracture properties. In addition, flow simulation of discrete fracture network (DFN) models remains computationally demanding (Garcia et al., 2007; Liu et al., 2019). Due to the significant disparity in scales, estimating the distributions of secondary/natural fracture properties is more challenging than the hydraulic fracture properties.

Data from different sources, including static/geologic and dynamic/flow measurements, should be integrated during the characterization process. Interpretations of the microseismic response cloud are often used to infer the approximate size and shape of the stimulated reservoir volume or SRV (Aminzadeh et al., 2013). The inference of SRV alone does not provide detail about connectivity between different fractures and secondary fracture properties. Yu et al. (2016) applied the Hough-transform technique and moment-tensor analysis to generate DFN models constrained by microseismic locations and fracture plane orientations. Many rate transient analysis (RTA) models have been developed over the years to analyze flowing data (fluid rates and flowing pressures) for estimating unknown fracture and reservoir parameters. One of the earlier works was by Bello (2009), who developed a model consisting of five flow regimes for a dual-porosity (DP) medium. The model was used to estimate matrix drainage area, fracture half-length, and formation damage. There have been many improvements in the topic of RTA; however, given that RTA models are based on analytical solutions of idealized models (e.g., homogeneous properties and simplified boundary conditions), their applications are limited by these many assumptions (Yue et al., 2016). Therefore, in this work, interpretations derived from RTA are used to infer initial distributions of the model parameters for the PPM history-matching analysis.

Many different strategies are available for the numerical multiphase simulation of fractured reservoir systems. They primarily differ on how the geometries of the fracture systems are described and how the fracture-matrix fluid flow is presented. In a dual-porosity (DP) formulation, only the fracture system or network is directly connected to the wellbore. Therefore, fracture-to-fracture flow and inter-porosity flow from matrix system to fracture system are considered, while matrix-to-matrix flow and matrix-to-wellbore connection (Barenblatt et al., 1960; Warren and Root, 1963; Al-Ghamdi and Ershaghi, 1996) are not. In a dual-porosity dual-permeability (DPDK) formulation, both the fracture and matrix systems are connected to the wellbore, where inter-porosity flow between matrix and fracture systems are considered (Hu and Huang, 2002; Degraff et al., 2005; Uba et al., 2007). Both DP and DPDK models generally work well if the fractures are densely populated and well connected (Sun and Schechter, 2015; Kumar et al., 2019; Xu and Leung, 2021). In situations where the detailed description of the actual geometries and locations of individual fractures are necessary, local grid refinement (LGR) can be applied in the fracture regions to represent these fracture elements in the computational domain explicitly. Although this modelling approach can offer a more accurate representation of the complex fracture system than the DP or DPDK models, it is much more computationally demanding. Therefore, many simulation studies still adopt DP or DPDK models (Sarda et al., 2001; Nejadi et al., 2017; Nwabia and Leung, 2020).

The aforementioned simulation techniques generally employ a structured (e.g., Cartesian) mesh. Unstructured grids have become increasingly popular to model fracture systems. Advanced higher-order discretization schemes, such as mixed finite-element or finite volume with multiple-point flux approximation, can more accurately simulate fluid flow in fracture systems. These discrete fracture models (DFM) are also more computationally intensive (Cipolla et al., 2010). The recent and widely adopted embedded discrete fracture model (EDFM) discretizes fractures into structured cubical matrix cells (Li and Lee 2008; Shakiba et al., 2018). The EDFM is considered more computationally efficient in calculating fluid transport than DFM, where fractures are embedded explicitly within the matrix; fluxes between sub-grid fracture segments and the background matrix block are computed grid without refinement.

In reservoir systems where both hydraulic and secondary fractures are present, secondary data such as seismic can improve predictions of fracture intensity in between the wells. In this work, fracture intensity at pilot (e.g., well) locations are used as conditioning data in a sequential indicator simulation to populate secondary fractures to the rest of the domain. Reservoir model parameters are adjusted during history matching such that the model predictions can closely reproduce the historical data (e.g., flow rates and pressures). History matching is inherently an ill-posed inverse problem with non-unique solutions. A combined gradient simulator and the adjoint method were formulated by Cui and Kellar (2005) to update the flow properties of a reservoir based on the correlation between fracture intensity and fracture permeability, matrix permeability, and a coupling factor. Gradient-based optimization techniques require several gradient calculations and are prone to converging at local minima. Other non-gradient-based or global optimization techniques can be applied: stochastics search algorithms (e.g., genetic algorithm, simulated annealing), optimization-based methods (e.g., maximum a-posterior), and sampling-based (e.g., gradual deformation, MCMC), have been used to infer discrete fracture parameters or some effective (or equivalent DPDK) properties. De Lima et al. (2012) implemented the gradual deformation approach to estimate realizations of fault distribution (i.e., spatial locations, intensity, and length). However, this method only works for modelling properties that follow a Gaussian distribution. It is not applicable for modelling non-Gaussian fracture properties. The MCMC technique has been applied to calibrate subsurface models and quantify their uncertainties in a Bayesian probabilistic framework (Maucec et al., 2007). A combined two-stage MCMC with EDFM was proposed by Chai et al. (2016) for characterizing different porosity systems corresponding to the organic matrix, inorganic matrix, secondary fractures, and hydraulic fractures of shale reservoirs. The MCMC tends to require many forward simulations, especially when dealing with a large number of unknown model parameters. Evolutionary techniques have been implemented to estimate fracture distribution. For example, a multi-scale scheme was formulated by Chen et al. (2019) for the history-matching of dual-porosity models; they calibrated coarse-scale and local-scale fracture parameters from a variety of dynamic and static data. Finally, ensemble-based techniques such as Ensemble Kalman Filter or EnKF (Aanonsen et al., 2009; Emerick and Reynolds, 2011) and ensemble smoother or EnS (Chai et al., 2018; Chang and Zhang, 2018) are also popular for data assimilation and uncertainty quantification. They utilize the covariance matrix to update an ensemble of parameters. Its major limitation is that it assumes a multi-Gaussian distribution on model and data variables and a linear relationship between all variables. These assumptions do not hold for fractured reservoirs, compromising their convergence behaviour. Emerick and Reynolds (2012) assessed the results of a very long MCMC as a reference solution to scrutinize the sampling performance of the ensemble-based methods by combining MCMC with EnKF. Despite acknowledging a high data mismatch, the MCMC formulation offered noticeable improvement to the EnKF formulation. However, though these extensions and hybrid formulations may retain the utility of an ensemble, they do not depend on a linear update; thus, they provide only a partial approximation for cases with highly non-Gaussian variables or nonlinear system dynamics.

A workflow addressing some of the concerns above is proposed for production history matching of multi-scale fractured reservoirs. Integrated information from both microseismic data, RTA results, and knowledge from previous studies can be used to infer prior probability distributions of fracture network parameters. A sampling-based history-matching method (PPM – probability perturbation method) is adopted for updating the non-Gaussian hydraulic and secondary fracture parameters; it facilitates the approximation of the posterior probability distributions based on the dynamic (production) data. Although this method has been used to calibrate permeability distribution in conventional reservoirs (Kashib et al., 2006) and unconventional reservoirs (Suzuki et al., 2007; Nwabia and Leung, 2021a), its application in scenarios where the secondary fractures are disconnected to and not within the vicinity of the hydraulic fractures is lacking. In our previous works, the technique was used to estimate the properties of hydraulic fracture and nearby secondary fractures (those that are induced or connected to the hydraulic fractures). Information from microseismic events and results from RTA was also used to construct the initial distributions of unknown fracture parameters. To history match the production data, an indicator-based probability perturbation method was employed (Nwabia and Leung, 2021a; Nwabia and Leung, 2021b).

This thesis aims to extend the technique to modelling secondary fractures throughout the entire domain. To handle the spatially varying secondary fracture distribution, a pilot-point parameterization scheme and sequential simulation are integrated into the indicator-based PPM workflow to update the unknown DFN model parameters: primary fracture transmissivity (T_{pf}) at each stage of the hydraulic fracture, secondary fracture aperture (r_e), secondary fracture transmissivity (T_{sf}), secondary fracture length (L) and height (H), local fracture intensity of the secondary fracture (P^{sf}_{32L}). Similar to the previous works, RTA interpretations, microseismic data, and knowledge of the updated fracture parameters are used to construct the initial distributions of the unknown DFN parameters. In the PPM framework, a realization of the DFN model is sampled, upscaled to an equivalent DPDK model, and subjected to flow simulation (forward modelling). The mismatch between the simulation predictions and the actual production profiles is computed. The novelty in our proposed workflow is the description of uncertainties in fracture parameters through several DFN models capturing both HF and SF properties and the equivalent upscaled flow-simulation models, resulting in an ensemble of DFN realizations conditioned to both static and dynamic data.

6.3 METHODS

The proposed PPM framework integrates data from different sources to infer unknown multi-scale fracture parameters. Static (geologic) information such as those extracted from microseismic data, as well as RTA estimates of fracture parameters, are employed to construct the initial (prior) distributions of various uncertain discrete fracture parameters. Parameters including T_{pf}, T_{sf}, r_e, H and L are assumed to be constant, while secondary fracture intensity represented by P_{32L} are assumed to vary spatially. The pilot point technique is used to parameterize P_{32L}, such that the number of unknown parameters is reduced and to provide a means of reintroducing the spatial distribution through sequential simulation. In particular, P_{32L} values at selected pilot point locations are updated and used as conditioning data in the sequential indicator simulation or *SISIM* (Deutsch and Journel, 1998) to populate its values for the rest of the grid. In this thesis, well locations with conditioning data (microseismic data and RTA estimates of fracture properties) are selected as the pilot locations. The PPM algorithm is used to perturb the probability distributions of all unknown parameters (e.g., H, P_{32L} at pilot points, etc.) until a match with the production data is attained: first, a realization of the reservoir (or DFN) model is constructed by sampling from the initial distributions of all unknown parameters; second, the model is upscaled into an equivalent DPDK model and subjected to numerical flow simulation using a commercial black-oil simulator (Schlumberger, 2020); (3) a Brent 1-D optimization algorithm is applied to minimize the objective function update the unknown fracture parameters. A localization scheme or two-step history matching process is employed: early-time production data is used to update only some of the hydraulic parameters, while late-time production data is used to perturb only the secondary fracture parameters.

6.3.1 DFN Modeling and Simulation

6.3.1.1 Generation and Upscaling of Initial Realization of DFN Model

The HF and SF properties are inputted into a commercial DFN modelling package (Golder Associates, 2018) to generate different DFN model realizations and perform the upscaling step.

Fig. 6-1 represents a complex fracture system with primary fractures conceptualized as elliptical fissures intersected by secondary fractures, as Fisher et al. (2005) proposed. It comprises four hydraulic fracturing stages, modeled as elongated penny-shaped fissures and secondary fractures throughout the domain. An editable macro script is used to implement these steps. Consider a mesh of $n_x \times n_y \times n_z$ grid cells. Each grid cell is populated with secondary fractures according to its values of P_{32L}, T_{sf}, r_e, H, and L. If a primary fracture is also present, then other parameters of the hydraulic fracture, including T_{pf} are used to generate an initial realization of the DFN model.

To model the multivariate distribution of P_{32L}, it would require modelling their values at all $n_x \times n_y \times n_z$ locations. As mentioned earlier, a pilot point scheme is adopted to parameterize P_{32L}. For example, in the case study presented next, $n_x \times n_y \times n_z = 50 \times 50 \times 10$, five pilot points are selected such that P_{32L} values at these selected locations are updated and used as conditioning data in *SISIM* to populate the rest of the grid. P_{32L} is modeled as a categorical variable: high, relatively high, medium, and low intensities. There are many possible ways of choosing these pilot points. A few considerations are made when selecting these locations: (1) they are intersected by well perforations or hydraulic fracture planes (where microseismic data and RTA estimates of fracture properties are available); (2) they are placed randomly throughout the domain to ensure sufficient variability is captured. In addition, instead of selecting five cells from all locations, five *subregions* (each consisting of 7 × 7 × 10 grid cells) are chosen. The pilot subregions represent about 10% of the total reservoir domain, ensuring a sufficient level of conditioning is achieved without exarcerbating the computational load.

To summarize, the model parameters are:

- T_{pfi} at each hydraulic fracture stage: i = 1,.., number of hydraulic fracture stages. It is assumed that they follow a Gaussian distribution.
- P_{32Lj} at each pilot point: j = 1,…, number of pilot points. It is assumed that they follow a lognormal distribution, and *SISIM* is used to simulate P_{32L} at other grid locations.
- $T_{sfj'}$ at each specified perturbing location: j' = 1,…, number of perturbing locations. It is assumed that they follow a bimodal distribution, and initialized based on the assumption that the probability distributions of T_{sf} facilitated through RTA estimates of induced fractures obtained from previous studies are suitable. At other non-perturbing locations of

the reservoir, the bimodal distributions of $T_{sfj'}$ remain unchanged and values are sampled randomly from these probability distributions.

- $r_{ej'}$, $L_{j'}$, and $H_{j'}$ at each specified perturbing location: j' = 1,…, number of perturbing locations. It is assumed that they follow a lognormal distribution. $r_{ej'}$ is initialized based on the assumption that the probability distributions of r_e facilitated through RTA estimates of induced fractures obtained from previous studies are suitable. The initial distributions of $L_{j'}$ and $H_{j'}$ are assumed based on knowledge of the field. At other non-perturbing locations in the reservoir, the lognormal distributions of these parameters remain unchanged and their values are sampled randomly from their lognormal distributions.

The probability distributions of the secondary fracture network parameters (i.e., r_e, T_{sf}, L, and H) are adjusted only at specific perturbation locations. The assumption is that fracture intensity (P_{32L}) is most uncertain and significantly impacts the overall conductivity of the SF network.

Next, the DFN model is upscaled to an equivalent DPDK model using a static upscaling procedure developed by Oda (1985). In this work, a static upscaling scheme is employed for its computational efficiency; however, other flow-based techniques can also be used. This Oda upscaling technique works well when all the secondary fractures are well connected to the primary fractures, which is assumed to be valid in this research (Dershowitz et al., 2000).

The upscaled DPDK parameters are (1) Oda permeability tensor; (2) fracture porosity – defined as the total fracture volume (average cross-sectional area × aperture) divided by the cell volume; (3) shape factor – related to the flow area between the matrix and fracture systems within a grid block. The Oda permeability tensor is computed by projecting the isotropic fracture permeability onto the fracture plane, thereafter scaling it in line with the fracture porosity, resulting in a 3 × 3 permeability tensor.

$$K_{ij} = \frac{1}{12}(F_{kk}\delta_{ij} - F_{ij}) \ , \tag{6-1}$$

In the equation above, while δij is the Kroenecker's delta, K_{ij} represents an element in the permeability tensor. F_{ij} is the element of fracture tensor which simplifies fracture flow as a vector along the unit normal from the fracture plane and is estimated by summing individual fractures within the upscaled grid block, weighted by their transmissivity and area described in Eq. (6-2).

$$F_{ij} = \frac{1}{V}\sum_{r=1}^{N} A_r T_r n_{ir} n_{jr} \ . \tag{6-2}$$

The total number of fractures in a grid cell is represented as N. n_{ir}, n_{jr} is the component of a unit normal to the fracture r, T_r is the transmissivity of fracture r, A_r is the area of fracture r, while V is the grid cell volume. The shape factor describes the interporosity flow between the matrix and fracture domains and is mathematically represented as:

$$\sigma = 4\left(\frac{1}{L_i^2} + \frac{1}{L_j^2} + \frac{1}{L_k^2}\right), \tag{6-3}$$

where L_i, L_j, L_k are the fracture spacings in x, y, z directions, respectively. Fig. 6-2 shows the first diagonal element of the upscaled DPDK Oda permeability tensor.

6.3.1.2 History Matching – Probability Perturbation Method

This probability perturbation method (PPM) is used to update the posterior probability distribution of unknown model parameters depending on the mismatch between model predictions and the actual production histories at each perturbation step (Caers 2003; Caers 2007). The tuning of the probability distributions corresponding to the unknown DFN model parameters is achieved through the variable r_D (a deformation parameter). An indicator-based formulation based on Kashib and Srinivasan (2006) is applied here to model the non-Gaussian distributions of model parameters (Nwabia and Leung, 2021a, 2021b):

$$
\begin{aligned}
&P\{I^{l+1}(u)=k \mid I^{l}(u)=k,\ C\}=r_{Dn}\cdot P\{I(u)=k'\}\forall k'\neq k\\
&P\{I^{l+1}(u)=k \mid I^{l}(u)=k,\ C\}=1-\sum_{k^{i}\neq k} r_{Dn}\ \cdot P\{I(u)=k'\}
\end{aligned}
\tag{6-4}
$$

The equation describes the probability of transitioning from the indicator category k at step l to the category k' at step l+1 utilizing the perturbation factor $r_{Dn}\in[0,1]$, for n = 1, …, number of distinct types of model parameters (e.g., n = 6 for T_{pf}, T_{sf}, P_{32L}, r_e, L, and H). $P\{I(u) = k'\}$ is the prior probability while $P\{I^{l+1}(u) = k|I^{l}(u) = k, C\}$ is the posterior probability considering C as the production data. For this research, the probability distributions of the uncertain DFN model parameters (i.e., T_{pfi}, T_{sfj}, P_{32Lj}, r_{ej}, H_j, and L_j) are adjusted. u represents the locations of the unknown multivariate distributions of T_{pfi}, T_{sfj}; r_{ej}; H_j; L_j; and P_{32Lj}. The indicator-based formulation facilitates the handling of the non-Gaussian distributions.

An efficient 1D optimization scheme suggested by other authors (Caers 2003) is adopted here to handle limitations associated with the PPM perturbation, which depends on the perturbation factor only. As $r_D \rightarrow 0$, there is little or no perturbation implying that the probability of staying at category k at step l+1 is 1.0. As $r_D \rightarrow 1$, the probability of staying at category k at step l+1 is 0 since more perturbation is expected. The adopted parameterization scheme preserves the nonlinear relationship between the set of uncertain DFN model parameters and the corresponding reservoir flow response since the perturbation of these parameters is executed in the DFN space. DPDK upscaling is performed after the sampling of a DFN model.

The PPM procedure is summarized in Fig. 6-3. The process consists of an inner and outer loop, where different levels of optimization are performed to attain the desired global optimal. For the inner loop, a 1D optimization scheme (Brent, 1973) is used to obtain a local optimal value of r_D for a given initial realization. In other words, the goal of the inner loop is to find the optimal r_{Dn}, considering a particular initial realization of the model parameters. The single-variable function is optimized using the golden section search and successive parabolic interpolation, as outlined in Eq. (6-5).

$$\frac{x^{(2)} - x^{low}}{x^{high} - x^{low}} = \frac{x^{high} - x^{(1)}}{x^{high} - x^{low}} = \varphi = 0.618 \tag{6-5}$$

where x^{high} and x^{low} are the upper and lower bounds for the search interval equivalent to a unimodal function; $x^{(2)}$ and $x^{(1)}$ are points on the function such that the distances from x^{low} to $x^{(2)}$ and $x^{(1)}$ to x^{high} are equal. Either $x^{(2)}$ and $x^{(1)}$ is selected as the minima for the next search interval, and the procedure is repeated until the minimum is achieved (i.e., below a user-defined tolerance). φ represents the ratio of equal distances to the overall interval distance ($x^{high} – x^{low}$), and this is a factor related to what is applied in the golden section search algorithm. Once an optimal value of "r_D" is obtained, the entire inner loop is repeated using a different initial realization, as denoted by the outer loop. In other words, during the execution of the outer loop, a different initial realization of the model parameters is examined. An optimal set of r_{Dn} values (for n model parameters) and the corresponding posterior distribution are updated according to Eq. (6-4). Each r_{Dn} value is perturbed and optimized individually since different r_D values should be used for different variables.

The normalized objective function is formulated as the L2 norm of the mismatch between the historical data and the model forecast:

$$\Delta O = \int \left(\frac{Q_{g_s}(t) - Q_{g_h}(r_{Dn}^*, t)}{Q_{g_{h\max}}(r_{Dn}^*, t)} \right)^2 dt + \int \left(\frac{Q_{w_s}(t) - Q_{w_h}(r_{Dn}^*, t)}{Q_{w_{h\max}}(r_{Dn}^*, t)} \right)^2 dt + \int \left(\frac{P_{wf\,s}(t) - P_{wf\,h}(r_{Dn}^*, t)}{P_{wf\max}(r_{Dn}^*, t)} \right)^2 dt \quad (6\text{-}6)$$

where Q_g, Q_w, and P_{wf} are the gas production, water production, and bottom-hole pressure, respectively, while the subscripts *s*, *h* and *max* are the historical data, simulation prediction and the upper limit for a specific variable, respectively.

The PPM algorithm is summarized below. It follows the algorithm descriptions given by Caers (2007) and Kashib and Srinivasan (2006):

- [**Outer Loop**] Generate an initial realization of the DFN model by sampling from probability distributions of $T_{pfi}, T_{sfj'}$ $r_{ej'}$ $H_{j'}$ $L_{j'}$ and P_{32Lj}. Perform upscaling and flow simulation to compute ΔO.
- [**Inner Loop**] Perform a set of 1D optimizations for r_{Dn} to yield r_{Dnopt} [i.e., optimizing all n r_D's simultaneuosly]:
    - Repeat until ΔO is minimized
        - Guess a value for r_{Dn} for each of *n* parameters [Eq. 6-5];
        - Calculate $P\{I^{l+1}(u(x)) = k \,|I^l\,(u(x)) = k,\ C\}$ for T_{pfi}, $T_{sfj'}$ $r_{ej'}$ $H_{j'}$ $L_{j'}$ and P_{32Lj} [Eq. 6-4];
        - Perform *SISIM* and generate a new realization of the DFN model by sampling from the updated posterior distributions of $I^{l+1}(u(x))$;
        - Perform upscaling and flow simulation to compute ΔO.
    - Set $I^{l+1}(u(x))$ computed using the optimal "r_D" values → $I^l(u(x))$.

The outer loop [step 1] is repeated until minimum mismatch in the objective function is achieved, and the most optimal $I^{l+1}(u(x))$ [step 2b] with the lowest minima is selected as the final updated posterior distributions.

Following Nwabia and Leung (2021b), a novel localization strategy is formulated using the flow regimes identifiable from RTA. First, the early-time data is used to perturb and optimize only T_{pfi}. Next, the late-time data is used to perturb and optimize $T_{sfj'}$, P_{32Lj}, $r_{ej'}$, $L_{j'}$, and $H_{j'}$ while T_{pfi} remains fixed at its optimal value from the first stage. This scheme is adopted since it is known that secondary fractures typically remain un-propped, and their hydraulic conductivity and aperture strongly depend on the inner-fracture fluid pressure; communication between the hydraulic and secondary fractures are significant during the late time when much of the water in the active secondary fractures has been displaced by gas influx from the matrix (Ezulike and Dehghanpour, 2015). First, the r_D perturbation for T_{pfi} at the four hydraulic fracture stages is done independently until optimal r_{Dn} and the corresponding updated distributions of T_{pfi} are attained. Then, independent r_{Dn} for each secondary fracture parameter at the different locations are perturbed and combined until r_{Dnopt} or minimum objective function mismatch is achieved. The algorithm is computationally efficient and exhibits good convergence behaviour.

6.4 CASE STUDY

A field example of a four-stage hydraulically fractured reservoir with secondary fractures in the Horn River Basin is modelled to assess the validity of the designed workflow. The model domain is 244 m × 244 m × 76 m (50 × 50 × 10 grid cells along the x-, y-, and z- directions, respectively). As mentioned earlier, to facilitate the parameterization of P_{32L}, five sub-regions of 7 × 7 × 10 grid cells (each) are selected as pilot points. Model parameters (as shown in Table 6-1) are extracted from a previous study (Nwabia and Leung, 2020). The average aperture of NFs in the HRB is approximately 0.8 mm, with most of the NFs ranging from 0.1 to 2.5 mm (Yang et al., 2018).

A reference DFN model is created representing a multifractured shale gas well in the Horn River Basin. This reference model is considered as the "true case" here. As discussed in the previous study, the trend and plunge of each primary fracture were inferred from interpreted microseismic events (Nejadi et al., 2015). The reference DFN model is upscaled to an equivalent DPDK model. This step is carried out within the FracMan® software facilitated by macros, which are scripts of function calls for generating and upscaling the DFN models. The upscaled DPDK model is then subjected to numerical flow simulation to compute the production profiles over 12 months. The 12-month production profiles of water production rate, gas production rate, and bottom-hole pressure are employed as the *historical* data. A sensitivity analysis is performed to ensure the prior distributions of all model parameters are reasonable (e.g., the ranges exhibited are sufficient to capture the variability in the production histories). The summary of the parameters of the DFN model and the corresponding upscaled dual-permeability model are presented in Table 6-1. The orientation parameters for the secondary fractures are assumed similar to those of the primary fractures. Values of storativity for the primary and secondary fractures are similar to those reported in Cinco-ley (1996).

Table 6-1: Parameters for the reference discrete fracture network (DFN) model and the corresponding dual permeability simulation model.

Discrete Fracture Network Parameters:	
Primary Fractures	
Storativity, S_{pfrac}	1.0×10^{-6}
Equivalent radius, e_{peq}	30, 45, 26, 55m (98.4, 147.6, 85.3, 180.4ft)

Permeability k_f	($k_{f1} = k_{f2}$ 10, k_{f3} 15, k_{f4} 5) mD
Trend (Stage 1)	247˚
Trend (Stage 2)	244˚
Trend (Stage 3)	177˚
Trend (Stage 4)	226˚
Plunge (Stage 1)	55˚
Plunge (Stage 2)	29˚
Plunge (Stage 3)	69˚
Plunge (Stage 4)	19˚
Compressibility, c_{pfrac}	0.0226 MPa^{-1} (0.000156 psi^{-1})
Secondary Fractures	
Storativity, S_{sfrac}	1.0×10^{-6}
Equivalent radius, e_{seq}	3.0, 4.9, 2.4, 5.5 m (9.8, 16.1, 7.9, 18 ft)
Trend	Assigned based on the nearest neighbor model from the primary fracture
Plunge	
Compressibility, c_{sfrac}	Similar to the primary fracture
Dual Permeability Model Parameters:	
Number of grids	50 × 50 × 10
Model dimensions	244 × 244 × 76 m^3 (800 × 800 × 250 ft^3)
Matrix Permeability	0.00004 to 0.00007 mD
Matrix Porosity	5 to 6%
Reservoir depth	1959 m (6425 ft)
Initial reservoir pressure	34.47 MPa (5000 psi)
Parameters for Variogram Model:	
2 0.0	-nst, nugget effect
1 0.15 0.0 0.0 0.0	-it, cc, azm, dip, tilt (ang1, ang2, ang3)
5 5 0.0	-a_hmax, a_hmin, a_vert (ranges)
1 0.85 0.0 0.0 0.0	-it,cc,azm,dip,tilt (ang1,ang2,ang3)

5 5 0.0	-a_hmax, a_hmin, a_vert (ranges)
,, ,, ,,	
Structure type (it):	
1 - spherical variogram model	

Table 6-2: Reservoir Fluid Properties (Shale Gas)

Gas Density, ρ	0.812 kg/m^3 (0.0507 lb./ft^3)
Viscosity, μ	0.015 cp
Compressibility, c_{fluid}	5.787 e-4 MPa^{-1} (3.99 e-7 psi^{-1})

Next, the PPM workflow is applied to history match the production data collected from the reference case. An initial realization of the DFN model is constructed and upscaled (using the macros as described earlier). The macro can be executed repeatedly within a loop, enabling the generation of multiple DFN realizations at each iteration or updating step. The entire PPM workflow is implemented in Matlab™ R2018a (MathWorks, 2018), and it also acts as the interface between multiple software platforms.

The initial (prior) probability density functions of the uncertain DFN parameters are shown in Fig. 6-4. They are formulated based on static information and RTA results, as discussed in the previous studies (Nwabia and Leung, 2021b). These initial probability density functions are set so that their means are widely apart. To test the robustness and validity of the proposed technique, the initial (prior) distributions are constructed such that the means (indicated in red) are different from the true case (indicated in green – it is assumed that the initial distributions for each of the i, j, and j' locations are the same).

Thirty indicator levels are used to parameterize each unknown model variable. The midpoint corresponding to each level is used for the back-transform. There are a total of 29 model parameters, including T_{pfi} (i = 1,…,4), $T_{sfj'}$ (j'=1,…,5), P_{32Lj} (j =1…5), $r_{ej'}$, $L_{j'}$, and $H_{j'}$ (j'=1,…,5). In this thesis, it is assumed that the perturbation locations of the secondary fracture properties (i.e., j') are the same as those pilot point locations j. The use of different notations is to emphasize that *SISIM* is performed for P_{32Lj} only, while the other secondary fracture parameters ($T_{sfj'}$, $r_{ej'}$, $H_{j'}$, $L_{j'}$) are updated during history matching process at the locations j' only. Finally, the variogram model for P_{32L} are shown in Table 6-1. A localization scheme is adopted where T_{pfi} (i = 1,…,4) is tuned at the early time production period (0 – 90 days), and the other secondary fracture parameters ($T_{sfj'}$ (j'=1,…,5), P_{32Lj} (j =1…5), $r_{ej'}$, $L_{j'}$, and $H_{j'}$ (j'=1,…,5) are adjusted at the late time (91 – 365 days). This scheme is achieved by dividing the PPM workflow into two separate stages, and different parameters are adjusted in each stage.

An additional case is set up to examine the sensitivity of the pilot points (or subregions) on the performance and the developed history matching framework – Fig. 6-5. The model set up and workflow implementation is the same as described earlier. The only difference is that there are only four pilot points (subregions) intersecting the hydraulic fractures. They represent about 8% of the reservoir domain.

6.5 RESULTS AND DISCUSSION

The quality of the history match is quantified according to the mismatch in the objective function. The iterations are terminated after approximately 300 – 363 iterations when the mismatch is less than 5%. This is typically achieved after 10 outer loops and 30 inner loops (3 iterations for each outer loop).

The (final) updated posterior distributions with the minimum objective function mismatch are presented in Fig. 6-6 & 6-7. The figures show the distributions of T_{pfi} for different hydraulic fracturing stages and those of the secondary fracture parameters – (P_{32Lj}) and ($T_{sfj'}$, $r_{ej'}$, $L_{j'}$, $H_{j'}$) at the pilot locations and locations j', respectively. Selected successive changes in the prior and posterior distributions from iteration l to iteration $l+i$ during the final outer loop are shown, representing the probabilities of staying at the current category k at step $l+1$ or transitioning to category k' at step $l+1$. The spikes observed in the figure reveal a reduction in the sampling variance, indicating convergence to a solution at the final iteration step. A reduction in the model parameter uncertainty is observed in the posterior distributions, reflecting the conditioning effect in the model uncertainty due to the integration of additional dynamic data. The results demonstrate that the procedure can adequately capture the non-Gaussian characteristics for the individual distributions during the parameter updating process.

The means of the initial and updated (posterior) distributions are compared to the reference (true) values in Table 6-3. Despite the vast disparity between the initial models and the true case, the updated models are close to the true case. It suggests that the history matching workflow can progressively perturb the posteriors to match the actual production data in both case implementations: where pilot points are placed either randomly throughout the domain, or placed near the hydraulic fractures. Since the updated posterior distributions of the DFN parameters closely matches the true case for the case where pilot points are placed near the HF's, it is suggested that the fluid flow is more sensitive to the parameters of the SF's near the HF's than those of SF's away from the HF's. The slight variability exhibited by the final updated models, compared to the reference (true) case, further illustrates the inherent non-uniqueness (ill-posed nature) of all history-matching inverse problems.

Table 6-3. Updated realizations of the DFN model parameters are compared with the reference (true) and initial models.

DFN Parameter	Reference Model	Initial Model (Mean Values)	Updated Model for both cases (Mean Values)
Transmissivity T_{pfi}, ft^2/sec	277.06	851.000	289.050, 280.060
	282.40		273.501, 279.630
	287.90		280.092, 283.690
	698.00		711.010, 705.000
Transmissivity T_{sfj}, ft^2/sec	91.36	137.400	102.500, 101.950
	113.30		126.85, 125.680
	82.19		88.072, -
	83.95		80.024, 81.402
	67.78		65.809, 66.470
Fracture Intensity (P_{32Lj}), /ft.	0.093	0.218	0.051, 0.058
	0.097		0.060, 0.063
	0.055		0.047, -
	0.209		0.190, 0.210
	0.200		0.199, 0.202
Aperture $r_{ej,}$ in.	0.050	0.087	0.048, 0.052

	0.065		0.064, 0.066
	0.075		0.082, -
	0.074		0.083, 0.080
	0.045		0.033, 0.034
Length L_f, in.	10.90	11.710	11.594, 11.520
	10.95		11.699, 11.600
	10.00		10.780, -
	10.25		10.793, 10.710
	10.45		10.804, 10.778
Height H_f, in.	12.95	14.400	13.374, 13.296
	12.50		12.661, 12.618
	13.90		14.197, -
	10.90		11.190, 10.802
	14.25		14.202, 14.242

Typically, in a robust optimization process as presented in this work, an ensemble of model realizations is used for the assessment of uncertainties in the fracture parameters. Intuitively, these realizations appear equiprobable or statistically similar with similar patterns and similar spatial variability, since they are generated by the same perturbation method using the same data, same grid and same parameter settings. Three additional realizations are sampled from the final posterior probability distributions. These realizations are useful in optimizing reservoir management decisions such as the proposed fracture sizes, fracture location, fracture spacing and their varied impacts on production, future reservoir performance predictions and the decisions about future development (with minimized risks). Table 6-4 compares the objective functions of the three realizations. Their profiles of gas production rate, water production rate, and P_{wf} are compared with the historical data in Fig. 6-8 & 6-9.

Table 6-4: Contrasts in the objective function of the history matched realizations

Days	**ΔO_{tol} %**	**Realization #1 %**	**Realization #2 %**	**Realization #3 %**
Early time (0 – 90)	5	0.7043	0.1039	0.6313
Late time (91 – 365)	5	0.9467	0.1947	0.7031

A comparison in model assumptions, computational time, and model accuracy between the developed technique with other sampling-based methods are presented in Table 6-5.

Table 6-5: Comparison between the developed PPM framework and other sampling-based methods

	Model Assumptions	Computational Time	Accuracy
Gradual Deformation	Relies on the perturbation of random numbers for stochastic realizations. Applied to only systems that can be represented	Converge exponentially to the global minimum for only linear problems after long run. Difficulty in convergence for non-linear problems.	Inaccurate sampler for non-Gaussian cases.

	by a Gaussian distribution.		
EnKF	Gaussian prior joint probability distribution. Linear model assumptions.	Difficulty to converge to correct distribution if the prior joint probability distribution has non-Gaussian contribution.	Partial approximation for cases with non-Gaussian variables or nonlinear system dynamics.
MCMC	Relies strongly on the statistical assumptions of the error model.	Large number of iterations to converge.	Approximately sample the space defined by the model.
Developed PPM Framework	Relies on probability models to generate realizations.	Computationally efficient and exhibits good convergence behaviour.	Better approximations to both Gaussian and non-Gaussian posterior probability.

It should be emphasized that the forward model does not couple the flow computations with geomechanics calculations. In addition, other reservoir parameters, such as relative permeability functions or compaction tables, are not considered during the history matching. The proposed workflow can be extended in future work to consider these additional parameters.

6.6 CONCLUSION

- A probabilistic-based assisted history matching workflow is applied to update unknown DFN model parameters from static and dynamic (production) observations. The method is used to update posterior probability distributions of hydraulic and secondary fractures of a shale gas reservoir.
- An indicator formulation is adopted to facilitate modelling uncertain distributions of several fracture parameters (T_{pf}, P_{32L}, T_{sf}, r_e, L, H).

- The method is flexible in handling both Gaussian and non-Gaussian uncertain fracture parameters. It is suitable for handling the nonlinear relationship between discrete fracture network parameters and reservoir flow response. Perturbation of model parameters is performed in the DFN space instead of the upscaled reservoir parameters. The uncertainties in model parameters are represented using multiple DFN models and their corresponding upscaled DPDK models.
- Secondary fractures, including those in the vicinity of the hydraulic fracture and those disconnected from the hydraulic fractures, are modeled. The spatial variability is handled using a pilot-point parameterization scheme and sequential simulation with the indicator-based PPM workflow.
- The significance of this work is that while the workflow was developed for analyzing hydraulically fractured reservoirs with secondary fractures, it can be applied to other unconventional hydrocarbon formations with multiple wells. Future studies should test this technique for modelling other complex field cases involving numerous well pads.
- The history-matching results are achieved within the low user-defined tolerance ($\Delta O_{tol} \leq 5\%$), suggesting the modelling workflow can infer a reasonable representation of the reservoir's primary and secondary fracture distributions.

6.7 REFERENCES

Aanonsen, S. I., Oliver, D. S., Reynolds, A. C., Vallès, B. 2009. The Ensemble Kalman Filter in Reservoir Engineering – A Review. SPE-117274-PA. SPE J. 14(03): 393–412. SPEJ Sept. 2009. https://doi.org/10.2118/117274-PA

Al-Ghamdi, A., Ershaghi, I. 1996. Pressure transient analysis of dually fractured reservoirs. SPE 26959-PA. SPE J. 1(1): 93–100. doi:10.2118/26959-PA

Aminzadeh, F., Tafti, T. A., Maity, D. 2013. An Integrated Methodology for Sub-surface Fracture Characterization Using Microseismic Data: A Case Study at the NW Geysers. Computers and Geosciences, 54, 39–49. https://doi.org/10.1016/j.cageo.2012.10.015

Barenblatt, G. I., Zheltov, Y. P., Kochina, I. N. 1960. Basic concepts in the theory of seepage of homogeneous liquids in fissured rocks, J. Appl. Math. Mech., Engl. Transl. 24(5): 1286-1303. https://doi.org/10.1016/0021-8928(60)90107-6

Bello, R.O. 2009. Rate Transient Analysis in Shale Gas Reservoirs with Transient Linear Behaviour [Doctoral dissertation, Texas A&M University, Texas, USA]. Retrieved from http://oaktrust.library.tamu.edu/bitstream/handle/1969.1/ETD-TAMU-2009-05-316/BELLO-DISSERTATION.pdf;jsessionid=D2B4A7BDAE325ED80B822D637F2FFEEC?sequence=2

Boisvert, J. 2018. *Geostatistical methods* [lecture note]. Edmonton, AB: University of Alberta, MIN E 612.

Brent, R.P. 1973. Algorithms for Minimization without Derivatives. Prentice- Hall, Englewood Cliffs, New Jersey. ISBN: 0-13-022335-2.

Caers, J. 2003. History Matching Under Training-Image-based Geological Model Constraints. SPE Journal, 8(03): pp.218-226. 10.2118/74716-PA

Caers, J. 2007. Comparing the Gradual Deformation with the Probability Perturbation Method for Solving Inverse Problems. Mathematical Geology 39(1), 27-52. https://doi.org/10.1007/s11004-006-9064-6

Chai, Z., Tang, H., He, Y., Killough, J., Wang, Y. 2018. Uncertainty Quantification of the Fracture Network with a Novel Fracture Reservoir Forward Model. SPE-191395-MS. SPE Annual Technical Conference and Exhibition, Dallas, Texas. https://doi.org/10.2118/191395-MS

Chai, Z., Yan, B., Killough, J.E., Wang, Y. 2016. An Efficient Method for Fractured Shale Reservoir History Matching: The Embedded Discrete Fracture Multi-Continuum Approach. SPE-181765-MS. SPE Annual Technical Conference and Exhibition, Dubai, UAE. https://doi.org/10.2118/181765-MS

Chang, H., and D. Zhang. 2018. History Matching of Stimulated Reservoir Volume of Shale-Gas Reservoirs Using an Iterative Ensemble Smoother. SPE-189436-PA. SPE Journal 23 (2): 346-366. https://doi.org/10.2118/189436-PA

Cinco-ley, H. 1996. Well-Test Analysis for Naturally Fractured Reservoirs. SPE-31162-JPT. Journal of Petroleum Technology 48(01). https://doi.org/10.2118/31162-JPT

Cipolla, C., L., Lolon, E. P., Erdle, J. C., Rubin, B. 2010. Reservoir Modeling in Shale-Gas Reservoirs. SPE Res Eval & Eng, 13 (2010): 638–653. doi:https://doi.org/10.2118/125530-PA

Cui, H., Kelkar, M. 2005. Automatic History Matching of Naturally Fractured Reservoirs and a Case Study. SPE-94037-MS. Western Regional Meeting, Irvine, California. https://doi.org/10.2118/94037-MS

Degraff, J.M., Meurer, M.E., Landis, L.H., Lyons, S. 2005. Fracture network modeling and dual-permeability simulation of carbonate reservoirs. SPE 10954-MS. international petroleum technology conference, Doha, Qatar. doi:10.2118/10954-MS

De Lima, A., Lange, A., Schiozer, D.J., 2012. Assisted History-Matching for the Characterization and Recovery Optimization of Fractured Reservoirs using Connectivity Analysis. SPE 154392. SPE Europec/EAGE Annual Conference. https://doi.org/10.2118/154392-MS

Dershowitz, B., LaPointe, P., Eiben, T. et al. 2000: Integration of Discrete Feature Network Methods with Conventional Simulator Approaches. SPE Res Eval & Eng 3 (2): 165-170. SPE-62498-PA. http://dx.doi.org/10.21186/62498-PA

Deutsch, C. V. 2002. Geostatistical Reservoir Modeling. Oxford University Press, Inc., New York, New York.

Deutsch, C.V., and A.G. Journel. 1998. GSLIB Geostatistical Software Library and User's Guide, 2nd Edition, Applied Geostatistics Series, Oxford University Press, Inc. New York, NY.

Dershowitz, W.S. 1993. Geometric Conceptual Models for Fractured Rock Masses: Implications for Groundwater Flow and Rock Deformation. ISRM-EUROCK-1993-010, Second European Conference of the International Society for Rock Mechanics, Lisbon, Portugal, 21–24 June. https://www.onepetro.org/conference-paper/ISRM-EUROCK-1993-010

Emerick, A. A., Reynolds, A. C. 2011. History Matching a Field Case Using the Ensemble Kalman Filter With Covariance Localization. SPE -141216-PA. SPE Res Eval & Eng 14 (04): 443-452. https://doi.org/10.2118/141216-PA

Emerick, A. A., Reynolds, A. C. 2012. Combining the ensemble Kalman Filter with Markov-chain Monte Carlo for Improved History Matching and Uncertainty Characterization. SPE-141336-PA. SPE J. 17(2): 418–440. https://doi.org/10.2118/ 141336-PA

Ezulike, O. D., Dehghanpour, H. 2015. A Complementary Approach for Uncertainty Reduction in Post-Flowback Production Data Analysis. J. Nat. Gas Sci. Eng., 27(2), 1074 – 1091. https://doi.org/10.1016/j.jngse.2015.09.059

Fisher, M.K., Wright, C.A., Davidson, B.M., Goodwin, A.K., Fielder, E.O., Buckler, W.S., Steinsberger, N.P. 2003. Integrating Fracture Mapping Technologies to Optimize Stimulations in the Barnett Shale. SPE-77441-PA. SPE Production & Facilities. 20 (02), 85-93. https://doi.org/10.2118/77441-PA

Golder Associates. 2018. FRACMAN 7.70 User Documentation. Copyright 1999 – 2018.

Garcia, M.H., Gouth, F.M., Gosselin, O.R. 2007. Fast and Efficient Modeling and Conditioning of Naturally Fractured Reservoir Models Using Static and Dynamic Data. SPE-107525-MS. EUROPEC/EAGE Conference and Exhibition, London, U.K. https://doi-org /10.2118/107525-MS

Hu, B.X., Huang, H. 2002. Stochastic analysis of reactive solute transport in heterogeneous, fractured porous media: a dual-permeability approach. Trans. Porous Med. 48(1): 1–39. doi:10.1023/A:1015671227317

Kashib, T., Srinivasan, S. 2006. A Probabilistic Approach to Integrating Dynamic Data in Reservoir Models. Journal of Petroleum Science and Engineering. 50, 241 – 257. https://doi.org/10.1016/j.petrol.2005.11.002

Kumar, S., Rey, A., Dufour, G., Ogunyomi, B. 2019. Understanding Fluid Flow Behavior in Fractured Reservoir using Dual Porosity Dual Permeability and Discretized Fracture Model. SPE-196038-MS. SPE Annual Technical Conference and Exhibition, Calgary, Alberta, Canada. doi:https://doi.org/10.2118/196038-MS.

Li, L., Lee, S.H. 2008. Efficient field-scale simulation of black oil in a naturally fractured reservoir through discrete fracture networks and homogenized media. SPE-103901-PA. SPE Res. Eval. & Eng. 11(4): 750-758. https://doi-org /10.2118/103901-PA

Liu, Y., Leung, J.Y., Chalaturnyk, R., Virues, C.J.J. 2019. New Insights on Mechanisms Controlling Fracturing Fluid Distribution and its Impacts on Well Performance in Shale Gas Reservoirs. SPE Production & Operations 34(3): 564-585. https://doi-org/10.2118/185043-PA.

MathWorks, 2021. *MATLAB Documentation*. www.mathworks.com/help/matlab/index.html

Maucec, M., Douma, S. G., Hohl, D., Leguijt, J., Jimenez, E., Datta-Gupta, A. 2007. Streamline-Based History Matching and Uncertainty--Markov-Chain Monte Carlo Study of an Offshore Turbidite Oil Field. SPE-109943-MS. SPE Annual Technical Conference and Exhibition, California, USA. https://doi.org/10.2118/109943-MS

Nejadi, S., Trivedi, J.J., Leung, J. 2017. History Matching and Uncertainty Quantification of Discrete Fracture Network Models in Fractured Reservoirs. Journal of Petroleum Science and Engineering. 152, 21–32. http://dx.doi.org/10.1016/j.petrol.2017.01.048

Nwabia, F.N., and J.Y. Leung. 2020. Probabilistic History Matching of Multi-Scale Fractured Reservoirs: Integration of a Novel Localization Scheme Based on Rate Transient Analysis. SPE-199988-MS. SPE Canada Unconventional Resources Conference, Calgary, Canada. https://doi.org/10.2118/199988-MS

Nwabia, F.N., Leung, J.Y. 2021a. Inference of Hydraulically Fractured Reservoir Properties from Production Data Using the Indicator-Based Probability Perturbation Assisted History-Matching Method. Journal of Petroleum Science and Engineering 198, 108240. ISSN 0920-4105. https://doi.org/10.1016/j.petrol.2020.108240

Nwabia, F.N., Leung, J.Y. 2021b. Probabilistic History Matching of Multi-scale Fractured Reservoirs: Integration of a Novel Localization Scheme Based on Rate Transient Analysis. J. Nat. Gas Sci. Eng., 94 (2021): p. 104067, https://doi.org/10.1016/j.jngse.2021.104067

Oda, M. 1985. Permeability Tensor for Discontinuous Rock Masses. Geotéchnique **35** (4): 483 – 495. https://doi.org/10.1680/geot.1985.35.4.483

Sarda, S., Jeannin, L., Bourbiaux, B. 2001. Hydraulic Characterization of Fractured Reservoirs: Simulation on Discrete Fracture Models. SPE Reservoir Simulation Symposium, Houston, Texas, USA. SPE-66398-MS. https://doi-org/10.2118/66398-MS.

Shakiba, M., de Araujo Cavalcante Filho J., Sepehrnoori, K. 2018. Using Embedded Discrete Fracture Model (EDFM) in Numerical Simulation of Complex Hydraulic Fracture Networks Calibrated by Microseismic Monitoring Data. Journal of Natural Gas Science and Engineering, 55(2018), 495-507. ISSN 1875-5100. https://doi.org/10.1016/j.jngse.2018.04.019

Schlumberger, 2020. ECLIPSE Reference Manual Version 2020.2.

Sun, J., Schechter, D. S. 2015. Optimization-Based Unstructured Meshing Algorithms for Simulation of Hydraulically and Naturally Fractured Reservoirs with Variable Distribution of Fracture Aperture, Spacing, Length and Strike. SPE-170703-PA. SPE Res. Eval & Eng 18(04): 463 – 480. https://doi-org /10.2118/170703-PA

Suzuki, S., Daly, C., Caers, J. K., Mueller, D. 2007. History Matching of Naturally Fractured Reservoirs using Elastic Stress Simulation and Probability Perturbation Method. SPE-95498-PA. SPE J. 12 (1): 118–129. https://doi.org/10.2118/95498-PA

Uba, H.M., Chiffoleau, Y., Pham, T., Divry, V., Kaabi, A., Thuwaini, J. 2007. Application of a hybrid dual-porosity/ dual-permeability representation of large-scale fractures to the simulation of a giant carbonate reservoir. SPE 105560-MS. SPE middle east oil and gas show and conference, Bahrain. doi:10.2118/105560-MS

Xu, Z., Leung, J. Y. 2021. Analyzing the Impacts of Meshing and Grid Alignment in Dual-Porosity Dual-Permeability Upscaling. SPE-208573-PA. SPE Res Eval & Eng 1-20. https://doi.org/10.2118/208573-PA

Yang, S., Harris, N.B., Dong, T., Wu, W., Chen, Z. 2018. Natural Fractures and Mechanical Properties in a Horn River Shale Core From Well Logs and Hardness Measurements. SPE-174287-PA. SPE Res Eval & Eng 21(03): 671–682. https://doi-org/10.2118/174287-PA

Yu, X., Jim, R., Scott, L., Maxwell, S. 2016. Discrete-Fracture-Network Generation From Microseismic Data by Use of Moment-Tensor- and Event-Location-Constrained Hough Transforms. *SPE J.* 21 (01): 221–232. https://doi-org/10.2118/168582-PA

Yue, M., Leung, J.Y., Dehghanpour, H. 2016. Numerical Investigation of Limitations and Assumptions of Analytical Transient Flow Models in Tight Oil Reservoirs. Journal of Natural Gas Science and Engineering 30: 471-486. https://doi.org/10.1016/j.jngse.2016.01.042

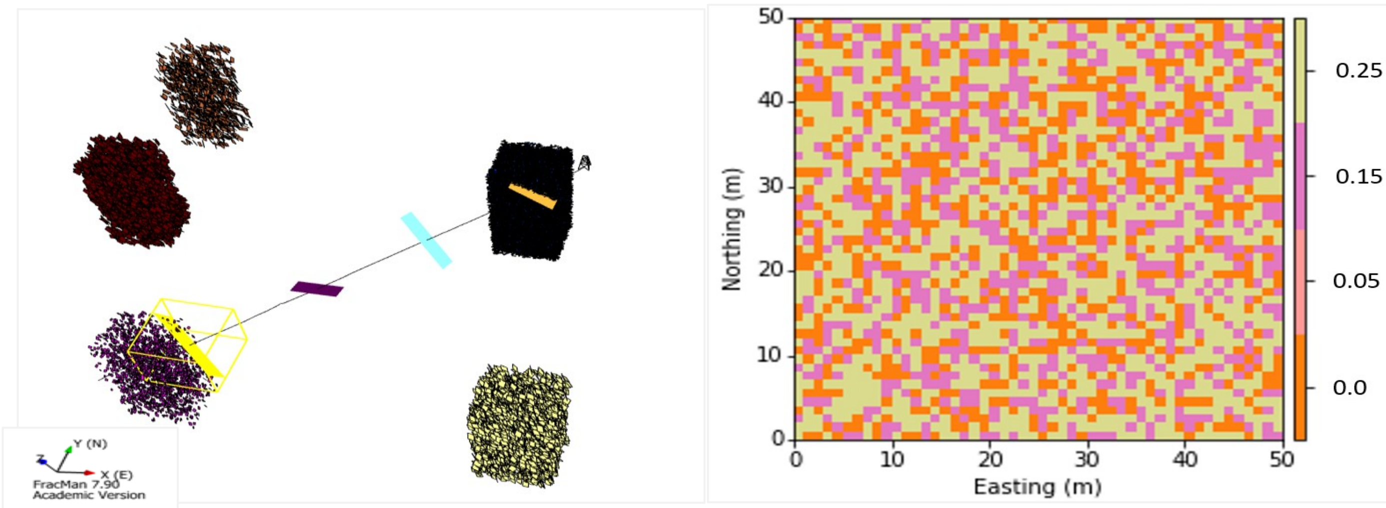

Fig. 6-1 (a): The discrete fracture network model with the hydraulic and secondary fractures: pilot points (left) and *SISIM* realization of P_{32L} (right).

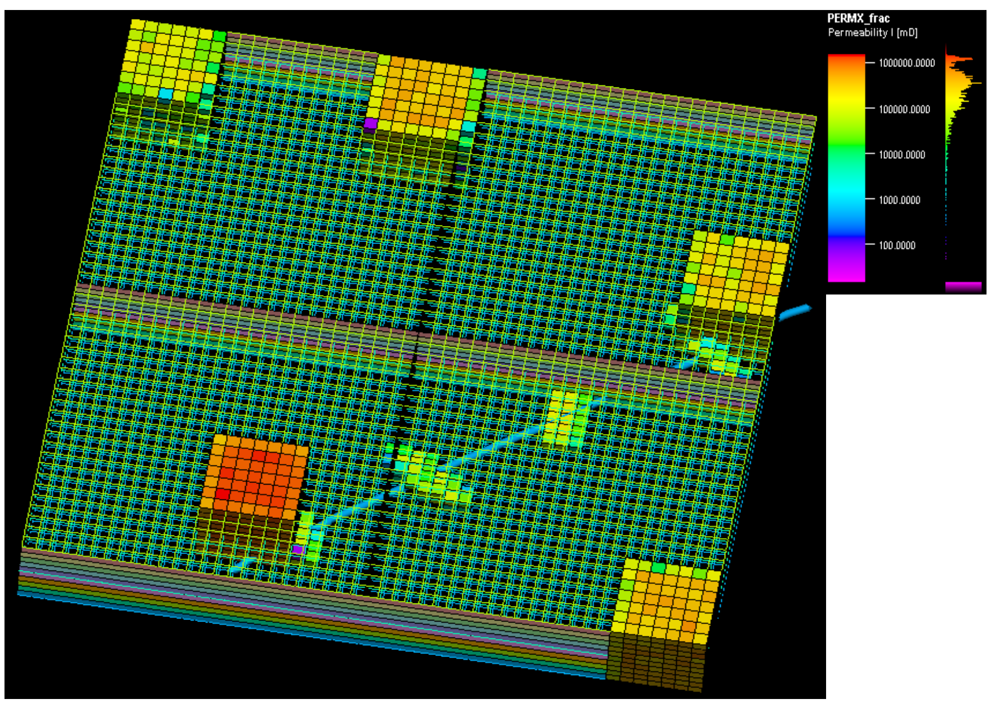

Fig. 6-2: The upscaled DPDK Oda permeability tensor (PERMXX – 1st diagonal element). Only the regions near the hydraulic fractures and several pilot locations are displayed.

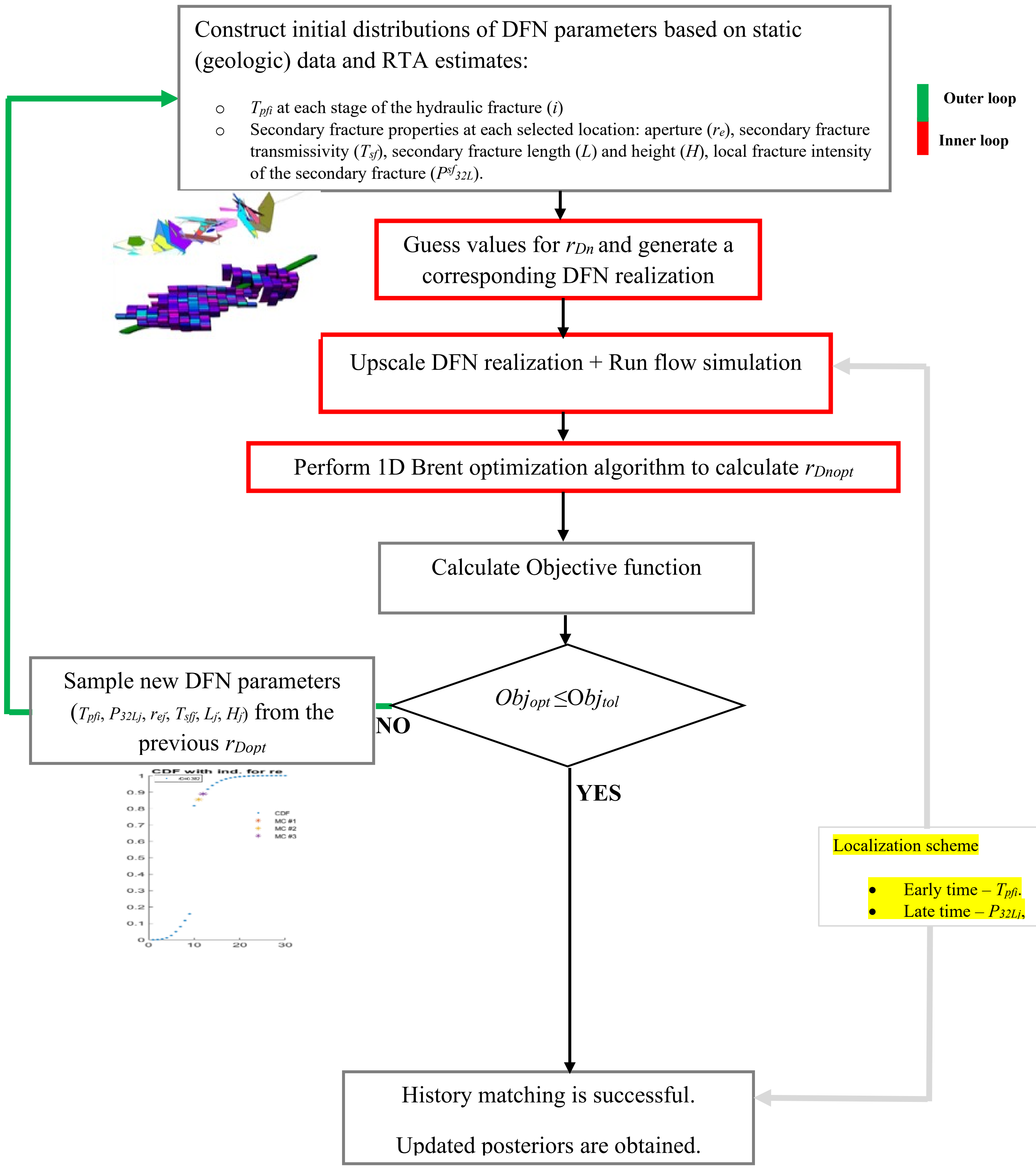

Fig. 6-3: Schematic description of the PPM procedure.

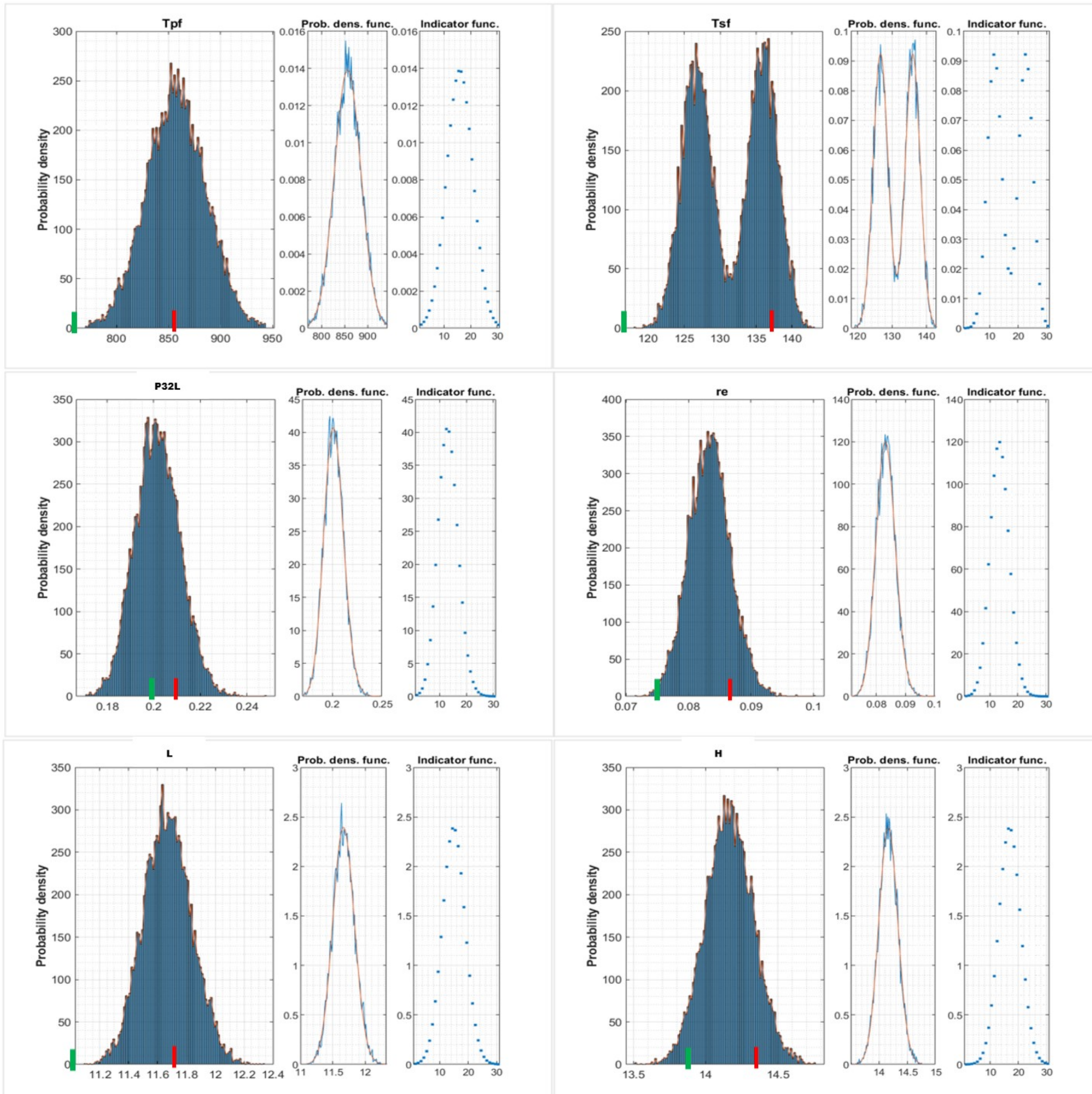

Fig. 6-4: Initial probability density functions of the primary and secondary fracture DFN parameters.

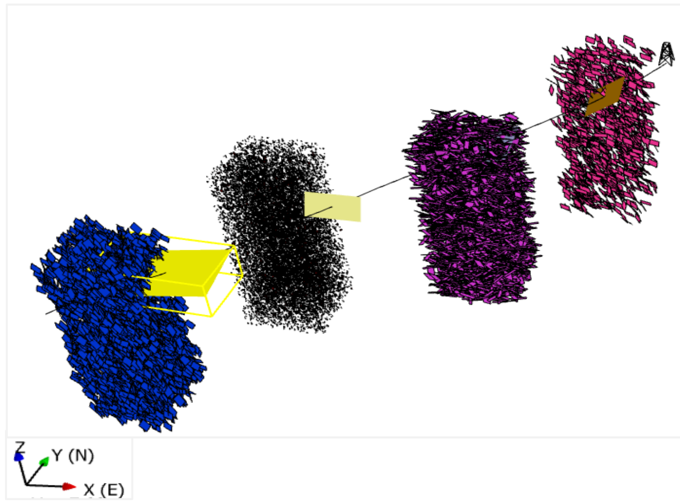

Fig. 6-5. The DFN model with the hydraulic and secondary fractures for the case where the pilot points are placed near the hydraulic fractures.

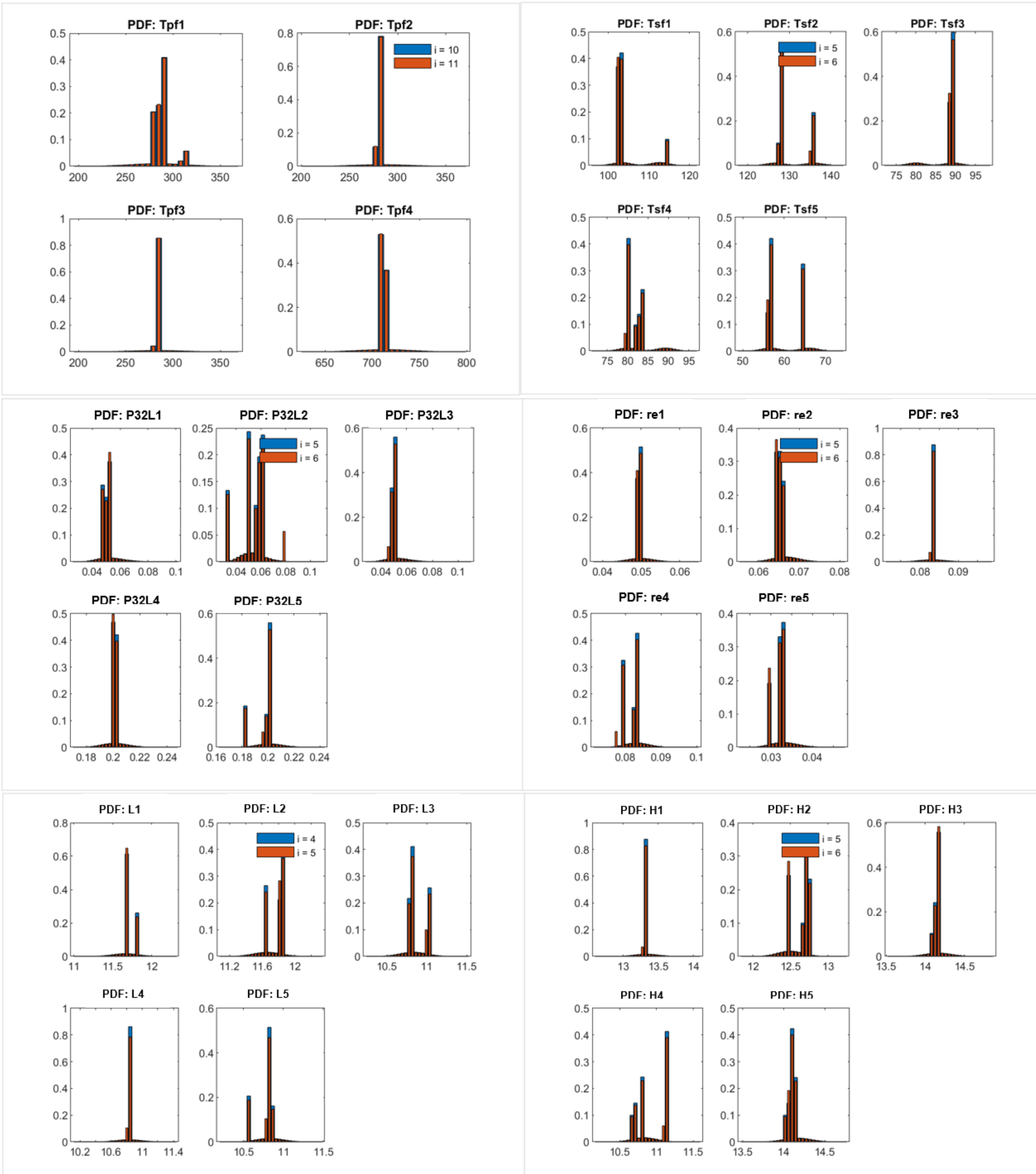

Fig. 6-6: Final posterior distributions of the hydraulic and secondary fracture DFN parameters for the iteration step $i + 1$, where. $i = l$ = iterative index

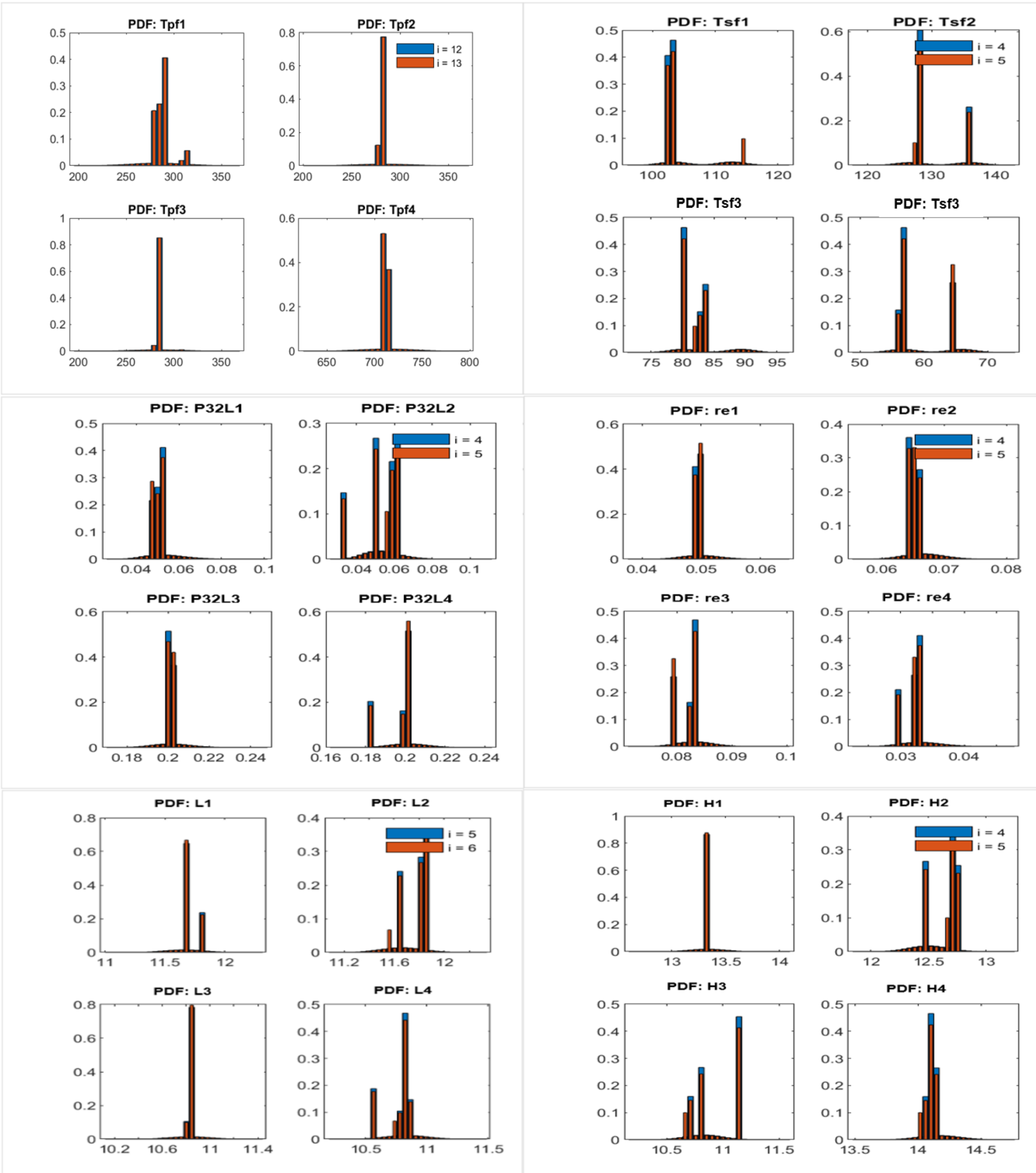

Fig. 6-7. Final posterior distributions of the hydraulic and secondary fracture DFN parameters for the iteration step $i + 1$, where $i = l$ = iterative index, for the case where pilot points are located near the hydraulic fractures.

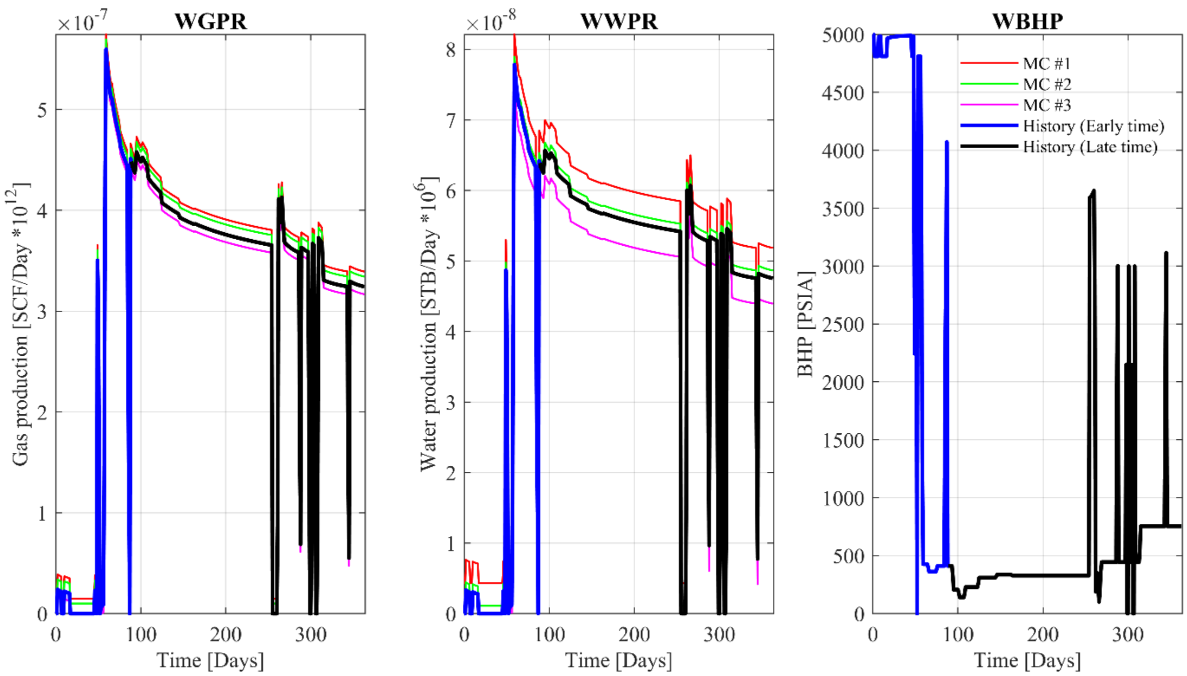

Fig. 6-8: Three random history-matched realizations of gas production rate, water production rate, and BHP profiles sampled from the final posterior probability distributions.

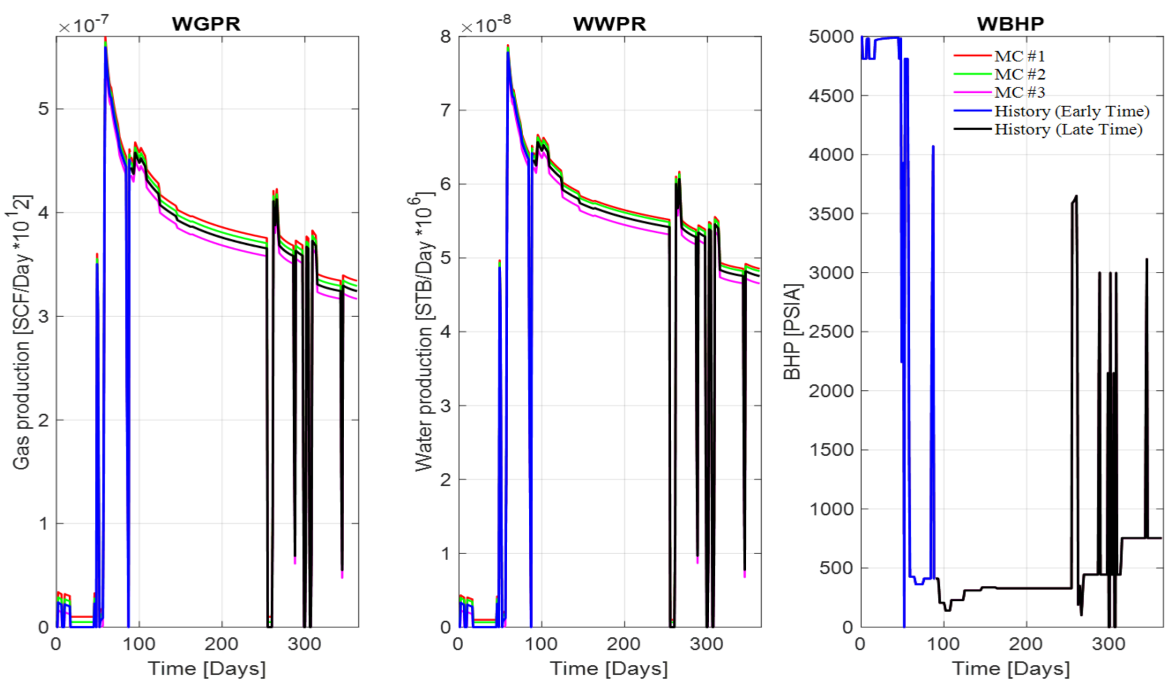

Fig. 6-9: Three random history-matched realizations of gas production rate, water production rate, and BHP profiles were sampled from the final posterior probability distributions for the case where pilot points are located near the hydraulic fractures.

Chapter 7: Conclusions and Recommendations for Future Work

7.1 OVERVIEW

In this thesis, a robust probability-based assisted history matching framework for the characterization of fracture networks in fractured shale reservoirs is reported. The research improved the existing history matching routines for hydraulically fractured reservoirs by handling both Gaussian and non-Gaussian fracture parameters and the non-linear relationship between fracture parameters and upscaled reservoir model properties while maintaining a low computational cost and honouring both the static and dynamic data. This chapter presents the conclusions derived from the work, the academic and industrial contributions, and finally, recommendations for future work.

7.2 CONCLUSIONS

Available datasets from a four-stage hydraulically fractured reservoir in the Horn River Basin, including production data and microseismic information, are gathered from previous field reports. An RTA study is conducted to derive possible estimates of the reservoir fracture parameters. The resulting RTA estimates are combined with the microseismic information to constrain the description of the fracture network. Secondary fractures, including those in the vicinity of the hydraulic fracture and those disconnected from the hydraulic fractures, are modeled. Their spatial variability is handled using the pilot-point parameterization technique and sequential indicator simulation.

A robust probabilistic-based assisted history matching workflow is developed and employed to characterize the hydraulically fractured reservoirs from the static and dynamic observations and update the posterior distributions of the uncertain fracture network parameters.

The developed PPM workflow integrates data from different sources to infer unknown multi-scale fracture parameters by perturbing the probability distributions of the unknown model parameters until a match with the production data is attained. An efficient multiple 1D optimization scheme based on golden section search and successive parabolic interpolations is incorporated with the PPM framework to obtain a local optimal value of a perturbation parameter r_{Dn} for a given initial realization. Perturbation of r_{Dn} is performed individually for each variable. The results are posterior distributions of the uncertain DFN parameters after integrating the production data.

A novel localization strategy is formulated based on the flow regimes identified from RTA where the early-time data is used to perturb and optimize only the hydraulic fracture parameters and the late-time data is used to perturb and optimize the secondary fracture parameters while the hydraulic fracture parameters remain fixed at its optimal value from the first stage. The incorporation of this scheme into the PPM workflow achieved reliable history matching results within a low pre-set objective function tolerance.

The developed fractured system characterization methodology is implemented to handle both Gaussian and non-Gaussian uncertain fracture parameters and has the capabilities of characterizing any other type uncertain fracture parameters, which is usually impossible through other sampling-based techniques where a Gaussian posterior distribution are normally expected. It further accounts for highly nonlinear relationships between fracture model parameters and the corresponding flow responses, and yields good characterization results through an ensemble of DFN realizations that honor both static and dynamic data, as well as the related upscaled flow-simulation models.

This thesis presents a robust probabilistic-based assisted history matching workflow which can efficiently characterize and update the posterior distributions of the uncertain fracture network parameters of fractured reservoir systems. The methodology presented in this thesis is targeted at improving the existing history matching routines for unconventional reservoirs used in both the academics and the industry by providing a robust and efficient workflow for the characterization of the fracture systems of shale gas reservoirs.

7.3 CONTRIBUTIONS

The significant contributions of this work can be summarized as follows:

a) A robust and efficient probabilistic-based history matching framework capable of characterizing hydraulically fractured reservoirs from static and dynamic (production) observations and updating unknown fracture network parameters is developed.

b) An incorporated pilot-point parameterization scheme and sequential simulation with the indicator-based PPM workflow efficiently handled the spatial variability of secondary fractures in the reservoir volume, including those in the vicinity of the hydraulic fractures and those disconnected from the hydraulic fractures. Thus, a proper representation of the fluid flow in a fractured reservoir system where flow is contributed by both the primary fractures and secondary fractures (NFs), and not only the primary fractures and induced fractures, is captured.

c) The developed workflow flexibly handled both Gaussian and non-Gaussian uncertain fracture parameters. This is usually impossible using other sampling-based techniques where a Gaussian posterior distribution is normally expected. In addition, it appropriately handled the nonlinear relationship between discrete fracture network parameters and reservoir flow response by perturbing model parameters in the DFN space instead of the upscaled reservoir parameters.

d) A formulated localization scheme using the flow regime rationale facilitated a reliable history matching process by perturbing the impacting model parameters according to the specific flow region.

e) An important benefit of this method is that the uncertainties in fracture parameters are quantified using multiple DFN models and their corresponding upscaled DPDK models.

f) The history-matching results achieved within a low user-defined tolerance ($\Delta O_{tol} \leq 5 - 10\%$), suggest that the modelling workflow can infer a reasonable representation of both primary and secondary fracture distributions in the reservoir.

g) The probabilistic-based assisted history matching workflow is applied to update unknown DFN model parameters (T_{pf}, P_{32L}, T_{sf}, r_e, L, H) from static and dynamic (production) observations. The method is used to update posterior probability distributions of hydraulic and secondary fractures of a shale gas reservoir.

7.4 APPLICATIONS

A major significance of this research is that while the workflow was developed for analyzing hydraulically fractured reservoirs with secondary fractures, it can be applied to other unconventional hydrocarbon formations with multiple wells.

The developed framework is also useful for CO_2 storage in terms of the improved knowledge of a competent reservoir to be used for the storage, derived from the characterization of its fracture network. An example is the reservoirs in the Horn River Basin, which is studied in this research. It originally contains about 12% CO_2 and can be classified as a good candidate for CO_2 storage, thus contributing to the vision of 2050 net-zero emissions target.

7.5 RECOMMENDATIONS FOR FUTURE WORK

(i) Application of the developed technique to characterize other complex unconventional hydrocarbon formation cases involving multiple well pads.

(ii) Coupling flow computations with geomechanics calculations in the forward model to capture the dynamic changes in stresses and temperatures, and their consequent impacts on production.

(iii) Adoption of the technique for other multiphase fluids such as wet gas and gas condensates, other than a (water-wet) dry gas reservoir where the gas remains in the gas phase during pressure depletion in the reservoir. Consideration of relative permeability function during the history matching.

(iv) Consideration of other possible hydraulic fracture shapes such as the plane strain and the elliptically shaped cross-section fracture and compare them with the elongated penny-shaped fissures used in this research.

(v) Modification of the workflow by integrating other simulation tools that can explicitly model fractures within matrix grid without refinement for the efficient calculation of fluid transport within SRV.

Bibliography

Aanonsen, S. I., Oliver, D. S., Reynolds, A. C., Vallès, B. 2009. The Ensemble Kalman Filter in Reservoir Engineering – A Review. SPE-117274-PA. SPE J. 14(03): 393–412. SPEJ Sept. 2009. https://doi.org/10.2118/117274-PA

Agarwal, R.G, D.C. Gardner, S.W. Kleinsteiber, and D.D. Fussell. 1999. Analyzing Well Production Data Using Combined-Type-Curve and Decline-Curve Analysis Concepts. SPE Reserv. Eval. Eng. 2, 478–486.

Ahmed, R., Edwards, M.G., Lamine, S., Huisman, B.A.H., Pal, M. 2015. Three-Dimensional Control-Volume Distributed Multi-Point Flux Approximation coupled with a Lower-Dimensional Surface Fracture Model. Journal of Computational Physics, 303(2015), 470 – 497. https://doi.org/10.1016/j.jcp.2015.10.001

Al-Ghamdi, A., Ershaghi, I. 1996. Pressure transient analysis of dually fractured reservoirs. SPE 26959-PA. SPE J. 1(1): 93–100. doi:10.2118/26959-PA

Ali, A.J., Siddiqui, S., Dehghanpour, H. 2013. Analyzing the Production Data of Fractured Horizontal Wells by a Linear Triple Porosity Model: Development of Analysis Equations. Journal of Petroleum Science and Engineering. 112 (2013), 117 – 128. https://doi.org/10.1016/j.petrol.2013.10.016

Al-Shaalan, T.M., Fung, L.S.K., Dogru, A.H. 2003. A Scalable Massively Parallel Dual-Porosity Dual-Permeability Simulator for Fractured Reservoirs with Super-k Permeability. SPE 84371-MS, SPE Annual Technical Conference and Exhibition, Denver, Colorado, 5–8 Oct 2003. https://doi:10.2118/84371-MS

Alshehri, N.S. 2010. Quantification of Reservoir Uncertainty for Optimal Decision Making. [Doctoral Thesis, Civil and Environmental Engineering, University of Alberta].

Amarante, F. A., Rolo, R.M., Costa, J, F. 2019. Assessing Geological Model Uncertainty – A Case Study Comparing Methods. REM –International Engineering Journal, 72(4), 643 – 653. https://doi.org/10.1590/0370-44672019720037

Aminzadeh, F., Tafti, T. A., Maity, D. 2013. An Integrated Methodology for Sub-surface Fracture Characterization Using Microseismic Data: A Case Study at the NW Geysers. Computers and Geosciences, 54, 39–49. https://doi.org/10.1016/j.cageo.2012.10.015

Babak, O., Deutsch C.V. 2008. Accounting for Parameter Uncertainty in Reservoir Uncertainty Assessment: The Conditional Finite-Domain Approach. Natural Resources Research, Vol. 18, 7-17. https://doi.org/10.1007/s11053-008-9084-7

Barenblatt, G. I., Zheltov, Y. P., Kochina, I. N. 1960. Basic concepts in the theory of seepage of homogeneous liquids in fissured rocks, J. Appl. Math. Mech., Engl. Transl. 24(5): 1286-1303. https://doi.org/10.1016/0021-8928(60)90107-6

Bayes, T., Price, R. 1763. An Essay Towards Solving a Problem in the Doctrine of Chances. By the Late Rev. Mr. Bayes, F. R. S. Communicated by Mr. Price, in a Letter to John Canton, A. M. F. R. S. Philosophical Transactions (1683-1775), 53, 370-418. www.jstor.org/stable/105741

Bello, R.O. 2009. Rate Transient Analysis in Shale Gas Reservoirs with Transient Linear Behaviour [Doctoral dissertation, Texas A&M University, Texas, USA].

Bello, R.O., Wattenbarger, R.A. 2010. Multi-stage Hydraulically Fractured Shale Gas Rate Transient Analysis. SPE-126754-MS, SPE North Africa Technical Conference and Exhibition, Egypt. https://doi.org/10.2118/126754-MS

Blasingame, T.A., Johnston. J.L., Lee. W.J. 1989. Type-Curves Analysis Using the Pressure Integral Method. SPE-18799-MS. SPE California Regional Meeting, 5 – 7 April, Bakersfield, California. https://doi.org/10.2118/18799-MS

Bogdanov, I.I., Mourzenko, V.V., Thovert, J.F., Adler, P.M. 2007. Effective Permeability of Fractured Porous Media with Power-Law Distribution of Fracture Sizes. Phys. Rev. E, 76 (036309), 1–15.

Boisvert, J. 2018. *Geostatistical methods* [lecture note]. Edmonton, AB: University of Alberta, MIN E 612.

Bourbiaux, B., Cacas, M.C., Sarda, S., Sabathier, J.C. 1998. A Rapid and Efficient Methodology to Convert Fractured Reservoir Images into a Dual-Porosity Model. Oil & Gas Science and Technology. 53 (6), 785–799. https://doi.org/10.2516/ogst:1998069

Bourdet, D. 2002. Well Test Analysis: The Use of Advanced Interpretation Models. Handbook of Petroleum Exploration and Production, ISSN 1567-8032; Vol 3. Elsevier Science.

Brent, R.P. 1973. Algorithms for Minimization without Derivatives. Prentice- Hall, Englewood Cliffs, New Jersey. ISBN: 0-13-022335-2.

Bui, T.D., Mamora, D.D., Lee, W.J. 2000. Transient Pressure Analysis for Partially Penetrating Wells in Naturally Fractured Reservoirs. SPE 60289-MS, SPE Rocky Mountain Regional/Low Permeability Reservoirs Symposium and Exhibition, Denver, Colorado, 12–15 Mar 2000. https://doi:10.2118/60289-MS

Bustin, R.M., Bustin, A.M.M., Cui, X., Ross, D.J.K., Pathi, V.S.M., 2008. Impact of Shale Properties on Pore Structure and Storage Characteristics. In: Presented at the SPE Shale Gas Production Conference, Fort Worth, Texas, USA, 16–18 November. SPE 119892. https://doi.org/10.2118/119892-MS

Caers, J. 2003. History Matching Under Training-Image-based Geological Model Constraints. SPE Journal, 8(03): pp.218-226. 10.2118/74716-PA

Caers, J. 2007. Comparing the Gradual Deformation with the Probability Perturbation Method for Solving Inverse Problems. Mathematical Geology 39(1), 27-52. https://doi.org/10.1007/s11004-006-9064-6

Chai, Z., Tang, H., He, Y., Killough, J., Wang, Y. 2018. Uncertainty Quantification of the Fracture Network with a Novel Fracture Reservoir Forward Model. SPE-191395-MS. SPE Annual Technical Conference and Exhibition, Dallas, Texas. https://doi.org/10.2118/191395-MS

Chai, Z., Yan, B., Killough, J.E., Wang, Y. 2016. An Efficient Method for Fractured Shale Reservoir History Matching: The Embedded Discrete Fracture Multi-Continuum Approach. SPE-181765-MS. SPE Annual Technical Conference and Exhibition, Dubai, UAE. https://doi.org/10.2118/181765-MS

Chang, H., and D. Zhang. 2018. History Matching of Stimulated Reservoir Volume of Shale-Gas Reservoirs Using an Iterative Ensemble Smoother. SPE-189436-PA. SPE Journal 23 (2): 346-366. https://doi.org/10.2118/189436-PA

Chen, H., Yang, C., Datta-Gupta, A., Zhang, J., Chen, L., Liu, L., Chen, B., Cui, X., Shi, F., Bahar, A. 2019. A Hierarchical Multiscale Framework for History Matching and Optimal Well Placement for a HPHT Fractured Gas Reservoir, Tarim Basin, China. IPTC-19314-MS. International Petroleum Technology Conference, Beijing China. https://doi.org/10.2523/IPTC-19314-MS

Chen, Y., Oliver, D.S., 2012. Ensemble Randomized Maximum Likelihood Method as an Iterative Ensemble Smoother. Math. Geosci. 44 (1), 1–26. https://doi.org/10.1007/ s11004-011-9376-z

Chen, Y., Durlofsky, L.J., Gerristen, M., Wen, X.H., 2003. A Coupled Local-Global Upscaling Approach for Simulating Flow in Highly Heterogeneous Formations. Advances in Water Resources. 26 (10), 1041–1060. https://doi.org/10.1016/S0309-1708(03)00101-5

Chow, C.C. 2015. Sampling from a Probability Distribution. Scientific Clearing House. https://sciencehouse.wordpress.com/2015/06/20/sampling-from-a-probability-distribution/

Cinco-ley, H. 1996. Well-Test Analysis for Naturally Fractured Reservoirs. SPE-31162-JPT. Journal of Petroleum Technology 48(01). https://doi.org/10.2118/31162-JPT

Cipolla, C., L., Lolon, E. P., Erdle, J. C., Rubin, B. 2010. Reservoir Modeling in Shale-Gas Reservoirs. SPE Res Eval & Eng, 13 (2010): 638–653. doi:https://doi.org/10.2118/125530-PA

Clarkson, C.R, and P.K. Pedersen. 2010. Tight Oil Production Analysis: Adaptation of Existing Rate-Transient Analysis Techniques. SPE-137352-MS. *In Proceedings of the Canadian Unconventional Resources and International Petroleum Conference, Calgary, AB, Canada, 19–21 Oct.*

Cui, H., Kelkar, M. 2005. Automatic History Matching of Naturally Fractured Reservoirs and a Case Study. SPE-94037-MS. Western Regional Meeting, Irvine, California, 30 March-1 April. https://doi.org/10.2118/94037-MS

Daniel, C. 1973. One-at-a-Time Plans. Journal of the American Statistical Association, 68(342), 353-360. https://www.jstor.org/stable/2284076

Degraff, J.M., Meurer, M.E., Landis, L.H., Lyons, S. 2005. Fracture network modeling and dual-permeability simulation of carbonate reservoirs. SPE 10954-MS. international petroleum technology conference, Doha, Qatar. doi:10.2118/10954-MS

De Lima, A., Lange, A., Schiozer, D.J., 2012. Assisted History-Matching for the Characterization and Recovery Optimization of Fractured Reservoirs using Connectivity Analysis. SPE 154392. SPE Europec/EAGE Annual Conference. https://doi.org/10.2118/154392-MS

Dershowitz, B., LaPointe, P., Eiben, T. et al. 2000: Integration of Discrete Feature Network Methods with Conventional Simulator Approaches. SPE Res Eval & Eng 3 (2): 165-170. SPE-62498-PA. http://dx.doi.org/10.21186/62498-PA

Dershowitz, W. S. 1984. Rock Joint Systems. [Doctoral Thesis, Massachusetts Institute of Technology, Cambridge, Massachusetts].

Dershowitz, W.S. 1993. Geometric Conceptual Models for Fractured Rock Masses: Implications for Groundwater Flow and Rock Deformation. ISRM-EUROCK-1993-010, Second European Conference of the International Society for Rock Mechanics, Lisbon, Portugal, 21–24 June. https://www.onepetro.org/conference-paper/ISRM-EUROCK-1993-010

De Swaan, O.A. 1976. Analytical Solutions for Determining Naturally Fractured Reservoir Properties by Well Testing. SPE 5346-PA. SPE J. 16(3), 117–122 (1976). https://doi:10.2118/5346-PA

Deutsch, C. V. 2002. Geostatistical Reservoir Modeling. Oxford University Press, Inc., New York, New York.

Deutsch, C. V. 2004. A Statistical Resampling Program for Correlated Data: Spatial_Bootstrap. Center for Computational Geostatistics Annual Report (Vol. 6). University of Alberta, Edmonton, Canada. Retrieved from http://www.ccgalberta.com/ccgresources/report06/2004-401-spatial_bootstrap.pdf

Deutsch, C.V., and A.G. Journel. 1998. GSLIB Geostatistical Software Library and User's Guide, 2nd Edition, Applied Geostatistics Series, Oxford University Press, Inc. New York, NY.

Emerick, A. A., Reynolds, A. C. 2011. History Matching a Field Case Using the Ensemble Kalman Filter With Covariance Localization. SPE -141216-PA. SPE Res Eval & Eng 14 (04): 443-452. https://doi.org/10.2118/141216-PA

Emerick, A. A., Reynolds, A. C. 2012. Combining the ensemble Kalman Filter with Markov-chain Monte Carlo for Improved History Matching and Uncertainty Characterization. SPE-141336-PA. SPE J. 17(2): 418–440. https://doi.org/10.2118/ 141336-PA

Emery, A.F. 2016. Advances in Heat Transfer: Parameter Estimation, Volume 48. ISSN 0065-2717. http://dx.doi.org/10.1016/bs.aiht.2016.08.001

Endo, H. K., and Long, J. S. 1984. A Model for Investigating Mechanical Transport in Fracture Networks. Water Resources Research, 20(10), 1390-1400. https://doi:10.1029/WR020i010p01390

Ezulike, O.D., Ghanbari, E., Siddiqui, S., Dehghanpour, H. 2015. Pseudo-Steady State Analysis in Fractured Tight Oil Reservoirs. Journal of Petroleum Science and Engineering. 129 (2015), 40 – 47. https://doi.org/10.1016/j.petrol.2015.01.009

Ezulike, O. D., Dehghanpour, H. 2015. A Complementary Approach for Uncertainty Reduction in Post-Flowback Production Data Analysis. Journal of Natural Gas Science and Engineering. 27(2), 1074 – 1091. https://doi.org/10.1016/j.jngse.2015.09.059

Emerick, A.A., Reynolds, A.C. 2012. Combining the Ensemble Kalman Filter with Markov-Chain Monte Carlo for Improved History Matching and Uncertainty Characterization. SPE-141336-PA. SPE Journal 17 (2): 418–440. https://doi-org/10.2118/141336-PA

Endo, H. K., and Long, J. S. 1984. A Model for Investigating Mechanical Transport in Fracture Networks. Water Resources Research, 20(10), 1390-1400. https://doi:10.1029/WR020i010p01390

Fisher, M.K., Wright, C.A., Davidson, B.M., Goodwin, A.K., Fielder, E.O., Buckler, W.S., Steinsberger, N.P. 2003. Integrating Fracture Mapping Technologies to Optimize Stimulations in the Barnett Shale. SPE-77441-PA. SPE Production & Facilities. 20 (02), 85-93. https://doi.org/10.2118/77441-PA

Fisher, R.A. 1953. Dispersion on a Sphere. The Royal Society of London. Series A, Mathematical and Physical Sciences. A217 (1130), 295-305. https://doi.org/10.1098/rspa.1953.0064

Garcia, M.H., Gouth, F.M., Gosselin, O.R. 2007. Fast and Efficient Modeling and Conditioning of Naturally Fractured Reservoir Models Using Static and Dynamic Data. SPE-107525-MS. EUROPEC/EAGE Conference and Exhibition, London, U.K. https://doi-org /10.2118/107525-MS

Golder Associates. 2018. FRACMAN 7.70 User Documentation. Copyright 1999 – 2018.

Gringarten, E. 2009. Uncertainty Assessment Using 3D Modeling. AAPG Geol. Tech. Workshop - Geological Aspects of Estimating Petroleum Resources and Reserves #120025.

Guidelines for Application of the Petroleum Resources Management System (2011). Sponsored by Petroleum Engineers (SPE), American Association of Petroleum Geologists (AAPG), World Petroleum Council (WPC), Society of Petroleum Evaluation Engineers (SPEE) and Society of Exploration Geophysicists (SEG)

Heinemann, Z. E., Mittermeir, G. M. 2011. Derivation of the Kazemi–Gilman–Elsharkawy Generalized Dual Porosity Shape Factor. Transp Porous Med 91, 123–132. https://doi-org./10.1007/s11242-011-9836-4

Hu, B.X., Huang, H. 2002. Stochastic Analysis of Reactive Solute Transport in Heterogeneous, Fractured Porous Media: a Dual-Permeability Approach. Trans. Porous Med. 48(1), 1–39. https://doi:10.1023/A:1015671227317

Hu, L. Y. 2000. Gradual deformation and Iterative Calibration of Gaussian Related Stochastic Models. Mathematical Geology 32(1), 87–108.

Hu, L. Y. 2002. Combination of Dependent Realizations within the Gradual Deformation Method. Mathematical Geology 34(8), 953–963.

Hu, L.Y., Jenni, S. 2005. History Matching of Object-Based Stochastic Reservoir Models. SPE Journal 10 (3), 312–323. https://doi.org/10.2118/81503-PA

Jo, H. 2013. Optimal Fracture Spacing of a Hydraulically Fractured Horizontal Wellbore to Induce Complex Fractures in a Reservoir Under High In-Situ Stress Anisotropy. IPTC-16717-MS. International Petroleum Technology Conference, 26-28 March, Beijing, China. https://doi-org/10.2523/IPTC-16717-MS

Johansen, K. 2008. Statistical Methods for History Matching. PhD Dissertation, Department of Chemical and Biochemical Engineering, Technical University of Denmark.

Johansen, K., Caers, J., Suzuki, S. 2007. Hybridization of the Probability Perturbation Method with Gradient Information. *Comput Geos* 11, 319 – 331 (2007). https://doi.org/10.1007/s10596-007-9055-9

Kalman, R.E. 1960. A New Approach to Linear Filtering and Prediction Problems. Transactions of the ASME – Journal of Basic Engineering 82(Series D): 35 – 45.

KAPPA Engineering, 2019. Dynamic Data Analysis – v5.20.02 - ©KAPPA 1988 - 2019

Kashib, T., Srinivasan, S. 2006. A Probabilistic Approach to Integrating Dynamic Data in Reservoir Models. Journal of Petroleum Science and Engineering 50(3–4), 241 – 257. https://doi.org/10.1016/j.petrol.2005.11.002

Kazemi, H. 1969. Pressure Transient Analysis of Naturally Fractured Reservoirs with Uniform Fracture Distribution. SPE-2156-A. *SPE J.* 9(04), 451-462.

Kazemi, H., Gilman, J.R., Elsharkawy, A.M. 1992. Analytical and Numerical Solution of Oil Recovery from Fractured Reservoirs Using Empirical Transfer Functions. SPE-19849-PA. SPE Reserv. Eng. 7(2), 219–227. https://doi-org/10.2118/19849-PA

Kazemi, H., Merrill, L.S., Porterfield, K.L., Zeman, P.R. 1976. Numerical Simulation of Water-Oil Flow in Naturally Fractured Reservoirs. SPE-5719-PA. SPE Journal 16(6), 317-326. https://doi.org/10.2118/5719-PA

Khani, H., Hamdi, H., Nghiem L., Chen, Z., Sousa, C.S. 2018. Geologically Consistent History Matching of SAGD Process Using Probability Perturbation Method. SPE-189770-MS. SPE Canada Heavy Oil Technical Conference, Calgary, 13-14 March. https://doi.org/10.2118/189770-MS

Kumar, S., Rey, A., Dufour, G., Ogunyomi, B. 2019. Understanding Fluid Flow Behavior in Fractured Reservoir using Dual Porosity Dual Permeability and Discretized Fracture Model. SPE-196038-MS. SPE Annual Technical Conference and Exhibition, Calgary, Alberta, Canada. doi:https://doi.org/10.2118/196038-MS.

Lee, P.M. 1997. Bayesian Statistics, An Introduction, Second Edition. John Wiley & Sons Inc., New York.

Li, G and Reynolds, A.C. 2009. Iterative Ensemble Kalman Filters for Data Assimilation. SPE-109808-PA. SPE Journal 14(3), 496–505. https://doi-org/10.2118/109808-PA

Li, L., Lee, S.H. 2008. Efficient field-scale simulation of black oil in a naturally fractured reservoir through discrete fracture networks and homogenized media. SPE-103901-PA. SPE Res. Eval. & Eng. 11(4): 750-758. https://doi-org /10.2118/103901-PA

Linde, N., Renard, P., Mukerji, T., Caers, J., 2015. Geological Realism in Hydrogeological and Geophysical Inverse Modeling: A Review. Adv. Water Resour. 86 (Part A), 86–101. https://doi.org/10.1016/j.advwatres.2015.09.019

Liu, S., Wei, J., Ma, Y., Liu, X., Yan, B. 2021. Numerical simulation on the effect of fractures geometries for shale gas development with discrete fracture network model. *J Petrol Explor Prod Technol*.

Liu, Y., Leung, J.Y., Chalaturnyk, R., Virues, C.J.J. 2019. New Insights on Mechanisms Controlling Fracturing Fluid Distribution and its Impacts on Well Performance in Shale Gas

Reservoirs. SPE Production & Operations 34(3): 564-585. https://doi-org/10.2118/185043-PA.

Liu, Y., Liu, L., Leung, J. Y., Moridis, G. J. 2020. Sequentially Coupled Flow and Geomechanical Simulation with a Discrete Fracture Model for Analyzing Fracturing Fluid Recovery and Distribution in Fractured Ultra-Low Permeability Gas Reservoirs. Journal of Petroleum Science and Engineering, 189, 107042. https://doi.org/10.1016/j.petrol.2020.107042

Long, J. S., Remer, J. S., Wilson, C. R., & Witherspoon, P. A. 1982. Porous Media Equivalents for Networks of Discontinuous Fractures. Water Resources Research, 18(3), 645-658. https://doi:10.1029/WR018i003p00645

MathWorks. 2018. MATLAB Documentation. www.mathworks.com/help/matlab/index.html

MathWorks, 2020. MATLAB Documentation. www.mathworks.com/help/matlab/index.html

MathWorks, 2021. MATLAB Documentation. www.mathworks.com/help/matlab/index.html

Maucec, M., Douma, S. G., Hohl, D., Leguijt, J., Jimenez, E., Datta-Gupta, A. 2007. Streamline-Based History Matching and Uncertainty--Markov-Chain Monte Carlo Study of an Offshore Turbidite Oil Field. SPE-109943-MS. SPE Annual Technical Conference and Exhibition, California, USA. https://doi.org/10.2118/109943-MS

Mishra, S. 1998. Alternatives to Monte-Carlo Simulation for Probabilistic Reserves Estimation and Production Forecasting. SPE-49313-MS. SPE Annual Technical Conference and Exhibition held in New Orleans, Louisiana. https://doi.org/10.2118/49313-MS

Monteagudo, J.E.P., Firoozabadi, A. 2004. Control-Volume Method for Numerical Simulation of Two-Phase Immiscible Flow in Two-and Three-Dimensional discrete-Fractured Media, Water Resources Research. 40(7) (2004) W074051–W0740520, http://dx.doi.org/10.1029/2003WR002996

Morris, M. D. 1991. Factorial Sampling Plans for Preliminary Computational Experiments. Technometrics, 33(2), 161–174. https://www.jstor.org/stable/1269043

Nejadi, S., Leung, J.Y., Trivedi, J.J. 2015. Integrated Characterization of Hydraulically Fractured Shale-Gas Reservoirs - Production History Matching. SPE Res Eval & Eng **18** (04): 481–494. SPE-171664-PA. https://doi.org/10.2118/171664-PA.

Nejadi, S., Trivedi, J.J., Leung, J. 2017. History Matching and Uncertainty Quantification of Discrete Fracture Network Models in Fractured Reservoirs. Journal of Petroleum Science and Engineering. 152, 21–32. http://dx.doi.org/10.1016/j.petrol.2017.01.048

Neufeld, Chad and Deutsch, Clayton V. (2007) CCG Software Catalogue. 9th Annual CCG Meeting.

Nwabia, F.N., Leung, J.Y. 2021a. Inference of Hydraulically Fractured Reservoir Properties from Production Data Using the Indicator-Based Probability Perturbation Assisted History-Matching Method. Journal of Petroleum Science and Engineering 198, 108240. ISSN 0920-4105. https://doi.org/10.1016/j.petrol.2020.108240

Nwabia, F.N., Leung, J.Y. 2021b. Probabilistic History Matching of Multi-scale Fractured Reservoirs: Integration of a Novel Localization Scheme Based on Rate Transient Analysis. J. Nat. Gas Sci. Eng., 94 (2021): p. 104067, https://doi.org/10.1016/j.jngse.2021.104067

Nwabia, F.N., and J.Y. Leung. 2020. Probabilistic History Matching of Multi-Scale Fractured Reservoirs: Integration of a Novel Localization Scheme Based on Rate Transient Analysis. SPE-199988-MS. SPE Canada Unconventional Resources Conference, Calgary, Canada. https://doi.org/10.2118/199988-MS

Oda, M. 1985. Permeability Tensor for Discontinuous Rock Masses. Geotéchnique **35** (4): 483 – 495. https://doi.org/10.1680/geot.1985.35.4.483

Oliver, D., Chen, Y., 2011. Recent Progress on Reservoir History Matching: A Review. Computational Geosciences. 15(1), 185–221. https://doi.org/10.1007/s10596-010-9194-2

Pyrcz, M.J., Deutsch, C.V. 2014. Geostatistical Reservoir Modeling. Oxford University Press. ISBN: 978-0-19-973144-2.

Rwechungura, R.W., Dadashpour, M., Kleppe, J. 2011. Advanced History Matching Techniques Reviewed. SPE -142497-MS. SPE Middle East Oil and Gas Show and Conference, 25 – 28 September, Manama, Bahrain. https://doi.org/10.2118/142497-MS

Sahimi, M. 2011. Flow and Transport in Porous Media and Fractured Rock (2nd ed.). Weinheim: Wiley-VCH.

Sandve, T.H., Berre, I., Nordbotten, J.M. 2012. An Efficient Multi-Point Flux Approximation Method for discrete Fracture–Matrix Simulations. Journal of Computational Physics. 231(09), 3784–3800. https://doi.org/10.1016/j.jcp.2012.01.023

Sarda, S., Jeannin, L., Bourbiaux, B. 2001. Hydraulic Characterization of Fractured Reservoirs: Simulation on Discrete Fracture Models. SPE Reservoir Simulation Symposium, Houston, Texas, USA. SPE-66398-MS. https://doi-org/10.2118/66398-MS.

Scheidt, C., Li, L., Caers, J. 2018. Quantifying Uncertainty in subsurface Systems. Geophysical Monograph 236, First Edition. https://doi.org/10.1002/9781119325888.ch4

Schlumberger, 2017. ECLIPSE Reference Manual Version 2017.2.

Schlumberger, 2017. ECLIPSE Technical Description Version 2017.2.

Shakiba, M., de Araujo Cavalcante Filho J., Sepehrnoori, K. 2018. Using Embedded Discrete Fracture Model (EDFM) in Numerical Simulation of Complex Hydraulic Fracture Networks Calibrated by Microseismic Monitoring Data. Journal of Natural Gas Science and Engineering, 55(2018), 495-507. ISSN 1875-5100. https://doi.org/10.1016/j.jngse.2018.04.019

Solow, A.R. 1985. Bootstrapping Correlated Data. Journal of the International Association for Mathematical Geology 17, 769-775. https://doi.org/10.1007/BF01031616

Sun, J., Schechter, D. S. 2015. Optimization-Based Unstructured Meshing Algorithms for Simulation of Hydraulically and Naturally Fractured Reservoirs with Variable Distribution of Fracture Aperture, Spacing, Length and Strike. SPE-170703-PA. SPE Res. Eval & Eng 18(04): 463 – 480. https://doi-org /10.2118/170703-PA

Suzuki, S., Daly, C., Caers, J.K., Mueller, D., 2007. History Matching of Naturally Fractured Reservoirs using Elastic Stress Simulation and Probability Perturbation Method. SPE-95498-PA. SPE J. 12 (1), 118–129. https://doi.org/10.2118/95498-PA

Torres, F., A. Jia, Y. Wei, W. Yunsheng, W. Junlei, X. Hongbing, L. Ning, and M. Jijun. 2020. Comparison of Dual Porosity Dual Permeability with Embedded Discrete Fracture Model for Simulation Fluid Flow in Naturally Fractured Reservoirs. ARMA-2020-1462. In Proceedings of the 54th US Rock Mechanics/ Geomechanics Symposium, Houston, Texas, USA.

Tripoppoom, S. 2019. Assisted History Matching Workflow for Unconventional Reservoirs. [MSc Thesis, University of Texas at Austin].

Uba, H.M., Chiffoleau, Y., Pham, T., Divry, V., Kaabi, A., Thuwaini, J. 2007. Application of a hybrid dual-porosity/ dual-permeability representation of large-scale fractures to the simulation of a giant carbonate reservoir. SPE 105560-MS. SPE middle east oil and gas show and conference, Bahrain. doi:10.2118/105560-MS

Uleberg, K., and J. Kleppe. 1996. Dual Porosity, Dual Permeability Formulation for Fractured Reservoir Simulation. Paper from the NTNU Trondheim RUTH Seminar, Stavanger.

Uzun, I., B. Kurtoglu, and H. Kazemi. 2016. Multiphase Rate-Transient Analysis in Unconventional Reservoirs: Theory and Application. SPE Reserv. Eval. Eng. 19, 553–566.

Van Heel, A.P.G., Boerrigter, P.M., Van Dorp, J.J. 2008. Thermal and Hydraulic Matrix-Fracture Interaction in Dual Permeability Simulation. SPE 102471-PA. SPE Reservoir Evaluation Eng. 11(4), 735–749. http://doi:10.2118/102471-PA

Vo, H., J. Kamath, and R. Hui. 2019. High Fidelity Simulation of Recovery Mechanisms in Complex Natural Fracture Systems. SPE-193864-MS. *In Proceedings of the SPE Reservoir Simulation Conference, 10-11 April, Galveston, Texas*.

Wang, H. 2018. Discrete Fracture Networks Modeling of Shale Gas Production and Revisit Rate Transient Analysis in Heterogeneous Fractured Reservoirs. Journal of Petroleum Science and Engineering. 169, 796 – 812. https://doi.org/10.1016/j.petrol.2018.05.029

Wang, M., Leung, J.Y. 2015. Numerical Investigation of Fluid-Loss Mechanisms During Hydraulic Fracturing Flow-Back Operations in Tight Reservoirs. Journal of Petroleum Science and Engineering 133: 85-102. https://doi.org/10.1016/j.petrol.2015.05.013

Warren, J.E., Root, P.J. 1963. The Behavior of naturally Fractured Reservoirs. SPE 426-PA. SPE J. 3(3), 245–255. http://doi:10.2118/426-PA

Yang, S., Harris, N.B., Dong, T., Wu, W., Chen, Z. 2018. Natural Fractures and Mechanical Properties in a Horn River Shale Core From Well Logs and Hardness Measurements. SPE-174287-PA. SPE Res Eval & Eng 21(03): 671–682. https://doi-org/10.2118/174287-PA

Yu, X., Jim, R., Scott, L., Maxwell, S. 2016. Discrete-Fracture-Network Generation From Microseismic Data by Use of Moment-Tensor- and Event-Location-Constrained Hough Transforms. *SPE J.* 21 (01): 221–232. https://doi-org/10.2118/168582-PA

Yu, W., K. Wu, M. Liu, K. Sepehrnoori, and J. Miao. 2018. Production Forecasting for Shale Gas Reservoirs with Nanopores and Complex Fracture Geometries Using an Innovative Non-intrusive EDFM Method. SPE 191666. *In Proceedings of the SPE Annual Technical Conference and Exhibition, September 2018, Dallas, Texas.*

Yue, M., Leung, J.Y., Dehghanpour, H. 2016. Numerical Investigation of Limitations and Assumptions of Analytical Transient Flow Models in Tight Oil Reservoirs. Journal of Natural Gas Science and Engineering 30: 471-486. https://doi.org/10.1016/j.jngse.2016.01.042

Xu, Z., Leung, J. Y. 2021. Analyzing the Impacts of Meshing and Grid Alignment in Dual-Porosity Dual-Permeability Upscaling. SPE-208573-PA. SPE Res Eval & Eng 1-20. https://doi.org/10.2118/208573-PA

Yang, S., Harris, N.B., Dong, T., Wu, W., Chen, Z. 2018. Natural Fractures and Mechanical Properties in a Horn River Shale Core From Well Logs and Hardness Measurements. SPE-174287-PA. SPE Res Eval & Eng 21(03): 671–682. https://doi-org/10.2118/174287-PA

Yu, X., Jim, R., Scott, L., Maxwell, S. 2016. Discrete-Fracture-Network Generation From Microseismic Data by Use of Moment-Tensor- and Event-Location-Constrained Hough Transforms. *SPE J.* 21 (01): 221–232. https://doi-org/10.2118/168582-PA

Zidane, A., Firoozabadi, A. 2014. An Efficient Numerical Model for Multicomponent Compressible Flow in Fractured Porous Media, Advances in Water Resources. 74, 127–147. https://doi.org/10.1016/j.advwatres.2014.08.010

Zuo, L, W. Yu, and K. Wu. 2016. A fractional Decline Curve Analysis Model for Shale Gas Reservoirs. *Int. J. Coal Geol.* 163, 140–148.

Appendix

A.1 RATE TRANSIENT ANALYSIS

<u>Matrix transient linear flow</u>:

The transient linear flow regime is characterized by a half-slope representing matrix drainage into fractures with infinite conductivity. The analysis data obtained during this flow regime is useful in estimating the total matrix surface area draining into the fracture system.

The plot of $\frac{\left[m(P_i)-m(P_{wf})\right]}{q_{sc}}$ versus $\sqrt{t}$ is derived from the following equation;

Considering oil flowing at constant rate, $\frac{P_i-P_{wf}}{q_{sc}}=\frac{4.06B}{h}\sqrt{\frac{\mu}{\phi c_t k X_f^{\,2}}}\sqrt{t}$ (A.1-1)

$$P_D=\sqrt{\pi t_{Dxf}} \qquad \text{(A.1-2)}$$

where $t_{Dxf}=0.0002637\frac{k}{\phi\mu c_t X_f^{\,2}}t$ (t in days) (A.1-3)

$$P_D=\frac{1}{141.2}\frac{kh}{qB\mu}(P_i-P_{wf}) \qquad \text{(A.1-4)}$$

$$\frac{1}{141.2}\frac{kh}{qB\mu}(P_i-P_{wf})=\sqrt{\pi 0.0002637\frac{k}{\phi\mu c_t X_f^{\,2}}t} \qquad \text{(A.1-5)}$$

$$(P_i-P_{wf})=141.2\frac{qB\mu}{kh}\sqrt{\pi 0.0002637\frac{k}{\phi\mu c_t X_f^{\,2}}t} \qquad \text{(A.1-6)}$$

$$(P_i-P_{wf})=(141.2\sqrt{\pi 0.0002637})\frac{B}{h}\sqrt{\frac{\mu^2}{k_m^{\,2}}\frac{k}{\phi\mu c_t X_f^{\,2}}t}=4.0641\frac{B}{h}\sqrt{\frac{\mu}{\phi k_m c_t X_f^{\,2}}}\sqrt{t} \qquad \text{(A.1-7)}$$

For a gas case,

$$\frac{\left[m(P_i)-m(P_{wf})\right]}{q_g}=1447.8\frac{TP_{sc}}{hT_{sc}}\sqrt{\frac{1}{\pi(\phi\mu c_t)_{f+m}k_m X_f^{\,2}}}\sqrt{t} \qquad \text{(A.1-8)}$$

Plot of $\frac{\left[m(P_i)-m(P_{wf})\right]}{q_g}$ versus $\sqrt{t}$ yields, Slope, $m = \dfrac{TP_{sc}}{hX_f T_{sc}\sqrt{k_m}\sqrt{\pi(\phi\mu c_t)_{f+m}}}$ (A.1-9)

Note that, $X_f = \dfrac{A_{cm} \times L_w}{2A_{cw}}$ (A.1-10)

$A_{cw} = 2 \times L_w \times h$ (A.1-11)

Thus, $\sqrt{k_m}A_{cm} = \dfrac{TP_{sc}}{m.T_{sc}\sqrt{\pi(\phi\mu c_t)_{f+m}}}$ (A.1-12)

If k_m is known, A_{cm} is estimated.

<u>Pseudo steady-state or SRV flow:</u>

This flow regime is characterized by a unit slope representing pressure interference between consecutive hydraulic fractures. Its analysis is based on the log-log plot of *RNP* versus *MBT* on a cartesian graph. The equation for the plot of *RNP* versus *MBT* is originally derived from the material balance equation into the governing equation during the PSS flow regime.

Material balance equation $q\rho\Delta t\,|_{x+\Delta x} - q\rho\Delta t\,|_x = \rho\phi_m V_m\,|_{t+\Delta t} - \rho\phi_m V_m\,|_t$ (A.1-13)

$\dfrac{dP_m}{dt} = -\dfrac{q}{V_m\phi C_t}$ (A.1-14)

Linear diffusivity equation $\dfrac{d^2P_m}{dx^2} = \left(\dfrac{\phi_m\mu c_t}{k_m}\right)\dfrac{dP_m}{dt}$

(A.1-15)

Average pressure of control volume $\overline{P_m} = \dfrac{\mu BqL_f^{\,2}}{12k_mV_m} + P_f$ (A.1-16)

where $V_m = 2X_f hNL_f$

Governing equation $\dfrac{P_i - P_f}{q_{(t)}} = \left(\dfrac{B}{\left(2X_f hNL_f\right)\times\left(\phi c_t\right)_m}\right)\dfrac{Q_{(t)}}{q_{(t)}} + \left(\dfrac{\mu BL_f}{12k_m\left(2X_f hN\right)}\right)$ (A.1-17)

As hydraulic fractures are considered highly permeable, pressure drop during the PSS is negligible and thus P_f (fracture pressure) $\equiv P_{wf}$.

$$\frac{P_i - P_{wf}}{q_{(t)}} = \left(\frac{B}{\left(2X_f hNL_f\right)\times\left(\phi c_t\right)_m}\right)\frac{Q_{(t)}}{q_{(t)}} + \left(\frac{\mu BL_f}{12k_m\left(2X_f hN\right)}\right) \qquad \text{(A.1-18)}$$

$$\equiv \quad RNP = \left(\frac{B}{\left(2X_f hNL_f\right)\times\left(\phi c_t\right)_m}\right)MBT + \left(\frac{\mu BL_f}{12k_m\left(2X_f hN\right)}\right)$$

$$\text{Slope} = \left(\frac{B}{\left(2X_f hL_w\right)\times\left(\phi c_t\right)_m}\right) \qquad \text{(A.1-19)}$$

$$\text{Intercept} = \left(\frac{\mu BL_f}{24k_m X_f hN}\right) \qquad \text{(A.1-20)}$$

For a gas reservoir,

$RNP = \dfrac{m(P_i) - m(P_{wf})}{q_{(t)}}$ is plotted against $t_e = \dfrac{Q_{(t)}}{q_{(t)}}$

To preserve the signatures corresponding to the flow regimes by suppressing the noise level, the integral of *RNP* and its derivative are plotted with t_e.

Integral of normalized pressure $\dfrac{1}{t_e}\displaystyle\int_0^{t_e}\frac{m(P_i) - m(P_{wf})}{q_{(t)}}dt$ versus t_e

Derivative of the integral of normalized pressure $\dfrac{\partial}{\partial \ln t_e}\left(\dfrac{1}{t_e}\displaystyle\int_0^{t_e}\frac{m(P_i) - m(P_{wf})}{q_{(t)}}dt\right)$ versus t_e

The slope of the log-log plot of *RNP* versus *MBT* of the PSS region facilitates the estimation of X_f. Thus, *SRV* is calculated as $2 \times L_w \times X_f \times h$. The line intercept on the other hand is used for the estimation of k_m.

MBAL (normalized rate cumulative) plot:

The gas material balance is formulated in terms of pseudo pressures. At PSS boundary dominated flow, it obeys the equation,

$$q_D = \frac{1}{2\mu} - Q_{DA} \qquad \text{(A.1-21)}$$

Where,

Dimensionless rate $q_D = \dfrac{1422Tq}{kh(m(P_i) - m(P_{wf}))}$ (A.1-22)

and

Cumulative production $Q_{DA} = \dfrac{4.5Tz_iG_i\left[m(P_i) - m(\overline{P})\right]}{\phi hAP_i\left[m(P_i) - m(P_{wf})\right]}$ (A.1-23)

Thus,

$$\frac{1422Tq}{kh(m(P_i) - m(P_{wf}))} = \frac{1}{2\mu} - \frac{4.5Tz_iG_i\left[m(P_i) - m(\overline{P})\right]}{\phi hAP_i\left[m(P_i) - m(P_{wf})\right]} \tag{A.1-24}$$

A plot of $\dfrac{q}{m(P_i) - m(P_{wf})}$ versus $\dfrac{G_i\left[m(P_i) - m(\overline{P})\right]}{\left[m(P_i) - m(P_{wf})\right]}$ converges towards a straight line as the system goes into PSS flow and intercepts can be used to estimate STGIIP:

$$\frac{\phi hAP_i}{4.5\times 2\pi Tz_i} = \frac{PV\times P_i}{4.5\times 2\pi Tz_i} = \frac{PV\times P_i\times P_{sc}\times T}{4.5\times 2\pi TB_{gi}T_{sc}P_i} = \frac{PV}{B_{gi}} = G_i \text{ or STGIIP}$$

These equations representing the solutions of the flow regimes are embedded in the ©KAPPA - Topaze NL tool and were adapted for a dry gas analysis.

A.2 OPTIMIZATION ALGORITHM FOR rDn

algol60.m

```
function [x,fx,vec,vec2,paramVals]=algol60(func,a,b,t,iter_out,MCno,vec,vec2,paramVals,debug)
% function [x,fx]=algol60(a,b,t,debug)
iter=1;
c=(3-sqrt(5))/2;
x= a + c*(b-a);v=x;w=x;e=0;
[fx,vec,vec2,paramVals]=func(x,iter,iter_out,MCno,vec,vec2,paramVals,debug);fw=fx;fv=fx;
while true
    iter=iter+1;
    m=(a+b)/2;          % Line 10
    tol=eps*abs(x)+t;
    t2=2*tol;
```

```
if abs(x-m)>t2-(b-a)/2
    p=0;q=0;r=0;
    if abs(e)>tol
        r=(x-w)*(fx-fv);
        q=(x-v)*(fx-fw);
        p=(x-v)*q - (x-w)*r;
        q=2*(q-r);
        if q>0
            p=-p;
        else
            q=-q;       % Line 20
        end
        r=e;            % Line 30
        e=d;
    end
    if ( (abs(p) < abs(q*r/2)) && (p < q*(a-x)) && (p < q*(b-x)) )  % Line 40
        d=p/q;
        u=x+d;
        if ( ((u-a) < t2) || ((b-u) < t2) )
            if x<m
                d=tol;
            else
                d=-tol;     % Line 50
            end
        end
    else        % Golden section step
        if x<m
            e=b-x;
        else                % Line 60
            e=a-x;          % Line 70
        end
        d=c*e;              % Line 80
    end
    if abs(d) >= tol
        u=x+d;
    elseif d>0          % Line 90
        u=x+tol;
    else                % Line 100
        u=x-tol;        % Line 110
    end

    [fu,vec,vec2,paramVals]=func(u,iter,iter_out,MCno,vec,vec2,paramVals,debug);   % Line 120
    if fu<=fx
        if u<x
            b=x;
        else
            a=x;        % Line 130
        end
        v=w;            % Line 140
```

```
            fv=fw;
            w=x;
            fw=fx;
            x=u;
            fx=fu;
        else
            if u<x
                a=u;
            else            % Line 150
                b=u;        % Line 160
            end
            if( (fu<=fw) || (w==x) )    % Line 170
                v=w;
                fv=fw;
                w=u;
                fw=fu;
            elseif( (fu<=fv) || (v==x) || (v==w) )  % Line 180
                v=u;
                fv=fu;
            end
        end
       if debug
           %fprintf('rD_cb = %d  |  obj.= %d\n',x,fx);
       end
    else
        break;
    end
end
fprintf('Found local minima in %d iterations at:\nx=%d | f(x)=%d\n',iter,x,fx);

end
```

getParamsFromRD.m

```
function [Iy,newVal,CI]=getParamsFromRD(rD,ci,Ix,Iy,pdfX,pdfY,I2PDF,iter,iter_out,figNo,lege,MCno,debug)

NoOfIndicators=length(Ix);

if isempty(ci)
    [~,ci]=max(Iy);
end

P=double(false(size(Iy)));      % Variable for the probabilities of the indicators at the next step. This is PPM.
for i=1:NoOfIndicators
    if i~=ci
        P(i)=rD*Iy(i);
    end
end
P(ci)=1-sum(P);
Iy=P;
```

```
if debug
    figure(figNo);clf;subplot(1,3,1);hold on;
    plot(Ix,Iy,'.','DisplayName',sprintf('rD=%.3f',rD));
    title(['PDF with ind. for ',lege]);legend show;
end

% Transform PDF to CDF and plot it in Fig
cumu=getCDF(Iy);

% N - Monte-Carlo sampling
idx=double(false(MCno,1));newVal=double(false(MCno,1));
CI=MCSamples(cumu,MCno);
newVal=I2PDF(CI);

% cmuO=getCDF(pdfY);
% cmuO=cmuO/max(cmuO);
% for i=1:MCno
%     [~,idx(i)]=min(abs(cmuO-cumu(CI(i))));
%     newVal(i)=pdfX(idx(i));
% end

if debug
    figure(figNo);
    subplot(1,3,2);hold on;
    plot(Ix,cumu,'.','DisplayName','CDF');
    for i=1:MCno
        plot(Ix(CI(i)),cumu(CI(i)),'*','DisplayName',['MC #',num2str(i)]);
    end
    title(['CDF with ind. for ',lege]);
%     legend show;
    figure(figNo);
    subplot(1,3,3);hold on;
    plot(I2PDF(Ix),cumu,'.','DisplayName','CDF');
    for i=1:MCno
        plot(newVal(i),cumu(CI(i)),'*','DisplayName',['MC #',num2str(i)]);
    end
    title(['CDF for ',lege]);
    legend show;set(legend,'Location','EastOutside','Box','off');
    saveas(figNo,[lege,'_CDF_',num2str(iter_out),'_',num2str(iter),'_distri.png']);
end
```